OPEN ACCESS

University of BRISTOL

This electronic thesis or dissertation has been downloaded from Explore Bristol Research, http://research-information.bristol.ac.uk

Author:
Hinitt, Andrew

Title:
Integration and Coupling of High Performance Dielectric Elastomer Actuator Systems

General rights
Access to the thesis is subject to the Creative Commons Attribution - NonCommercial-No Derivatives 4.0 International Public License. A copy of this may be found at https://creativecommons.org/licenses/by-nc-nd/4.0/legalcode This license sets out your rights and the restrictions that apply to your access to the thesis so it is important you read this before proceeding.

Take down policy
Some pages of this thesis may have been removed for copyright restrictions prior to having it been deposited in Explore Bristol Research. However, if you have discovered material within the thesis that you consider to be unlawful e.g. breaches of copyright (either yours or that of a third party) or any other law, including but not limited to those relating to patent, trademark, confidentiality, data protection, obscenity, defamation, libel, then please contact collections-metadata@bristol.ac.uk and include the following information in your message:

• Your contact details
• Bibliographic details for the item, including a URL
• An outline nature of the complaint

Your claim will be investigated and, where appropriate, the item in question will be removed from public view as soon as possible.

Integration and Coupling of High Performance Dielectric Elastomer Actuator Systems

By
Andrew Hinitt

Department of Mechanical Engineering
University of Bristol

A dissertation submitted to the University of Bristol in accordance with the requirements of the degree of Doctor of Philosophy in the Faculty of Engineering.

Word count: 58,916

Abstract

Dielectric Elastomer Actuators (DEAs) are a novel soft actuator technology which has been shown to be highly efficient, fast acting, proprioceptive and soft. These actuators have been investigated for their impressive performance, but they do have significant drawbacks due to their high voltage operation, failure modes and high stress concentrations around soft-rigid couplings.

This thesis presents three main areas of research into DEAs to enhance their material coupling and integration into practical applications by maximising performance through innovative design concepts, and implementation optimisation.

A novel method of creating multi-layer actuators is presented where laminated dielectric and conductive layers form an inter-penetrating network with captured strain energy. A proof-of-principle DEA demonstrator produced active strain comparable to mammalian muscle.

A new design space is explored to conceive a mechanically coupled DEA that produces a stiff actuation output from a soft actuator. This mitigates key risks of failure of DEAs. The design space includes potential for development of rotational and linear drives and a proof-of-concept multi-state actuator implementation is characterised.

DEAs exhibit self-sensing capability, however high resolution sensing is difficult to implement. An innovative approach for sensing coupling DEA actuation with a soft optical touch sensor is presented. This active-touch system is demonstrated using a palpating coupled module to detect objects.

This thesis has shown high performance DEAs can be integrated and coupled into rigid and soft systems, producing state of art actuators and sensing. Additionally this work demonstrates that the high performance characteristics implemented in thin-film actuator, can be captured in a scaled-up multi-layer actuator through novel bonding, prestrain and lamination methods.

Dedication and Acknowledgements

For the help they have given me whilst I have studied for this thesis I would like to thank firstly, my wife, Olivia for her constant love and unwavering support. Also my parents who have helped me where I have lost my way. I would like to thank my supervisors Andrew Conn and Jonathan Rossiter. Jonathan supported me when Andy could not. Since his return Andy has helped me through my time working on this thesis with great patience and whose guidance has enabled this work to be completed. Finally, I would like to thank all those in the department (both BCCS and BRL) whose friendly disposition and support have helped me through.

I would like to dedicate this thesis to my son, Gregory, who has spurred me on to complete this work.

Author's Declaration

I declare that the work in this dissertation was carried out in accordance with the requirements of the University's Regulations and Code of Practice for Research Degree Programmes and that it has not been submitted for any other academic award. Except where indicated by specific reference in the text, the work is the candidate's own work. Work done in collaboration with, or with the assistance of, others, is indicated as such. Any views expressed in the dissertation are those of the author.

SIGNED: ..... DATE: .....

Contents

List of Publications 9

1 Integration and Optimisation of Dielectric Elastomer Actuators (DEAs) 20

1.1 Overview of Polymer Actuators 20

1.2 DE Actuator Overview 24

1.3 DEA Actuator Applications 27

1.4 Limitation and Opportunities in DEA Research 29

1.5 Research Objectives 32

1.6 Research Methodology 33

1.7 Structure of Thesis 35

1.8 Contributions 37

2 Literature Review 38

2.1 Introduction 38

2.2 Dielectric Elastomer Actuator Overview 41

2.2.1 Principles of Operation 41

2.2.2 Failure Modes 44

2.3 Further Exploitable Properties 45

2.4 DEA Materials 47

2.4.1 Dielectric Membrane Material 47

2.4.2 Conductive Material 48

2.5 DE Actuator Fabrication and Preparation 56

2.6 DEA Configurations 58

2.7 Energy Efficient Configurations 61

2.7.1 DEA Coupling 64

2.8 Prestrain of Dielectric Membranes 65

2.8.1 Methods of Capturing and Integrating Pre-strain in Systems and Devices . . . 67
2.9 Hyperelastic Modelling . . . 68
2.10 Union of Intrinsically Soft & Rigid Components . . . 71
2.11 Soft Sensing Technology Review . . . 74
2.11.1 Sensors Variants . . . 74
2.12 Summary . . . 77

3 Mesoscale Thickness-mode Multi-layer Actuator Optimisation 79
3.1 Introduction . . . 79
3.2 Evaluation of Multi-layer Actuator Implementations, Configurations, and Formulation . . . 80
3.2.1 Multi-layer Actuator Implementations . . . 80
3.2.2 DEA Multi-layer Actuator Configuration . . . 88
3.2.3 Breakdown of Multi-layer Actuator Components . . . 91
3.3 Criteria for Improving Multi-layer Actuator with Single Layer Actuator Characteristics . . . 93
3.3.1 Selection of Design of Multi-layer Development . . . 95
3.3.2 Defining Scope for Optimisation of Multi-layer Actuator . . . 97
3.4 Novel Thin-layer Fabrication Process . . . 99
3.4.1 Lamination . . . 100
3.5 Electrode Development . . . 103
3.5.1 Electrode Characterisation . . . 106
3.6 Multi-layer Bonding and Pre-Stretch . . . 114
3.6.1 Mechanical Strength Characterisation of Multi-layer Structure . . . 121
3.7 Multi-layer DE Actuator Implementation . . . 123
3.7.1 L-IPN Stacking Techniques . . . 123

3.7.2 Multi-layer Actuator Proof of Concept 124
3.7.3 Automation of L-IPN Stack Fabrication 131
3.8 Summary 140

4 Multi-stable Soft Actuator with Rigid Position Control 143
4.1 Introduction 143
4.2 Finite Displacement Actuators 145
4.3 Mechanical Output of a DEA System 146
4.4 Coupling Soft and Stiff Sub-Systems 148
4.5 DEA Stable State Actuator Concept 150
4.5.1 Ratchet Mechanisms 151
4.5.2 Actuator Configuration 153
4.5.3 Multi-state Actuator Concept 156
4.6 Mechanism Design Space 160
4.6.1 Actuation System Operation Modes and Applications 161
4.7 Antagonistic Cone Pair Characterisation 164
4.7.1 Materials and Methods 165
4.7.2 Experimental Setup 166
4.7.3 Characterisation Results 167
4.8 Lock Pin Functionality Test 172
4.9 Experimental Setup 174
4.10 Concept Proof Results 175
4.11 Summary 180

5 Development of an Actively Sensing Pneumostatic Probing Device 182
5.1 Introduction 182
5.2 Understanding Tactile Sensing and Nature's Design 185
5.2.1 Tactile Sensing 186

5.2.2 Nature's Design . . . 187
5.3 Touch Sensing Modes . . . 190
5.3.1 Robotic Tactile Sensing Implementations . . . 191
5.4 TACtile sensor and artificial fingerTIP - TACTIP . . . 192
5.5 Embodied Active Touch . . . 194
5.6 Pressurised Active-Touch Sensing Module . . . 198
5.6.1 Pressurised Vessel Sensor . . . 198
5.6.2 Sensory Skin Actuation . . . 199
5.7 ActivePneumostaticTIP Concept . . . 200
5.8 Materials and Methods . . . 203
5.9 AP-TIP Characterisation . . . 209
5.9.1 Experimental Setup . . . 209
5.9.2 APTIP Static Tests . . . 209
5.9.3 APTIP Dynamic Tests . . . 218
5.10 APTIP Module Object Palpation . . . 222
5.11 Experimental Setup . . . 223
5.12 Image Processing of Camera Video . . . 223
5.12.1 Image Processing Methods . . . 224
5.12.2 Summary of Image Processing Development . . . 231
5.13 Analysis of Test Objects Contact . . . 232
5.13.1 Square Object Test . . . 233
5.13.2 Triangular Object Test . . . 234
5.13.3 Circular Object Test . . . 235
5.14 Summary . . . 236

6 Conclusions and Further Work 238
6.1 Introduction . . . 238

6.2 Conclusions 239
6.3 Discussion of Applications of Developed Technologies 243
6.3.1 Multi-Layer Actuator Optimisation and Fabrication 243
6.3.2 Multi-state Device Future Development 244
6.3.3 Soft Active-Touch Sensor 247
6.4 Further Work 249
6.4.1 Multi-Layer Actuator Optimisation and Fabrication 249
6.4.2 Multi-state Device Future Development 250
6.4.3 Soft Active-Touch Sensor 250

References 251

Appendices 270

A Equilibrium Mechanics of L-IPNs 270

B DE Membrane Fabrication For Multilayer Actuators 271
B.1 Spin Coating 272
B.2 Spin Coating Sample Analysis 272

C High Voltage Test Rig 273

D PIV Frames of Palpation of Circular Object 275

List of Publications

[1] A.D. Hinitt, J. Rossiter, and A.T. Conn. *WormTIP: An invertebrate inspired active tactile imaging pneumostat*, volume 9222. 2015.

[2] Andrew D. Hinitt and Andrew T. Conn. A novel method of fabricating laminated silicone stack actuators with pre-strained dielectric layers. *SPIE*, 9056:90560D, 2014.

[3] A.T. Conn, A.D. Hinitt, and P. Wang. Soft segmented inchworm robot with dielectric elastomer muscles. In *Proceedings of SPIE - The International Society for Optical Engineering*, volume 9056, 2014.

[4] Andrew Hinitt, Jonathan Rossiter, and Andrew Conn. Non-back-drivable binary bistable DEA device. 15(2):141903, 2015.

[5] Aaron Fishman, Martin Stephen Garrad, Andrew Hinitt, Plinio Zanini, Tim Barker, and Prof Jonathan Rossiter. A Compliant Telescopic Limb with Anisotropic Stiffness. i(February):1–8, 2017.

List of Figures

1 Chart of stress-strain characteristics of actuator technologies (reproduced from [Conn, 2008]). 24

2 Chart of the research methodology used in the developments set out in this thesis 34

3 DEA actuation principle showing (a) at rest and (b) actuated with application of high voltage across dielectric 42

4 Graphical illustration of general voltage - stretch relationship and breakdown voltage curve 43

5 Examples of DEAs with wrinkling (reproduced from [Conn and Rossiter, 2012b, Conn and Rossiter, 2012a]) 46

6 Graphical illustration of effects of particulate density on electrical conductivity and mechanical strength. 53

7 Graphical illustration of general volume resistivity - particulate weight relationship with percolation threshold 54

8 Illustration of the potential affect of contact resistance at the connection interface. 55

9 Illustration of state tranistion of displacement in a multi-stable system, showing relative energetic states. 62

10 Examples of coupled pairs of DEA membranes in two common configurations 65

11 Illustration of mechanical strain of DEA membrane. 66

12 Photographic depiction of zone with uniform strain on Hoberman platform. 67

13 One dimensional rheological model of viscoelasticity in hyperelastic materials (reproduced froml [Bergström and Boyce, 1998]). 71

14 Graphical exploration of the component space of robots considering actuator and links (body/end-effector). 72

15 Example of a multi-layer stack fabrication rig (reproduced from [Kovacs and Düring, 2009]). 82
16 Images of two developed multi-layer actuators 83
17 CAD depiction of conceptual multi-layer actuator valve (reproduced from [Maas et al., 2015]) 84
18 A step guide to a manual fabrication process of a DEA stack (reproduced from [Maas et al., 2015]) 85
19 Spring stack leg concept and implementation (reproduced from [Nguyen et al., 2014]) 86
20 Arm wrestling implementation demonstrated at EAPAD 2005 (reproduced from [Kovacs, 2006]) 87
21 Illustration of process for creating thin films of silicone dielectric using developed laminator. 101
22 Microscopy image of cross-section of laminated silicone layer (target thickness 100microns). 102
23 Experimentally calculated uniaxial force-strain relationship of Xiameter 3483 silicone 102
24 Plot of experimental results of two-wire resistance for composite silicones with different carbon black weightings at 1kV using a Megger high voltage resistance meter 107
25 Comparison of photographic imagery of samples with different carbon black weights analysing homogeneity. 108
26 Illustration of experimental set up of straining rig for testing conductivity change with strain. 109
27 Illustration of experimental setup for straining conductivity samples of varying thickness. 110
28 Graph of experimental data on effects of uniaxial material strain on resistance for silicone conductive composite samples with varying carbon black weightings. 110

29 Illustration of set up for force-strain characterisation of conductive silicone composites. 112
30 Plot of relationship between applied tensional force and uniaxial strain of silicone conductive composite samples with varying carbon black weightings. 112
31 Effect of weighting of carbon black in a silicone conductive composite on material stiffness 113
32 Plot of the effect of conductive composite thickness on sheet resistance with a constant carbon black weighting of 5% 114
33 Depiction of the process of laminating two dielectric silicone membranes together with a silicone-carbon black conductive composite. 116
34 Process of capturing pre-strain of a silicone elastomer in preparation for forming an L-IPN 117
35 Illustration of three resultant three layer L-IPN with silicone - carbon black composite sandwiched between two dielectric membranes with caputred pre-strain. 118
36 L-IPN Uniformity Images 119
37 Meaurements of layer thickness uniformity from cross-section of L-IPN. . 120
38 Example Tensile Sample 122
39 Experimental set up and breakdown of test sample. 122
40 Arrangement of equipment for actuation test of pre-strain silicone multi-layer actuator 125
41 Multi-layer sample actuator in situ for experimental test. 127
42 Actuator input voltage and current profile (3.2kV) for actuation test. . . . 127
43 Differential laser actuator displacement response for 3.2kV input voltage actuation test. 128
44 Individual laser displacement measurements 129

45 Microscopy image of slice cross-section of actuated pre-strained LIPN multi-layer actuator. 130
46 Prototype Stacking Rig Iteration 133
47 Illustration of arrangement of components for stacking layers. 134
48 CAD drawing of arranged components for conceived stacking rig. 135
49 Complete prototype stacking rig. 136
50 Photograph illustrating the nature of peelable inconsistent bonding between layers encountered. 138
51 Prototype stack cross-section consisting of 16 dielectric layers fabricated using stacking rig. 139
52 Microscopy image of prototype stack in sliced cross-section showing layer thickness consistency and uniformity. 140
53 Flexidrive prototype rotary drive (reproduced from [Tse et al., 2011]). . . 147
54 DSMPA - Dielectric shape memory polymer actuator - state concept transition illustration. (reproduced from [Rossiter et al., 2010]) 150
55 Exploded view detailing a design of an indexing cam (reproduced from [Sclater, 2011]) 153
56 Illustration of linearised conceptual multi-state mechanism design 156
57 Illustration of state tranistions of multi-state mechanism for a 120 degree cycle 158
58 Illustration of forces involved in the state transitions 159
59 Conceptual illustration of an linearised N-state mechanism configuration . 162
60 Image of cross-section of linear screw mechanism CAD design. 163
61 Antagonistic coupled cone actuators cross-sectional schematic 165
62 Experimental rig schematic of antagonistic cone actuator characterisation. 167
63 Plot of force - displacement for strut length 80mm 168
64 Plot of force - displacement for strut length 90mm 168

65 Plot of force - displacement for strut length 100mm 169
66 Plots of force - displacement for strut length 110mm 169
67 Plot of work output of single side actuation of antagonistic cone pair. . . 171
68 CAD desing of multi-state actuator prototype demonstration rig. 172
69 Illustration of defrees of freedom of multi-state mechanism design 173
70 Photo of multi-state actuator with component descriptions. 174
71 Series of figures showing state steps of actuation cycle of prototype unit. . 177
72 Plot of translational displacement of end effector along the axis of DEA actuation displacement. (Letters a-e mark states referred to in Figure 71). 178
73 Plot of the rotational displacement of the end effector about the axis of DEA actuation displacement. (Letters a-e mark states referred to in Figure 71). 179
74 Images of human finger structure and illustration of the use of papillae in haptic sensory feedback. 188
75 Photo of original TACTIP device and corresponding casting moulds (reproduced from [Chorley et al., 2009]). 193
76 Photo of prototype Whiskerbot. 197
77 Diagrammatic representation of APTIP actuation and sensing of object. . 201
78 Fabrication steps for production of silicone sensory membrane. 206
79 Photo of test pieces of sensory membrane. 207
80 Illustration of deflection of papillae on sensory membrane resultant from contact with test object. 207
81 Schematic of characterisation rig setup for APTIP. 209
82 Actuation of APTIP at varying voltages 211
83 Photographic evidence of wrinkles on pneumostatic DEA when actuated with voltages approaching material breakdown. 212

84 Plot of pole height and pressure against voltage for pneumostatic characterisation. 213
85 Plot of sensory membrane retraction on actuation recorded from video frames. 214
86 Plot of actuator membrane expansion on actuation recorded from video frames. 215
87 Illustration of APTIP volumetric changes between states. 217
88 Illustrative plot of dynamic variation of parameters with actuation of DEA pneumostat. 218
89 Processed data of internal camera video frames of sensory membrane protraction. 221
90 External Photos of ActivePneumostaticTIP 222
91 Photo of test blocks used in sensory membrane object detection tests . . . 223
92 Schematic of APTIP set up for object detection tests 223
93 Unprocessed frames from camera of circular object test 224
94 PIV of succcessive frames at key state changes. 226
95 Circle object test individual pin vector tracking. 228
96 Output of image processed frames from circular object detection test . . . 230
97 Output of image processed frames from square object detection test . . . 233
98 Output of image processed frames from triangular object detection test . 234
99 Concept of an antagonistic finger prosthesis 244
100 Photo of common braille display device (reproduced from [Runyan and Blazie, 2010])246
101 Illustration of conceptual DEA braille display device. 246
102 Illustration of APTIP as a robotic arm attachment 247
103 Ilustration of active pneumostatic device as worm end effector 248
104 Concept of APTIP as standalone senory device 249

105 Set of schematics illustration the strain mechanics in producing a layered actuator with captured pre-strain. 270
106 Laminations In an Envisaged Stack 271
107 Illustration of measurements of spun silicone sheet 273
108 Depiction of high voltage experimental rig. 274
109 Photo of high voltage experimental rig. 275
110 Complete set of frames of video of circular object test palpation. 278

List of Tables

1 A comparison of prevalent alternatives to conventional actuator technologies [Mirvakili et al., 2014, Carpi and Rossi, 2007, Bar-Cohen, 2004] . . . 22

2 Description of customisable characteristics of DEAs and developmental methods 26

3 Conceived applications of DEA actuators and sensors 28

4 Performance of dielectric materials from material characterisation papers [Carpi et al., 2007, Brochu and Pei, 2010] 48

5 Table of common conductive materials used for electodes in DEAs 50

6 Tabulate list of common DEA configurations with distinctive characteristics of type of strucutre and operation, with short description of features. 60

7 Tabulation of current forms of multi-layer DEA configurations and categorisations of structure and output. 90

8 Table of high-level development issues in the development and fabrication of stack actuators. 94

9 Design Selection Decision Matrix 95

10 Table of main characteristics and addtional description of common conductive powders for DEAs 105

11 Tabulation of comparison of actuators matching concept desired parameters155

List of Abbreviations and Symbols

SMA - Shape Memory Alloys

SMP - Shape Memory Polymer

DEA - Dielectric Elastomer Actuator

EAP - Electro-active Polymer

IPMC - Ionic Polymer Metal Composite

MES - Minimum Energy Structures

GI - Gastro-intestinal

TCA - Twisted Polymer Coil Actuator

NBR - Acrylonitrile Butadiene Rubber

FOV - Field of View

PIV - Particulate Image Velocimetry

E – Electric Field

P – Pressure

C – Capacitance

A – Overlapping surface area of electrode plates

t – Distance of separation between conductive plates (i.e. membrane thickness).

ε_r – Relative permittivity

ε_0 – Permittivity of free space

X_C – Capacitive reactance

f – Frequency

L – Initial length

l – Final length.

λ – Stretch

e – Strain

W – Helmholtz free Energy

μ – Small-strain shear modulus

J_{lim} – Strain-stiffening constant

μ_i and α_i – Non-physical material parameters that are experimentally measured

ξ_α and ξ_β – Time-dependent variables of the dielectric elastomer

1 Integration and Optimisation of Dielectric Elastomer Actuators (DEAs)

Research in novel actuators has seen rapid expansion in recent years especially within soft actuators including dielectric elastomer actuators (DEAs). There is a rich environment for research within this class of polymer actuator with scope for innovation. The characteristics of DEAs in their most basic form are comparably impressive in the field. They show high efficiency, high strain, fast response time and repeatability of actuation cycles. These features should enable a whole range of devices to be developed, however when applied to real world applications, the actuators exhibit some limitations. DEAs require mechanical optimisation to achieve the characteristics described, and the delivery of mechanical energy from the active strain of an actuator membrane is difficult to transfer to an external load. Additionally, the soft nature of these actuators requires a more holistic consideration of actuator reliability and performance including integration to external structures.

1.1 Overview of Polymer Actuators

In the last two decades there has been a renewed interest in the investigation of soft actuators and soft robots. This reinvigoration is due to a number of factors in the fields of engineering and robotics. As industrial robots have increased in complexity to take on more tasks performed by humans, the requirements have shifted from large-scale repeated actions in a structured* environment carrying out mass-production tasks with minimal feedback, to human-scale† unstructured environments with variable workspaces and dynamic complex tasks. The set of tasks where there are limitations in current actuation technologies also encompasses a wide range of applications beyond humanoid robots, including medical devices (e.g. surgical tools [Cianchetti et al., 2014]), search

*Structure is used to define the type of environment the robot is used in. If it is structured, the workspace is considered ordered

†In this instance, human-scale refers to tasks that are capable to be undertaken by humans and includes a range to the lower limit of human operational capabilities

and rescue robots [Tolley et al., 2014], or pipe inspection [Kornbluh et al., 1998]. These tasks require reliability, repeatability, flexibility, compact high power density (over a range of scales) and feedback for control. As such there has been an increasing desire to find alternative actuators and structures that offer potential to exhibit these characteristics, and to be able to implement specialised devices in these expanding areas of desired operation.

Of the many possible novel actuator choices available, electrostatic polymer actuators are of particular interest and they are a type of electroactive polymers (EAPs). EAPs encompass a wide range of materials and actuation types (e.g. ionic polymer metal composite (IPMC), electrostatic, twisted-coil actuators (TCAs), shape memory alloys (SMA)), each with specific benefits and limitations, which all use a polymeric based material for actuation [Haines et al., 2014, Carpi et al., 2007]. Within this class of actuators, dielectric elastomer actuators (DEAs) are a particular group of electrostatic EAP actuator that show promise as efficient high energy, high strain, soft actuators and have been used across a range of scales from millimetre to metre [Chiba et al., 2008].

Table 1 shows a comparison of maximum performance between a selection of smart material actuators, and a biological actuator (mammalian muscle).

Actuation Types	Mammal Skeletal Muscle	DEA (Silicone)	DEA (VHB)	TCA	SMA (TiNi)	IPMC
Strain (%)	20 - 40	<120	<380	40	>5	<3
Stress (MPa)*	0.1 (0.35†)	3.2	7.7	70	>200	<3
Efficiency (%)	∼40	<80	<80	<2	<5	<5
Response (cyclic)	Medium/ Fast	Fast	Medium/ Fast	Slow	Slow	Medium
Voltage (V)	<1	>1000	>1000	N/A (Thermal)	Low	<7
Cycle Life	10^9	10^6 at 10% strain	10^6 at 50% strain	10^4 at 2% strain	10^7 at 0.5% strain	10^4

Table 1: A comparison of prevalent alternatives to conventional actuator technologies [Mirvakili et al., 2014, Carpi and Rossi, 2007, Bar-Cohen, 2004]

(†) - Only sustainable for short periods

Mammalian muscle is used as a benchmark when comparing how these actuators perform, as many applications of soft actuators require the same range of characteristics (however it should be noted, there are some signifiant exceptions). Mammalian muscle has evolved to provide an efficient method of providing actuation to a skeletal framework, which can operate across scales from sub-millimetre to metre. They offer a high power density and function over the lifetime of the mammals in some cases exceeding a century

*Peak Stress that can be sustained

of continuous use. Nature's methods of repair and continual replacement facilitate this capability. DEAs potentially offer capabilities in excess of those attained by mammalian muscle (in their thin film form). Scaling these results to the high power requirements of larger muscles in mammals is still in active development. At a smaller scale DEAs are already being applied to devices including haptic feedback units, and an autofocus lens [O'Halloran et al., 2008, Matysek et al., 2010, SRI, 2010]. To apply an electric field of the strength needed for actuation, the voltage required is high, and as such, a significant drawback, especially for high power applications, where the energetic release on failure would potentially be fatal for humans. Methods of protection and ways to reduce the voltage amplitude required may be developed to mitigate this drawback. The parameters of response time, efficiency and lifespan are exceptional and show the potential of this technology. Twisted polymer coil actuators (TCAs) and shape memory alloys (SMAs) use thermal response to actuate - by thermal conduction and electrical resistive heating respectively -, producing high energetic output; greater than DEAs, but taking longer to respond with a significantly slower response time. Additionally, their efficiency is comparatively much lower than DEAs or mammalian muscles. Ionic polymer-metal composite (IPMCs) offer another alternative actuation technology, even considering their relatively fast response time, the energetic output of this actuator type is not considered comparable to other technologies shown in Table 1.

DEAs can be seen to be a close approximation to their biological counterparts, but have some drawbacks which affect how the technology can be used (especially in human robot interaction applications) discussed in Section 1.4. With response time and efficiency improvements TCAs and SMAs could offer some competition to DEAs at mimicking the actuation potential of muscle. For all actuators described, the technologies can be applied to real world problems requiring novel actuation. Figure 1 gives a comparison between competing actuator technologies, showing their optimum stress and strain response.

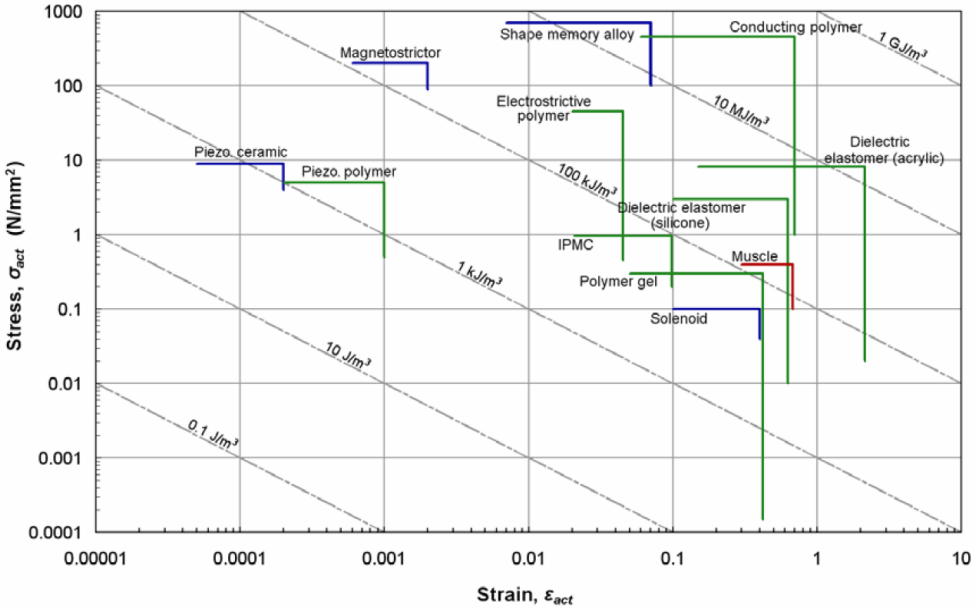

Figure 1: Chart of stress-strain characteristics of actuator technologies (reproduced from [Conn, 2008]).

From the figure above, the maximal stress-strain performance of envelopes can be compared. The electrostatic actuators fabricated from VHB and silicone straddle the output of muscle, and outperform most non-conventional actuators and some more conventional actuator technologies. As a mimetic for biological muscle DEAs can be shown to, at present, have outputs that can match this capability. In addition, due to the lack of significant breakthroughs in the chemical engineering of the dielectric materials for DEAs, it can be assumed that further performance enhancements may be found.

1.2 DE Actuator Overview

From the very beginnings of the discovery of electricity, actuation of biological muscles excited and intrigued. With the advent of the harnessing of electrical energy in the late 19th century early experimentation involving dielectric actuation of balloons was carried out [Breazeal and Bar-Cohen, 2003]. In the re-genesis of DEAs, the properties of numerous elastomers have been explored.

Due to the breadth of possible configurations, materials and applications that DE actuators can be formed with, the categorisation of specific system types is difficult to define. However, DE actuators can be divided into two broad categories of operation - higher power multi-layer implementations and thin films (usually single layer). Across both operation types, DEA research efforts have included improving the actuators through endeavours in material science and modelling, mechanical design and fabrication. The characterisation of DEA actuation has led to an understanding of the parameters that determine the actuation and failure modes of the actuator. This research is aimed at optimising the coupling of DEAs to external loads through a number of configurations. The exploitable characteristics and methods intrinsic to the actuator design and construction detailed in Table 2 are utilised along with novel design approaches to create coupled DE actuators.

Characteristic/ Method	Description
Material Composition	Dielectric and conductive materials make up the electrostatic actuator. The material compositions and characteristics can be improved to achieve required levels of performance
Fabrication Methods	Uniform dielectric membranes and consistent conductivity are critical to optimal operation of DEAs. In stacks layering techniques also help optimise performance.
Modalities	To use the mechanical work done by the actuator, it needs to be converted into a useful form. The modality will depend on the design of the actuator and the modality, which in planar arrangements includes transverse contractive actuation or planar relaxation actuation. Other modalities will be discussed in reviewing relevant literature in section2.6
Actuator Modelling	A better understanding of the mechanical dynamics enables further enhancement of the actuator within quantified stable boundaries.
DEA Specific Parameters	Optimisation of parameters such as pre-strain and response time of the DEA membrane and use of characteristics of the actuator will enable increases in performance.
Design and Integration	DEAs are inherently soft, and need to have external support or be self-supporting. Their operation can be enhanced through structurally supported configurations, such as antagonistic cone pairs. The design of the actuator and its system integration are important in developing real world applications.

Table 2: Description of customisable characteristics of DEAs and developmental methods

A DEA's operation is governed by the electrostatic compression of an elastomer through the application of high electric field*. To maximise the performance of the actuator, the parameter and methods tabulated can be used. Inherent in the optimisation and reliable operation of a DEA, the design of its integration into a structure is paramount. In spite of achieving outstanding characteristics in thin film form, the actuators are not resilient to high physical stresses generated from external interactions especially during operation where over-stressing localised points of the material can cause mechanical failure. Additionally, failure may be induced by electrical breakdown (dielectric failure either through inhomogeneous material facilitating breakdown, or pull-in failure†. Due to the capacitive nature of the membrane, a single point of failure causes the whole device to fail, hence the importance of reducing these failure mechanisms.

1.3 DEA Actuator Applications

In principle DEA actuators offer a method of producing a variety of devices from high-power large-scale, to efficient millimetre scale and proprioceptive devices (in both passive and active operation). As such there are wide range of applications that this exciting technology can be applied to. To classify particular groups of interest, Table 3 shows some of the popular conceived applications.

*The voltage is of a high magnitude due to the distance over which it acts. The Maxwell pressure needed to compress the elastomer is proportional to the inverse square of the distance acted over. At a material thickness where reliable dielectric layers can be produced the voltage is broadly in the order of 1kV to 10 kV with present materials and fabrication techniques

†Pull-in failure refers to an instability where Maxwell pressure continually exceeds film compressive stress resulting in breakdown

Application	Description
Prosthetics	Multi-layer - Artificial Muscle for use as the high power actuator in prosthetic or supportive actuation for stroke rehabilitation
Surgical Robots	A manipulator to produce precise control at small scale.
Gastrointestinal Investigation	A stand-alone robot to locomote and sense features of the GI tract related to health conditions.
Damage Assessment	A better understanding of the mechanical dynamics enables further enhancement of the actuator within quantified stable boundaries.
Search and Rescue	The ability to locomote and explore an environment adapting to traverse small gaps and unstructured environments.
Pump	For the movement of fluids in a system (e.g. artificial heart).
Valve	For the control of high pressure fluids as a control mechanism for a high-power system (e.g. air muscle control valve).
Micro space system deployment	Unfurling systems and sensors using lightweight minimum energy structure (MES) designs.
Artificial Skin	For the development of areal sensory feedback of external interaction forces on a robotic system.

Table 3: Conceived applications of DEA actuators and sensors

Soft materials can be used for a variety of applications as shown in Table 3. They can be used for actuators as stand-alone devices, sensors, actuators with intrinsic position sensing, and form entirely soft robots. DEA soft actuators are aimed to outperform existing technology in manipulation and efficiency at a humanoid scale in particular applications where large strain and compliance can be utilised. Many of these possible

functions surround human compatibility and capability, but include a far broader range of bio-mimicking technologies, which encapsulate a wide range of applications. The research in the field has involved a broad array of specialised devices, which fill specific gaps in the application space. In these cases particular features of the DEAs are exploited with some success in proof of concept [Carpi et al., 2011, Araromi et al., 2015a]

1.4 Limitation and Opportunities in DEA Research

DEAs are an excellent candidate for generating actuation outputs that cannot be adequately produced using conventional electric motor technology. This includes in applications requiring lightweight systems, non-metallic actuators, and as artificial muscles mimicking the contractile actuation found in natural muscle. They have been shown to have class-leading characteristics, and can self-sense, be used as an artificial sensory surface (or skin) and are scalable [Gisby et al., 2013]. They are inherently compliant, and based on analysis of characterisation data, DEAs appear to be a viable replacement for popular conventional actuators* over a wide variety of applications, both current and novel. However, there are some significant gaps between the current state-of-art and the targeted spectrum of applications. Additionally, there are some significant drawbacks due to the high voltages required for actuation (i.e. the need for protection from failure), realisation of reliable actuation with different application requirements (especially high-power) and resilience to interactions with external environment bodies (especially rigid or sharp objects) that may adversely affect actuator functionality [Kovacs and Düring, 2009]. Considering the benefits and the need for further optimisations, and the current limitations of the actuators in their current form, a key focus of addressing problems with coupling and integration of DEAs was identified. Specific opportunities with significant potential have been identified:

*Popular conventional actuators used are predominantly electric motor driven systems

Integration of DEAs to Real World Actuation Systems - Soft actuators such as DEAs have been purposefully used in combination with soft structures to assert a useful output. This work will look at how to integrate DEAs into modules compatible with popular conventional actuation systems* to produce useful and reliable interactions. The integration of soft actuators into rigid systems is a currently under-explored area of this field.

The research has however focused on thin film actuators (single layers) at a small scale. This is partly due to the ease of fabrication with existing materials to create proof of concepts, and partly due to the ease of optimisation of DEAs in their single layer form. There are a few applications which have used larger scale membrane and, some that have used multiple layers. [Kovacs and Düring, 2009, Carpi and Rossi, 2007]. As planar actuators, DEAs can be designed to be used in a number of modes to provide simple and complex planar, and out-of-plane actuation.

Development of Multi-layer Actuators for Integration in High Power Systems - The development of a high performance large-scale actuator has applications in a number of fields. It can be used as a mimetic for mammalian muscle, or soft robot actuation - for locomotion and manipulation. As a muscular mimetic, the DEA can be used for humanoid robotic systems and prostheses, but more broadly can be used to replicate muscular actuation in bio-mimetic designs.

Soft robotic actuators have been used for a range of novel, specialised small-power devices. These have facilitated the development of soft devices and are inherently part of the field of soft robotics. However, it has been found that high output multi-layer actuators are much harder to construct, optimise and deliver a usable output in the region characterised in single layers. The necessity of actuator supporting structure and thickness mode configuration for multi-layer compressive strain is complex.

A significant proportion of large scale developments have focused on energy gen-

eration rather than actuation, due to removal of high voltage requirements and the acceptance of higher losses or lack of maximised optimisation in the operation of the soft capacitor.

Multi-modal Compliant Sensing - In precise manipulation robots, the requirements for sensing and actuation are closely linked, especially as researchers move to investigate increasingly complex unstructured environments that we aspire to develop robots to operate in future [Tiwana et al., 2012]. There is a need for feedback from robotics arms and end-effectors. These sensors must provide multi-point sensing with a sensing density high enough to give an emulation of skin that can be used to enable more precise dextrous manipulation. The development of a robotic skin or complex sensing system seems likely to be an essential part of future humanoid robotic systems especially with close proximity to humans, due to need to protect people from damaging movements of robots. Additionally, its uses on a range of robots with complex behaviours make it a sought after technological advancement.

Previous research has been undertaken to utilise the properties of the DEA to provide a form of sensing [Gisby et al., 2013]; intrinsic to the capacitive form is the complex impedance (capacitive reactance) of the actuator. Superimposing a high frequency input signal can allow the reactance to be detected at high or low voltage [Jung et al., 2008, Huu Chuc et al., 2008]. The actuation of a sensing component (e.g. skin or proboscis) whilst simultaneously sensing enables the use of a *passive* sensor in an *active* mode. This method has been shown to provide precise sensing. However, only one sensing parameter can be outputted per DEA. Additionally, bi-axial expansion cannot be distinguished from uni-axial strain with the same area change. This fundamentally limits the capability of this sensing method when considering zonal sensing.

This is not the only method of sensing whilst using a DE actuator. Other proven technologies such as optical or resistive sensing, as well as other capacitive sensing methods

can be used whilst still leveraging the advantageous properties proffered by soft actuators [Dahiya et al., 2010].

In summary, the field of soft robotics offers a wealth of new possibilities to implement novel and high performance robotic systems that provide exceptional characteristics that cannot be replicated in current popular robotic systems. These include pseudo-muscular mimicry, intrinsic compliance and proprioception properties. There is a clear need for flexible, bio-mimicking, sensory robots to work with humans and improve on the current state-of-art in a number of sectors; from medical tools and prostheses, to close proximity robot interaction with humans (where safety is paramount) and in a number of other fields (such as space systems, or search and rescue robots). DEAs do have potential to fulfil all of these tasks, however, there are some key limitations to be overcome including safety, for high voltage required for operation, and realisation of optimised characteristics in real world systems reported in literature [Pourazadi et al., 2017].

1.5 Research Objectives

This work is aimed at filling some of the gaps in the current actuator and sensing technology for use in soft robots, muscles or actuating structures. The field and the possibilities for the technology are still not fully explored. Soft actuators have been explored as low power and broadly planar systems, where actuation has been optimised and shown to have high performance characteristics. Some have been shown to have sensing capabilities. Harnessing these performance characteristics to produce devices with useful output requires novel specialisation, design, and fabrication methods. In summary the objectives are as follows:

1. Analyse current state-of-art developments to provide insight into:
    - Fabrication methods of actuators including materials and optimisation pa-

rameters.

- Mechanical designs and structures used to provide specialised performance characteristics.
- Actuator configurations and modalities of actuation for integration into electromechanical devices.

2. Use that analysis to identify key areas where DEA systems can be improved.

3. Develop innovative solutions to limitations of DEA system coupling

   - Ideate novel concepts
   - Develop requisite processes and methods to create proof-of-concept
   - Test conceptual implementations and analyse performance.

1.6 Research Methodology

The motivation of this PhD is to enhance the current state-of-art of DEAs through analysing their form and creating innovations in the optimisation of DE actuator development and their integration and use in a variety robotic structures and implementations. Three defined technological gaps were identified and solutions developed as part of the investigations:

1. Multilayer actuators

2. Low-power or control actuation systems*

3. Sensory systems

An approach of defining and characterising technological innovation was proceeded by a unit system and integrated system design process as part of an engineering design process. The methodology used is described in the flowchart in Figure 2:

*The term 'control actuator' is used to refer to an assistive actuator that enables or controls the primary (or power) output (e.g. valve in a pneumatic system).

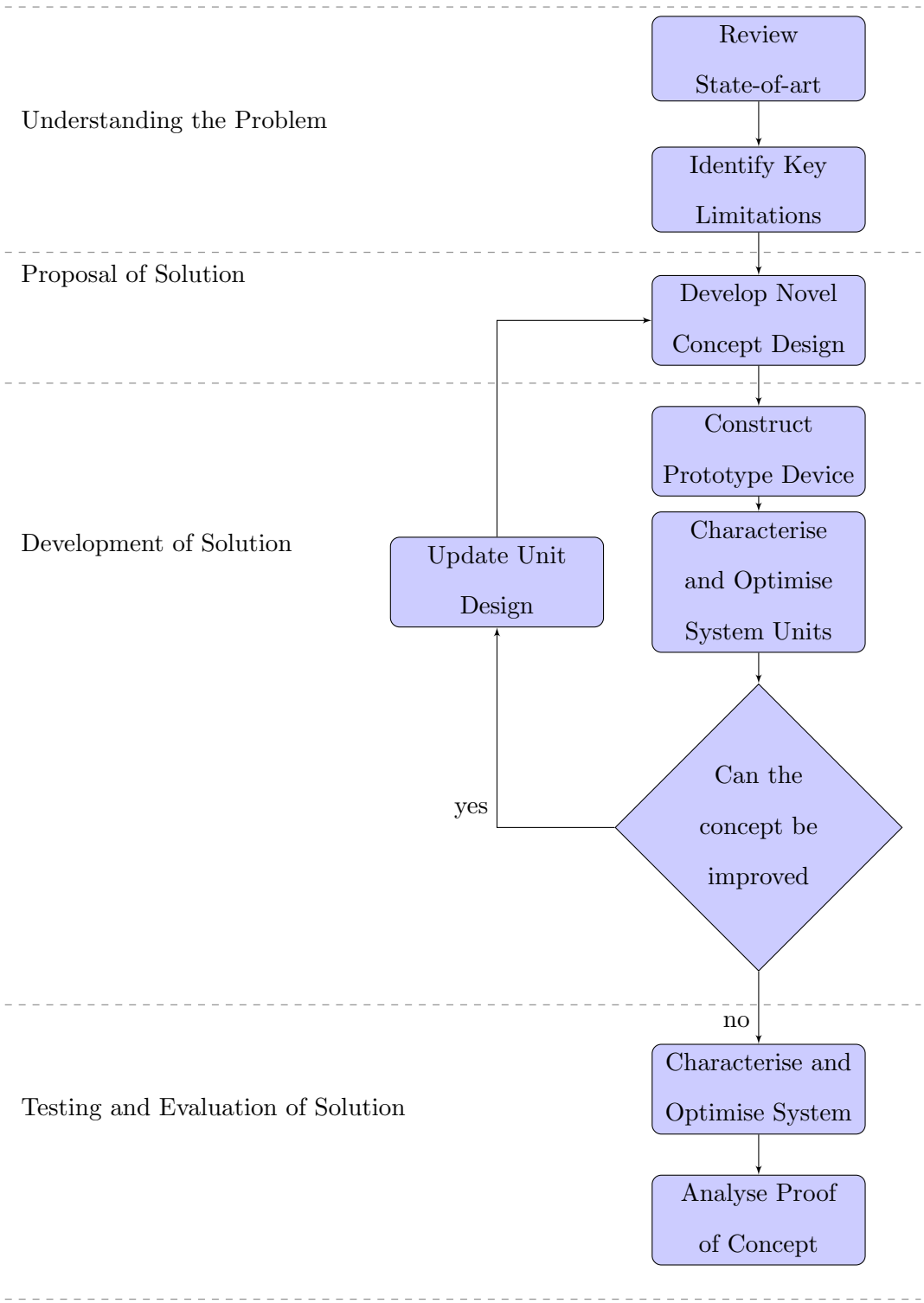

Figure 2: Chart of the research methodology used in the developments set out in this thesis

As described in Figure 2, a review of the literature surrounding DEAs was followed by identifying key limitations within the application of soft actuators to real-world robotic problems. This involved the targeted study of configurations, modes of operation, state-of-art fabrication and modelling techniques.

A concept with innovative approaches to DEA utilisation was devised to solve limitations within the current state-of-art of DEA. From this concept, steps/problems required to be solved were identified. These were undertaken in the development of a prototype, where these problems were individually or in combination resolved in the design and fabrication of components and mechanisms for the system. Major unitised components were individually characterised to ensure unit functionality of each element of the solution. If required, elements were redesigned and retested where they failed to meet the requirements of the design. When the system was fully integrated in a working prototype, the whole system was tested and its performance analysed. This method was repeated in three areas where particular gaps were found in the development of DEA actuators.

1.7 Structure of Thesis

The integration of optimised DEAs to operate in complement or in place of current actuation technologies is under-explored. This work will attempt to change this by exploring and optimising novel concepts for specific classes of applications to which DEAs are suited. This introduction is followed by a literature review of the current state-of-art in the field of soft actuation and sensing. The current attainable performance will be discussed and how novel specialisation has provided a breadth to the field.

- Chapter 2 - Literature Review - a review of the current state-of-art in the field of soft actuation and sensing. This will provide a more specific in-depth review of DEAs, which form the main focus of the thesis. It will include modalities, materials, fabrication, modelling, design, and structure. The current attainable

performance will be discussed and how novel specialisation can be applied to the field to attain some key benefits.

- In Chapter 3 - Mesoscale Thickness-mode Multi-layer Actuator Optimisation - , the requirements for the development of a high performance multi-layer actuators will be investigated. How certain technological limitations could be overcome are investigated.

- Chapter 4 - Multi-stable Soft Actuator with Rigid Position Control - will cover the development of an enabling technology, providing secondary actuator with application in valves. The use, configurations and optimisation of DEAs for this purpose will be explored.

- In Chapter 5 - Development of an Actively Sensing Pneumostatic Probing Device - use of soft materials in the development of active-touch sensing technology when paired with optical sensors will be considered. The capabilities and possible methods of information retrieval about a surface will be researched.

These chapters will introduce the concepts and research pertinent to the endeavour and describe the models, methods and experiments used. The outcome of investigations and developments will be discussed and summarised.

The thesis focuses on the development of novel devices based on characterised materials. However, the novelty in each case is through the innovative pairing and coupling of actuators, structures, and sensors. As such, the focus was on the optimisation of individual technologies and integrating them to form devices with highly useful functionality. Due to the innate properties of the soft materials, the pairing combinations/coupling, and the complex designs and manufacturing used, the developments are empirical as it is highly unlikely to produce useful and comparable models in the cases presented. In addition the focus on the prediction of output would have reduced the achieved innovation

in design and function delivered.

1.8 Contributions

This thesis makes the following contributions to the field of DEAs:

- Advancement of the techniques to enhance performance of multi-layer stack DE actuators with specific emphasis on requirements for high-power tensile operation actuation.
- Development of innovative pairing of a soft actuator with a multi-state mechanism with rigid output and the creation of a prototype demonstration of a bistable actuation device with zero-energy-fixity.
- Devise a novel active-touch zonal sensor, combining soft actuation and sensing membranes to create a lightweight modular device.

2 Literature Review

2.1 Introduction

The field of electrostatic actuators has expanded dramatically over the past two decades, even though the principles and technologies have been described and understood for over a century [Breazeal and Bar-Cohen, 2003]. The resurgence has grown from key findings in new research within the field of soft actuators which have resulted in larger performance increases [Carpi et al., 2007], as well as the current technological drive to fill gaps in next generation robotics where more biomimetic properties are desired. New types of actuator, materials and methods in a range of soft actuators, including twisted polymer actuators, SMAs, DEAs and IPMCs have shown great promise and have exposed the potential benefits still to be realised from innovations in novel actuation technologies. The popular and standardised actuation technologies (such as electric motors) used in most current commercial actuation systems are chosen for their power, scalability, relative efficiency, and the gained economies of scale found in mass-production. There are considerable economic, technological and research barriers to changes of actuation technology, which may limit future commercialisation potential of DEAs until they are proven to reach certain milestones of reliability and utility. However, there has been a shift towards investigating alternative actuator solutions as robots (especially those of a human-scale with future requirements of human manipulation) are being developed where:

- Safer interaction characteristics currently are actively governed through complex control systems of rigid bodies rather than inherent compliance and self-sensing.
- Actuator instantaneous power output in compact designs reaches the limits of electric motors especially with high repetition, rather than with low loss, highly responsive high strain direct actuation.

- Haptic feedback is limited to optical, torque joint control and point-sensing feedback, rather than proprioceptive, biomimetic actuation with tactile skin.

These are the aims and outputs of some of the state-of-art soft actuation technologies being developed today in the soft robotics field. The potential for soft actuators to provide alternative actuation in a near unexplored class of actuator has meant characterising this group from the ground up.

Arguments made against developing this actuator class have included the comparable high power, utility and scalability of electric motor technology, which have been the primary drivers of a worldwide electrical motor industry for a century. The difficulty in developing soft actuation technologies has been in the creation of new systems (including designs, configurations, and devices) based on the basic principles and the formation of a niche in which these technologies can surpass existing incumbent conventionally actuated systems. However, the need for compliant sensors and actuators has become increasingly clear from research endeavouring to further expand and leverage robotic capabilities in both industrial and consumer applications. Research to solve these issues has focussed on soft actuation and soft robots due to their bio-mimicry and comparable output (to biological muscle) [Carpi et al., 2007]. The research and development in novel actuation has expanded into many of the facets of the field, which has fuelled competition in differing technologies and actuation methods internal to the soft robotics. The majority of the outcomes of research in soft actuation are still developmental or proof of concepts, however there have been commercial applications in the fields of wave energy generation [Chiba et al., 2008], and in some haptic technologies [Haruna et al., 2007, Matysek et al., 2009]. Additionally, many exploratory implementations in the soft robot space have been created by Festo in their Bionic Learning Network [Fes, 2018].

There are significant hurdles in the development of soft robotics and soft actuators to be overcome in order to reach these goals with the reliability and resilience expected in industrial applications. The potential for specialised optimisation to an application

is a potentially very beneficial feature, but also an "Achilles Heel" in the research, as a large number of designs and types of actuation are possible, leading to a lack of targeted aims. The breadth of research in materials, configurations, parameters and applications will be discussed. These areas all play an important role in leveraging the technology and enabling the current state-of-art through a mixture of optimisations to produce specialised output.

Conventional actuation* for manipulation tasks has been mainly comprised of rigid joint-and-link structures coupled with electric motors or hydraulic systems. Commercially they have been mainly designed for industrial fabrication and manipulation. The aim is to provide robots with the ability to deliver precise movements repeatedly with high accuracy (in some cases with heavy loads). Large scale conventional robots have excelled at these tasks, due to their well understood and proven dynamic movement and control, enabling the robotic overhaul of industrial production. To automate a new range of operations, robots are required to perform more complex tasks in semi-structured environments at a human scale (potentially with human interaction).

However, as robots are aimed towards less structured environments with more human interactions, reducing the scale of these systems whilst maintaining required performance is hindered by limitations of the robotic components. The rigidity is an issue for Human-Robot Interactions (HRI) due to the possibility of injury. This is compounded by component weight and size.

Soft robots offer a potential solution to this and other problems. They may be actuated by conventional and non-conventional actuators. Depending on the type of actuation the robot can be tethered or untethered. Generally soft robots tend to be small at present with a few exceptions (for example, Ant Roach by Pneubotics which is a large hexapedal robot [Albert, 2016]), due to the early development stage of the technology.

*For the purposes of this study, conventional actuation will encompass the use of electric motors (linear, rotary, and geared), and rigid pneumatic/hydraulic systems

Mostly they are produced at the lower end of the macro-scale for manufacturing*, where they are used in a mixture of primary and secondary actuation systems (such as pumps and low-power muscles [Lotz et al., 2009, Gu et al., 2017a]).

This work, and hence the literature review, focuses on the development and optimisation of soft systems using DEAs to facilitate further progress in soft robotic implementations, from multilayer actuators and their potential use for high power applications to secondary actuators to control the actuation developed by other high power systems.

When considering soft robots with soft actuators, the supporting structure is an inherent part of the actuator and vice versa (whether it is soft or rigid). The parts are inseparable due to the actuators reliance on the support to enable applied force generation for external interactions. There are relatively few large scale soft robot implementations with some exceptions [Albert, 2016, Tolley et al., 2014]. One of the major factors in this is the actuation technologies. Dielectric elastomer actuators are the technological focus of this work and their characteristics and operation will be discussed in detail.

2.2 Dielectric Elastomer Actuator Overview

2.2.1 Principles of Operation

Actuation - DEAs are constructed of three formative layers; a central dielectric elastomeric membrane separates two electrodes. The dielectric in DEAs is chosen to develop high strain, whilst functioning as a continuous dielectric barrier. The electrodes are chosen to be soft, so as not to inhibit the actuation - in sensors the electrodes can be stiffer as high strain is not their primary task. The electrode material is tailored to apply a continuous and uniform high electric field across the actuating surface area of the elastomer, and maintain conductivity and coverage with a large expansion in the coated surface. Figure 3 shows the actuation states.

*macroscale denotes a range from 1 millimetre to 1 metre size components [Kalpakjian S., 2000]

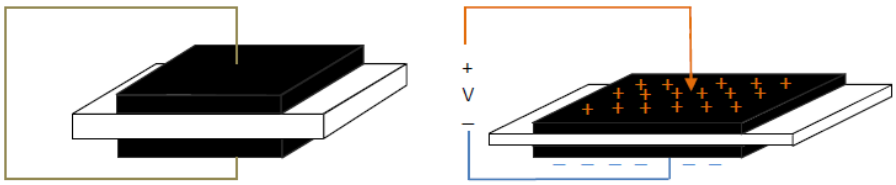

(a) Short-circuited DEA (passive state)

(b) High Voltage Applied to DEA (active state)

Figure 3: DEA actuation principle showing (a) at rest and (b) actuated with application of high voltage across dielectric

The DEA shown in Figure 3 is a single layer actuator. When a high voltage is applied to the conductive plates either side of the dielectric material Figure 3b, an effective pressure is generated by the electric field created across the dielectric. The pressure can be calculated using Maxwell pressure, P, expressed as:

$$P = \varepsilon_r \varepsilon_0 E^2 = \varepsilon_r \varepsilon_0 (V/t)^2 \tag{1}$$

where ε_r is the relative permittivity, ε_0 is the permittivity of free space, E is the electric field, V is the applied voltage, and t is the separation between conductive plates (i.e. membrane thickness) [Carpi et al., 2007].

Stretch and strain are used to describe the deformation of elastomers depending on their applicability. In Cartesian space, the stretches can be defined in each of the three dimensions, where λ_1, λ_2, λ_3 are the principal stretches in the directions x,y,z respectively (x and y represent the in plane membrane lengths and z its thickness) [Carpi et al., 2007]. Stretch and strain are related such that:

$$\lambda = l/L \tag{2}$$

$$e = \frac{l - L}{L} = \lambda - 1 \tag{3}$$

where λ is stretch, e is the strain, L is the initial length and l is the final length. Elastomers used as dielectrics for DEAs are considered incompressible (having a Poisson ratio that can be approximated to 0.5), which means that the pressure causes the membrane to biaxially strain due to the relationship:

$$\lambda_3 = 1/(\lambda_1 \lambda_2) \tag{4}$$

The stretch can be plotted against voltage to show how the material expands when actuated (shown in Figure 4) from Zhigang Suo's Theory of Dielectric Elastomers [Suo, 2010]. The amount of stretch is dependent on the material properties of the dielectric membrane and the pressure generated by the electric field. The mechanical strain limit of the dielectric is shown as λ_{lim} and the breakdown voltage as $V_B(\lambda)$. The electrical breakdown voltage is determined experimentally for a particular elastomer by pre-straining a membrane and using rigid electrodes to apply voltage while ensuring the membrane strain is kept constant. The voltage at failure is the determined breakdown voltage. The voltage-strain curve V(λ) is defined by the strain of an unconstrained dielectric membrane due to an applied voltage.

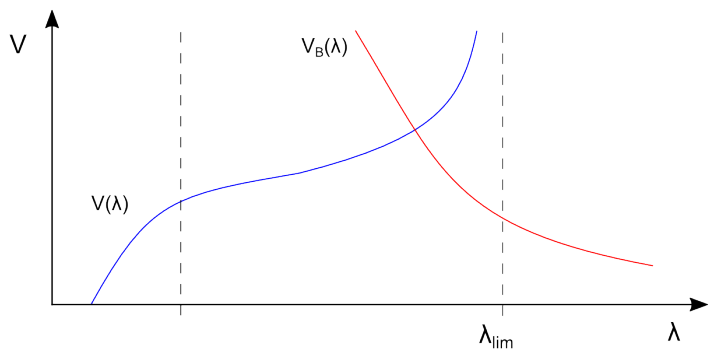

Figure 4: Graphical illustration of general voltage - stretch relationship and breakdown voltage curve

Sensing - The DEA as an electrostatic actuator can be considered in the same way as

a capacitor – two conductors separated by a dielectric. To sense the current areal state of the actuator a high frequency signal can be superimposed to calculate the capacitive reactance of the actuator and hence its active area, which will vary with strain of the soft capacitor. This method can be used for accurately calculating strain in active or passive stretchable capacitors and can be used as control feedback [Gisby et al., 2011, Schmitz et al., 2010, O'Brien et al., 2014].

The capacitance of the effective capacitor created can be written as:

$$C = \frac{\varepsilon_r \varepsilon_0 A}{t} \tag{5}$$

where C is capacitance, ε_r is relative permittivity, ε_0 is permittivity of free space, A is the overlapping surface area of electrode plates, and t is the distance of separation between conductive plates (i.e. membrane thickness) [McKay et al., 2009].

The capacitive reactance can be measured through the application of a high frequency input signal to the DEA, which can be applied with or without actuation high voltage. The capacitance can be evaluated from:

$$X_C = \frac{1}{2\pi f C} \tag{6}$$

where X_C is capacitive reactance, f the frequency of signal, and C the capacitance [Horowitz and Hill,]. From Equations 5 & 6 the area over which the capacitor acts can be calculated and determine the strain of the capacitor and hence its position in a controlled strain cycle.

2.2.2 Failure Modes

The simple operation of the actuator belies the complexity and fabrication issues, when optimal performance is targeted. Further to the principles of operation for actuation and sensing, failures are known to occur for three main reasons [Plante and Dubowsky, 2006]:

- Mechanical failure (breaking strength) - The elastomer used of the dielectric membrane is a soft material, that contains cross-linked chains. As the material is stretched, these tighten and will reach an elastic limit determined by the materials composition. If this is exceeded, the material will mechanically fail. Approximate limits can be determined, but materials are not ideally fabricated leading to a margin of error. The direction of pre-strain also affects the limit (discussed in Section 2.8).

- Dielectric strength failure - A dielectric material has a quantifiable dielectric constant which defines the electric field strength per unit thickness at which the material will breakdown. This parameter has been found to vary with changes to initial stretch of the dielectric (discussed in Section2.8).

- Pull-in failure - Pull-in failure is caused by a pull-in instability, where the Maxwell pressure generated by the electric field applied across a soft dielectric is greater than the elastic stress of the material. Due to this, the material expands causing it to thin, which increases the Maxwell pressure. This leads to runaway compression in the elastomer material and failure by one of the previous failure modes.

2.3 Further Exploitable Properties

In addition to the simple behaviour described, DEAs also exhibit additional characteristics under certain conditions, which can be utilised to affect the actuation dynamic (potentially positively).

Wrinkling

When the effective Maxwell pressure generated through actuation is greater than the planar stress in the material in a given direction, it expands. If the expansion in area is large enough, it leads to wrinkling of the material where there is no axial tension. If

the material is equi-biaxially strained, this can lead to a complex wrinkle patterning, where bifurcation points lead to irregular mosaics of directional wrinkling due to the non-linearities of biaxial wrinkling (shown in Figure 5b). Although wrinkling should be avoided in most instances due to it being a precursor to material failure through pull-in instability described, it can be used to preferentially instigate directional strain behaviour. This can be used to develop traits such as effective uniaxial expansion in a membrane facilitating, for example, rotational actuation [Conn and Rossiter, 2012b] (shown in Figure 5b).

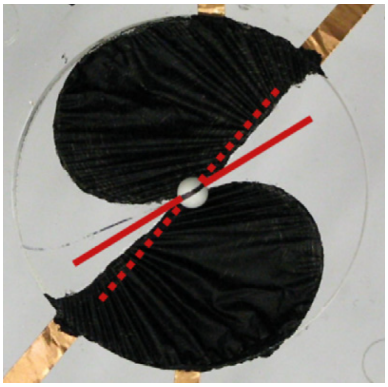

(a) Wrinkling used for rotational actuation

(b) Complex bifurcations in biaxial wrinkling

Figure 5: Examples of DEAs with wrinkling (reproduced from [Conn and Rossiter, 2012b, Conn and Rossiter, 2012a])

Controlling Snap-through* Instability with Giant Expansion

Snap-through instabilities in DEAs can be achieved by using a pressure gradient to control the stress-strain equilibrium in a soft dielectric membrane. A diminishing mechanical load (for example from a pressurised fluid) counteracts mechanical instability and creates a stable state. The negative feedback caused by the drop in pressure stops the membrane reaching unstable state, creating a loading path that does not induce failure.

*Snap-through is synonymous with pull-in

This effect has been explored by a number of groups and has included exploration of pairing DEA membranes to facilitate the mechanical load, thus providing bi-stability in a self-pressurising DEA system [Hines et al., 2016, Huang et al., 2012, Keplinger et al., 2012].

2.4 DEA Materials

DEAs have two main constituent parts; electrodes and a dielectric. These can be constructed of homogeneous material or form a composite of materials combining certain beneficial characteristics to enhance performance or optimise the actuator for a specific function.

2.4.1 Dielectric Membrane Material

Dielectric materials were first investigated whilst searching for alternative means of generating actuation for artificial muscles to produce a man-made analogue to natural muscle. Kornbluh et al made the suggestion of using electrostatic forces at micro scales to produce actuation [Kornbluh et al., 1991]. A significant breakthrough came when Pelrine et al at SRI realised the resultant Maxwell stresses generated by the application of high voltage on a polymeric sheet produced deformation at macro scale. Research in the field was accelerated by Pelrine's discovery of high strain in polyacrylate elastomer materials, which led to peak strains increasing from 10-30% to greater than 300% in polyacrylate elastomer.

Although silicone and acrylic are the two major choices for DEA fabrication, they can also be made from a range of materials from biodegradable gelatine and natural rubber (latex). The choice of material will depend heavily on application, due to performance optimisation. For example, in space applications, the glass transition temperature must be taken into account for the lower operation temperatures required. Natural rubber and gelatine offer an option for novel robots that degrade and as such could be deployed to operate and perform tasks in remote or inaccessible locations without long-term en-

vironmental impact. An overview of a few of the possible combinations that have been characterised are listed in Brochu and Pei's review paper [Brochu and Pei, 2010].

Dielectric Material	**Strain (%)**	**Electric Field Strength (MV/m)**	**Dielectric Strength**	**Overall Efficiency (%)**
Silicone	120	350	2.5 - 3.0	>80
Acrylic	380	8.2	4.5 - 4.8	>80

Table 4: Performance of dielectric materials from material characterisation papers [Carpi et al., 2007, Brochu and Pei, 2010]

Table 4 shows the maximal attained performance characteristics of two popular dielectric membranes. The criteria of the target application can influence the choice of dielectric to attain higher task specific performance*

2.4.2 Conductive Material

The conductive material holds the charge to the opposing sides of the dielectric material. It should produce a uniform field, which is consistent and repeatable throughout the straining action of the dielectric. A number of compositions have been used shown in Table 5.

Conductive Material	**Description**
Graphite Powder	A powder that can be sprayed when mixed with an alcohol or directly deposited. When spread onto a dielectric, this electrode is thin, but can be prone to loss of function due to cracking causing a break in the conductive pathways especially with high strains.

Continued on next page

*Performance can be defined in a number of ways, but power output and overall efficiency are used as generally indicators of performance.

Conductive Material	Description
Carbon Nano-tubes (CNTs)	The molecules of CNTs for a non-uniform lattice of pathways working as an effective electrode over large strains. CNTs have been shown to provide 'self-healing' properties by 'clearing' an area on electrical breakdown allowing the rest of the actuator to function [Yuan et al., 2007]. They are applied by spraying through a template.
Carbon Black	Amorphous carbon black has been shown to have conductive properties and due to its shell-like structure and agglomerative properties, can be used to produce high conductivity through percolation even with particle sizes in the order of 10nm.
Metal Powders	Metal nano powders work similarly to carbon black, but can offer superior conductivity above percolation threshold. Some effects of quantum-tunnelling have been postulated to give rise to low percolation especially in pointed particulates [Bloor et al., 2006].
Laser-scribed Carbon	Carbon based compounds can be heated by a laser to produce a conductive ash layer. This can be used to print electrodes from a variety of materials. This is a novel method of producing electrodes and an active research area [El-Kady et al., 2012].

Continued on next page

Conductive Material	**Description**
Ultra-thin film metal	Ultra-thin film metal coatings can be used to produce electrodes, using particular cutting patterns to allow flexibility for example, biaxially crumpled silver thin-film electrodes [Low et al., 2012]. Through vacuum sputtering this has also been used on a commercial scale roll-to-roll method by Danfoss [Kiil and Benslimane, 2009]. Additionally similar patterned thin film metal electrodes have been used as sensors [Lu and Kim, 2014].
Carbon Grease	Applied through a number of methods, the grease (comprising carbon black homogeneously mixed in with an oil) enables adhesion to the dielectric, whilst exhibiting good conductivity and compliance.
Conductive - Silicone Composites	These are cured electrodes using bulk silicone with a conductive filler (carbon black is a common compound). This produces a reliable electrode, but does - to a small extent -inhibit strain due to the stiffening effects of the carbon black filler. As a curable electrode it can be bonded to the dielectric which can be desirable.
Metal Weave	*Specifically for Sensing.* This flexible material provides a tightly woven planar resilient electrode that can be used for capacitive sensing [Low and Lau, 2014]. Due to its stiffness metal weave does not perform well as an actuation electrode as it inhibits strain.

Table 5: Table of common conductive materials used for electodes in DEAs

Powders and Greases:

Conductive powders can be single elements, compounds, or coated micro-structures.

They have no chemical bonding and do not affect straining performance of an actuator. However, as the material expands, the gaps between conductive particles increase leading to the loss of conductivity. This loss of conductivity can be counteracted by encapsulating the powder in a grease, which remains a viscous fluid allowing enhanced percolation over much larger strains. In the formation of electrodes for DEAs, this is very useful, as it offers negligible resistance to strain in the material due to actuation, but thins and spreads on the surface of the dielectric maintaining a conductive film over the expanded soft membrane. However, the grease does potential spread, causing unwanted cross connection between electrodes on the same surface, and it can dry out, causing cracks and loss of conductivity. These factors can affect reliability in real world applications, but can be countered using encapsulation materials (which may cause an additional reduction in performance due to the extra passive stiffness added). Grease can also leach into the dielectric and affect the actuation over time.

Composites and Conductivity:

Mixing a conductive compound into a base material (usually a dielectric material), enables the composite to exhibit conductive properties. These properties can be enhanced by material molecular form, material mixing ratios and quality of mixing process to achieve high conductivity with low particulate weight - at the percolation threshold [Foulger, 1999].

- Percolation Theory - Mathematically it describes the behaviour of connected points in a random space. The level of connection across a space is dependent on the probability of occupation of points in a given lattice space (p). When the cluster concentration reaches a critical level (p_c), there is a cluster spanning the whole system [Stauffer and Bunde, 2008]. The probability of an infinite chain (p_∞) is zero below the critical level and increases above this level. This is illustrated in

Equation 7.

$$p_{\infty} = (p - p_c)^{\beta} \tag{7}$$

where β is the critical exponent. When applied to a physical medium where the points represent conductive particles and the medium is a bulk insulator material, the theory can be used to evaluate the conductivity of the resultant composite. When a certain ratio of conductive particles is introduced to the composite via a mixing method, there is an exponential increase in conductivity, due to the filler density creating continuous chains of particles forming conductive paths [Xiao et al., 2014]. In Figure 6 the effect of particulate density on conductivity and mechanical strength is depicted in a series of 2D illustrations. As the particle density increases (from ***(a)*** to ***(b)***), the electrical conductivity increases very slowly, due to marginal increases in leakage current. This continues until the percolation threshold zone (***(c)***), where there is a rapid change in the resistivity, as chains conjoin forming large conductive pathways. As the particulate density increases above a certain level, the cross-linking of the silicone is affected significantly (from ***(c)*** to ***(d)***), which has the effect of reducing the mechanical strength. Additionally, if the material is made thinner, the probability of conductive pathways being formed for a given particulate density decreases, hence reducing conductivity (seen in ***(e)*** and ***(f)***), where $X_1 > X_2 > X_3$. The particle size and shape also affects the number of connections or chains formed. The size of particles also affect the bulk material mechanical properties as mentioned [Altalhi et al., 2017].

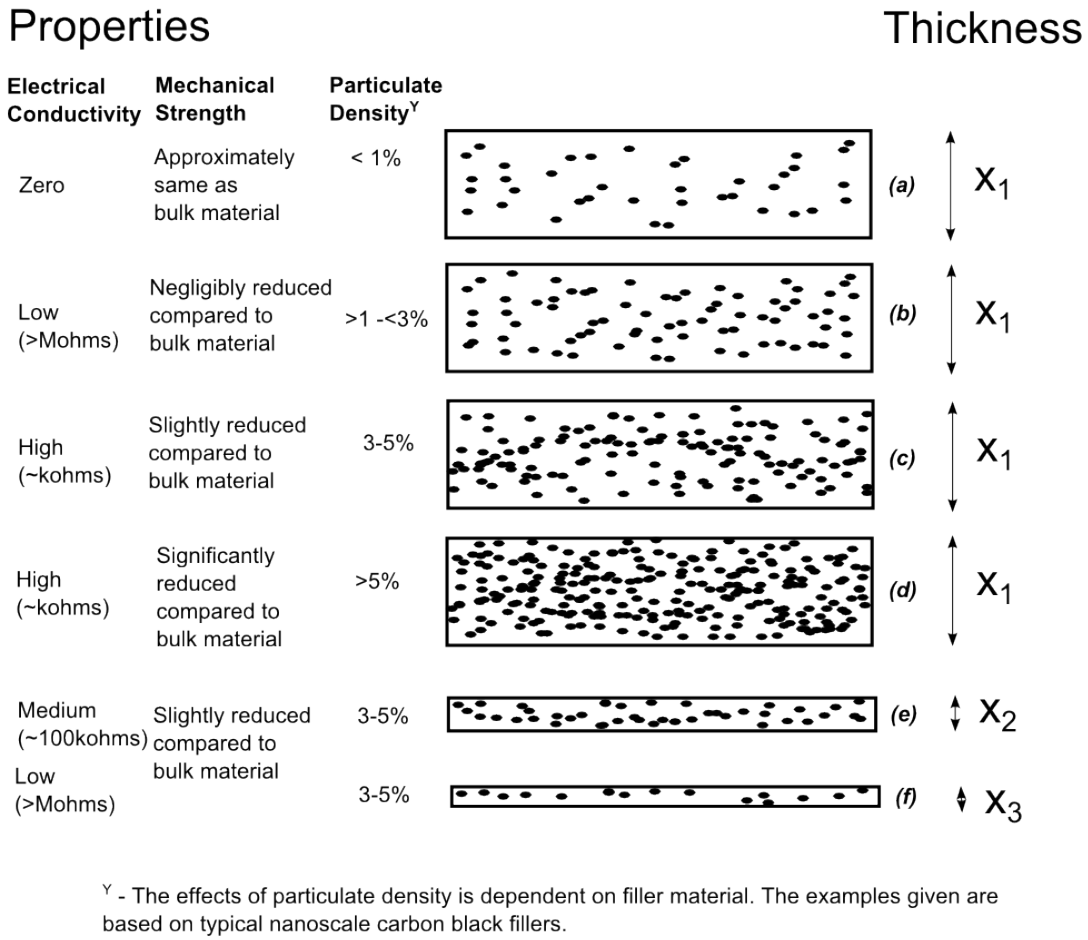

Figure 6: Graphical illustration of effects of particulate density on electrical conductivity and mechanical strength.

There are a range of solutions currently being researched from arranged nanotubes [Romasanta et al., 2011, Sugino et al., 2012], to using the smallest available particles of carbon black [Carpi et al., 2008, Araromi et al., 2015b]. The graph in Figure 7 shows the general volume resistivity response to increased weightings of carbon black in silicone. There is a large variation in the weighting at which the critical threshold is reached between different carbon blacks, due to the different fabrication processes, sieve sizes and dispersion in the bulk material

[Medalia and Heckman, 1969, Xiao et al., 2014].

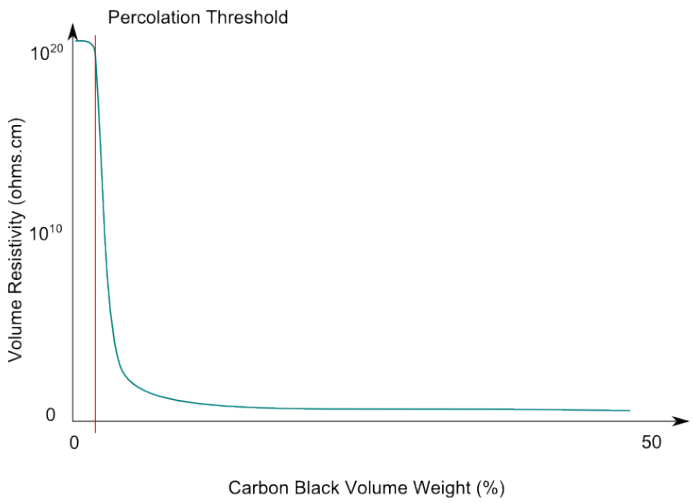

Figure 7: Graphical illustration of general volume resistivity - particulate weight relationship with percolation threshold

The point at which the resistivity of the bulk material drops below a measurable level is defined as the percolation threshold, where the chains of molecules conduct. The curve of volume resistivity depicted in Figure 7 is calculated experimentally, through testing samples with defined weightings of a particular filler mixed with a chosen bulk material.

A curable compound can be mixed with a conductive material, forming a stretchable solid conductive compound film. To remain conductive under strain, care needs to be taken to include enough conductive particulates to maintain connectivity as strain can separate chains of particles leading to a reduction in conduction. The production of conductive compounds requires homogeneous mixing of the constituents to optimise conductivity. Proprietary conductive greases are readily available (such as MG Chemical^{TM} carbon grease [MG Chemicals, 2012]), and are a popular electrode choice. However, curable conductive elastomer composites are not generally commercially available. As such, these need to be produced in the

lab. The weighting is chosen empirically to provide sufficient level of conduction, whilst remaining mechanically able to undergo strain up to 100%.

- Electrical Contact Resistance (ECR) - This resistance has a potentially large influence on the overall resistance of a composite sheet and the response time of the actuator due to its impact on the connectivity between the external power source and the conductive composite [Carpi et al., 2015, Rosset et al., 2007]. A high contact resistance will significantly increase the time required to charge the capacitive plate the conductive composite forms in the DEA. The surface of a conductive silicone sheet is a cut through the filler compound trees, providing a 2D surface of possible connections. The number of points of connection define the contact resistance. Additionally the surface of the sheet is not perfectly flat and hence does not meet a connector surface (such as copper tape) perfectly leading to air gaps. To reduce the contact resistance and resolve related connectivity issues.

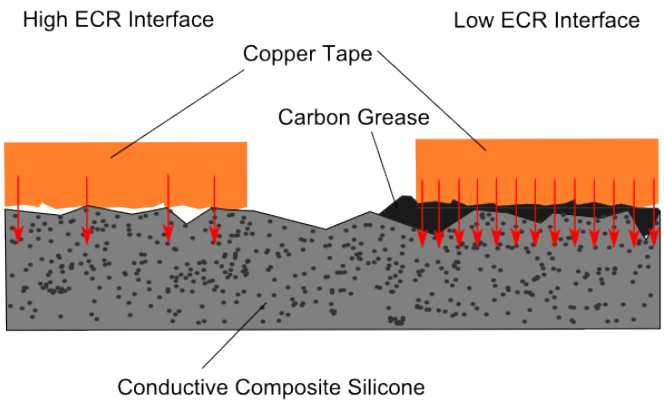

Figure 8: Illustration of the potential affect of contact resistance at the connection interface.

2.5 DE Actuator Fabrication and Preparation

The fabrication of DEAs is an active area of investigation. Thin uniform layers are essential in the effective performance of fabricated actuators. Any unwanted particulates can lead to physical failure of the dielectric, either through affecting the uniformity of the membrane or causing a rupture. It is preferable to reduce the thickness of dielectric films to decrease the driving voltage. Dielectric layers $<100\mu$m thick are considered a good target, but dielectric membranes of thicknesses $< 10\mu$m have been produced [Lotz et al., 2008]

Spin-coating is a technique devised for repeatedly producing membranes of a defined thickness with a known profile and margin of variation in thickness. The method uses a commercialised technology used in silicon wafer preparation and etching. The method employs centrifugal forces to thin the silicone producing a thin film on top of a flat substrate. Lotz et al set out spin-coater parameters and an implementation to test the resulting actuators [Lotz et al., 2011].

Spray Deposition includes two methods at present:

- Airbrush uses an airbrush to deposit fine coatings of material. This can be used to fabricate layers of DEAs (of either dielectric or conductor) with a dielectric component or in the case of the conductor as a conductive solution [Araromi et al., 2011].
- Inkjet uses a piezoelectric actuator and a jet nozzle to deposit small quantities of material to form electrodes [Pede et al., 1998]

Doctor Blading is a method of thin film fabrication using a sharp blade pulled across a flat substrate at a controllable height. The resultant film's thickness can be precisely controlled and is consistent over a wide area.

K-bar Rolling is a technique similar to doctor-blading, in which a wire is wrapped around a bar in a spiral with gaps of a known height and spacing. From these parameters, the amount of material 'rolled' can be specified. The material flows into the space created by the wire to form a continuous membrane before curing.

Pad Printing uses a soft rubber pad to transfer material from an engraved plate to deposit on an object. The material is usually an ink, as the system is usually used in mass production labelling systems, but can be used for application of conductive material. The layer thickness can be very thin (in the order of microns) [Rosset et al., 2016].

Proprietary Films are used in some cases, especially dielectric layers that are commercially produced. These pre-fabricated materials offer standardised parameters and consistent performance (e.g. Parker EAP film [Parker,], Wacker Elastosil [WackerChemie, 2014]) . Some companies specifically produce dielectric layers for DEAs, others produce materials for an unrelated purpose, but still offer good performance. In both cases there may be a lack of information due to intellectual property, material composition and fabrication methodology protection. In the case of unrelated materials (a key example being VHB^{TM} - a proprietary acrylic material), sometimes properties have been seen to vary in a way that affects DEA performance [McKay et al., 2009]. Additionally quality control is not aimed at DEA applications and can lead to large error margins in breakdown being accounted for.

Actuator Depiction	Type	System Output	DE Actuation	Description
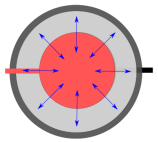	Planar Film (Spot Actuator)	Planar Biaxial Expansion	Planar Biaxial Expansion	A relaxation planar actuation is used for material characterisation.
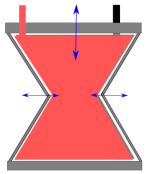	Bow Tie	Linear Translation	Planar Expansion	Hinged sprung joints of the bow tie allow the planar expansion of the bow-tie to be translated to a linear actuation output.
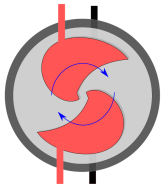	Rotary Film	Rotation	Planar Expansion with wrinkling	Rotary actuation is generated in a planar form through careful electrode shape, designed to accentuate wrinkling effects, causing rotation of the centroid of the membrane (marked in blue) [Conn and Rossiter, 2012b].

Continued on next page

Actuator Depiction	Type	Type	Operation	Description
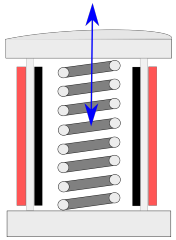	Spring Roll	Spring assisted translation	Cylindrical planar Expansion	The spring roll uses a spring to oppose the elastic strain of the parallel DEA membranes. When actuated the spring roll DEA relaxes enabling the spring to extend until a new equilibrium is found with the opposing DEA.
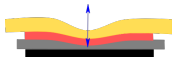	Thickness-mode Amplification	Transverse Contraction	Planar Expansion	A layer of soft material (yellow) is adhered to a DEA. The thickness contraction of the actuator is amplified by the soft material, forming a deep channel.
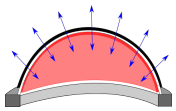	Diaphragm	Volumetric expansion and/or peak translation	Non-linear biaxial strain	A pressurised membrane forms a hemisphere, which can be used as a pump by varying the pressure on the internal fluidic media. As with the cone the diaphragm can be arranged as an antagonistic pair, to provide a double-cycle.

Continued on next page

Actuator Depiction	Type	Type	Operation	Description
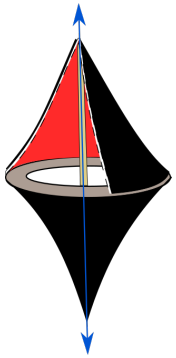	Antagonistic Cone Pair	Linear Translation	Non-linear biaxial strain	The cone configuration can be made with a spring and membrane, or more commonly (as depicted) as an antagonistic matched actuator. This arrangement allows a naturally balanced equilibrium between two duplicated cones. If both act as actuators a double actuation cycle maximises overall displacement.
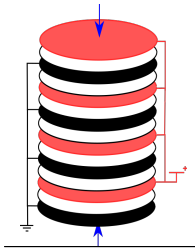	Individual Layer Stack	Transverse Contraction	Planar expansion	For transverse contractile actuation multi-layer DEAs are used. Typically operating without support various multi-layer specifications are discussed in Section 3.1.

Table 6: Tabulate list of common DEA configurations with distinctive characteristics of type of strucutre and operation, with short description of features.

2.7 Energy Efficient Configurations

An area of particular interest is the use of DEAs in energy efficient secondary actuation and switching. The groups of technologies in this area are reviewed with specific focus on DEAs as the actuation mode.

Minimum Energy Structures (MES) - MES are structures which move to a locally minimal energy state based on the initial conditions of a structure's spatial arrangement, constituent material stiffness, and acting stresses and initial strains. A system can have multiple minimum energy states. The system can be mechanically storing energy whilst in a state. The transition between each of the states are made through application of energetic impulses enabling the transfer of the system between minimal energy states, causing spatial arrangement alteration of the structure. The specific application of MES to dielectric elastomers is known as DEMES - dielectric elastomeric MES. In mechanical systems there are many uses for bistable transition systems, where fixed displacement states can be set and released, through the application of an energetic source. The number of states can be arbitrarily chosen to match tasks, but in its simplest form a transitioning MES is a bistable. A simple example is a switch, where two stable states are attained by applying sufficient directed mechanical energy to surpass the energy saddle point. Minimum energy structures can have actively or passively maintained stable states. If the energetic input used to transition the structure between minimum energy states is required to remain active in order to hold the structure in its state, the system is considered active. The stable states are local minima in the Figure 9 with a local maxima (or saddle point) separating the states in a two dimensional illustration of the energy surface of a arbitrary system. The energetic input (shown by orange arrow), allows the system to move from one stable local minima to another (marked by dashed lines).

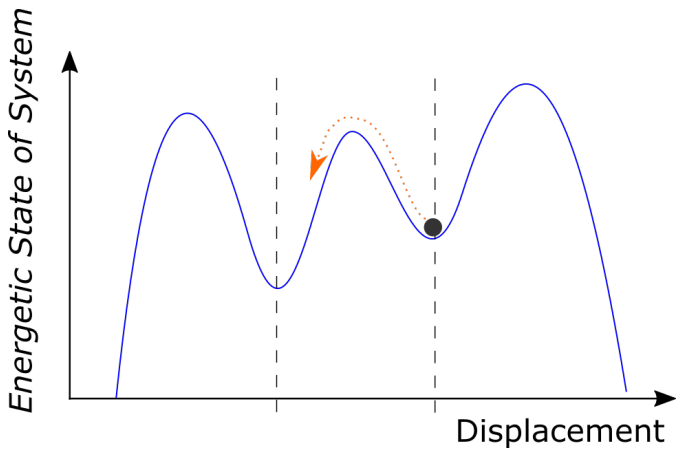

Figure 9: Illustration of state tranistion of displacement in a multi-stable system, showing relative energetic states.

This simple system is used throughout engineering systems, and has also been found in nature (used by the venus fly trap to catch prey [Shahinpoor and Thompson, 1995]). Bistable minimum energy structures have been developed to show how DEAs can be used to provide this type of actuation [Follador et al., 2014]. DEAs are used in an antagonistic configuration in combination with a buckling beam to provide bistability.

Zero Energy Fixity - As explained by Rossiter et al [Rossiter et al., 2010], DEAs currently available are soft - to allow high strain required - and operate in a window of approximately constant elastic modulus throughout their operation cycle. Considering the DE on its own as an actuating system, once the energetic impulse to change state (i.e. strain the DE) is removed, it will return to its initial state. The proposed solution is to alter the elastic modulus of the structure in which the energy is stored providing fixity - a property of a structure exhibiting the ability to be locked into a fixed, rigid configuration -, enforcing bistability. DEAs are inherently soft and to optimise their performance in their most common use - single layer film - need a structural body to provide support to maintain pre-strain*.

*In Chapter 3 an alternative method for maintainingg pre-strain internal to the DEA is discussed

The ability to put a system in a stable state through the application of directed energetic input is very useful in the class of application considered in this chapter, but state fixity improves on this as it provides resistance to state change of energy input greater than the energy required for state change, adapting the state transition parameters. We have discussed how DEAs have characteristics that could prove useful in some displacement control systems. They could use structural configurations such as buckled beams to enter minimum energy states. However, due to the operation of DEAs, the elastic modulus is approximately linear, and due to the direct application of energy from the DEA, the mechanical energy in the buckled beam must be below the maximum output of an antagonistic actuator pair as described by Follador et al [Follador et al., 2015]. The use of symmetry in the bistable system limits the blocking force able to be provided as the actuator is mechanically linked with the bistable mechanism. Rossiter et al [Rossiter et al., 2010] consider the use of creating an actuator with variable elastic modulus to overcome this problem.

Binary Robots - Binary robotics is the application of discrete stable state as a paradigm for robotic manipulators [Chirikjian, 1994]. The benefits include operation without feedback control, high repeatability and inexpensive implementation. The paradigm of binary robotics is in early developmental stages in actuation implementation. A robotic system can utilise the discretised actuation, described as binary robotics, when work done by the actuator shifts an end-effector between two stable spatial states (through a combination of translation and/or rotation). Binary robotics can be considered to be the mechanical equivalent of digital systems, providing discrete output position control from an actuation input. A collection of discrete actuation units can be used in the implementation of many manipulators - defined as n-bit manipulators, where n is the number of binary actuation units present - for example an articulated binary limb

using Inter-penetrating Networks [Brochu et al., 2013], but this is still in early development and is far from common practice.

[Lichter et al., 2001]. A paper by Follador et al [Follador et al., 2015], goes further, considering BiMES as bistable binary actuator units. The concept is novel, and enables separation of end effector and actuation components, but the applications are limited by the inherent flexibility of the structure. Hence it has few applications due to low blocking forces of soft film of dielectric elastomer especially considering the relaxation* actuation is used in this system.

2.7.1 DEA Coupling

DEAs are soft and inherently compliant in both passive and active states. They exhibit highly non-linear electro-mechanical behaviour and associated failure modes (Section 2.2.2). It is important that the coupling between the elastic DEA and the actuator output is optimised to improve performance and reliability. In out-of-plane configurations (commonly) planar membranes are stretched to enable out-of-plane actuation and optimise the characteristics. In most cases a spring or spring-like element is coupled with the membrane. Researchers have considered pairing DEAs with the same base dielectric material to exactly match the actuating membrane. In some cases both coupled elements have been DEAs enabling bi-directional pull-pull† actuation. The methods of coupling have taken two main forms - rigid link and fluidic - which each have separate benefits. A rigid link - as used in the cone configuration in Table 6 - directly attaches the membranes. This enables effectively instantaneous position coupling, ideal for antagonistic DEAs. However, the boundary interface between hard and soft materials is highly susceptible to failure due to the high stress concentration found (discussed further in Section 2.10). Instead of hard links between membrane, the coupling can be soft, for example with a fluid linking opposing membranes. This resolves potential issues with stress inherent to rigid coupling, however introduces potential issues with the weight of

*relaxation actuation describes the way the Maxwell pressure acts in opposition to the elasticity of the material lengthening it.

†pull-pull has been used to describe the coupling of relaxation actuators where the passive side pulling is the energy source for the work on the end effector.

the coupling fluid, or conversely its compressibility, both of which will affect actuation performance. For some applications such as pumps, this is not a problem as the application requires work on a fluid. A rigid link coupling has constant circumferential strain, and linear radial strain. A fluidic pressure coupling the strain is inhomogeneous - the balloon is fixed at the outer boundary -, giving rise to variations in strain from bi-axial at the tip of the balloon, to a combination of non-linear radial and circumferential strain in relation to the distance from the outer boundary. Examples of coupled DEAs are shown in Figure 10.

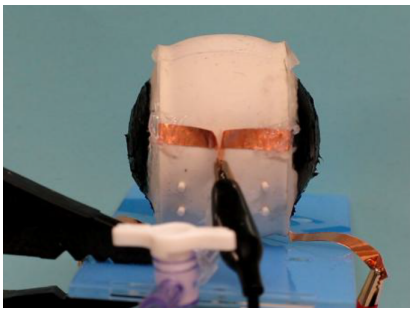

(a) Pneumatically coupled DEA segment for locomoting worm (reproduced from [Conn et al., 2014a]).

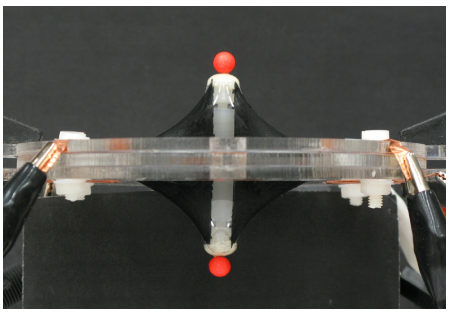

(b) Antagonistic rigid-link cone coupled DEAs (reproduced from [Conn and Rossiter, 2011]).

Figure 10: Examples of coupled pairs of DEA membranes in two common configurations

2.8 Prestrain of Dielectric Membranes

As part of the optimisation of DEAs for particular tasks, the dielectric membranes are mechanically strained and held in this state for operational actuation (known as pre-strain). The strain can be uniaxial or biaxial. The reasons for using pre-strain are due to a number of material mechanical factors already discussed (in Sections 2.3 & 2.4; namely limiting pull-in failure, reduction in wrinkling through tensioning, reduction in viscoelastic damping, and to alter actuation material strain conditions, leading to mechanical amplification and increase in dielectric strength [Carpi et al., 2007]. As such the ability to apply pre-strain to a material is advantageous in a number of configura-

tions and implementations.

Biaxial prestrain is used to enable equi-bi-directional straining on actuation. This is depicted in Figure 11:

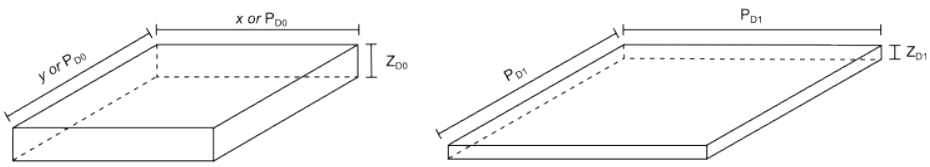

Figure 11: Illustration of mechanical strain of DEA membrane.

Assuming uniform prestrain and considering the membrane is approximately incompressible (Poissons ratio approaching 0.5), it can be said that:

$$\lambda_{l_{1,0}} = \frac{l_1}{l_0} \tag{8}$$

$$\lambda_x.\lambda_y.\lambda_z = \lambda_p^2.\lambda_z = 1\,, \tag{9}$$

where l_1 is final length, l_0 initial length, and λ_L is stretch ratio of length [Kikuuwe et al., 2004]. Hence, the material thins as the membrane is biaxially strained.

To achieve uniform biaxial prestrain, in this work a hoberman platform was used, which has been found to provide a practical method of applying biaxial to a pre-strain [Conn and Rossiter, 2010]. Although the strain is not perfectly uniform it can be seen in Figure 12b, where a silicone membrane is biaxially strained using this method, there is a zone where the strain can be considered uniform.

Figure 12 shows an element of material being strained and the zone of uniform

prestrain:

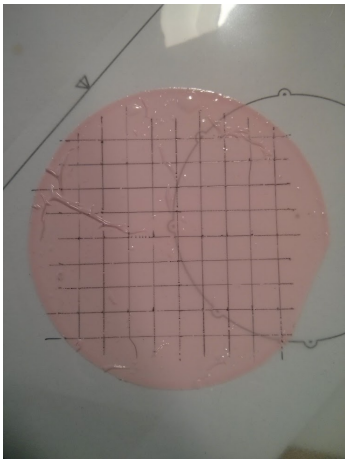

(a) Photo of relaxed silicone membrane with grid of lines.

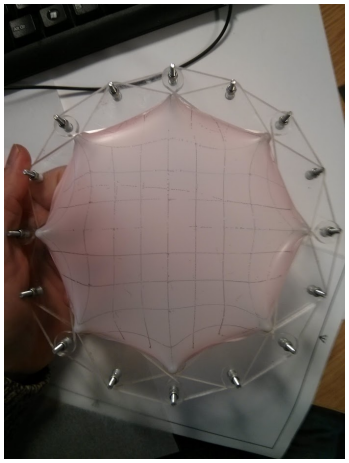

(b) Photo of strained silicone membrane with grid of lines on a Hoberman platform straining rig.

Figure 12: Photographic depiction of zone with uniform strain on Hoberman platform.

2.8.1 Methods of Capturing and Integrating Pre-strain in Systems and Devices

Pre-strain can be captured in a number of ways; the pre-strain maybe uni-directional or bi-directional and may vary across the dielectric membrane depending on the constraints of the configuration of the actuator.

Fluidic Inflation - When a membrane is inflated with a fluidic medium, it is strained as the pressure difference across the actuator increases until the stress in the material enables an equilibrium to be reached. In doing so the membrane forms a hemispherical shape with a combination of prestrains (see Section 2.7.1 for more detail). The membrane is attached to a ring (commonly rigid and inextensible, which enables the pressure difference to be developed).

Supporting Structure - The method of mechanically controlling the membrane can involve a supporting structure, which can be made from materials with a range of stiff-

nesses. The supporting structure may be planar or out-of-plane. Commonly an annular support is used, thus keeping the strain and stresses constant around the DEA. However, there are a wide variety of forms and structural complexity possible in the support structure, which can create specialised benefits. For example, a DEMES structure provides opposing spring stiffness which pre-strains the dielectric. A cone structure would be another example [Cao and Conn, 2017]. Each of these implementations utilise the direction and size of the pre-strain to maximise performance.

IPN - Inter-Penetrating Network - In the previous cases, a rigid or inextensible substrate is required to support the membrane in order to capture the pre-strain *. Interpenetrating Networks (IPNs) use an interlaced material - typically soft - to stop the strained primary dielectric from returning to its original size [Carpi et al., 2007]. In this way, a dielectric can be supported by a soft incompressible substrate. A mixture of silicones and acrylic materials can be used to enable an optimised strain.

2.9 Hyperelastic Modelling

Many models exist for determining the stress-strain relationship in hyper-elastic models [Suo, 2010]. Incompressible hyper-elastic materials can be considered (and modelled) using a number of methods.

- Physical Model - These use real physically definable parameters to model the behaviour of a material (e.g. Neo-Hookean and Gent Models [Suo, 2010, Gent, 1996])
- Phenomenological Model - In some cases a model is created for a material by fitting to experimental data, using parameters that do not have any physical meaning (e.g. Ogden mode [Ogden, 1972]).

*Pre-strain is the stretching of material to improve its properties using and external support. Capturing pre-strain uses a mechanism that is inherent to the actuator to maintain the pre-strain of the material. Examples of this include IPNs and S-IPNs [Carpi et al., 2007, Brochu et al., 2013].

The neo-Hookean model uses a single material parameter to describe, the dynamics of an elastomer. The elastomer stress-strain relationship can generally be considered linear initially, but exhibits strain stiffening at high strains. It takes the form:

$$W = \frac{\mu}{2}({\lambda_1}^2 + {\lambda_2}^2 + {\lambda_3}^2 - 3) \tag{10}$$

where W = Helmholtz energy, μ is small-strain shear modulus, and λ_1,λ_2,λ_3 represent strains in x,y and z respectively [Gu et al., 2017b]. The Gent model extends the neo-Hookean model by including a parameter for straining stiffening through the strain limiting term J_{lim} [Gent, 1996]. The model reduces to the neo-Hookean model as the strain term tends to infinity. The parameters in these two models are physically interpretable and are hence known as physical models. The Gent model has recently been popular within the modelling of DEAs due to its simplicity and good approximation to experimental outcomes. The parameters can be determined with relatively few experimental data points which also reduces complexity of use. It is expressed as:

$$W = \frac{\mu J_{lim}}{2} log\left(1 - \frac{{\lambda_1}^2 + {\lambda_2}^2 + {\lambda_3}^2 - 3}{J_{lim}}\right) \tag{11}$$

where μ is the small-strain shear modulus, and J_{lim} is the strain-stiffening constant [Gu et al., 2017b].

The Ogden model is a phenomenological model as the model parameters do not have direct physical meaning as they are directly determined by the fitting of the models curve to experimentally attained holistic data of the stress-strain relationship [Ogden, 1972]. Due to this fitting to specific materials through experimental data, the model can be considered to have superior approximation, but the parameters are difficult to determine and with a 3rd order approximation 6 parameters are required.

$$W = \sum_{i=1}^{N} \frac{\mu_i}{\alpha_i}({\lambda_1}^{\alpha_i} + {\lambda_2}^{\alpha_i} + {\lambda_3}^{\alpha_i} - 3) \tag{12}$$

where μ_i and α_i are non-physical material parameters that are experimentally measured. N is the model order (N=3 is a popular choice providing accuracy without high complexity [Gu et al., 2017b].

Viscoelastic Dynamics

Some hyperelastic materials have a pronounced viscoelastic response - one of the most popular dielectric membrane (3M VHB^{TM} 4905/4910) has a distinctly damped response - and this can be modelled through the Bergström - Boyce model. This includes internal variables for the material to account for time-dependent effects of viscosity in the dielectric material (such as Mullins effect, hysteresis and frequency based dynamics) [Chang et al., 2017, York et al., 2010, Hong, 2011, Suo, 2010]. The Helmholtz free energy density due to the stretch in the material can be described as:

$$W_{stretch}(\lambda_1, \lambda_2, \xi_\alpha, \xi_\beta, ...) \tag{13}$$

where ξ_α and ξ_β are time-dependent variables of the dielectric elastomer (more variables may be needed to describe materials fully).

Assuming a system in mechanical and electrostatic equilibrium, the non-linear viscoelastic behaviour can be described by:

$$\sum_\gamma \frac{W_{stretch}(\lambda_1, \lambda_2, \xi_\alpha, \xi_\beta, ...)}{\delta \xi_\gamma} \delta \xi_\gamma \leq 0 \tag{14}$$

where ξ_α and ξ_β are time-dependent variables of the dielectric elastomer [Gu et al., 2017b].

The thermodynamics are accounted for in the model shown in Figure 13, where A is a spring and B is a spring in series with a linear damper. The models discussed can be used to describe the elastic springs in this model. However, the task of modelling DEAs is still an open area of research and is not always consistent with experimental data.

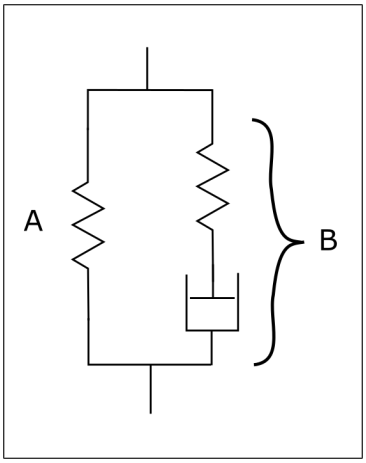

Figure 13: One dimensional rheological model of viscoelasticity in hyperelastic materials (reproduced froml [Bergström and Boyce, 1998]).

2.10 Union of Intrinsically Soft & Rigid Components

Electro-mechanical systems have been developed to predominately drive rigid components from rigid motors*. An example could be a servo driven industrial robotic arm, where rigid motors drive rigid links and end effector. With the rapidly developing research in soft actuators and robots, true soft robots have been developed which are mimetics of some of natures' diverse species. Figure 14 shows differing robotic systems compared by the stiffness of their actuation and body/end-effector†.

*Rigid in this context is used to describe the major proportion of a components constituent parts

†It should be noted electronic driver systems used for supplying power to systems are considered an essential component in the power feed system of any robotic system irrespective of drive or form. Pneumatic and hydraulic systems however are still considered part of the components that make the robotic system even though they can be remotely separated from the actuation unit.

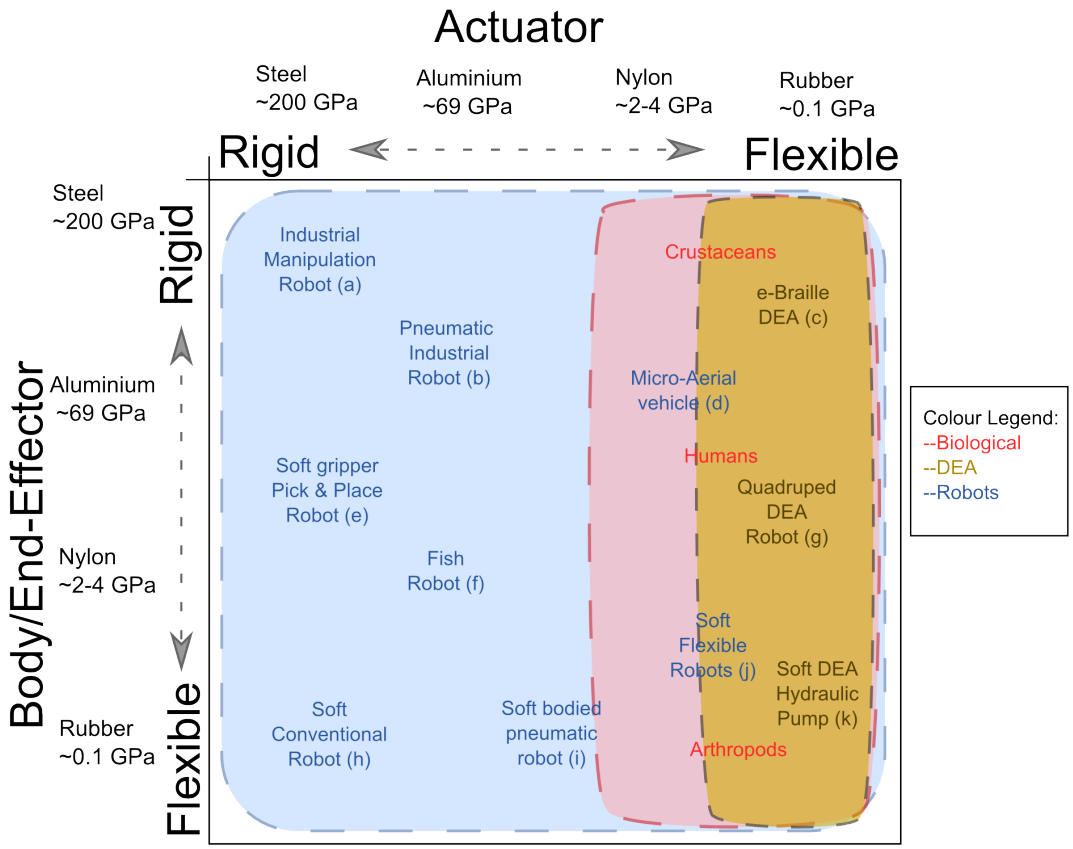

Figure 14: Graphical exploration of the component space of robots considering actuator and links (body/end-effector).

Examples of each of the robots types listed in Figure 14 are given here:

(a) - ABB motorised Arm [ABB, 2018]

(b) - Festo Bionic Cobot [Festo, 2018]

(c) - E-braille DEA [Runyan and Blazie, 2010]

(d) - Micro Aerial Vehicle [Conn et al., 2007]

(e) - FlexShapeGripper [Stoll,]

(f) - Autonomous Soft Robotic Fish [Marchese et al., 2014]

(g) - A small biomimetic quadruped robot [Nguyen et al., 2014]

(h) - Seal-like therapeutic robot [Chang et al., 2013]

(i) - Robots Made from Interesting Materials [OtherLab,]

(j) - Artificial muscles and soft gripping [Bogue, 2012]

(k) - Electroactive elastomeric actuator for all-polymer linear peristaltic pumps [Carpi et al., 2010b]

The figure shows a lack of robots that have soft actuators and rigid end-effectors. This is partly due to the current power outputs achieved in soft actuation technologies (excepting pneumatic systems due to their tethered supplies). However, considering this is where nature has evolved to be most successful, there is a juxtaposition between engineered and evolved systems. Considering the expectation of closer operation of robots and humans, this current gap has been under-explored and may yield possible innovative approaches. For example, multi-material printing has enabled the addition of flexible materials to deliver a variation of stiffness in a continuous body [Ward-Cherrier et al., 2016]. The possibilities of this area of research will be considered in this thesis.

Relative Rigidity

When considering the development of robotic devices operated by soft actuators with soft or rigid linkages, the rigidity of the components relative to each other becomes an important factor in the kinematics of systems and devices. To this point the strain of a material due to the maximum stress applied on it by another material should be negligible (i.e. its form remain intact). The rigid materials are the supporting substrates used, which are made of cast acrylic. The soft materials are silicone (Dow Corning HSIII) and acrylic elastomer (VHB4910). The maximum stress of VHB with a high strain rate (0.05 % strain per second)* at a strain of 100%† is <100KPa [Nenno and Wetzel, 2014]. Dow Corning HSIII has a stress of ¡300Kpa at a strain of 100% [Yao et al., 2005]. Cast

*due to the viscoelastic properties of VHB a higher strain rate will give a higher stress at a given strain

†100% strain is greater than that used in any prestrain conditions.

acrylic attains a strain of $\leq$ 5% when a stress in the region of $\geq$65 MPa is applied. At a stress of <300KPa - the highest stress the dielectric material applies - the strain on the supporting frame is negligible. Applying this to the context of the thesis, the frames can be considered rigid relative to the soft actuator materials.

2.11 Soft Sensing Technology Review

Sensor feedback has been a key part of the development of robot technologies to enable them to complete tasks. This is especially true with humanoid robots; the inherent aim requires the ability to manipulate objects in a way that humans do.

2.11.1 Sensors Variants

There are a large number of transducers of different materials and structures too numerate to explore in full, however current major sensor research modalities are described, discussed and then compared here. The discussion focuses on the features of state-of-art sensors and the road blocks that have to be overcome in their development.

1. Capacitive

The electrostatic interaction between two conductive materials separated by an insulator can be measured through analysis of reactance using a high frequency input signal and measuring the resultant impedance, as mentioned in Section 2.2.1. Using soft materials, a capacitor can be developed into a physical sensor from which a capacitance value can be calculated at high frequency providing a continuous approximation of the capacitance of the sensor. The capacitor's construction can be of hard or soft conducting plates and a separating insulator. Their physical arrangement can be used to provide three dimensional data of force - normal application and a 2-D surface shear force [Schmitz et al., 2010, Viry et al., 2014].

The possible material properties, arrangements, and designs for capturing data of tactile

stimulus using capacitance are multitudinous, and as such are too numerous to explore fully. Two examples will be briefly discussed highlighting their individual properties and merits:

- I-cub fingertip - uses a combination of both hard (for the inner) and soft (for the outer) conductive plates in the construction of the sensor [Jamali et al., 2015]. The specifications of the chosen central processing unit limit the number of separate taxels forming the sensory skin and the soft and hard, compliance with underlying anthropomorphic bone-like structure.

- Dielectric elastomer sensors - There are a few implementations of DE stretchable sensors. An example StretchSense^{TM} uses a soft polymeric capacitor based on DE membranes to produce a sensor that can detect strain, pressure, shear and proximity/touch modalities [O'Brien et al., 2014]. These sensors are designed for feedback from compliant high degree of freedom movement found in humans. Similar technology has been developed using overlapping metal mesh flexible plates separated by a soft insulator to produce a highly sensitive artificial touch sensor providing information about shear and normal force to a high degree of accuracy [Viry et al., 2014].

Capacitive sensors have shown the potential for highly accurate measurement of multiple degrees of freedom. The sensors can be scaled to a size able to provide a significant resolution, however sensor signal processing and sensor hysteresis limit the potential for use as a touch skin on a robotic digit.

2. Variable Resistance Sensors

The variation in resistance found when observing bulk conductive materials under the application of external forces can be used to provide feedback. The resistive mate-

rial maybe homogeneous or a composite with specialised conductive materials providing complex interactions and properties when under compression or tension. The force registered is normal to the surface and cannot be easily expanded to provide more in depth shear data. In a simple form, as with capacitive sensing, the conductive terminals can be separated by a compressible conductive foam [Pang et al., 2016]. There is potential for more complex implementations however, which use percolative or quantum tunnelling conductivity to acquire more accurate sensing data (described in Section 2.4.2).

In conductive composites, percolation paths can also be reduced by using a foamed substrate for the filler. This enables paths to be reduced and specified, whilst giving high sensitivity to compression when pocket sides begin to touch.

Quantum tunnelling composites are a sub-class of filled conductive composites. Metal fillers are mixed with a polymeric base material. However, due to a specific mixing process, the nano-structure including spikes found on the surface of the metal particles are preserved within the filler [Bloor et al., 2005]. This spiky structure is theorised to give rise to quantum tunnelling through the polymer, producing conductive channels. The material produces linear conductivity behaviour at high and low stress, with high non-linearity in between, with resistivity varying from $10^{12}\Omega$ to less than 1Ω. It also increases in conduction when stretched, compressed, twisted or bent, which is contrary to the resultant attributes of filled polymers. This is significant in sensing technologies, due to its ability to discern very soft touch and hard forces repeatedly across a range of externally applied forces.

3. Optical Sensors

Optical sensors record many discrete values simultaneously multiple times per second in a mass-produced, cheap and compact architecture. In vision systems, monocamera temporal tracking paired with a set of spatial location markers enables tracking of movement in 3D space using SLAM - Simultaneous Localisation and Mapping

[Smith and Cheeseman, 1986]. When applied to tactile sensing, an intermediary layer, which makes contact with external surfaces, allows the same spatial tracking to perceive surface textures [Chorley et al., 2009]. The use of a specifically designed, compliant or bendable interactive surface as an intermediary layer, perceives resultant deformation from an external contact, and through surface slope variation can infer the location and force applied to it. The optical sensor can more readily monitor the deviations of points on the interactive surface (or skin) through the use of internal pins normal to the surface of the skin. The slope of the skin in a given region can be calculated due to its proportionality to the lateral displacement of the head of the pins [Chorley et al., 2009]. The pins act as a magnifier similar to the "contact lens" used in the car industry [Kikuuwe et al., 2004].

2.12 Summary

This chapter has reviewed the field of soft actuators with a specific focus on dielectric elastomer actuators and their features, configurations, and operation optimisation parameters. DEAs form a major topic in soft actuators and have the potential to produce significant performance enhancement in both actuators and sensor fields for robotic and wider actuator and sensing applications. The method of operation is well understood, but due to the huge range of possible dielectric material chemistries and physical characteristics, the modelling of such systems effectively is an open problem. Novel ideas of use and fabrication are possible in this relatively young field. The majority of research has focussed on single layer actuators and sensors, which can be fabricated to utilise optimisation parameters to create high performance characteristics. However, these works, although laudable for the results achieved, have avoided key questions on increasing power density and reliability. Some high power multi-layer actuators have been produced which are discussed further in Section 3. Fabrication is a particularly

complex process with multi-layer actuators due to a number of factors. Optimisation is also more problematic, as any frame or superstructure attached to the DEA stack will lead to a possible reduction in output due to the inherent coupling effects. This is augmented in stacks due to the layering. Even in soft body implementations an encapsulating insulating layer is required to avoid short circuiting at the dielectric boundaries. This layer does not compress with actuation, which creates a restraining structure as seen in 16a. Sensing using DEAs has been implemented with great effect leading to commercial products, however the sensing capability is limited by capacitance of, and size of the electrode. A single DEA acts as a capacitor to produce a strain or touch sensor. To create a sensory array hundreds of individual DEAs would be required. Some method of creating soft actuated touch would advance soft sensing state-of-art

To tackle the issues discussed above this work will aim to overcome these issues in the following research avenues:

- A solution to creating high performing stacks is to incorporate the enhancements made to single layer actuators in the multi-layer while mitigating or reducing the effects of any features of stacks that limit actuation performance.
- For the problem of reliability a method of protecting the soft actuator, whilst enabling strong coupled output will be explored.
- With regards to sensing, novel methods of creating sensory arrays in a soft skin or body will be investigated.

3 Mesoscale Thickness-mode Multi-layer Actuator Optimisation

3.1 Introduction

DEA actuators are based on thin films, which are compressed through the application of an electric field, causing useful mechanical work. Individual layer actuators tend to have relatively small active electrode areas producing low power outputs. These are still very useful actuators in this form for a large number of novel devices and systems, but advances in fabrication are needed for higher power applications. The attributes of single-layer DEAs would be very advantageous in larger scale actuator systems too, due to the high efficiency and power density exhibited in single layers [Carpi et al., 2007].

The chapter aims to devise an optimised thickness mode actuator to imitate biological muscle contractile actuation. This aim will enable further muscle mimetic actuator development in DEAs through the optimisation of performance characteristics in this actuation mode actuation. In this endeavour the chapter will explore barriers to optimisation that hinder the development of high powered layered actuators and, where possible, create novel methods to overcome them.

Below are the key performance characteristics for the improvement of multi-layer actuators that will be investigated:

- Tensile loading resilience (including best configuration type determination).
- Optimisation of actuation through material properties of both dielectric and conductive components (including layer uniformity, thickness, dynamic and electrical performance).
- Development of fabrication methods for the combining of individual components.
- Development of a fabrication method for creating high layer number multi-layer devices for high power actuation.

To meet these characteristics the features of materials, devices and fabrication methods need to be evaluated.The work has been divided into interlinked criteria of:

1. Conductive layer performance.
   - Layer thickness and uniformity.
   - Conductive performance under strain.
2. Dielectric layer performance.
   - Layer thickness and uniformity.
   - Optimisation of dielectric layer (enhanced strain).
3. Multi-layer fabrication methods.
4. Multi-layer passive characteristics.
5. Multi-layer actuation.

3.2 Evaluation of Multi-layer Actuator Implementations, Configurations, and Formulation

3.2.1 Multi-layer Actuator Implementations

State-of-art Stack Actuator Review

A number of stack actuators have been developed, from demonstrations of arm-wrestling using rolled actuators [Kovacs, 2006], to tensile stacks lifting weights [Kovacs and Düring, 2009]. Solutions to fabricating stacks have also been proposed using large fabrication rigs and rolling methods, which have had some success in stack creation for laboratory testing [Kovacs and Düring, 2009]. Some other examples of the top state-of-art actuators are shown in the images in Figures 16a-20. As well as the configurations and designs used, some research has been focussed on how to form a stack. Manual stacking can be used,

but is a painstaking process which is prone to human errors, with handling, alignment, and membrane damage. Additionally, due to the size of stacks desired and the fact that this is not a scalable process, a new approach is required. The production of DEAs is not yet a fully developed process, even though some components (such as DE membranes) are becoming more readily available. As such, research groups need to develop fabrication methods to be able to test and characterise these devices.

Contractive tension force stack DE actuator - This actuator was characterised and its operation demonstrated by Kovacs and Düring [Kovacs and Düring, 2009]. This actuator is one of the best demonstrations of the capability of DE stack actuators. The dielectric is pre-stretched to provide optimisation, using the IPN - Inter-penetrating Network - process, which involves spraying a pre-stretched film with monomer (TMPTMA), which is subsequently cured. A high number of optimised layers (order of 100) are stacked using very thin electrodes using rubbed carbon black of order of 100 nanometres. The stack was fabricated using two methods; manual and automated. These were both investigated to try to maximise the accuracy of the stack construction, due to the need for precise alignment to avoid premature breakdown and failure of the stack. However, the automated system was not able to use the pre-stretched membranes previously mentioned, and a maximum could only stack 200 layers due to the practical limitations of the stacking machine (Figure 15).

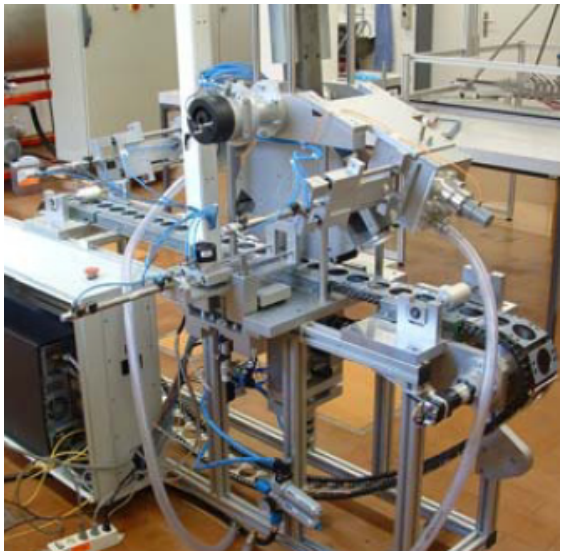

Figure 15: Example of a multi-layer stack fabrication rig (reproduced from [Kovacs and Düring, 2009]).

This is common problem with stacking machines due to the complexity of manipulation required for applying pre-stretch and capturing it in a stack. The actuators shown in operation show a considerable actuation strain even when loaded shown in Figure 16b. The characterisation tests showed up to 46% contractile strain when unloaded, with an actuation voltage of 4.1kV. It was noted that the border around the electrode (or margin - detailed in Section 3.2.3) did not alter shape leading to a stiff passive border (as shown in Figure 16a).

(a) Actuation of an encapsulated multi-layer stack actuator with stiff margin (reproduced from [Kovacs and Düring, 2009])

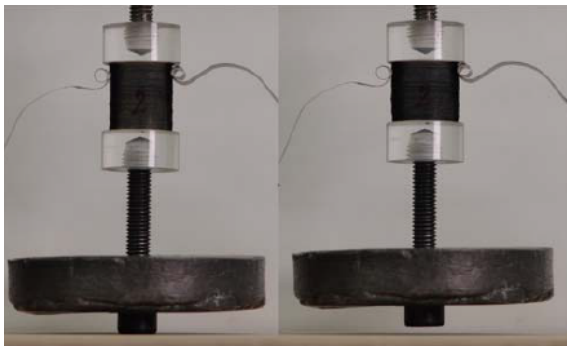

(b) Demonstraion of actuation of a multi-layer stack lifting a weight (reproduced from [Kovacs and Düring, 2009])

Figure 16: Images of two developed multi-layer actuators

The method of bonding between layers is not explicitly mentioned, and it is assumed the 3M VHB tape's acrylic dielectric pressure-sensitive adhesive nature is used to bond the layers. It is speculated that due to the separating carbon black this bond could be based mainly on the surface wetting and the vacuum formed between the layers (hence heavier weights are supported in images to avoid excessive strain in passive state).

Multi-layer DEA pneumatic valve - This is a multi-layer actuator designed for use as a pneumatic valve or linear actuator made from DEs requires high number of layers (Figure 17) [Tepel et al., 2014, Maas et al., 2015].

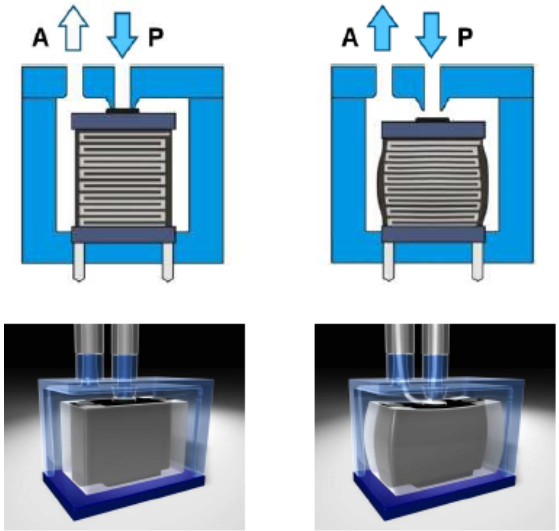

Figure 17: CAD depiction of conceptual multi-layer actuator valve (reproduced from [Maas et al., 2015])

This example shows that an automated fabrication process can be used to produce multi-layer actuators with a large number of layers. It uses a folding table which enables multiple stacks of a small number of layers to be made in parallel, and subsequently conjoined to form a larger actuator. The steps of the process are shown in Figure 18. It should be noted that the actuator is encapsulated with conductively coated DE material to form conductive channels to alternating layers. Additionally, the compliant electrode is applied using spray-coating, again forming surface adhesion between layers as mentioned with the previous actuator discussed. The whole actuator is additionally encapsulated which will aid in air-tight sealing avoiding any peel effects between layers.

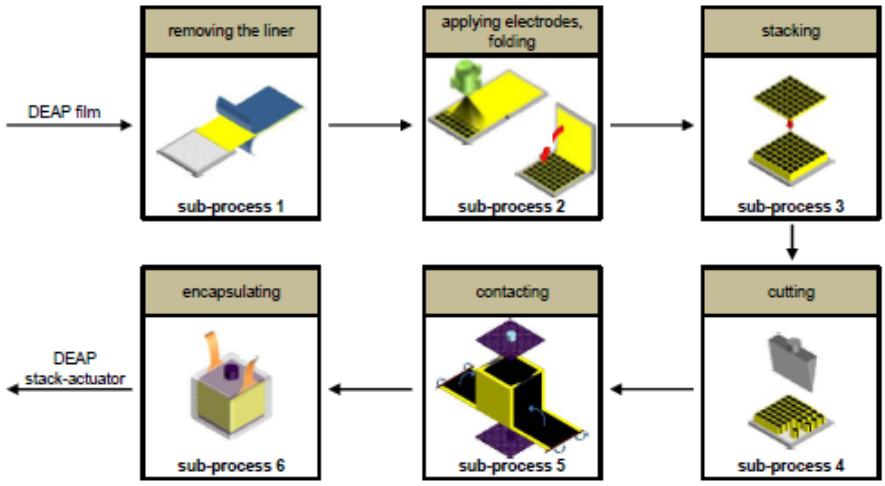

Figure 18: A step guide to a manual fabrication process of a DEA stack (reproduced from [Maas et al., 2015])

Spring-stack hexapod - A symmetric multi-layer stack is created using a manual fabrication method of cured 2-layer segments of alternating electrod and dielectric elastomer. When stacked to "approximately 58 layers" [Nguyen et al., 2014], the actuators contractile strain was recorded under an external load (no tension tests were undertaken). The stack was demonstrated in a robotic leg using a spring-stack arrangement to keep the stack under compression. This spring addition is speculated to be required to stop layer separation and hence ineffectual actuation (shown in Figure 19). The resultant walking stack actuator robot was demonstrated, delivering rotation of 25% of the angle of the femur.

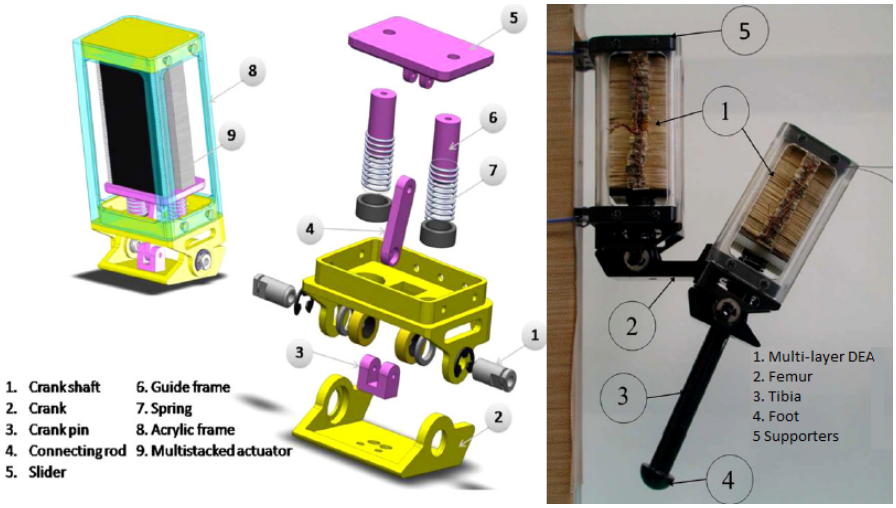

Figure 19: Spring stack leg concept and implementation (reproduced from [Nguyen et al., 2014])

Spring-Roll Arm-wrestling actuator - As part of a competition, EMPA - Swiss Federal Laboratories for Materials Testing and Research - presented a robot using 250 rolled actuators. These actuators use a large prestraining rig to create bi-axial pre-stretch and maintain it while it was captured round a spring core. Arranged in an antagonistic layout the system was large, but was able to perform the task (although not beat a human competitor) as shown in Figure 20. This system is mentioned as the competition was central to the push for higher power actuation from DEAs.

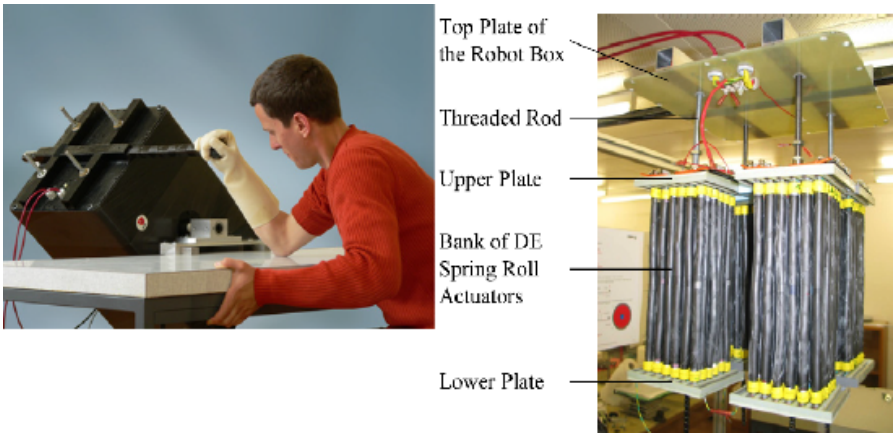

Figure 20: Arm wrestling implementation demonstrated at EAPAD 2005 (reproduced from [Kovacs, 2006])

Core-free roll DEA Actuator - This high power actuator is also put forward by Kovacs, Pei, Pelrine, Michel and Ha [Kovacs, 2006]. This actuator uses a free standing DEA roll to produce a relaxation actuation. This differs from most multilayer actuators, as the capacitor plane is in parallel with direction of actuation. It can produce a tensile force, but only when actuation energy is removed and the material undergoes areal contraction. Additionally, it uses no internal spring to maintain pre-stretch, which may be advantageous compared to the more conventional method, where the interface between the rigid support (spring) and the DE is a common point of failure. Spring-rolls also develop different layer strai,n on actuation related to distance from the axis leading to sub-optimal performance. However, using the L-IPN method as described in the contractive stack actuator from the same group, a stress-free prestretched material can be used to fabricate a rolled DEA. A large sheet of prestretched material is coated with a compliant electrode and rolled. A 10% strain was achieved at 6kV. Although the strain is not as great as previously mentioned implementations, the fabrication is far less complex.

These examples have each overcome the limitations of multi-layer actuator optimisation and fabrication using different techniques, which have resulted in several well

characterised proof-of-concept actuators that demonstrate the force and stroke that can be developed with larger DEA actuators.

3.2.2 DEA Multi-layer Actuator Configuration

Scaling up DEA sizes can be carried out in a number of ways as shown in Table 7. Rolling is a simple method of attaining higher power actuators, but the inherent relaxation actuation in this configuration leads to the requirement of additional antagonistic springs to perform extension/retraction behaviour [Zhang et al., 2006]. These additions also add bulk and potentially rigidity to the overall actuation system. However, the control of extension/retraction behaviour is very desirable, due to its muscle-like operation, which can be easily used in bio-mimetic and industrial applications. To attain this important trait, DEAs can be used to develop tensile strain on actuation, through active compression of the thickness of thin film DEAs, forming thickness mode tensile actuation. The contractile actuation operation mode, where contraction is produced through activation rather than relaxation, is advantageous in many applications. However, although these actuators can be constructed through a number of methods, they are hard to fabricate due to issues with film purity and thickness consistency, positional accuracy of layering, electrode conductivity and common rail conductivity, and layer optimisation.

Actuator Depiction	Type	System Output	DE Actuation	Description
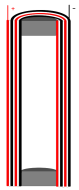	Multi-layer Roll	Transverse Relaxation	Planar expansion	A spring-free roll actuator is simple to produce, and can be enhanced through retained pre-strain on roll. However, it provides relaxation actuation, which although soft is harder to implement for robotic applications due to the limited stiffness under tensile strain.
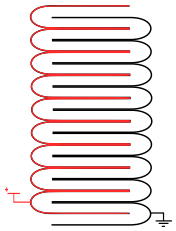	Folded Layer Stack	Transverse Contraction	Planar expansion	A Folded multi-layer stack consists of a single dielectric layer with conductive electrodes on each side. The dielectric is then folded back and forth to form a stack. This is easy to fabricate, but does lead to potential stress concentrations at folds. The folds also cause reduction in performance as the stiffness of the material in the fold leads to an effective passive region.

Continued on next page

Actuator Depiction	Type	System Output	DE Actuation	Description
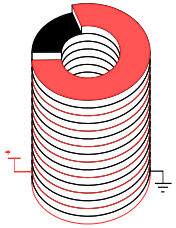	Bi-Film Helical Stack	Transverse Contraction	Planar expansion	A helical design actuator has been manufactured by slicing a dielectric tube using a spiraliser [Carpi et al., 2005]. A conductive coating can be applied to one side of the spiral, and then another helix inserted forming a second electrode. This has the advantage of not requiring electrode patterning, but cannot be easily enhanced through pre-straining techniques.
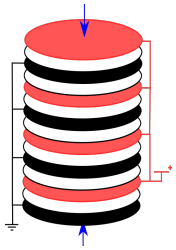	Individual Layer Stack	Transverse Contraction	Planar expansion	A stacked multi-layer actuator is potentially the hardest of the three configurations to fabricate, due to the requirement for separable layers. However, as the margins can be reduced to the minimum required to protect from breakdown, the performance can be maximised.

Table 7: Tabulation of current forms of multi-layer DEA configurations and categorisations of structure and output.

3.2.3 Breakdown of Multi-layer Actuator Components

To understand the components and processes involved in stack creation a detailed review is needed. The following list describes the features and processes used for construction.

Dielectric Elastomer Material - The choice of dielectric elastomer is a key factor in the creation of a DEA. It defines the maximal electric field and hence force that can be generated, as well as the actuation strain.

- Dielectric Layer Thickness - The layer thickness determines the voltage required to actuate. Reducing the actuation voltage is advantageous from safety, cost, and operational perspectives, reducing danger to health from harmful discharge to users (application dependent), whilst enabling simplification of high voltage electrical requirements.

- DE Optimisation - The DE material is still an ongoing chemical research topic and further advances are expected. Better characteristics will enable improvement of multi-layer actuator performance. Further, DEs have been shown to offer higher performance when pre-stretched due to the increase in dielectric constant this delivers, and can operate in softer straining region (i.e. the stiffness is reduced see Section 2.2.1).

Electrode Material - The electrode material must spread the charge across the DE surface to enable consistent actuation. If the electrode is too thin, the resistance may be too high when strained causing a slower response and inhibiting maximal strain.

Margins - Multi-layer actuators need good separation of electrodes between consecutive layers to avoid short circuiting through the air gap between high voltage electrodes. The dielectric separator must extend beyond the edge of the electrodes by a margin defined by the voltage to be applied to the actuator. An additional factor to be considered is for environment variation (such as humidity). Ideally a dielectric sealing all electrodes

would be created. However, the margin does affect the actuation as can be seen in Figure 16a.

Connections to Electrodes - The electrodes are alternately high voltage and ground, and in larger stack actuators, the number of layers may extend to hundreds or more. For these to be connected alternately requires an infrastructure of inter-connected wires. It should be noted that this is a key benefit of folded and helical high-power actuators, where the electrodes are constant planar linings on the dielectric as shown in Table 7. In stacked actuators, an electrode connection tab is required which will must follow the margin guidelines as set out above. These can then be connected to a common rail, but care should be taken to ensure the rails do not inhibit the actuation of the stack.

Fabrication - Single layers can be constructed with a well-documented relatively straightforward process. However, when this is extended to multi-layer stacks, the complexity of fabrication becomes much higher, due to the factors described previously in this list. Developing a fabrication method that resolves problems arising in implementing these features is required. The features used in the creation of a stack vary due to targeted aims of implementation and the specific optimisations proposed. Based on this, a fabrication system may be of a novel bespoke design. This is reflected in the state-of-art methods described in Section 3.2.1.

Packaging and Unitisation - To create a unit actuator, the stack must be able to connect to external components. Some method of connection is required, that can deal with the tensile load, whilst being spread across the stack surface area evenly to avoid local mechanical stress concentrations that could lead to premature failure. Furthermore, limiting z-axis (orthogonal to planar actuation surface) extension may be required to remove the potential for delamination. Due to the high voltage used, the unit electrodes and common rails would have to be electrically isolated through an encapsulating insulator to avoid harmful discharge.

3.3 Criteria for Improving Multi-layer Actuator with Single Layer Actuator Characteristics

To create a multi-layer actuator with the high performance characteristics of single layer actuators, certain characteristics must be incorporated into multi-layer implementations. These characteristics are presented in Table 8.

Single Layer Actuator Characteristics	**Description**
Mechanical Strength	The mechanical strength of the multi-layer actuator is critical to operation at high force contractile actuation. The mechanical strength in the case of a stack actuator can be defined by the strength at delamination as this is the mode of failure of the layered structure*.
Actuator Flexibility	The maintenance of DEAs inherent flexibility should be implemented for consideration in biomimetic applications.
Pre-stretch	Pre-strain has been shown to give a number of performance enhancements, including lower operating voltages resulting from thickness reduction
Maximisation of actuation area.	The framing required for voltage supply, separation of voltage rails, and stack support inhibits the performance of the actuator and reduces its effectiveness and should be minimised.

Continued on next page

*Due to a stacks construction this differs from the ultimate strength of the homgeneous silicone material that is used due to the layering process and fillers used in its fabrication.

Multi-layer Development Issue	Description
Uniformity of Thin Films	To reduce the risk associated with high voltage systems, and size of complimentary actuator electronics, thinner dielectrics are necessary. These films should be as uniform as possible, as the breakdown voltage will be related to the thickness at the thinnest point.

Table 8: Table of high-level development issues in the development and fabrication of stack actuators.

To produce a multi-layer actuator that integrates these features, the design and configuration need to be selected that offer potential for innovation and improvement in these areas. The development and optimisation of multi-layer actuators was a key focus of the work due to the limited progress of current state-of-art, and the possible utility of combining the single layer DEA characteristics, with the form of a tensile actuator and the potential of mimicking the dynamics of natural. This obvious goal is beset by many issues in developing a commercial actuator. The resolution of some of these issues is the focus of this chapter.

Stack actuators have been compared favourably alongside similar small-scale, and large-scale actuation alternatives [Poole and Booker, 2008]. However, large-scale stack implementations have yet to be realised with performance characteristics approaching power-to-weight or volume of biological counterparts.

3.3.1 Selection of Design of Multi-layer Development

Section 3.2 has discussed the possible options for the creation of a multi-layer actuator in terms of configuration and component, and considered how the features of single-layer actuators can be applied to layered actuators. Table 9 shows the analysis of the materials for the actuator and highlights the chosen configurations and materials that were decided on for combined enhancement.

Configuration	**Type**	Roll	Helix	Folded Stack			Layered Stack
	Ease of Fabrication	1 - High	4 - Low	2 - High			3 - Medium
	Separability of Components	4 - Low	3 - Medium	2 - Medium			1 - High
	Potential for Enhancement	3 - Medium	4 - Low	2 - Medium			1 - High
Component	**Electrode**	Carbon Grease	Carbon Powder	Carbon Nanotubes	Carbon-Silicone Composite	Metal - Silicone Composite*	Metal Powder	Metal Film
	Ease of use	1 - High	5 - Medium	7 - Low	4 - Medium	3 - High	2 - High	6 - Low
	Optimisation	6 - Not Possible	3 - Medium	4 - Low	1 - High	7 - Not Possible	2 - Medium	5 - Low
	Features	- Mass Produced - Well studied - Negligible strain limiting effects	- Powder variety - Negligible strain limiting effects	- High strain range - Negligible strain limiting effects	- Prefabricated membranes - Homogeneous bulk material	- Prefabricated membranes - Homogeneous bulk material	- Mass produced - Negligible strain limiting effects	- Films mass-produced
	Limitations	- Fluidic spread	- Limited effective strain range	- Hard to align - Specialist equipment required	- Strain limiting effects	- Strain limiting effects - IP protected	- Limited effective strain range	- Limited effective strain range - Low durability
						* - Specifically nickel-silicone composite developed by Bloor et al		
	Dielectric	VHB (Acrylic)	Silicone					Natural Latex Cast
	Optimisation	3 - Not Possible	1 - High					2 - Low
	Batch Size	1 - High (Reels)	3 - Medium. Batch size dependent					2 - Medium. Batch size dependent
	Dielectric Features	- Well studied	- Potential for bonding to silicone electrode					- Bio-degradable
			Spun	Doctor-Bladed	Spray			
	Uniformity	4 - Medium	2 - High	1 - Very High	3 - High			5 - Medium
	Thickness	5 - Medium (pre-defined)	2 - High Order of microns	1 - High Order of microns	4 - Medium Order of tens of microns			5 - Medium Order of tens of microns
	Thickness Variability	Unknown	- Distinct surface thickness variation	- Negligible variation				
	Issues	- Particulate inclusions - Variation in manufacture - Highly visco-elastic						

Table 9: Design Selection Decision Matrix

Reviewing the possible stack constructions, there are three ways of realising a stack shown in Table 7. The helical actuator concept requires layers to be sliced out of a

bar, if a uniform structure and strain is to be developed [Carpi et al., 2005]. Larger scale folded designs have been evaluated with circular and rectangular planar layers [Huu Chuc et al., 2008, Randazzo et al., 2008], demonstrating that effective stacks can be produced in this scale. Stack arrangements differ from folded stacks, due to the complete separation of dielectric layers. Both folded and stacked designs require electrodes of alternate layers to be connected to separate voltage sources. This leads to a complicated fabrication for a stacked approach, because each dielectric layer is isolated. Thus far, stack actuators have been created using a range of hand-assembled and semi-automated techniques [Huu Chuc et al., 2008, Randazzo et al., 2008].

To produce a multi-layer actuator the aim is to produce a stack of alternate conductive and dielectric layers that has sufficient lamination adhesion strength at limit in both active and passive states to remain bonded with sufficient tensile strength. The concept is able to be used for multiple implementations including valves, pumps and bio-inspired artificial muscles [Fes, 2018, Stoll, , Lotz et al., 2011]. The target application for this work specifically is to investigate steps towards the development, optimisation, and characterisation of an actuator. DEA technology has been shown to be able to produce output characteristics comparable to mammalian muscle, when the DEA is considered in its thin film form. As discussed in Section 3.2.3, there is a greatly increased level of complexity when stacking DEAs, making the design of a fabrication mechanism a difficult and intricate task.

3.3.2 Defining Scope for Optimisation of Multi-layer Actuator

The scope to be covered in this research on multi-layer actuator development can be broken down into three sections:

Layer Bonding

The bonding of consecutive layers of a multi-layer DEA stack enables the integrity of the actuator to be maintained under high loads in both passive and active conditions. The examples described in Section 3.2.1 have shown a variety of techniques which have used different adhesion of elements in the fabrication process. The layered smooth soft materials are adhered by Van der Waals forces at the molecular level. However, in the examples given, there is graphite or carbon (powder or similar) spread on one sheet - to form an electrode - before they are layered, leading to a mechanical adhesion with intermediary carbon particles. The bond between the silicone and acrylic described by Kovacs et al is likely diffusive where polymer chains diffuse into the other material (as acrylic can absorb silicone oil) [Kovacs and Düring, 2009, da Silva et al.,]. For the actuator to repeatedly operate effectively, the maximum tensile stress must be less that the yield strength. The yield strength of the stack is determined by the weakest layer adhesion leading to delamination and stack separation. This adhesion is not as strong as chemical bonding and may be too weak for requirements of high load applications. The methods of developing good inter-layer adhesion whilst maintaining performance will be explored as well as comparing the strength of different adhesions.

Capturing Pre-stretch

In DEAs, stretching the dielectric material prior to actuation has been shown to be beneficial to actuator performance and has been implemented and characterised [Carpi et al., 2007]. It would be highly advantageous to capture this performance in a multi-layer actuator whilst reducing the thickness of the actuator and maintaining

chemical bonding. The maintenance of a fixed strain of a DEA, for actuation (using a support material), is known as pre-stretch (or pre-strain). Pre-stretch has been captured using a silicone interpenetrating network with acrylic and silicone substrates [Kovacs and Düring, 2009, Brochu et al., 2013].

Multi-layer Fabrication

The high performance attributes of single layer DEA membranes have been thoroughly explored and characterised [Carpi et al., 2007]. The properties need to be shown to be implementable in multi-layer stacks. The two sections above are about developing performance characteristics. In order to test the functionality of a multi-layer actuator formed using the improved properties, a prototype needs to be fabricated with sufficient layers to allow experimental analysis. Methods of forming a stack actuator to deliver these optimisations will be explored and a multi-layer implementation tested.

These tasks are broad and cover every major component of the DEA, however they are separable into individual undertakings that can be combined to further improve the current state-of-art. As such, the following sections will discuss as individual projects the novel processes harnessed and the characterisation thereof, facilitating the creation of a multi-layer actuator which will be analysed and compared to other available technologies.

Materials and Experiments Note - In this Chapter, the investigation of stack actuators will focus on the use of a single silicone material, and all experiments will use this base material unless explicitly stated. This is to reduce variability in results due to a number of properties and side-effects of processing techniques used. The silicone base chosen is Dow Corning Xiameter 3483 (also known as HSIII), which has been characterised as a high performing silicone DEA material [Carpi et al., 2007]. It is also a readily available material and has been used by other groups in certain fabrication techniques

that are to be explored. This is a two part RTV - Room Temperature Vulcanisation - silicone, which can be readily mixed by hand in small or large quantities. As described in the technical data sheet it is highly recommended the mix should be degassed before use [Dow Corning, 2011]. Degassing uses a high vacuum to facilitate the removal of air from the mixture, enabling a homogeneous bulk to be produced with significantly reduced internal air pockets.

The materials are affected by humidity, temperature and fabrication [Boonstra, 1979, Guo et al., 2015]. As the materials were produced in house and were cured into forms required for testing, only small batches could be produced which were comparable. This has limited the number of tests able to be performed on samples and creates inherent variability between batches affected by environmental and accuracy factors. The predictive modelling of the materials is also limited due to the lack of precise understanding of the dynamics of the materials used. The use of phenomological models to describe the behaviour limits comparability between the samples, whereas physical models require more complex parameters. With the addition of filler materials and pre-strain used in this investigation methods for prediction are not currently available that can provide any support to the work.

3.4 Novel Thin-layer Fabrication Process

Creating uniform thin layers is critical to the formation of high performance DEAs. The layer thickness needs to be as small as possible to reduce voltage required to achieve significant actuation, while being as uniform as possible to achieve the highest thickness to dielectric strength ratio for any given layer (as this is dependent on the thinnest point of the membrane). The common thin film production methods are discussed in the Literature Review (Section 2.5). A new method which enabled a combination of forming thin layers whilst adhering to another silicone film was developed. Some methods do offer this ability, but do not investigate the utility that this bonding can

have on improving the properties of the DEA or for enabling for a higher yield strength in passive or active states.

3.4.1 Lamination

A process was devised to encapsulated uncured silicone between supporting films in a lamination process. The use of a fixed height aperture, between rigid components was used to produce a silicone layer of a given thickness. A method using shims of known thickness was used to adjust the aperture to produce a lamination gap of desired height. Once cured, the supporting films can be removed (acting as release films), revealing a highly uniform layer produced in a contained environment - hence preventing particulates from affecting the film uniformity. Figure 21 shows the lamination of a dielectric layer using a fixed spacing.

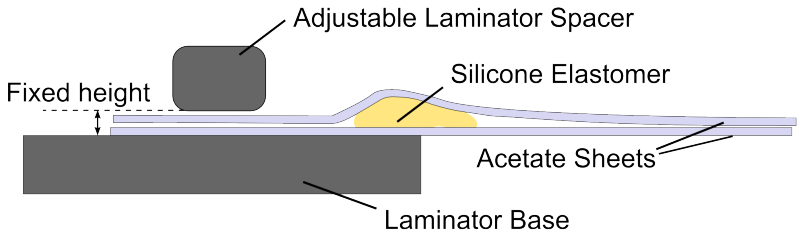

(a) Step 1. Setup of lamination thickness and appplication of silicone to substrate.

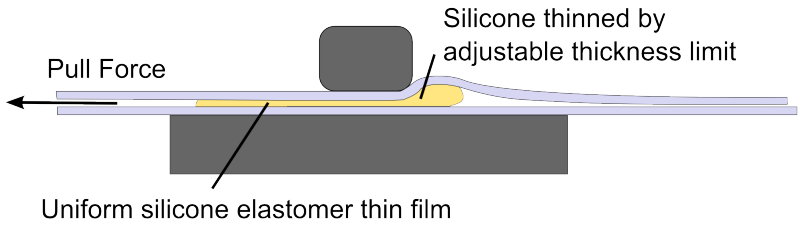

(b) Step 2. Application of force to pull substrate and squeeze silicone to set thickness.

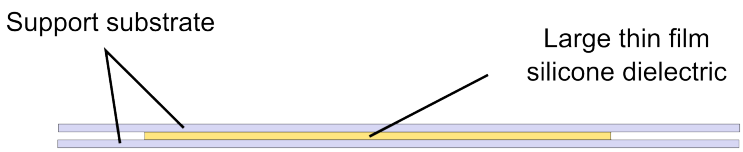

(c) Step 3. Allow the produced silicone thin film to cure

Figure 21: Illustration of process for creating thin films of silicone dielectric using developed laminator.

This process was shown to produce highly uniform layers as shown in Figure 22, where an 93 micron thick layer was produced.

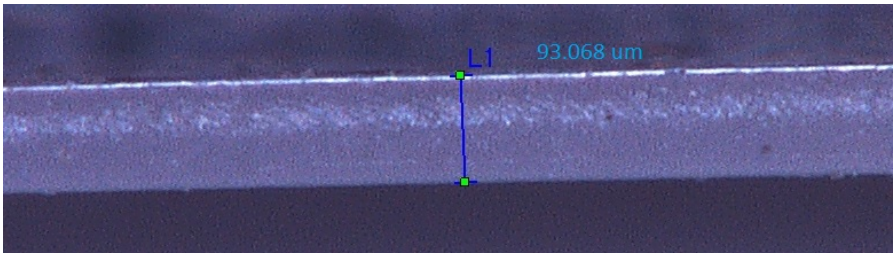

Figure 22: Microscopy image of cross-section of laminated silicone layer (target thickness 100microns).

A uniform silicone dielectric layer was created using the method described above to produce films of approximately 100 microns thickness. The Force-strain characteristics of the sheet were measured (shown in Figure 23). It can be seen after an initial linear phase there is some strain softening. This lower stiffness range is the area in which strain is greater for a given applied stress and hence the actuation would be enhanced through pre-strain.

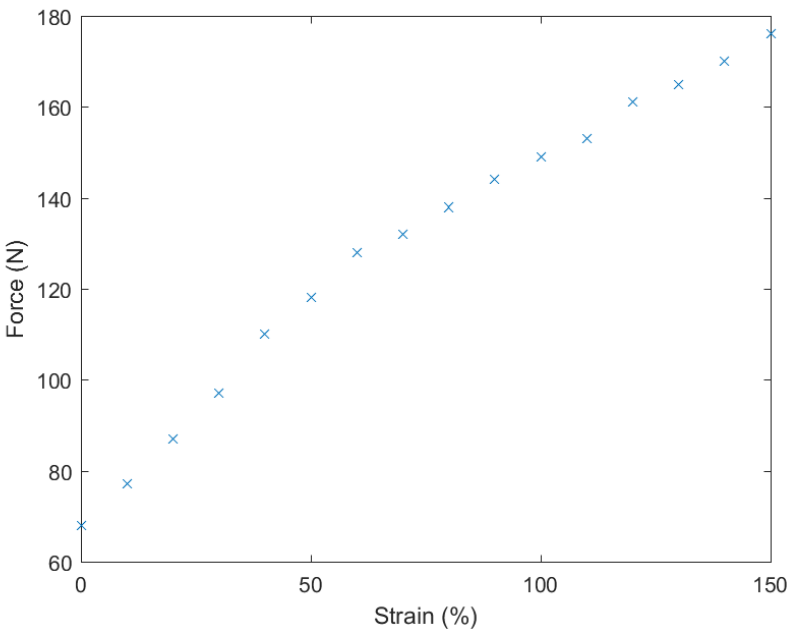

Figure 23: Experimentally calculated uniaxial force-strain relationship of Xiameter 3483 silicone

3.5 Electrode Development

As discussed in Section 2, there are many choices of electrode material; the selection of which varies on the application that it will be used for. However, there are some key features of the electrodes essential to providing good actuation.

- They must provide a consistent conductivity across the surface of the dielectric material
- They need to exhibit low stiffness and hence provide negligible resistance to strain.
- Conductivity should not significantly deteriorate over the full strain the actuator is required to achieve.

These requirements are consistent for all configuration types used in DEAs, but with specific reference to multilayer actuators, there are additional considerations. A multilayer actuator uses thickness-mode actuation to produce a useful strain. Hence, this type differs from most configurations of DEA, which utilise the relaxation of the membrane to deliver useful output in tandem with a spring or other energy store (even internal energy used in single layer planar actuation).

Conductive Filler

Conductive particles can be introduced into a bulk material (such as silicone) to make it conductive. For the creation of a conductive compound, the properties of conductive filler material are critical to achieving conductivity. Research into composite conductors for anti-static and sensor purposes have investigated a wide range of fillers [Bloor et al., 2005, O'Halloran et al., 2008]. Smaller particles have a lesser effect on the stiffness of the material compared to larger particles [Jha, 2008].

Metal and carbon powder based particulates are most commonly used as fillers due to their conductivity and lowparticle size. It has also been found that agglomerates are elec-

trically conductive at a lower volume ratio (weight and volume) [Wolff and Wang, 1993]. It is thought that the formation of chains of particles that are loosely grouped can form highly conductive pathways with low overall stiffness.

Table 10 shows the characteristics exhibited by a range of different conductive powder that have been used in recent research in DEAs and capacitive sensors. Conductive compounds are listed in the table, which are relevant to the research, but this is not an exhaustive list.

Filler Type	**Characteristic**	**Description**
Carbon Black	Particles Size	Carbon Black is a nomenclature for a range of carbon powders of different conglomerate sizes, which are grouped by sieving.
Carbon Black	Particle Aggregate - Mean Diameter of Spheres in Chain	The thickness of the chains formed of carbon black. This is generally inversely proportional to the surface area of carbon black [IARC, 2010].
Carbon Black	Particle Aggregate - Extent of branched Chain Aggregate	This is the aggregate size of the chain forming conductive pathways [Alsteens, 2005].
Carbon Black	Porosity	The porosity of carbon black is a key factor in aggregate to aggregate contact. Higher porosity (number of pores present) increases probability of contact and leads to higher conductivity [Jha, 2008].

Continued on next page

Filler Type	Characteristic	Description
Metal Powders	Quantum Tunnelling Conductivity	A spiky metal particle (Nickel) retains its shape leading to conductivity which is extremely sensitive to deformation [Bloor et al., 2005].
Carbon Nanotubes	Nanotube forests	The long single wall carbon nanotube molecules can be grown as forests and form collective aggregates, which leads to low percolation threshold conductivity [Ata et al., 2012]

Table 10: Table of main characteristics and addtional description of common conductive powders for DEAs

Carbon black has also been shown to improve the tensile strength of elastomers [IARC, 2010]. However, it does increase the stress for a given strain, hence increasing the stiffness of the conductive material and actuator. Both carbon nanotube and composites with quantum tunnelling effects (QTC^{TM}) are either IP protected or hard to produce in sufficient quantities, whereas carbon black is readily available due to its large number of industrial uses.

As described in Section 2.4.2 of the Literature Review, the weight of the conductive additive in the bulk material will reach a point where the bulk material becomes sufficiently conductive. This point is known as the percolation threshold (shown in Figure 7). Finding the combination of ratio of carbon black to provide the required level of conductivity, while keeping the overall actuator sufficiently soft to actuate effectively is the target of these experiments.

Mixing

The mechanics of mixing is still an area of research, but techniques have been developed and are currently used that give sufficient mixing for the research described herein. In order to get a homogeneous composite material, the conductive particles must be thoroughly mixed together to achieve the best conductivity. Mixing can be carried out in different ways from hand-mixing, high shear mixing, ball milling and sonication. After some initial tests, hand mixing was found to be laborious, inconsistent and overall had poor conductivity. High-shear mixing enabled well mixed composite samples to be quickly produced consistently, however, the process did introduce significant heat to the bulk material. Finally, sonication has been used in mixing solutions, but it was found that even when thinned, the viscosity of the material was too high to mix. High-shear mixing was chosen as the method to produce electrode material due to its effective and consistent processing and speed of production.

3.5.1 Electrode Characterisation

In order to understand the properties of the conductive compounds produced, a set of tests were undertaken to understand the conductivity characteristics of the composite material.

Sheet Resistance Tests

Using a process of high shear mixing with a consumer blender, carbon black was mixed with a silicone bulk material (Dow Corning Xiameter 3483) for a fixed period of time - 20 seconds. This time period was chosen to give a consistent output without overheating the sample in the process and causing premature cross-linking. The samples were laminated using the process described in Section 3.6 with a thickness of 150 microns. The samples were cured and then tested using a four wire measurement meter (Keithley

2001 series), to calculate the sheet resistivity at different strains. From precursory test samples a range of weightings around the percolation threshold was investigated shown in Figure 24 using a Megger insulation testing multimeter (MIT310) on a sample size of 100mm x 40mm. It can be clearly seen that there is a step change in resistance in 3.5 - 4.5 % weighting of carbon black, where the resistance falls by over 85% to 33.7kΩ.

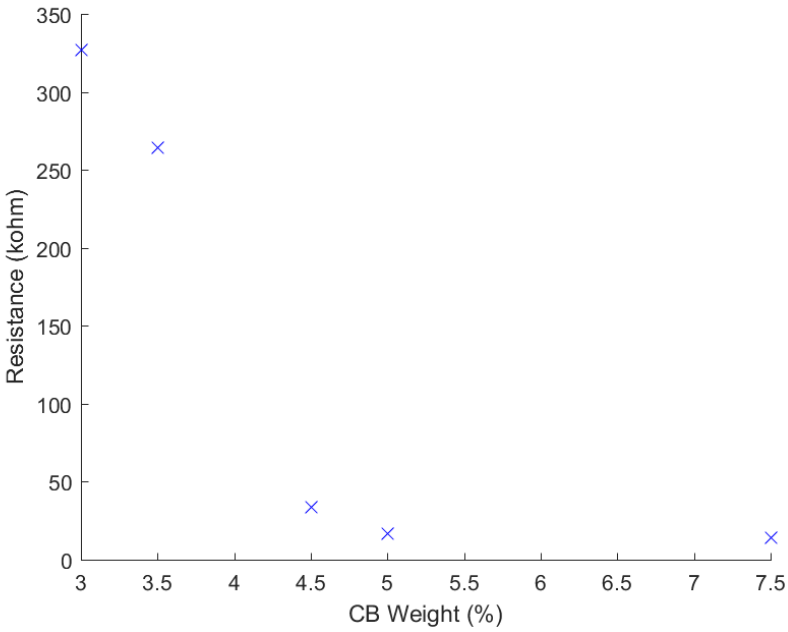

Figure 24: Plot of experimental results of two-wire resistance for composite silicones with different carbon black weightings at 1kV using a Megger high voltage resistance meter

At 3% carbon black (CB) weighting, the samples began to show some conductivity, and at 5% the resistance was over an order of magnitude lower. It was noted however, the mixture at this weighting was very viscous and hard to laminate. Additionally, unmixed carbon black agglomerations were found in the sample leading to holes from blocked cross-linking, suggesting inhomogeneous mixing due to the viscosity limiting the shear mixers capability (sample shown in Figure 25b). An additional a 7.5% weight sample was produced and was found to be significantly inhomogeneous, much stiffer,

more conductive, but mechanically weak, with a low tear resistance. Images of these samples are shown in Figure 25:

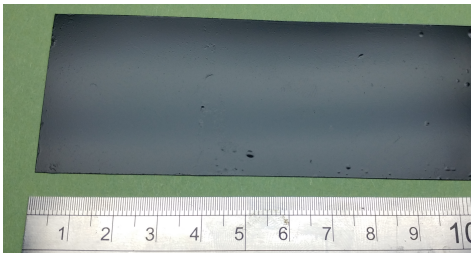

(a) Photograph image of surface of conductive composite sample with 3% carbon black by weight showing minor surface imperfections.

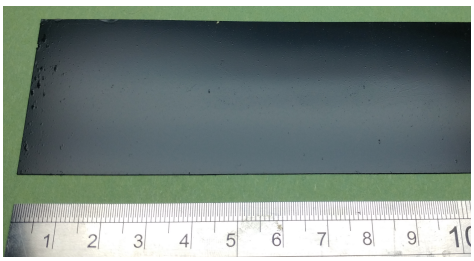

(b) Photographic image of surface of conductive composite sample with 5% carbon black by weight showing slightly larger surface imperfections.

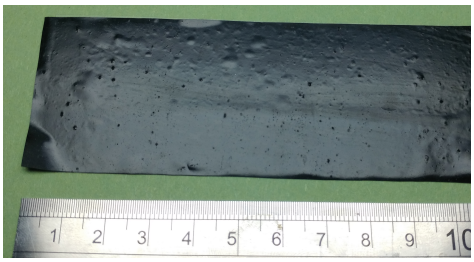

(c) Photographic close up image of surface of conductive composite sample with 7.5% carbon black by weight showing mm-scale surface imperfections and holes.

Figure 25: Comparison of photographic imagery of samples with different carbon black weights analysing homogeneity.

Samples were taken in the range of 3-7.5% weight and strained whilst recording sheet resistance. For these tests sheets of conductive composite silicone of dimensions 100mm x 40mm x 0.15mm (wxhxt) were cut using a guillotine (to avoid potential for tearing

from stress concentrations around small cutting defects). They were strained between two clamps to which copper tape was applied and a layer of carbon grease added to reduce contact resistance. Figure 26 shows the straining set up. A four wire resistance meter was used to accurately measure the resistance removing any effects of the lead resistance.

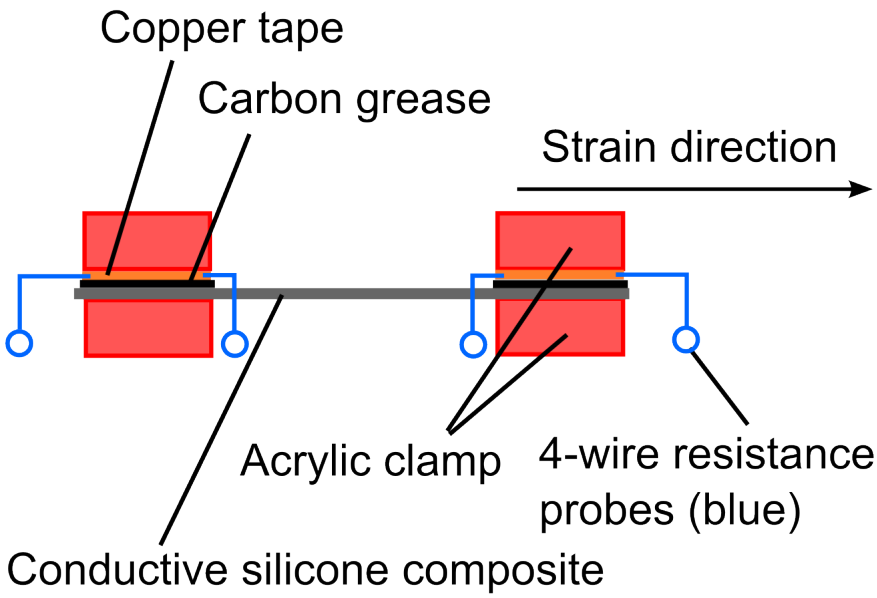

Figure 26: Illustration of experimental set up of straining rig for testing conductivity change with strain.

The setup used for the experiment is show in Figure 27. Carbon grease and copper tape were used to ensure the best practicable connectivity to the sample surface. The frame allowed for the samples to be incrementally strained and the resistivity measured:

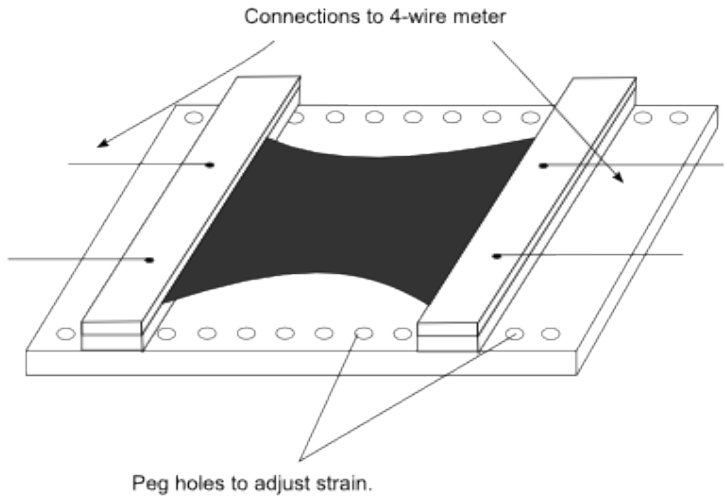

Figure 27: Illustration of experimental setup for straining conductivity samples of varying thickness.

The results of the tests are shown in Figure 28.

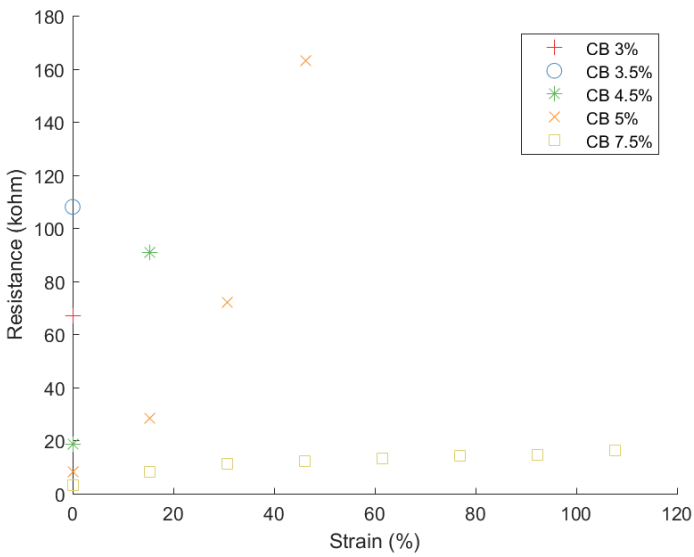

Figure 28: Graph of experimental data on effects of uniaxial material strain on resistance for silicone conductive composite samples with varying carbon black weightings.

It can be seen from the graph that the initial resistance drops significantly with increased weight of carbon black in this range. Another effect is that under strain con-

ditions the percentage increase in resistance decreases with weight of carbon black. This is due to the number of pathways allowing conductivity being much higher in these samples. The results show that conductivity is possible with thin composite samples that can conduct under strain. However, as more carbon black was mixed into the samples, the resultant material became significantly stiffer. This would be detrimental to the actuation of the multi-layer actuator, thus the stiffness was explored.

Force-Strain Test

The samples were found to be stiffer with a higher filler content, so the stress-strain characteristics of the conductive silicone samples was investigated due to its significant impact on the performance of the actuator produced. The samples used in the sheet resistance tests above were strained using weights to provide a uni-axial force-strain characterisation of the different samples. Uni-axial straining was used due to the ease and accuracy of measurement. A tensile strength testing rig would be normally used, but due to the thickness and delicate nature of the samples, the attachment and the force range required a simpler set up was considered with a mass attached on to a clamped, vertically held sheet of composite material. Figure 29 illustrates the setup used for the measurements:

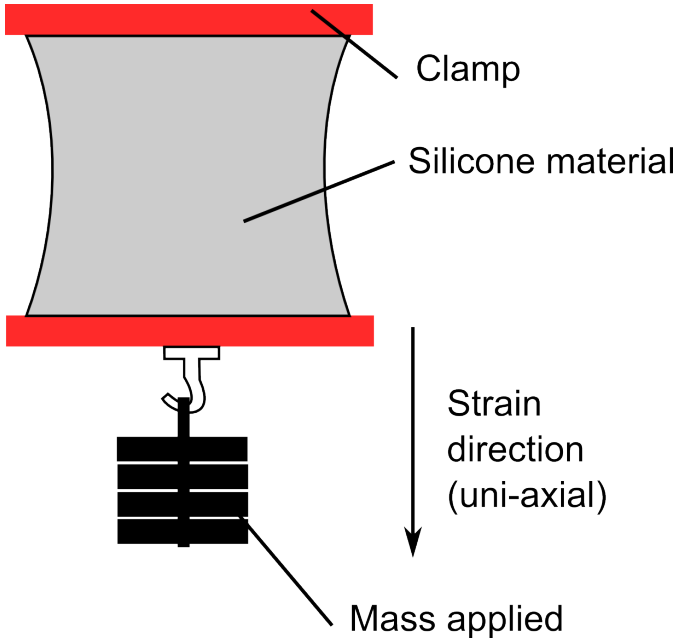

Figure 29: Illustration of set up for force-strain characterisation of conductive silicone composites.

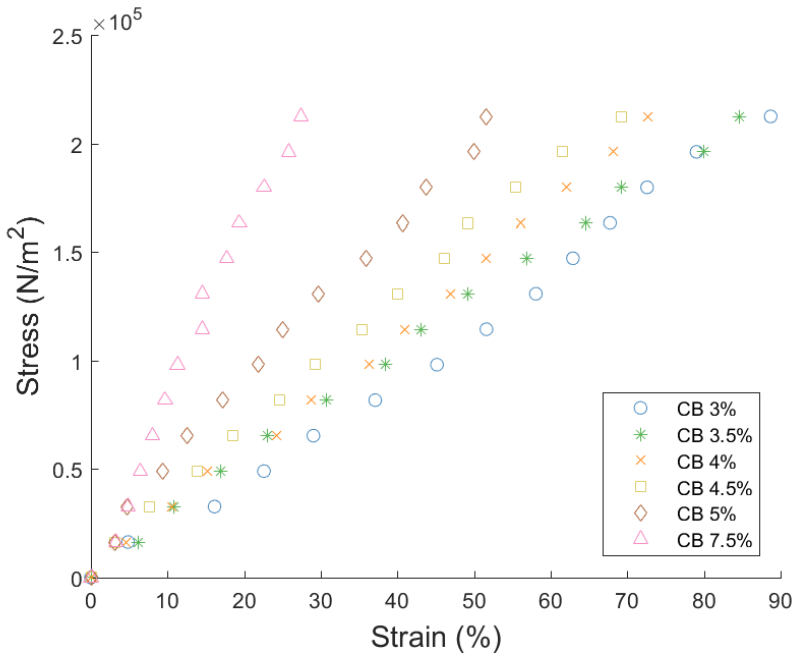

Figure 30: Plot of relationship between applied tensional force and uniaxial strain of silicone conductive composite samples with varying carbon black weightings.

The results presented in figure 31 show the stiffening effects of increased filler concentrations in the bulk material. It can be seen with higher levels of filler the rate of stiffening increases.

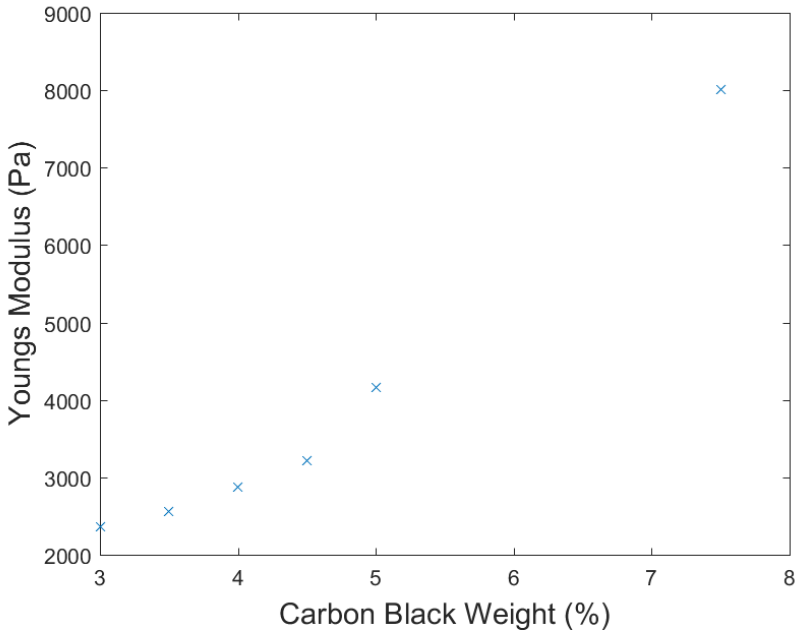

Figure 31: Effect of weighting of carbon black in a silicone conductive composite on material stiffness

Sheet Resistance Variation with Thickness

An optimum was needed to be found between thickness, stiffness and sheet resistance. The thickness of the material may affect the level of carbon black required to create pathways through the bulk material. This is due to the material transitioning from 3-dimensional to an effective 2-dimensional sheet. As the thickness reduces the agglomerate pathways are reduced hence increasing filler weighting at which the percolation threshold is found [Stauffer and Bunde, 2008]. This was tested with different sheet thicknesses with a 5% carbon black weighting, which is considered to offer a good compromise between resistance and stiffness. Two samples were tested per thickness as a significant variability in resistance was found between samples. The test setup is the same as used for sheet

resistance tests show in Figure 27 & 26.

The graph in Figure 32 shows some variability between samples, which may be due to low contact conduction, non-homogeneous final mixed state or variability due to unpredictability of internal connections of carbon black. However, a clear curve is discernable showing an exponential increase of resistance with reduction in layer thickness, as expected. The aim to reduce the conductive layer thickness led to the selection of 65 microns as the target conductive layer thickness, which would give a good compromise between conductivity and softness.

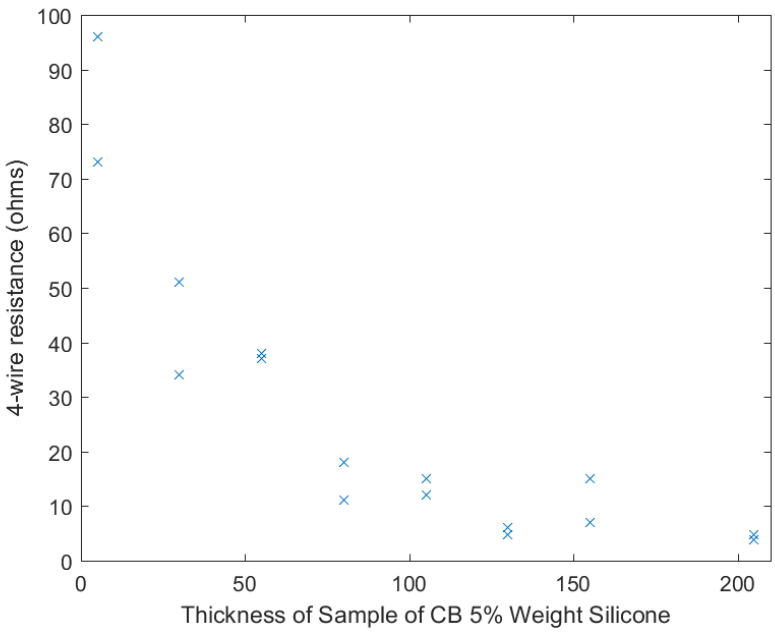

Figure 32: Plot of the effect of conductive composite thickness on sheet resistance with a constant carbon black weighting of 5%

3.6 Multi-layer Bonding and Pre-Stretch

With the aim of producing a tensile stress using a thickness-mode multi-layer actuation, there are a number of options for securing layers together, including chemical bonding, contact adhesion, and vacuum sealing. An alternative solution as mentioned in Section

3.2.1 is to use stacks under constant compression, however this requires extra structural components around the DEA, which limits the operation and flexibility of the actuator. The examples of previous tensile stack implementations in Section 3.2.1 use a mixture of contact adhesive or vacuum sealing in order to create an adhesion between layers. A chemically bonded layer could be much stronger, however optimisation is difficult to introduce to bonded multi-layers especially in thin layers (i.e. good conductivity, soft extensibility, mechanical efficiency, layer uniformity etc). To investigate whether it is possible to create an effective *chemically bonded* multi-layer stack actuator the composite electrode must be able to cross-link to the dielectric membrane when curing.

Laminated Inter-penetrating Networks (L-IPNs)

To consider methods of forming conductive layers for chemically bonded multi-layer actuators, it was considered that the formative layers of DEAs (conductive or dielectric layer) would need to be cured to each other. An additional layer of silicone could be used to enable cross-linking of layers, but this would increase the overall thickness of the dielectric layer and hence increase voltage. Maintaining layer thickness uniformity might also be a problem. Considering the methods of producing layers of elastomer discussed in the Literature Review (Section 2.5), doctor-blading was most promising for forming a bonding layer, due to the layer uniformity, thickness variability, and area coverage it could provide. Other methods had drawbacks which were too limiting to be used:

- Spray coating - Found to be inconsistent and block due to filler particulates [Cox, 2012].
- Spin coating - Fillers altered the even spreading of mixed conductive silicone, which led to streaking.
- Modified Doctor blading* - Found to give uniform thin film conductive output.

*Instead of direct contact with the film compound in the membrane fabrication, an acetate sheet of

To use doctor-blading to join cured dielectric layers, a backing substrate was used so that two layers could be laminated together, forming a chemical bond between two layers with the electrode material also acting as the chemical adhesive.

With two elastomer films on support acetate films, a conductive compound adhesive is prepared and applied in a line to one side of the films. The amount of compound is calculated to adequately fill the gap over an area larger than the film - this is to ensure no thinning of the adhesive layer during lamination. They are pulled through a laminator with a set thickness, as shown in Figure 33. Shim spacers were used to separate a machine bar and plate to ensure uniform thickness. Once formed, the laminated dielectric-electrode-dielectric sandwich is cured prior to the removal from the temporary support substrate. This process was found to produce a consistent electrode layer.

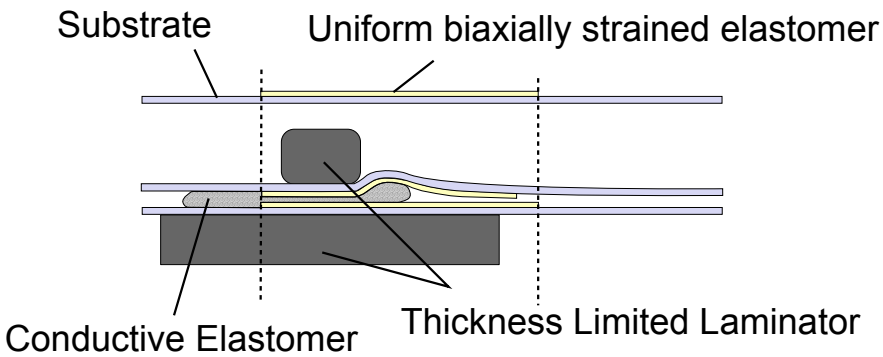

Figure 33: Depiction of the process of laminating two dielectric silicone membranes together with a silicone-carbon black conductive composite.

Pre-stretched Lamination

To enhance the properties of the DE, pre-stretch can be used to create a stress free membrane in the strain-softening region stress-strain curve of the material. To create an optimal stack actuator, a more complex construction method will be required. To

known thickness is used to increase layer uniformity

achieve this, thin films of cured elastomer are strained using a biaxial straining frame. The pre-strained film is placed on a supporting substrate forming a temporary adhesion (Figure 34a). Any excess to the uniform area of elastomer is removed (Figure 34b).

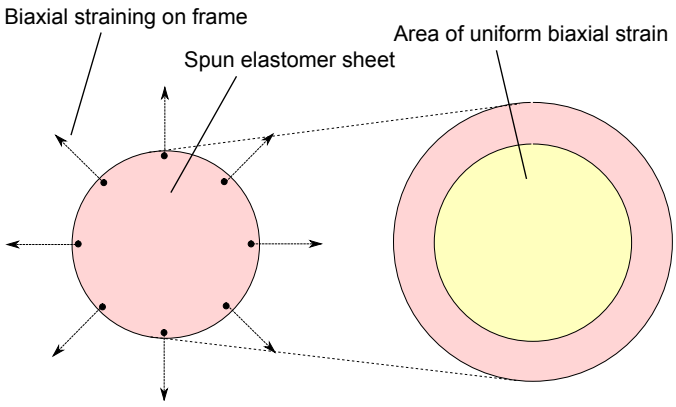

(a) Illustration of biaxial strain of a silicone elastomeric membrane

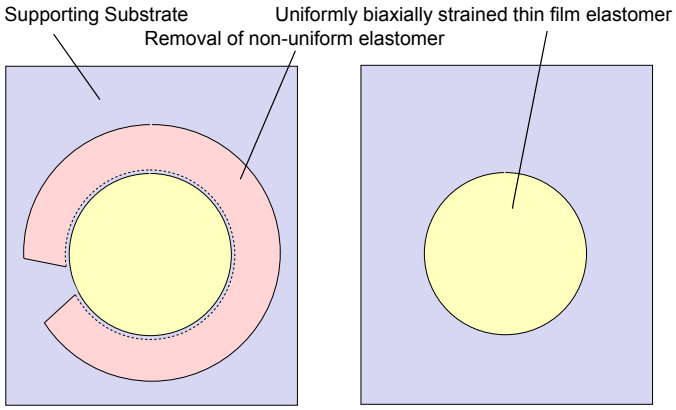

(b) Image of capturing uniform biaxial strain of a pre-strained silicone elastomer membrane using an acetate substrate.

Figure 34: Process of capturing pre-strain of a silicone elastomer in preparation for forming an L-IPN

Once cured, the uniform laminated two layer DEA can be removed from the temporary support, cut free from excess adhesive, and allowed to relax as shown in Figure 35.

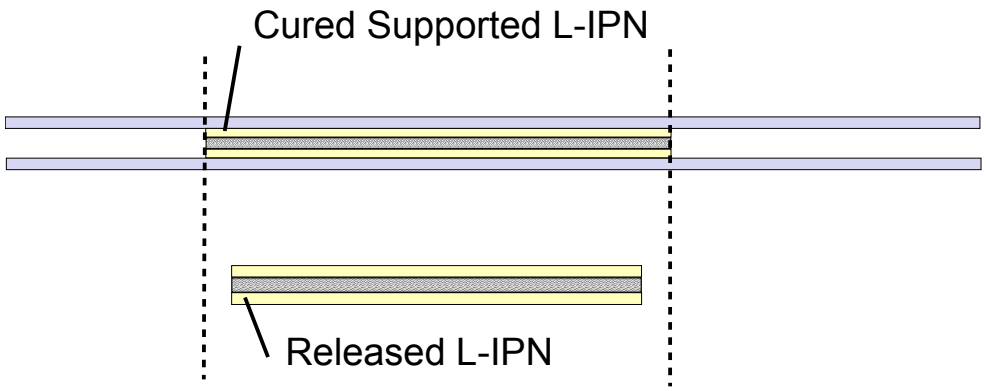

Figure 35: Illustration of three resultant three layer L-IPN with silicone - carbon black composite sandwiched between two dielectric membranes with caputred pre-strain.

When cured and released from the temporary support, the adhesive layer is deformed in the layers' plane by the contractile forces of the dielectric membrane. With the characterisation of chosen layer materials, this relationship can allow the device to be tuned for different levels of relaxed pre-strain. Additionally, the adhesive layer can be formed from the same base composition as the dielectric membrane enabling greater homogeneity of the stack. The insulator-electrode combination will need to be in effect actuated by each single dielectric layer (further analysed in Section 3.7.1). When actuating the laminated structure, the electrostatic pressure exerted over the dielectric layer strains both electrode and dielectric material. The force is generated solely based on the thickness of the dielectric, hence the ratio of electrode to dielectric layer thickness should be as low as possible, whilst maintaining high pre-stretch. An additional benefit is the compression of the electrode, which increases the range of strain in which it can conduct. The LIPN equilibrium is mathematically considered in Appendix A.

Sample Silicone L-IPN

The silicone L-IPN was observed using microscopy to confirm the thickness and structure of the samples. The thickness of each layer in the laminate was measured over a cross-section of the sample (as shown in Figure 36*).

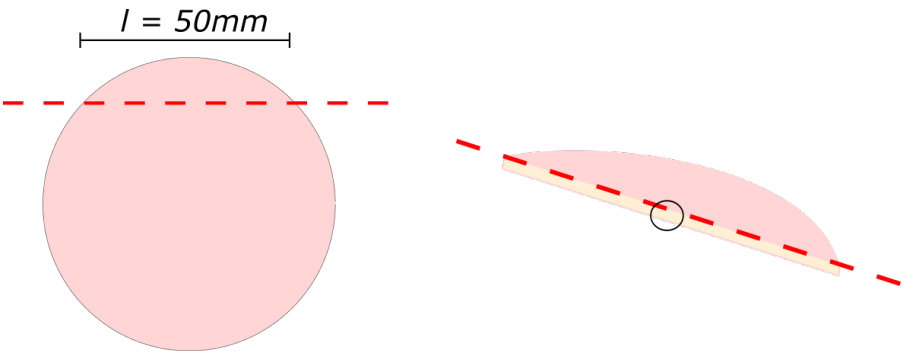

(a) Depiction of cross-section slice used for microscope image and uniformity measurements

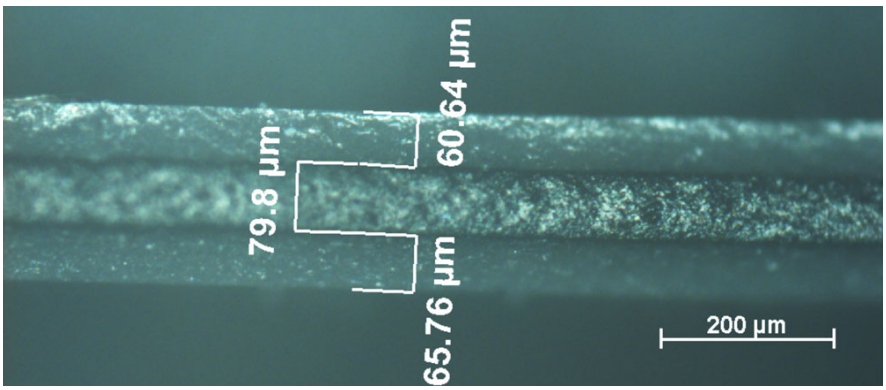

(b) Microscope image of L-IPN with captured pre-strain silicone layers adhered through lamination with siliicone - carbon black electrode composite.

Figure 36: L-IPN Uniformity Images

*The cross-section length was limited by the range of the microscope motorised axis (50mm travel), hence a sample of suitable length was taken

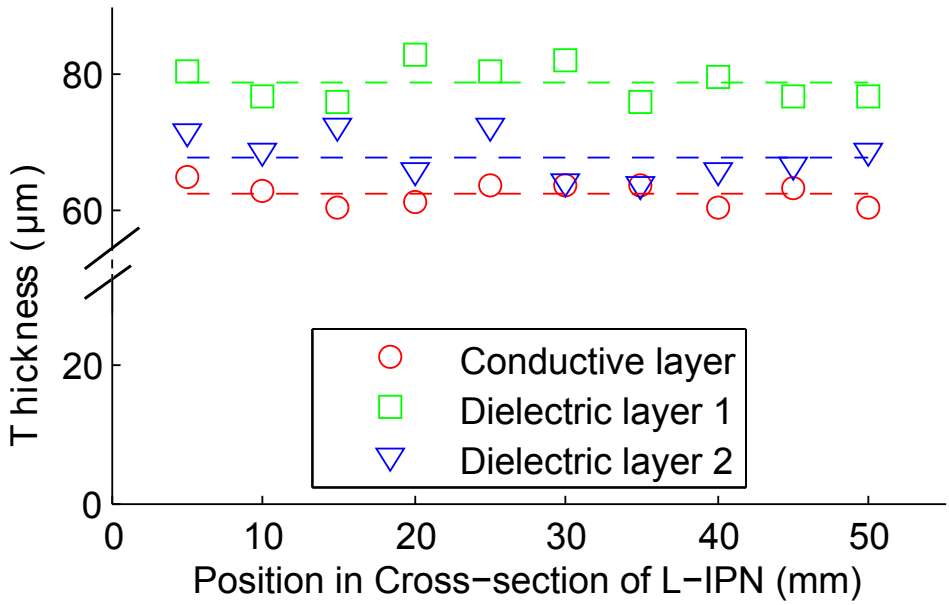

Figure 37: Meaurements of layer thickness uniformity from cross-section of L-IPN.

The L-IPN produced from the lamination method demonstrated global layer uniformity (Figure 36). The thicknesses of each layer were measured over the cross-section of a prepared sample. The conductive layer, dielectric layers 1 and 2, had coefficient of variance (CoV) of 2.55%, 3.23% and 4.87% respectively. These measurements demonstrated a consistent thickness profile, which is key to maximising the actuation potential of a stack. The conductive layer does show a markedly lower CoV, which may suggest that lamination between soft membranes may increase uniformity of a thin layer. It can be seen that the retained pre-strain is demonstrated by the reduced thickness of the outer (dielectric) membranes from the initial thickness. The initial silicone film sample diameter and the final relaxed L-IPN diameter were used to calculate the retained strain as 31%. The average thickness of the dielectric layer was 65μm when measured as part of the L-IPN, giving an initial thickness of 112μm. This was consistent when the measured laminate gap (based on a fully uncured lamination), was compared to the calculated

sum of layers using calculations demonstrated in Section 3.7.1. The measured thickness of the laminate gap was 130μm, and the L-IPN thickness was calculated as 158μm. The variation is attributed to local deformation of the elastomer as it passes through the laminator, leading to a thicker composite layer.

3.6.1 Mechanical Strength Characterisation of Multi-layer Structure

Stack actuators which will operate as a thickness mode tensile configuration, must stay mechanically linked through the cross-linking of the silicone. With any multilayer curing, where cured layers are bonded by the addition of an uncured silicone layer will cross-link. However, this bond is expected to be weaker than bulk cured material due to the reduced cross-linking between cured layers and the uncured silicone. Additionally in the process described in the L-IPN fabrication technique, the use of carbon in the silicone may inhibit the cross-linking. To test the maximum normal stress of the L-IPN, an hour glass mould (shown in Figure 38a) was produced using two conical segment moulds, allowing a circular sample of fixed initial area to be tested in a material testing frame. This allowed a defined cross-sectional area to be uniformly stressed. The test of a laminated structure showed an instantaneous failure when delamination occured.

(a) Tensile test of orthogonal lamination of silicone layers

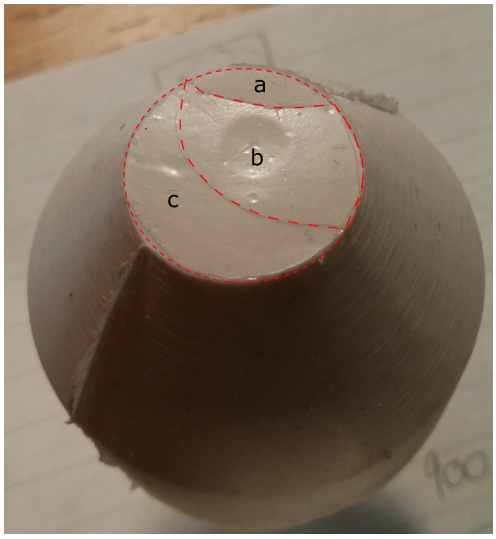

(b) Photo of delamination mechanical failure of orthogonal lamination silicone layer sample

Figure 38: Example Tensile Sample

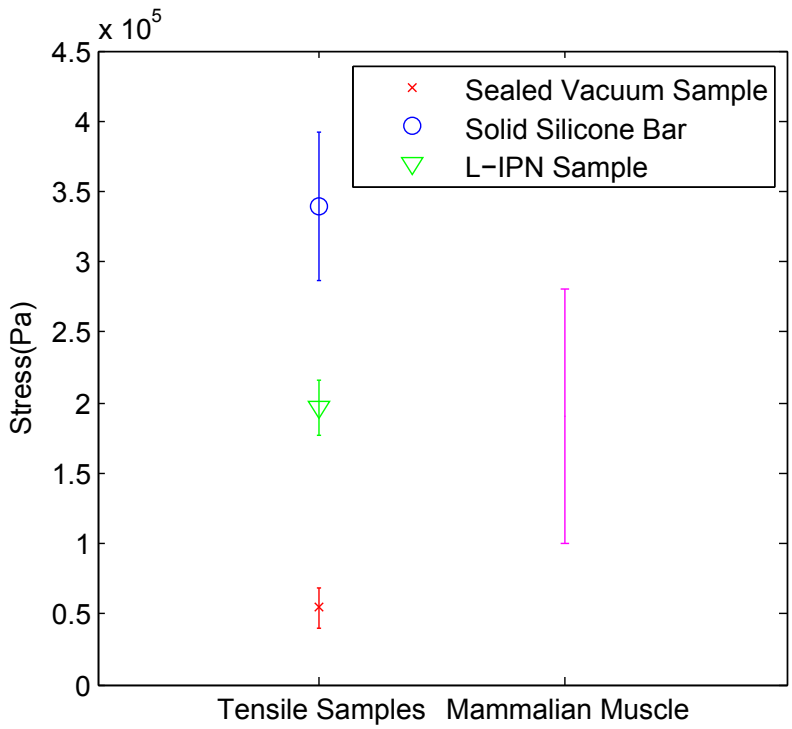

Figure 39: Experimental set up and breakdown of test sample.

It can be seen from Figure 38b that the L-IPN sample delaminated normal to the tensile force. The individual layers of the L-IPN are highlighted as a, b, and c which form the separate layers of the DEA. At mechanical breakdown, the layers separated and tore. The laminated sample was found to have a strong inter-layer bond with a peak stress of 200kPa, withstanding tensile stress in the same range as mammalian muscle (see Figure 39). The mould design allowed a sealed vacuum test sample to be created, by joining two conicals separated by carbon grease and sealing the edge with silicone. The vacuum sample gave a result in the region of the generated atmospheric pressure acting over the area. The results were slightly higher due to the presence of elastomer used to seal the mould. The solid bar, although degassed, was found to perform at an order of magnitude below the material specifications for Dow Corning Xiameter 3483, but was consistent over a number of tests. The mode of failure was tearing due to high surface stresses of the mould structure, which could have led to a lower value. This is also considered a cause for the lamination sample failure, as a small tear was found on the edge of each tested sample.

This section has shown that chemical bonding can be achieved between layers of dielectric and conductive silicone rubber. Additionally, it has shown that this bond is far superior to contact adhesion and vacuum suction, which have been previously used. The chemical bonding attains ultiamte tensile strength in the middle of the range found with mammalian muscle.

3.7 Multi-layer DE Actuator Implementation

3.7.1 L-IPN Stacking Techniques

The lamination process produces a uniform bonding layer, which provides a method of developing pre-strain and creating a self-supporting optimised actuator. The method can produce multi-layer actuators, however the method does have some significant limitations

beyond small numbers of layers:

- The process is time consuming involving multiple steps of capturing pre-strain, and single electrode layer curing per cycle (hence high layer number actuators would have high fabrication time).
- Lamination has inherent limitations in the number of layers that can be developed, due to the thickness of the substrate increasing as more layers are added, leading to increased deformation and error in layer height.
- The electrode patterning cannot be specified meaning that an alternative method of connecting electrode power lines is required.

3.7.2 Multi-layer Actuator Proof of Concept

In order to conjoin all of the performance characteristics found in the tests described, a novel method for producing a multi-layer proof of concept is required. The aim was to create a multi-layer actuator capturing pre-strain with compressed conductive silicone electrodes using thin silicone dielectric sheets. A process was devised combining earlier work on lamination with doctor blading and a more scalable stacking method.

Methods and Materials

To create samples, dielectric layers were created using the lamination method adapted for the formation of single layer thin uniform dielectrics. A thickness of 150 microns was chosen for the layers as this was considered sufficiently thick to handle, and thin enough to show the effect of the pre-strain on actuation. The dielectric layers were pre-strained and mounted on separable concentric circles which were stackable to form a multi-layer actuator. The aforementioned method for creating conductive compound was used to produce conductive silicone with a loading of 5% carbon black. The modified doctor-blading method was used to apply the electrode material to the dielectric, which involved

using a mask for the shape of the electrode, and a separating acetate sheet between the blade and the uncured material to protect the dielectric layer from tears and to form uniform layering. The layers were stacked and a three dielectric layer actuator was created using this method. Once the conductive layer was cured the actuator was released from the supporting frames, allowing it to contract and compress the conductive compound.

To test actuation of the samples, the multi-layer actuators were hung from a clip and the thickness measured through differential laser measurement. A method to calculate the blocking force was considered, however the device properties negated this option. As the actuator is soft and flexible, any external constraints would have to be attached directly to the actuator planar surface (as the actuation is thickness-mode), and would therefore inhibit the actuation by applying some extra stiffness. On a large scale blocking forces may be possible to extract, but the free measurement of actuation was considered the most effective test of the developed actuator in its present form.

The setup is shown in Figure 40.

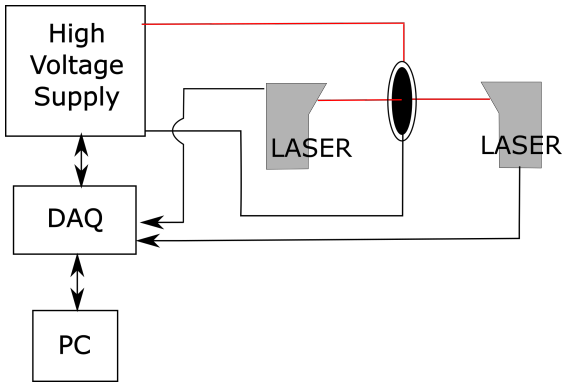

Figure 40: Arrangement of equipment for actuation test of pre-strain silicone multi-layer actuator

The lasers were aligned using a piece of paper - allowing the dots to be seen through the paper -, such that the laser dots could be centred reducing any measurement error.

The lasers were clamped symmetrically on a Thor Labs plate so that they were accurately aligned.

For the experiments the following equipment was used:

- DAQ - NI USB 8343
- Two Laser Units - Keyence LK-GD500
- PC - computer running MATLAB software

Strict safety protocol was used in the experiments, using an insulated test space and isolated high voltage supply. The setup is further described in Appendix C.

Characterisation

For the test sample, a pre-strain for mounting of 50% was used. Once the uncured conductive layers were applied, layers stacked and curing completed, the sample was released and the contraction measured. The resultant retained pre-strain was 29%. The overall thickness of the sample was measured a 0.7 mm thickness

The sheet resistance of the cured conductive silicone electrode on the surface of the actuator was measured using the 4-wire method. It was found to drop from 30 kOhms to 5 kOhms. This shows the compressive action of the dielectric causes a significant rise in the conductivity in the range of expected operation of the actuator. This clearly shows the benefit of the pre-strain on improving the conductivity.

The sample was set up as shown in Figure 41 and tested. As can be seen in the photo, although strain is retained in the silicone, the actuator is soft and flexible and requires no external structure. The resulting response from application of a high voltage was recorded and the maximal displacement response is shown in Figure 43.

Figure 41: Multi-layer sample actuator in situ for experimental test.

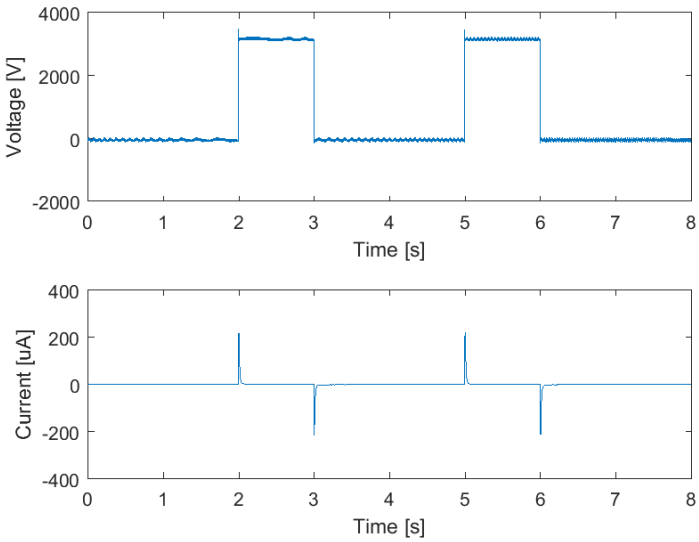

Figure 42: Actuator input voltage and current profile (3.2kV) for actuation test.

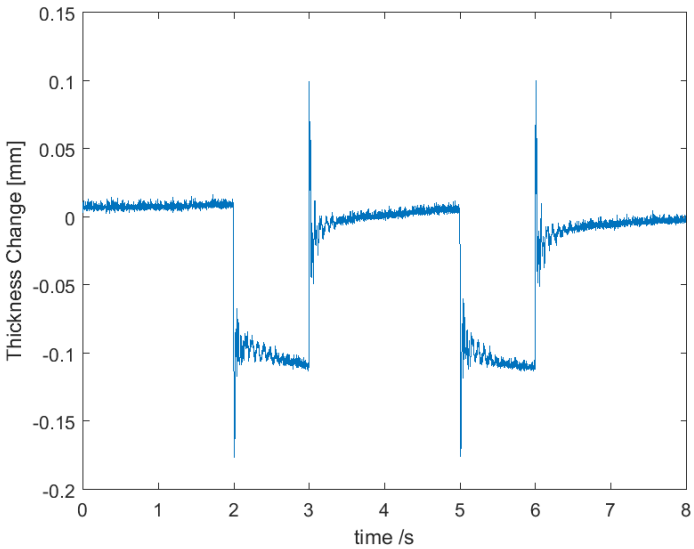

Figure 43: Differential laser actuator displacement response for 3.2kV input voltage actuation test.

From Figure 43, it can be seen that the actuator contracts by 0.11mm during each actuation cycle. The figure also shows some high amplitude dynamic oscillation, which was not directly observed during tests. On actuation (between 2-3 seconds), there is exponential rate of change decay observed as it approaches full displacement. When the voltage is removed (between 3-5 seconds) there is an exponential decay to equilibrium. Finally it is observed that there is some drift in the recorded thickness between the start and end of the experiment. To analyse these features in more detail the individual laser displacement measurements have been separated and plotted in Figure 44:

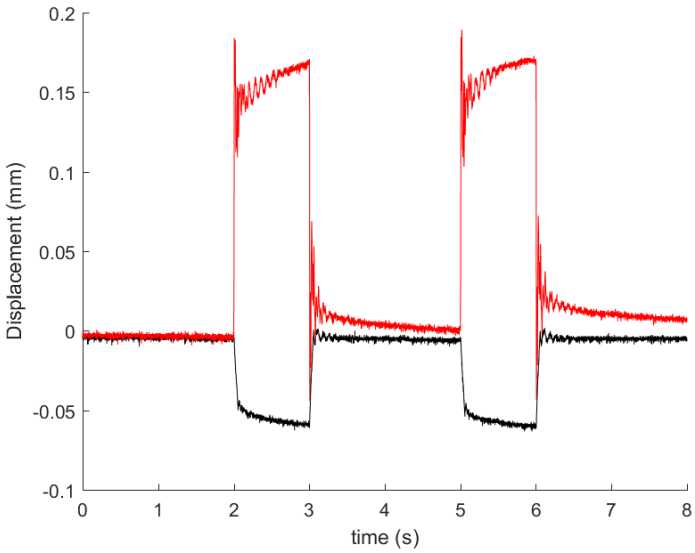

Figure 44: Individual laser displacement measurements

It can be seen that one laser signal in black is negative (meaning the actuator moved towards this laser). The signal shows minimal background noise, no continuous creep over the experiment, but does show a curve symptomatic of charging during actuation (a). The second laser signal in red is positive (meaning the actuator moved slightly away from this laser). The signal shows minimal background noise, shows symptomatic of charging during actuation (a), however exhibits oscillation on application of voltage (b), creep during actuation and global creep (c).

These three features can be individual analysed:

a The rate of change of contraction (measured by differential displacement) when charged and discharged would suggest the conductivity of the samples affecting the time constant of the conductive layer and hence the time taken to reach the maximum compression of the layers.

b The oscillation of the signal was not anticipated and was only observed at one side of the actuator.

- It is hypothesised it could be due to surface roughness affecting the point at which the displacement is measured. The near identical repetition in the cycles in both on and off states would suggest this is not the case.
- Intermittent connectivity of the outer conductive film on this side of the actuator could potentially cause this effect, where the contact resistance increases causing charging to stop, but this would not necessarily cause the negative change in displacement. However, the response does settle and the underlying signals rate of change reduces.

c To consider how this may have occurred, it is important to consider that the actuator was hung from a crocodile clip attached to a fix clamp. The lowest part of the actuator was connected to a free hanging crocodile clip. The top and bottom clips were the power supply (high voltage and ground respectively). A creep such as this could be caused by a slightly loose clamp and slight rotational slip of a component of the set up leading to the creep.

After testing the sample a cross-sectional microscope image was taken to show the internal uniformity of the actuator (see Figure 45).

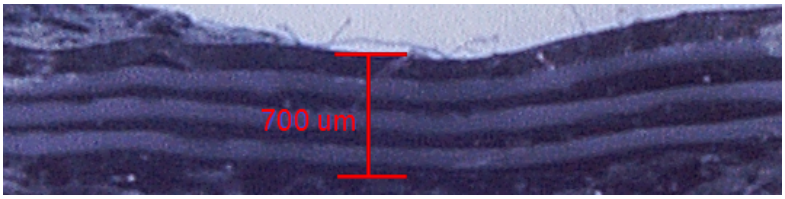

Figure 45: Microscopy image of slice cross-section of actuated pre-strained LIPN multilayer actuator.

It can be seen from the response, that the actuator had a significant change of thickness based on it's initial thickness of 0.7 mm. This is a resulting thickness contraction of 0.11mm giving a 16% strain which approaches the range of strain found in Mammalian

skeletal muscle of 20-40% [Carpi et al., 2007]. This was achieved using a method which involved retained pre-strain in a completely soft layered actuator of chemically bonded material of the same base silicone. However, a contractile actuator of 0.7mm thickness is still too thin to be useful for muscle-like actuation systems.

Comparing the strain developed by the tested sample with other multi-layer actuator works, the resulting output recorded is significant. Maas et al produced a contractile strain of 3% with a silicone DEA [Maas et al., 2015]. An acrylonitrile butadiene rubber (NBR) is created producing 10% contractile strain with a 50g mass applied [Nguyen et al., 2014]. Kovacs et al produced an acrylic stack with a maximal contraction of 46%. The final outcome of this experiment is a significant thickness contraction in a bonded multi-layer stack actuator.

3.7.3 Automation of L-IPN Stack Fabrication

The multi-layer bonded stack developed in this Chapter has shown a contractile strain on actuation of 16%, however, although proving the principle, the scale of the actuator is still too small for high power applications. To expand upon the prove concept of an inherently soft-bodied silicone stack actuator with captured pre-strained, a method of increasing the scale of the actuator was investigated.

Some research groups have developed semi-automated stacking systems for unstrained stacks (see Section 3.2.1). To produce a high-power actuator the current manual process of stacking needs to be improved to enable actuators of increased layer numbers to be produced, whilst harnessing the benefits developed. Automation of fabrication is critical due to the high number of layers (in the order of 100's) required for a large scale actuator. Additionally, the processing of thin films and the detailed patterning required to be precisely located relative to preceding and subsequent layers require an accurate forming mechanism.

The required stacking system is envisaged to produce stacks on a similar scale (in

terms of layers and diameter) to those produced in other groups (in the order of 100's of layers), whilst also enabling the production of pre-strained stacks using the L-IPN method. To do this certain criteria must be met:

Precise Placement - Accurate layer-to-layer placement aids efficient actuation through the alignment of electric field between sequential electrodes, across the dielectric layer . Considering actuation, at a voltage of 5kV, arcing can occur through air over a distance in the region of 5mm (hence a margin of 2.5mm required). However, to maximise actuation, the margins must be kept to a minimum, and as a result there is a need for accurate placement to reduce inefficient margins, yet avoiding arcing.

Scalable - The system must be able to stack a large number of layers in a single 'run', which should be repeatable through additional 'runs' to create joined units.

Pre-stretch - The layers must still be able to be pre-strained prior to stacking, to include the benefits discussed.

Multi-layer Stacking Rig

To consider a method of stacking, the principles that allowed the proof-of-concept actuator to be developed were considered. The layers must be supported (to capture pre-strain), stacked such that the gap between dielectric layers is minimised to the thickness of the conductive compound. This limited and focussed the design constraints of a mechanism. A concept was developed using a three-screw mechanism, which could lower membrane (which were attached to a ring of supporting substrate to maintain prestrain shown in Figure 47) on small tines whilst aligned by three sets of 'teeth' onto a central support plate. When all three screws were rotated in unison, the membranes could be lowered and deposited on top of each other. An initial model was constructed to test whether the stacking method devised was viable (Figure 46).

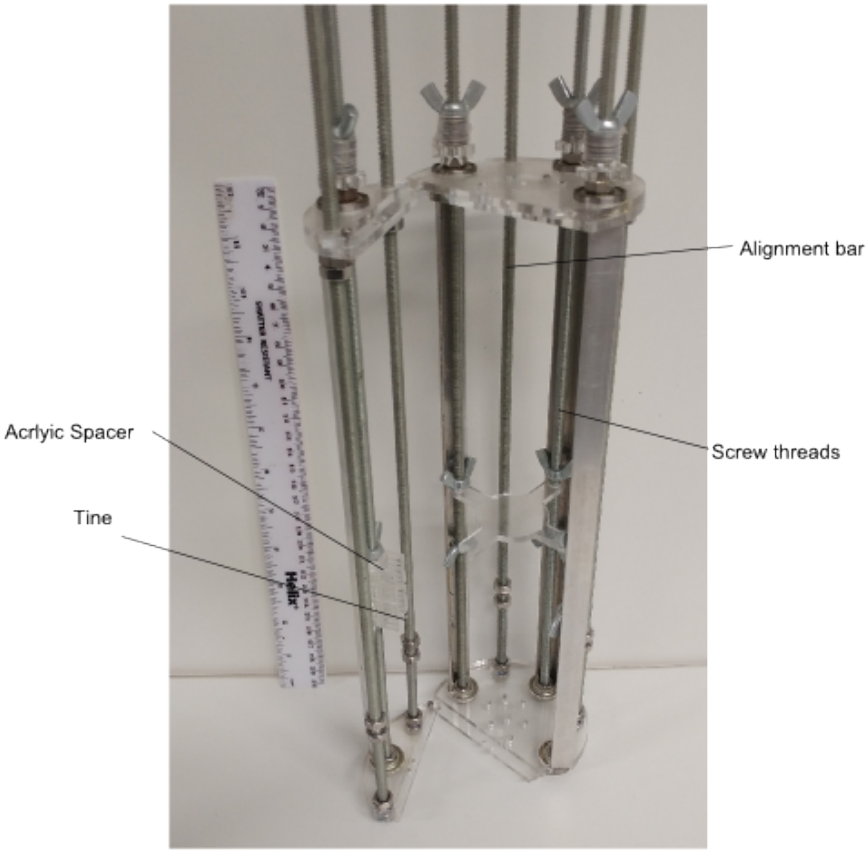

Figure 46: Prototype Stacking Rig Iteration

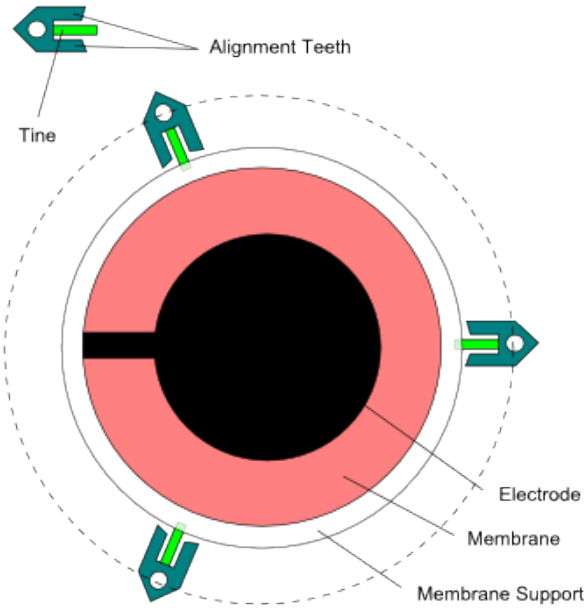

Figure 47: Illustration of arrangement of components for stacking layers.

The mechanism operated, but had the following issues:

- The mechanism was found to be too constrained in its design.
- There were reliability issues due to the materials used for the alignment supports (3mm acrylic) , which were too brittle for the purpose.
- Misalignment was found due to the alignment teeth being too inaccurate.

A new model was created in CAD using the lessons learned from the first iteration.The design was created to fulfil the criteria listed, and to allow for a large film size (up to the limit of the spin coating equipment). Plates (shown in orange) form separators of sequential disc layers of the actuator*. They have grooves design to allow tines, which support the layer to bend out of the way as the disc is lowered onto a central plate

*The individual actuator layers are prestrained and the uncured electrode applied in the same way as in the L-IPN multi-layer proof of concept

shown in pink in Figure 49. As the tines bend away the layer is deposited on the plate. This happens repeatedly until all layers are deposited accurately on top of each other. The discs are left to chemically bond before the stack is removed.

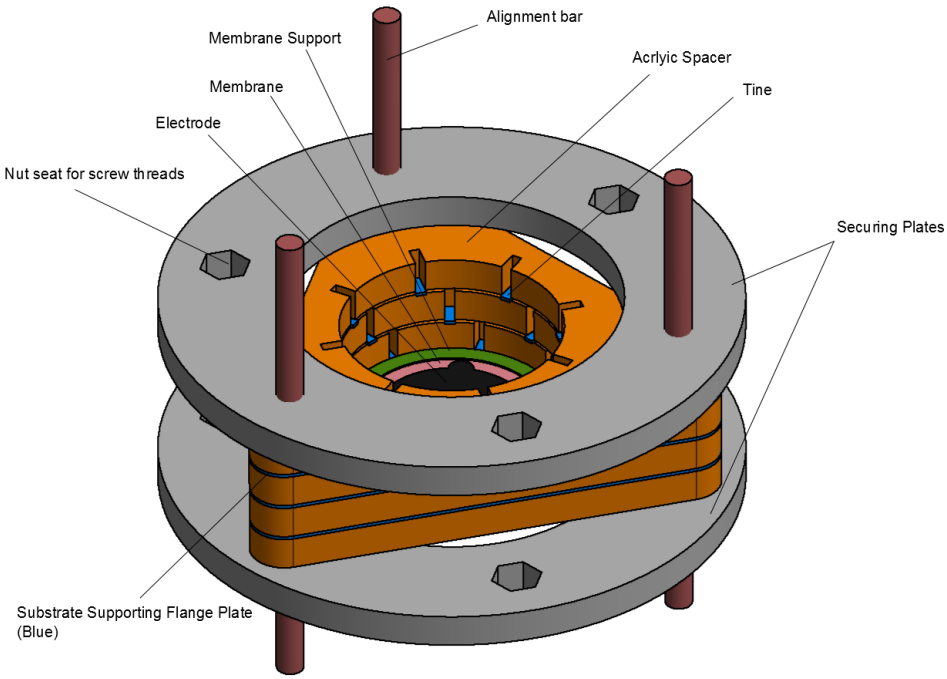

Figure 48: CAD drawing of arranged components for conceived stacking rig.

Improving on the first iteration involved a less structurally constrained design which was used to allow easier stacking, along with an improved spacer and film support mechanism allowing the reduction in misalignment on placement found on the earlier model.

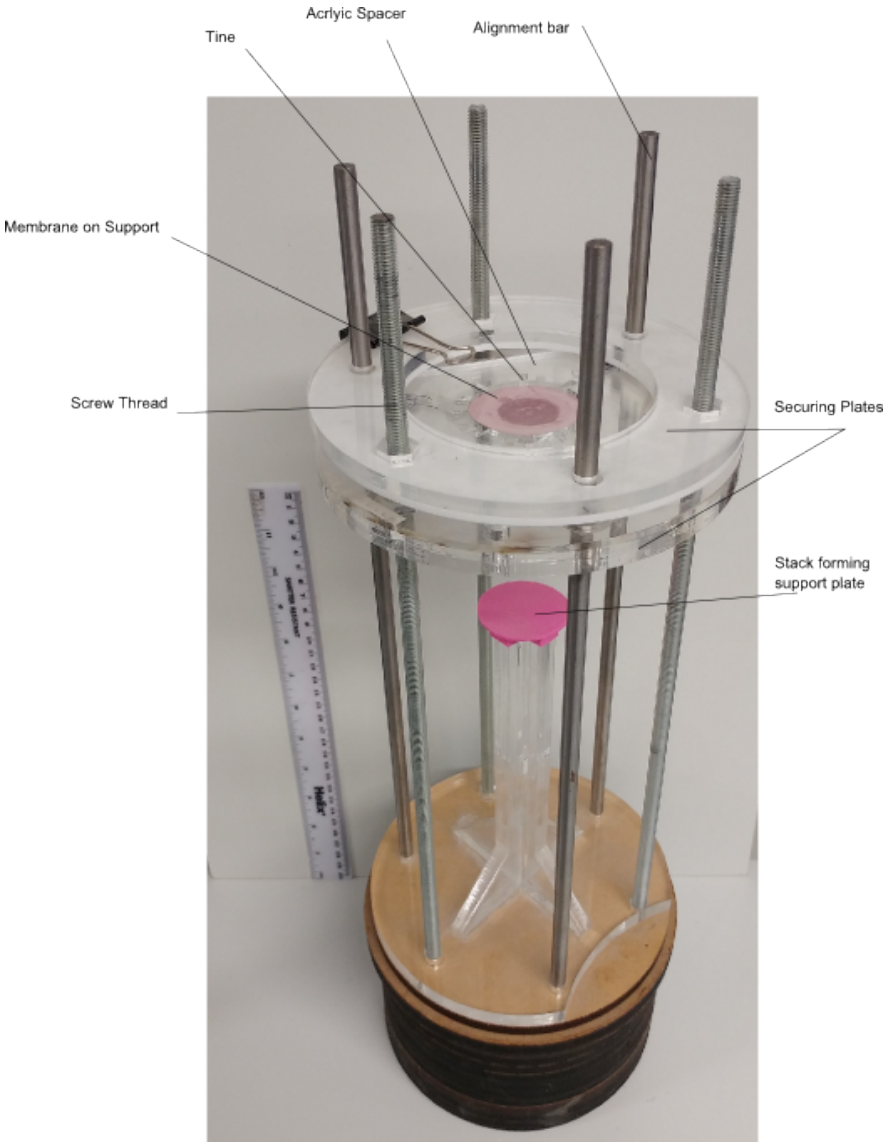

Figure 49: Complete prototype stacking rig.

Key Features:

Bendable Flange Plate - The flange and spacer are designed to fold out of the way allowing the membrane to settle accurately on the disc below, whilst exerting minimal force on the forming stack.

Uni-directional Stacking Mechanism - The flange and spacer are designed to sup-

port the individual film discs and hold them apart until deposited on the stacking column (Shown in Figure 48).

Scalable Design - The fabrication rig is designed to accept thin films up to the maximum disc size of the spin coater (120mm diameter), maximising the potential of the rig. This allows for more complex designs including more than one discrete actuator to be included in a single stack.

Support Discs - In the laminator rig, the L-IPN required a temporary substrate to maintain the pre-strain. With the stacking rig this is required for all discs to allow the manipulation required to apply a patterned electrode and to be adequately supported for uniform layering. A hollow disc is used to support the membrane, whilst allowing bonding to both sides of the dielectric.

Issues to Resolve:

Consistent Bond - Contaminates (chemical or particulate) can lead to poor bonding reducing the overall bond strength, maintained pre-strain, and electrode contact area for actuation. Air bubbles, for example, will significantly affect bonding and hence maximum tension stress and potentially actuation. An issue with effective bonding between layers during curing has occurred with subsequent stack outputs, following a successful first run (Figure 50). Potential causes include:

- Temperature - Either external or insufficient exothermic output of small quantities of bonding material.
- Inhibited chemical bonding - expired silicone active compound, or nitrogen compounds blocking cross-linking sites.

Figure 50: Photograph illustrating the nature of peelable inconsistent bonding between layers encountered.

Precise Repeated Electrode Patterning - To enable actuation each electrode layer must be patterned to include a connection to a voltage terminal. The patterning must be precise to allow the maximisation of effective electrode area. A pad-printer has been developed to mitigate this, but other methods of using a doctor blade, and spray deposition are still being investigated.

Automated Stacking Resultant Sample - The stacking rig operated as desired and has been used to produce a prototype actuator stack (Figure 51) using a non-conductive secondary bonding material, and a doctor blade material application technique. A non-

conductive bonding material was used as a temporary measure due to the unresolved issues described causing problems with the stack fabrication. It is considered however, once these problems are resolved, a conductive stack can be produced using the same method.

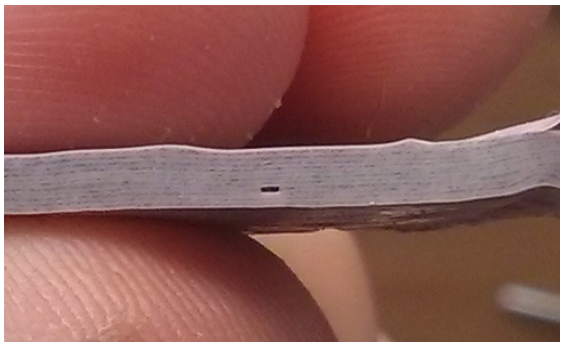

Figure 51: Prototype stack cross-section consisting of 16 dielectric layers fabricated using stacking rig.

The uniform laminations can be clearly seen and when viewed under a microscope (Figure 52) can be seen to be achieving a similar level of uniformity to the original lamination method. The layers are shown to be repeatably less than 100 microns thick. In Figure 51 a large air bubble can be clearly seen. This was anticipated as the prototype was not created in a vacuum. This reinforced the need for an air free environment for stack fabrication.

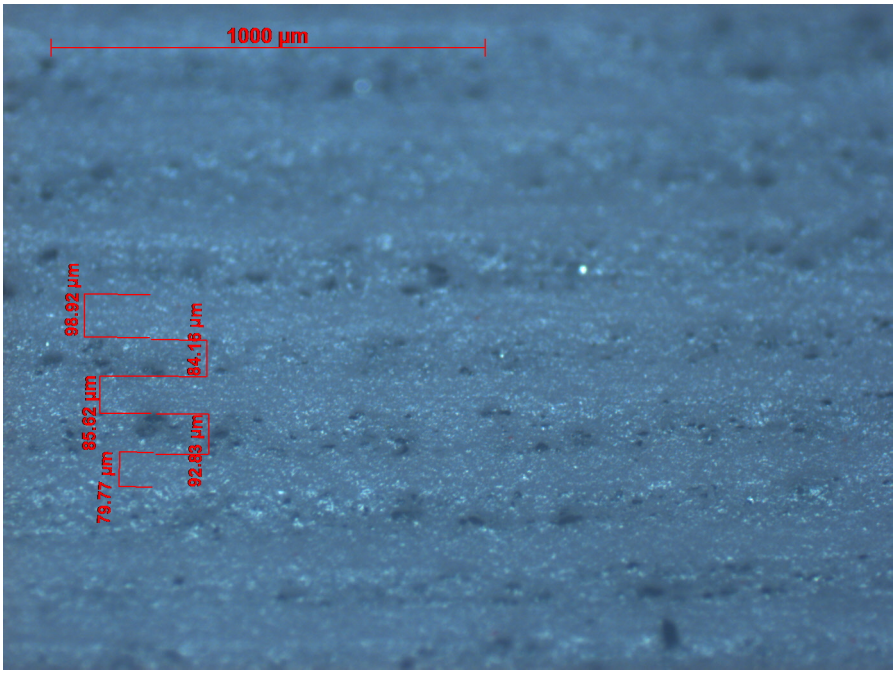

Figure 52: Microscopy image of prototype stack in sliced cross-section showing layer thickness consistency and uniformity.

3.8 Summary

This Section has covered a large number of innovation steps in design and fabrication, which have culminated in the production of a method to produce a high-performing pre-strained chemically bonded wholly silicone actuator, in a process that, at least in part, can be automated.

The investigations in this chapter have given rise to the following results:

1. *Dielectric layer performance.* Dielectric layers were developed using a fixed aperture lamination method and spin coating. The lamination fabrication system created was able to produce repeatable, thin and uniform dielectric membranes. The layer thickness was specified using shim spacers, but was also affected by the substrate layers between which the uncured silicone was squeezed. Layers of a thickness in the region of 100 microns were produced with a uniformity and a CoV for

all layers of below 5%.

2. *Conductive layer performance.* The investigation and experimentation of materials, fabrication methods and innovative ideas led to development and characterisation of a conductive soft silicone composite for electrode material. A method of producing replicable uniform silicone layers was developed and used for dielectric and conductive layer fabrication. The conductive silicone was characterised with varying parameters of straining, carbon weighting and layer thickness.

3. *Development of novel L-IPN Method.* Interpenetrating networks have been previously developed to capture pre-strain solely in the dielectric membrane. The lamination method and strain capturing innovation put forward in this chapter uses the conductive layer (in the form of a silicone composite) to capture the pre-strain, whilst compressing the conductive compound (aiding maintenance of conductivity with strain) and bonding the layers together forming a single silicone body.

   In this chapter the following results were attained with L-IPN:

   - Capturing of pre-strain - A strain of 31% was captured in a two dielectric layer LIPN, proving that strained dielectrics can be supported in a soft structure. Expanded on the lamination method to include the capturing and retention of pre-strain within dielectric layers, allowing them to perform with improved prestrain characteristics as developed in single layer actuators
   - Conductivity was shown in strained layers of carbon black - silicone composite. A trade-off between stiffness and conductivity led to the selection of a 5% weight filler mix, delivering a resistance of 8.3kohms with a Youngs modulus of 4.1kPa.
   - Confirm tensional loading in active and passive states in the range of that

found in mammalian muscle could be attained using laminated bonding techniques.

4. *Multi-layer bonded actuator with captured pre-strain.* Developed an alternative method of stacking layers using concentric supporting rings to retain pre-strain whilst multiple layers were cured together. A thickness mode strain of 16% was produced in a proof of concept sample containing three dielectric layers.

5. *Multi-layer actuator fabrication and characterisation* Due to the limitations of lamination for multi-layer stacking, the a new method evolved for creating multi-layer actuators with captured pre-strain using a stacking rig. The pre-strain of the dielectric could be temporarily maintained using a supporting substrate and a method called doctor blading was used to apply a conductive layer. Using a vertical stacking rig enabled these layers to be aligned and placed on top of each other forming a multi-layer device. The method allowed the bonding of pre-strained dielectric layers with conductive silicone, which captured the pre-strain once cured and could be released from the supporting substrates. A demonstration stack actuator with 16 dielectric layers (each of 100 micron thickness), bonded together, was produced using a developed multi-layer stacking rig and analysed.

The resultant proof of concept actuator and automated stack output show the feasibility of producing a stack with improved characteristics using a semi-automated process. This resulting multi-layer actuator is soft and flexible and mimics the actuation of biological muscle.

4 Multi-stable Soft Actuator with Rigid Position Control

4.1 Introduction

In the literature review (Section 2.10), the mechanical design space in which DEA actuators operate was discussed. Many implementations of DEA systems (robots and devices) have some compliance due to the DEA being directly coupled to the output [Carpi et al., 2007]. If the output of a DEA could be made more rigid - even for short periods of time - they could form a useful form of actuation which would overlap with existing technologies. Whereas DEAs are inherently soft, a large proportion of actuators need to operate with interfaces involving rigid components. This has led to DEAs being limited to use in soft body technologies, or in systems where they are directly linked to a substrate that reduces the potential for any reliability issues or failures. In this chapter, soft actuators in coupled systems will be considered for use as control actuators in rigid blocking systems. Generally blocking actuation technologies - existing and in development - require enabling technologies such as lightweight valves or locking mechanisms. For example, pneumatic systems require valves for flow control. In smaller (and in some cases soft systems), these control actuators need to be lightweight, responsive, and efficient. This type of task is an application that DEAs can be used for, where - when suitably designed -, the features of fast response can facilitate power output control.

It is proposed that the relaxation work, produced by the application of electrostatic force to a dielectric membrane, can be harnessed to deliver a number of useful motion modes which can be applied through a rigid framework to an external body. Modules created in this form could be used to replicate the function and, in some application under requirement constraints, replace conventional rigid actuators. To achieve this goal, methods of maximising power output and energy efficiency will be explored, whilst considering how to ensure reliable repeatable actuation in a usable form for real world application in a rigid system.

The aim of this Chapter is to develop a method to couple lightweight, efficient, and high-energy density soft DE-actuator membranes to a robust and controllable stiff output end effector, while mitigating or limiting the effects of the inherent electromechanical instabilities and failure modes of DEAs. Additionally it will require the development mechanism work over a range of scales (from millimetre to decimetre. In more detail this involves demonstrating that a scalable mechanism can be developed that can be powered by a DE-actuator to perform a range of applications including low energy miniature actuators (such as braille pins) and larger designs (individually such as lock-pins or in arrays such as dynamic surfaces). The mechanism should provide a non-back-drivable output, which will enable control of movement and ability to withstand intermittent high loading forces at end effector. The project aims for the mechanism to use bi-stability principles to increase energy efficiency of the device whilst ensuring isolation of the soft - and hence potentially fragile - part of the device from the rigid end-effector. This will create a a controllable bi-stable (and potentially a multi-stable) output device from a thin film actuator in a linear displacement configuration. Through the variation of the supporting structure design, and assembly of a connecting mechanism, these modules can be used to replicate or extend the performance of conventional rigid actuators.

The key performance criteria to be met in this chapter are:

1. Development of a lightweight efficient mechanism to transfer the energetic input of the DEA to a specific pin-locks.

2. Provide non-back-drivable with low energy consumption.

3. Create a compact actuator design that is scalable.

4. Expand the operation to include a variety of output formats for a range of applications.

To meet these criteria there are a number of targets to be met:

- Minimise the weight required to produce a useful output to meet concept criteria.
- Maximise the energetic output of the actuator per cycle.
- Enclose DEA actuator to make it resilient and hence reliable.
- Minimise energetic losses in the mechanism.
- Design a novel mechanism that can deliver the required outputs potentially in a range of formats.

4.2 Finite Displacement Actuators

To consider how to use DEAs most effectively for this purpose, the possible forms it can take will be analysed. Generalising this class of actuators, a set of desired characteristics can be extracted:

- High blocking force - The device must be able to hold its position once set.
- Low energy consumption - The device should require minimal energy once set in a control position.
- Fast response time - An input stimulus to alter position should be acted on quickly.
- Fast cycle time - The time required to reset or perform multiple full cycle repetitions should be as short as possible.

Evaluating these target characteristics, it is considered possible for the device attributes to be replicated by the design of a specific class of DEA system. To achieve this however, the method of application of forces from a soft membrane to a rigid structure would have to be addressed. It was realised that a possible solution could be devised through utilising minimum energy states and an arrangement that had a stiff output end-effector.

4.3 Mechanical Output of a DEA System

The use of soft actuators in real world applications has been relatively limited and focused mainly on soft robotic implementations [Gu et al., 2017a] and fluidic applications [Carpi et al., 2010a, Chiba et al., 2008], due to the inherent flexibility of the actuator used. The pairing of actuator and application has led to devices which cannot be created through the use of conventional actuator technologies (i.e soft pumps, pneumatic actuators, inchworm). The tendency to use unconventional actuation methods for these tasks has advantages over the conformation of the task to conventional actuators (motors or valves etc). Soft actuators can, not only be used to power inherently flexible devices, but can be used for manipulation of rigid structures. Complimenting soft materials with hard frames/structures can enhance the resilience and increase the reliability of soft actuator powered devices. A comparison found in nature are arthropods, which possess an outer shell which can be articulated with soft muscular tissue to provide external forces, but provides a dual purpose as a protection to the delicate organic structures contained in the outer shell. This creates a rigid interface with external objects protecting the soft muscles used for actuation.

DEAs are highly nonlinear in their electromechanical operation and have multiple failure modes. Hence, they require a safe working region of operation in order to maintain dependable actuation, which does reduce the maximum strain of the DEA. The strain can be used in different arrangements to produce useful output as discussed in Section 2. To maximise the power output of an actuator the force and displacement of the actuator must be maximised, as well as the cycle time of the device. The cyclic strain of an actuator is dependent on a number of material and control parameters. Some elastomers will provide a higher power output even though they have lower strain due to their superior cycle time.

DEA implementations have been popular in inherently soft systems or systems with flexible structures [Carpi et al., 2007]. The advantageous characteristics are not uniquely

useful to robotics but across mechanical systems for active damping, yet in robotics the actuators are limited in their use by their resilience to external interactions. This is in part due to the inherent material properties enabling easy coupling to soft structures, but also due to the complexity of developing a rigid output from a delicate actuator. Some configurations such as antagonistic cone pairs allow semi-rigid end-effectors to be controlled by a DEA* [Nguyen et al., 2017].

Rather than solely considering actuator configuration, some works have exploited the characteristics of DEAs when paired with with rigid support structures for rigid mechanical output. One novel exploitation uses segmented actuation to control movement of a soft orbital gear around a central geared shaft to elicit rotary motion and produce a DEA motor [Anderson et al., 2011, Tse et al., 2011]. This motor can easily suffer from slip due to the inherent elasticity of the drive gears mounting on the DEA (shown in Figure 53).

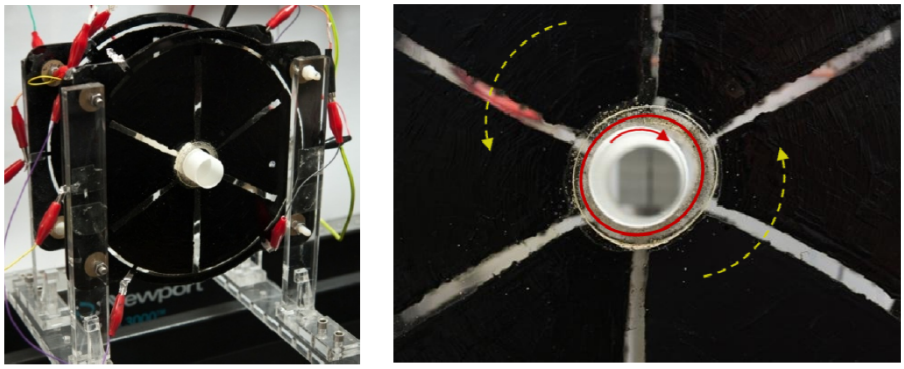

Figure 53: Flexidrive prototype rotary drive (reproduced from [Tse et al., 2011]).

Another novel device uses DEAs to shift a central mass, altering the center of gravity generating a rotation which can move a wheel and allow self commutation [Rosset and Shea, 2015]. This device could have applications as a vibrator motor using the resonance of the mass-spring dynamic system. However, there is no easy method

*the cone end-effector is considered semi rigid, as although a hard component interacts with the external environment, it is mounted on a DEA that is inherently flexible

to output the energetic motion generated for controlled displacement.

Both of these examples do convert the work done by the DEA into a useful output, through some rigid coupling, but in both cases, the inherent flexibility in the actuator can have a negative impact on the performance. These are not implemented in a form where there is a rigid end-effector and fixed position control. This is a key area that is currently underexploited in the actuation unit body/end-effector vs actuation stiffness space as discussed in Section 2.10. Hence, this Chapter aims to explore the potential for using DEAs in this way. Evaluating systems which provide bistable fixity, a key characteristic of valves and many applications of this class of actuator is the discrete application of force, where the device is required not only to provide enough energy to manifest state change under limited load, but hold position in the end states.

Defined State Transition Pathways - In Section 2, some examples of discrete state-space mechanical systems are discussed with reference to minimum energy actuation. It is shown that bistability can be used with the DEA technology to create binary robots that use minimum (or zero) energy states. The utility of such an output is clear in many applications using popular electromechanical actuation methods (i.e. switches, valves [FISHER, 2005]), and novel applications (i.e. self-deploying lightweight structures [Araromi et al., 2014]) which are made possible by specialised design of DEAs in flexible structures. To develop such a system using soft actuators would enable the beneficial features of DEAs to be exploited - the lightweight, fast response time, and efficiency in a rigid frame.

4.4 Coupling Soft and Stiff Sub-Systems

DEAs have outstanding operating characteristics and closely resemble the mode of operation of biological muscles, and as such are an excellent technology for replicating biological work. Using biological and other design inspirations, their uses include a

broad array of applications requiring lightweight, compact and soft structures. Many of the applications explore and optimise the soft and elastic characteristics of this actuator type, as the primary driving force in the formation of concepts. The actuators' soft and elastic structure does not have to limit it to operation devoid of rigid bodies or interactions. Unconstrained rigid bodies do have the potential to cause physical damage to the dielectric or conductive layers, but in a well designed supporting and containing structure the actuator can be used to produce a useful rigid end-effector mechanical output using some coupling method (such as a rod or strut as found in the DEA antagonistic cone configuration).

Soft components - in artificial muscles or limbs* - tend to be less resilient to point loads from interactions than stiff or rigid components. There are a plethora of benefits from using DEAs including weight, efficiency, response time and other application specific factors. Crucially, DEA materials currently available are soft so that the material can be highly strained for optimal performance; thus this property must be maintained. To consider using DEAs to provide energetic output to rigid systems, the resilience of the actuator must be addressed. The actuator performance should not be heavily compromised by the system, but the reliability of the actuator must be significantly increased, and the output should have rigid position control so as to hold position under loading.

One possible solution investigated alters the actuator material properties to increase the actuators structural rigidity enabling it to hold a specific state as demonstrated by Rossiter et al [Rossiter et al., 2010]. A material that acts as a DE and SMP -Shape Memory Polymer - is put forward forming a bimodal actuator. As a result zero energy fixity is generated after actuation. The design does leave the fragile actuator exposed however, and due to layering, affects the performance of the DEA. Additionally, the use of SMPs may significantly limit the time to fixity and the frequency of actuation due to

*Artificial muscles and limbs reflect the common replication or influence of biology in soft robot design, but robotic terminology would normally be actuator or link (and/or end-effector)

the heat cycling required for effective operation. Figure 54 shows the proposed design state transition diagram.

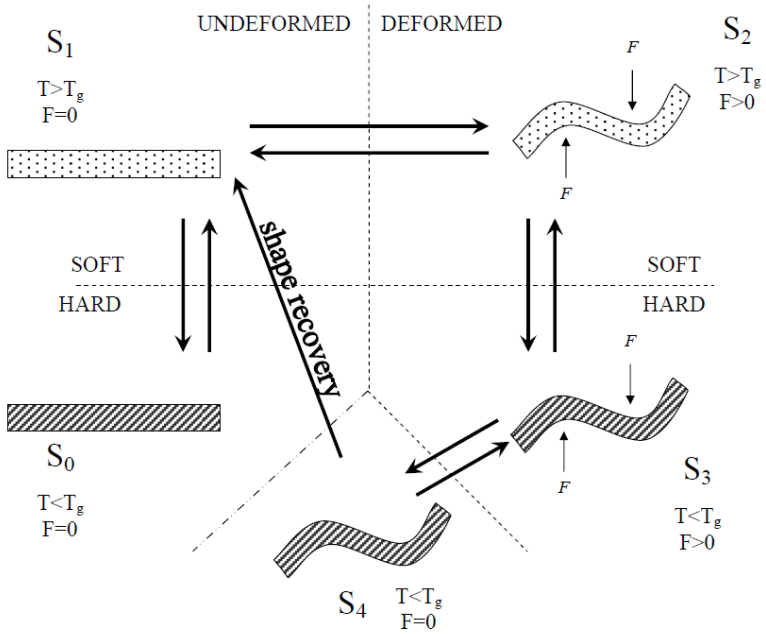

Figure 54: DSMPA - Dielectric shape memory polymer actuator - state concept transition illustration. (reproduced from [Rossiter et al., 2010])

DEAs, as mentioned are relatively fragile (see Section 2.2); any damage to the dielectric will cause the actuator to fail with few exceptions (self-healing has been shown in some DEAs [Yuan et al., 2008]), and the actuator would be irreparable if perforated. A similar mode of failure is found in batteries, which suffer from high energy failures on puncture. To counter this, batteries are encased in a rigid external structure, yet can still fail through external impacts. A protective skin or structure could be used likewise to protect the DEA, but this may impair the primary function - the DEAs actuation.

4.5 DEA Stable State Actuator Concept

The ideal solution is to produce a device which would use the minimum energy required to change between a number of stable states and provide an infinite blocking force at an

end effector, whilst consuming zero energy to hold position (i.e. zero energy fixity). The previous works discussed have focused on different aspects of these principal characteristics. To produce an improved system with this combination of features, other aspects of the system were considered. In DEA systems, a structure is required to support DEAs in many forms to provide optimal performance. This structure could also be used to provide some function through mechanical dynamics. Whilst reviewing popular systems for valves it was found that in some cases external mechanisms were used to convert a motors rotational output to mechanical translation to block flow [FISHER, 2005]. This transfer allows for the torque and hence force generated to be altered through the gear ratio. Other mechanisms may be able to be utilised to facilitate better transfer of work.

4.5.1 Ratchet Mechanisms

So far current state-of-art research on fixated resilient end-effectors able to translate between states has been limited to a small number of examples [Rossiter et al., 2010], although bistability has been explored in a broader set of research works. However, these implementations exhibit some significant performance drawbacks, from response time to fixed state position control. To try to further the development of fixed position bistability using DEAs, another possibility was considered; mechanisms. Mechanisms can be used to convert translational to rotary motion and vice versa, or produce a combination of the two. They can provide gearing to increase force/torque, while reducing displacement and ideally conserving input energy and outputting the work in the mechanical form required, however there are necessary losses in the system due to friction effects. Depending on the requirements of the application, this cost can be borne for the additional benefits the combination of actuator and mechanism provides. Hence, developing the actuation strategy and matching it to the system is essential for optimal performance.

Considering a mechanism for converting DEA displacement, output rotational devices have been devised but they do have drawbacks, such as slip and active membrane

area maximisation. Translational actuation has been used in a direct-drive format for a large number of systems, but it can also be used to drive a mechanism. In this way, the actuator can be physically separated from the external environment and encased. Additionally, the output can be adjusted to maximise performance for the task through variation of the mechanisms characteristics.

In servo motors, gearing is used to produce high torque output from a low torque high speed motor. The design of efficient gear mechanism, can be advantageous in terms of maximum power transfer efficiency and stall torque. Servo motors can be considered non-backdrivable due to the high torque required to reverse the gear ratio employed. Analogous to this gearing of a stepper motor, the mechanism proposed is non-backdrivable.

Combining the ideas described above, the functional objective is for the mechanism to convert the active elastic translation of the soft artificial muscle to a rigid position controlled output. With this in mind, an exploration of possible mechanisms was undertaken [Sclater, 2011]. It was discovered that fixity could indeed be introduced, controlling the movement of the end-effector due to directional forces, through the specific design of interactions of the mechanism, whilst enabling state change. A mechanism that fulfilled the purpose is an indexing barrel cam mechanism which can be adapted to provide multi-state fixity based on a translational input.

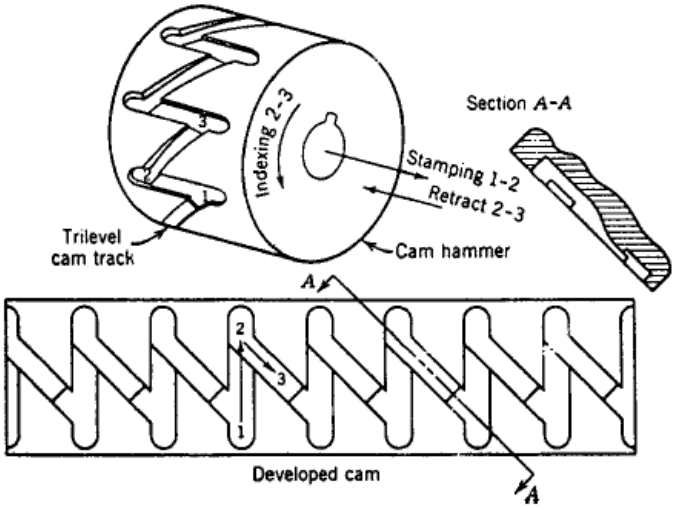

Figure 55: Exploded view detailing a design of an indexing cam (reproduced from [Sclater, 2011])

In Figure 55, the rotationally locked cam slides up and down a shaft, while a pin travels between cam track levels, creating uni-directional travel. This enables the pin to rotate in steps controlled by the translation of the barrel cam. A mechanism similar to this would enable the translational motion of the DEA to be converted into rotation. The control of the pin travel could also enable non-backdrivability.

4.5.2 Actuator Configuration

The actuator is the sole source of energetic input to the system and as such, its performance limits the output of the actuation mechanism. The particular configuration of the actuator can be used to enhance the actuator. The chosen configuration will inform the design of the supporting structure. For the design of a system using a soft actuator to drive a rigid end effector, some method is required to link the rigid mechanism to the soft DEA. For this to occur, a controlled displacing rigid point is required. From earlier discussions on DEA actuator configurations, it can be seen that an out-of-plane actuation mode is advantageous. A rigid connection point is preferable so that the membrane

is protected from potential damage from the interaction. For the electro-mechanical system to work optimally, the energetic output of the actuator is critical. A number of parameters characteristic of the configuration type can be used to classify and compare possible actuators for the required task.

Parameter	**Antagonistic DEA Cone**	**Antagonistic DEA Hydro-stat**	**Multilayer DEA**	**Planar DEA Motor**
Force Output	Low/Medium	Low/Medium	High	Low/Medium
Output Stroke	High	High	Low	Medium
Degree of Freedom	Translation	Translation	Translation	Rotation
Output Interface	Rigid	Soft*	Soft*	Soft*
Operational Reliability	Medium	Low	Medium	Medium/High

Continued on next page

*The interface can be made semi-rigid through reinforcement

Parameter	Antagonistic DEA Cone	Antagonistic DEA Hydrostat	Multilayer DEA	Planar DEA Motor
Coupling	Solid Rod	Pneumatic	Solid Soft Elastomer	Solid Gear
Resilience	Translation	Translation	High	Low (Slip)
Ease of Optimisation	High	Medium	Low	High

Table 11: Tabulation of comparison of actuators matching concept desired parameters

Numerous actuator designs could be considered and used for this system (shown in Table 11), but as discussed in the literature review (Section 2.6), each configuration has relative strengths. Specifically, cones seem to offer the best match to the desired function, hence this was chosen as the actuator configuration for this novel system.

Although the actuators all use passive and active elements to enable useful work output from the relaxation actuation of the dielectric elastomer, some can be enhanced by duplication of actuation in the opposite direction. This is a useful benefit of DEAs, where the passive element at one point of operation can be activated in another point. The antagonistic cone benefits from the ability for two active zones, enabling the increase of displacement control through sequential actuation.

4.5.3 Multi-state Actuator Concept

From the analysis above, for this application, the most usable energetic output is attained through an antagonistic cone pair producing a translational output. The pairing of the DEA with a mechanism can be advantageously used to lock the actuator position and hence fix the end-effector. Furthermore, at its most fundamental level, a mechanism can be used to alter the energy output (trading force/torque and displacement) with respect to the input, such that it can be transferred to a more useful form. Thus, a unit can be devised to fulfil the tasks of switching state and concurrently enable final state fixity from the input using a single actuation source. The optimisation of the mechanism will also minimise losses introduced to the system. For this mechanism to function, the forces applicable to the end-effector during transition must not exceed the force generated by the actuator; this is the blocking force of the actuator.

In Figure 56 an example multi-state actuator mechanism is shown as a linearised version showing the full circumference of the cylindrical system.

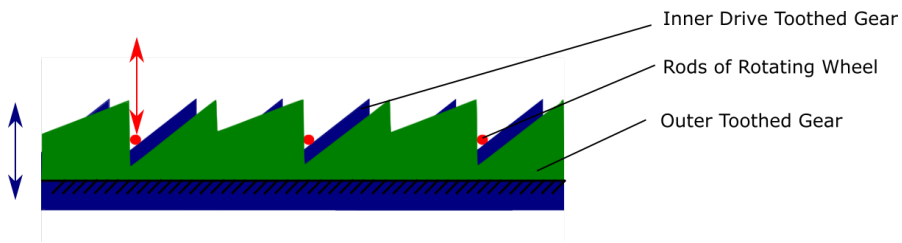

Figure 56: Illustration of linearised conceptual multi-state mechanism design

Plotting the polar coordinates of the barrel cam in planar form against the axial translation of the mechanism, the state transitions can be graphically presented as shown in Figure 56. In the figure:

- State (a) shows the pin wheel (represented by three red pins showing the spokes of the wheel in cross-section) in its high position locked in the teeth of the outer cam (marked in green).

- State (b) shows the upward translation of the index cam (marked in blue) transitioning through upward actuation force supplied by the paired actuator along the z-axis. This raises the pin wheel enabling it to rotate over the teeth of the outer cam in the direction controlled by the barrel cam teeth. (The movement of the pin wheel spokes during the state transition is shown in dark red).

- State (c) - shows the downward translation of the index cam transitioning through downward actuation force along the z-axis. The mechanism is now in locked low position.

- State (d) shows the upward translation of the index cam along the z-axis. This raises the pin wheel enabling it to rotate over the teeth of the outer cam once again.

- State (e) - shows the downward translation of the index cam along the z-axis. The mechanism is now in locked high position - repeating State (a).

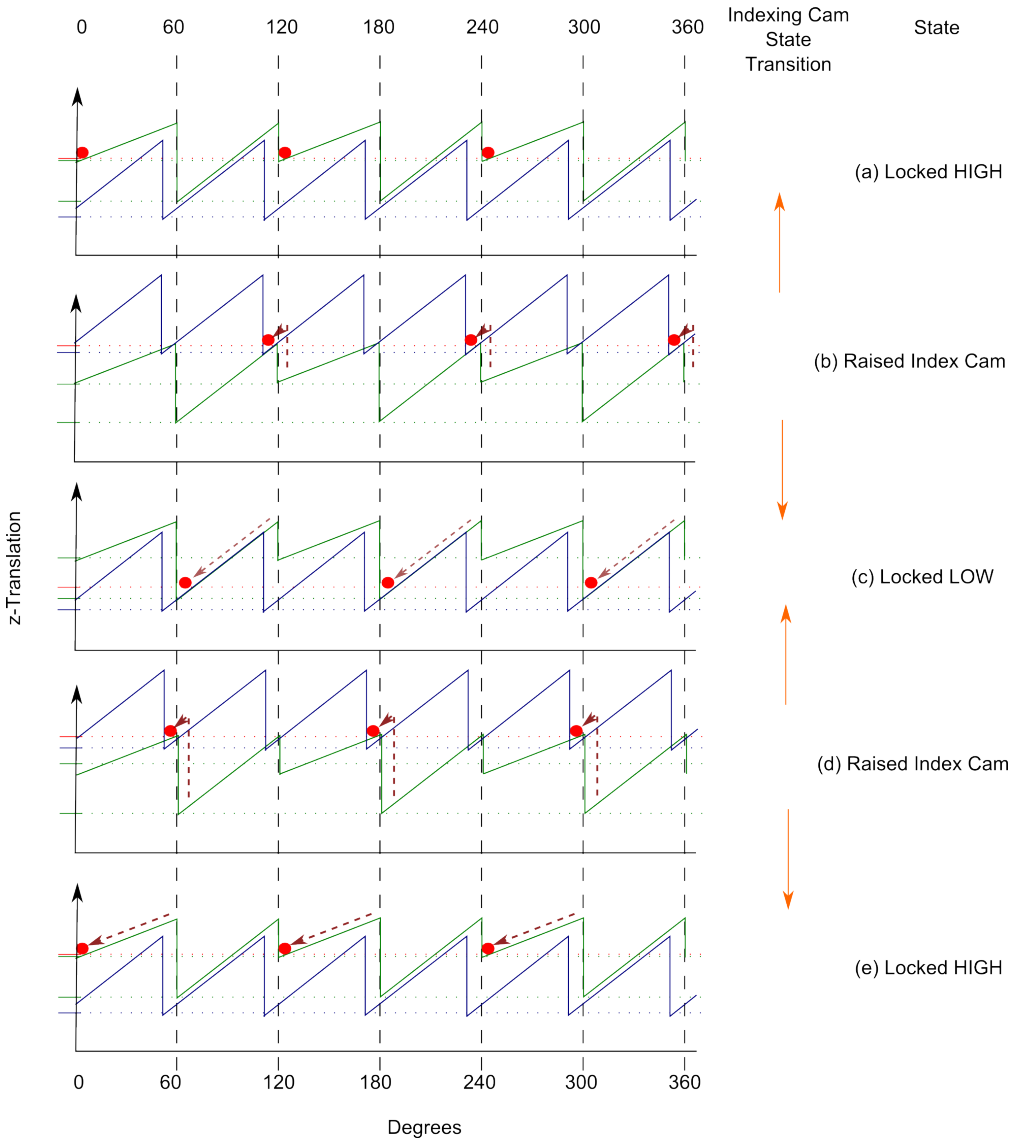

Figure 57: Illustration of state tranistions of multi-state mechanism for a 120 degree cycle

The mechanical constraints of the system state transitions are considered in Figure 58. The pin wheel is highlighted red, the outer cam green and the indexing cam blue consistent with the previous figure. In the actuation activation strokes in transition a to b, and c to d, the actuation force (F_a) must overcome the force from the mass of the pin wheel (m_p), and combined strut & indexing cam (m_s) acting under gravity (g).

There is also a friction force (F_fp) of the pin wheel as it moves in contact with the outer cam. Finally, there is a frictional force (F_fo) of the indexing cam moving through the outer cam. When the actuator returns to its steady state (b to c, and d to e), the actuator returns to a pair of passive elastomeric elements out of equilibrium resulting in elastic returning force (F_e), which along with the force from the strut & indexing cam acting under gravity must overcome the friction F_fo. The pin wheels mass m_p acting under gravity must overcome the friction on the slope of the outer cam as it slides into an output state (high or low). If the friction is reduced by material choices and the actuation force is large enough to lift the mass, the mechanism should be able to operate.

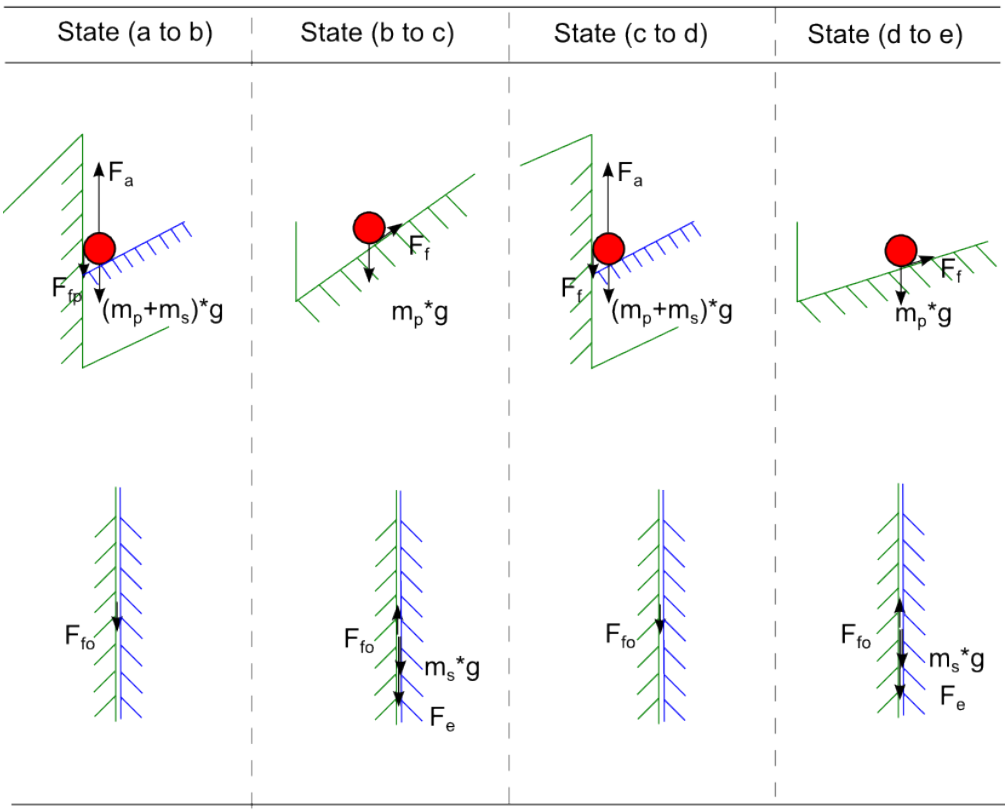

Figure 58: Illustration of forces involved in the state transitions

To enforce unidirectional mechanical interaction, a gearing system can be chosen with a high ratio, but this would add to losses and complexity. From rotation to translation worm gears can be used, whereby a transition in direction creates a controllable unidirectional movement. The inverted equivalent is not obvious however. A planar slider could be used with diagonal channels to drive a gear, for example. A cylindrical slide could be used, which would transfer the translation uni-directionally into rotational displacement*. This displacement can be used to relocate and lock an end-effector. In its simplest form, this mechanism is a non-backdrivable multi-state cam system (shown in Figure 56). The nature of the directed state transitions of this system mean that the system can benefit from feedforward control to track the position of the end-effector in the same manner as stepper motors.

The inspiration for the device pairing the actuator and mechanism was borne out of a desire to enhance the current designs and provide truly rigid position fixity. However it was realised that the design space of this simple non-backdrivable system could be expanded to produce an array of actuation modalities that are commonplace. Therefore this has opened up the possibility of using such a pairing in numerous applications where lightweight, scaleable and highly efficient actuators are needed. The revolute design creates a more compact actuator than a linearised mechanism. As no metals are used in the design, this could expand on current applications to medical technologies, where the system could be used in conjunction with live CT scanning. The possible designs that could be realised will be discussed in the next section.

4.6 Mechanism Design Space

Considering the separable components of the actuation system, a passive multi-state structure or mechanism can be used alongside an actuation source to transfer a mechanism between two stable output states. The mechanism allows the development of a

*The conversion is bi-directional, but once a new state is reached the conversion is non-reversible

system with translational output. The actuator enables controlled state change through discrete energetic application.

The multi-state non-backdrivable DEA concept described in Section 4.5, is an implementation of the novel combination of mechanisms with DEAs. This implementation is only a single example of a multitude of possible devices. The design space of the concept, and the rigid translation outputs made possible through the design will be explored. For the concept to function as a real world system, the chosen actuator is required to produce axial translational motion to drive the specific class of ratchet explored in this work. An indexing barrel cam mechanism can be designed to alter the translational actuation of the DEA into rotational or alternate axis translations or a combination of both. Hence, a broad spectrum of outputs can be created from the simple linear translation generated by the DEA antagonistic cone actuator.

4.6.1 Actuation System Operation Modes and Applications

Lock pin - A locking pin can be created with this orthogonal ratchet mechanism using a uni-directional bi-stable barrel cam ([Sclater, 2011]). This is the simplest form of the actuator and is the same as the conceptual multi-state non-backdrivable actuator described in Section 4.5. Figure 68 shows a CAD representation of the envisaged device. A barrel cam (or lifter), which is directly translated through the actuation of the DEA unit, is used to rotate a pin wheel. Once rotated, the lifter is retracted and the wheel relocated in a new state position on the static outer cam. This two-step extension and retraction enables the transition of the effective end-effector (the pin wheel) between two axially aligned translation locations.

N-State Translation Output - The circumference of the barrel and the size of the reciprocal pin define the number of states that can be created in a single rotation of the mechanism. The number of states and translation amplitude order can be varied (within the maximal energetic range of the paired actuator) to create a specific state transition

path for a particular application. The state path would enable a defined number of discrete amplitudes to be outputted using a set number of actuation pulses (shown in Figure 59). The order of consecutive states could be used to define state pathways.

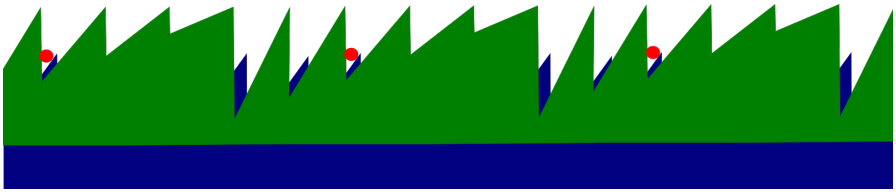

Figure 59: Conceptual illustration of an linearised N-state mechanism configuration

Stepper motor - The lock-pin mechanism can be seen to use the rotation of the bi-stable barrel cam to translate a reciprocating pin wheel between two positions on the z-axis. Evaluating the system from the perspective of the free cam, it can be seen that the pin and external cylinder control its movement. Driving the mechanism causes rotational movement of the barrel cam. The cam track can be designed such that the rotation of the stepper is non-back-drivable when there is no active drive. The mechanism can also be designed to allow for bi-directional rotation.

Linear Screw Drive - Extending the idea of the stepper motor further evaluation of the mechanism shows that it could be further extended to utilise the rotational drive to enable an axially aligned screw drive. This extension combined with the use of a bi-directional linear actuator (i.e. a twin-side active antagonistic cone actuator, as opposed to, single-side active antagonistic cone actuator), would enable the development of an indefinite (but pre-determined) height extending linear actuator (see Figure 60). This unit could be paired with many duplicates in a grid surface to produce a transitional active 3D surface, which could be used for topographical mapping, for example.

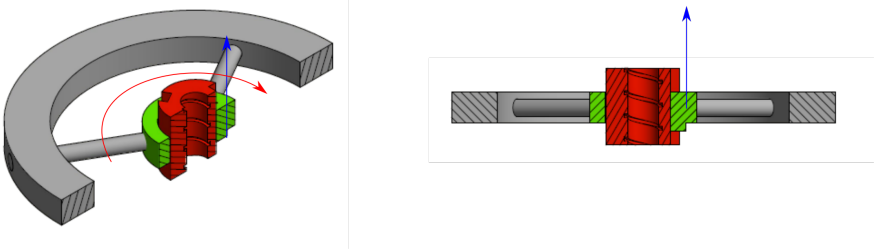

Figure 60: Image of cross-section of linear screw mechanism CAD design.

The chapter has, thus far, brought together concepts of position control mechanisms, soft actuators and minimum energy structures. Numerous applications and designs have been discussed as part of a broad possible design space, that can provide a range of modes of rigid actuation output, that could have broad uses and implications for future design and implementation of soft actuator based systems for applications currently using rigid actuators. However, to confirm that DEAs are capable of providing the force and stroke necessary, a device was devised to test the operation. A simple multi-state device as described and depicted in Section 4.5 was chosen for the test, as it would simplify the mechanism whilst still containing all the components needed in any multi-state actuator. A key consideration in such low-power devices is the losses in the system especially with the use of mechanisms, where friction due to part contact may inhibit the smooth operation of a device.

Development Note - The design of such a system, and the possible physical forms the actuator could take, will be analysed in detail. The actuator configuration and potential output mechanism design will be explored. This chapter uses DEAs in a studied arrangement and uses VHB4910, which is a characterised material described in the literature as a planar actuation membrane. However, the material has not been characterised in the particular arrangement used in this chapter and as such can only be compared to similar devices. The arrangement used applies a prestrain using an antagonistic cone which is non-uniform biaxial strain and varies between tested setups.

This has meant that empirical study rather than predictive analysis have been used.

4.7 Antagonistic Cone Pair Characterisation

The antagonistic cone DEA configuration has a number of optimisation parameters including pre-strain, rod/strut length, cap size. The use of an antagonistic pairing of DEA cones enables a high stroke and blocking force to be generated in both two-side or single-side active DE membrane forms. To characterise the antagonistic cone, the maximum force and stroke would be measured over a range of cone shapes. The cross-sectional shape of the cone is shown in Figure 61 with (a) the strut cap, (b) the strut, (c) carbon grease electrodes, (d) the supporting frame, and (e) DE membrane marked. The parameters l and w are the length of the strut (including tip), and the width of the strut tip respectively, which were varied as part of the characterisation. Length $I.D.$ is the internal diameter of the supporting acrylic frame. Due to the number of parameters that can be varied, the pre-strain of the DEA and the size of the aperture of the supporting frame were kept constant at 400% and 60mm respectively. The strut cap size varies the angle of slope of the cone. Due to the surface area of the cap, it also affects the available actuation area.

In order to find the optimum configuration with the parameters of strut cap size and strut length, a set of characterisations were undertaken.

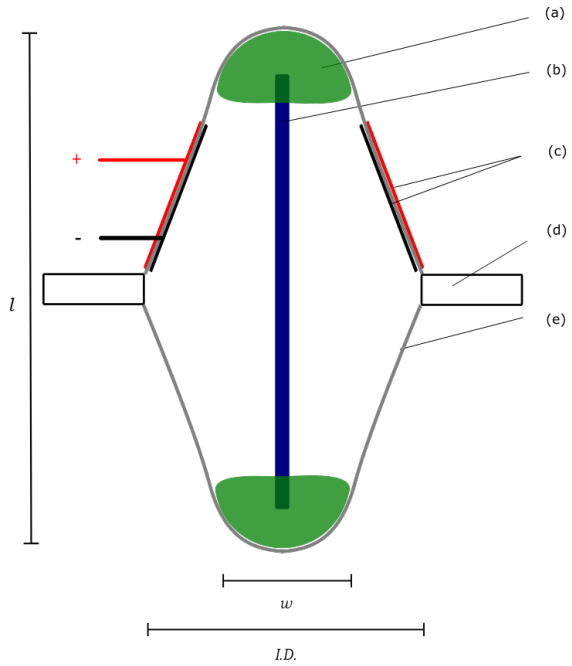

Figure 61: Antagonistic coupled cone actuators cross-sectional schematic

4.7.1 Materials and Methods

A proprietary dielectric was used for the experimentation (VHB 4910). This was due to its standardised material parameters enabling comparison between separate tests. Additionally it yields high strain on actuation, which is desirable in this system. A supporting frame for each cone was cut from 3mm cast acrylic sheet. VHB was pre-strained using the Hoberman platform method described in Section 2.8, and adhered to the frame, then a cap was centrally aligned on the membrane. The centering is crucial to forming an axisymmetric cone actuator. Any deviation leads to the cone leaning and thus, sub-optimal performance. Carbon grease electrodes were painted on to the active membrane and connected to the high voltage supply using copper tape connections. Care was taken not to to allow the active section -covered in carbon grease - to come within a 2mm boundary of the strut cap, due to the high stresses at the boundary due to boundary constraints potentially leading to premature material breakdown and hence

actuator failure.

Strut caps were 3d printed (using a Wanhao Duplicator 4s 3D printer) to and planar of 11μm and z-axis resolution of 100μm [Wanhao, 2016]. The caps high resolution printing enabled repeatable production and accurate cone alignment due to axial symmetry. The sizes of cap small, medium and large are 15mm, 20mm, and 30mm in diameter respectively. The rod was cut from extruded aluminium rod of O.D - Outer Diameter - 4mm, and wall thickness 0.5mm.

4.7.2 Experimental Setup

For the characterisation tests antagonistic cones were set up as described in Section 4.7, and a load cell rigidly located at varying distances from the active cone. As such the blocking force to displacement relationship over a range of voltages could be characterised. The set up is shown in Figure 62. The data was recorded for each of the configurations of three cap sizes and five rod lengths at voltages up to membrane breakdown. A DAQ was used to trigger actuation and recorded actual voltage (through sensing circuit via high voltage supply), displacement (from laser sensor) and blocking force (from load cell).

For the experiments the following equipment was used:

- DAQ - NI USB 8343
- Laser Unit - Keyence LK-GD500
- Load cell - Kyowa LMA-A-10N load cell with a Strain Amplifier Kyowa DPM-700B
- PC - computer running MATLAB software

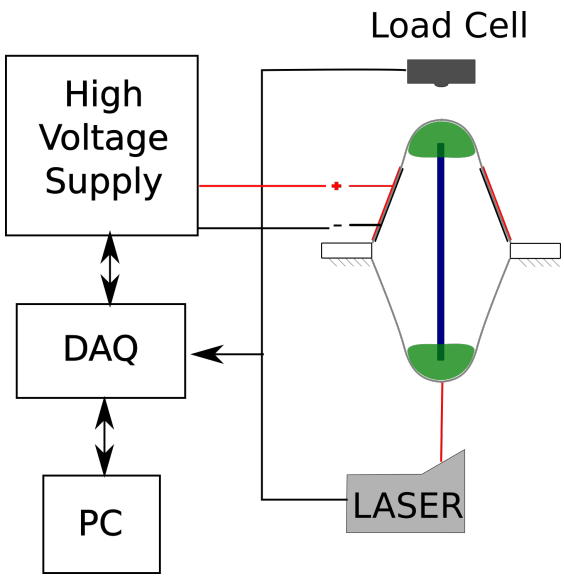

Figure 62: Experimental rig schematic of antagonistic cone actuator characterisation.

Strict safety protocol was used in the experiments, using an insulated test space and isolated high voltage supply. The setup is further described in Appendix C.

4.7.3 Characterisation Results

Using the materials and methods, and experimental setup as described, the antagonistic cone actuator was characterised and graphs of blocking force against displacement combined by strut length and plotting results for each strut cap size for the application of 3.5kV.

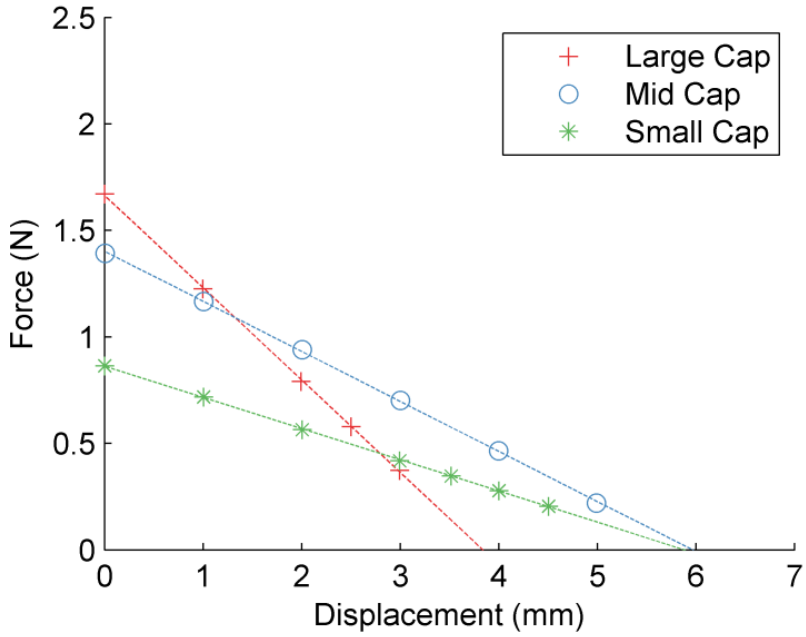

Figure 63: Plot of force - displacement for strut length 80mm

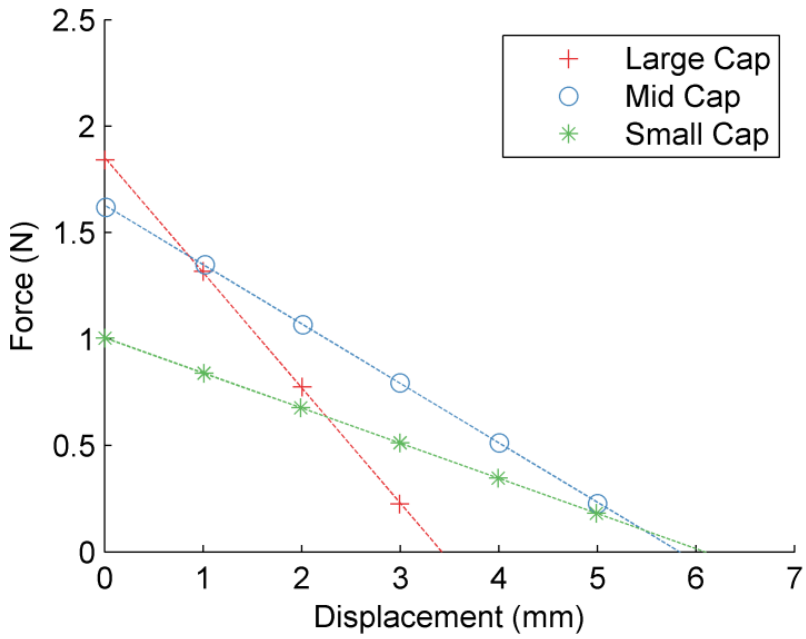

Figure 64: Plot of force - displacement for strut length 90mm

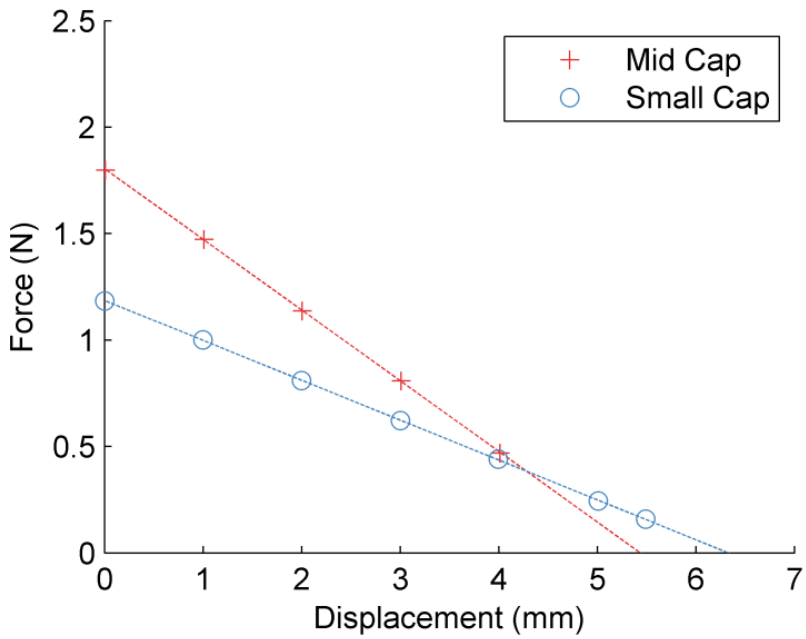

Figure 65: Plot of force - displacement for strut length 100mm

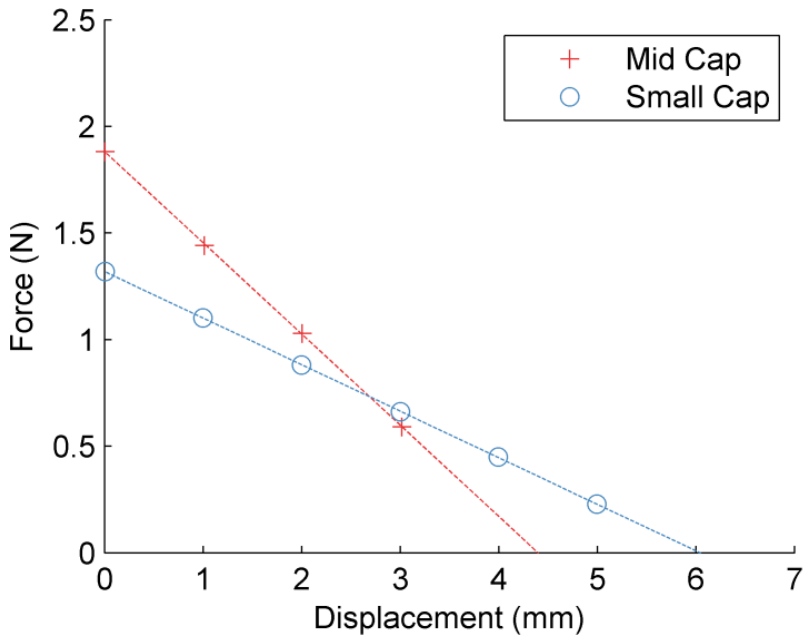

Figure 66: Plots of force - displacement for strut length 110mm

The graphs in Figures 63 - 66 show the blocking force vs. displacement characteristics of the cone actuator over a range of cap and strut length combinations*. The force-displacement relationship can be seen to be linear across all strut and cap sizes, which was unexpected due to the highly non-linear nature of the material and the variation in pre-stretch between samples - caused by the out-of-plane straining of the material by the insertion of the strut. However, due to the antagonistic membrane pairing, the non-linear attributes cancel out. Grouping measurements for each cap size, a longer strut length shows an increase in force due to the extra elastic energy stored in the membrane due to the increase in pre-stretch. This is countered by a reduction in displacement of the cone tip when actuated.

To compare the energetic output before membrane breakdown, the work done through actuation was calculated for each of the samples each combination of strut length and cap size (shown in Figure 67). With each cap size there is a clear peak in output†. The mid cap is shown to have the highest energy output.

*In arrangements with a strut length of 100mm and 110mm the testing of a cap size of 30mm (large cap) was not possible due to mechanical failure of the membrane on set up of the experiment. This was due to the combined pre-strain on the membrane being to great for it to withstand in a passive state.

†The peak in output for the large cap is with the maximum reliable pre-stretch (with 90mm strut)

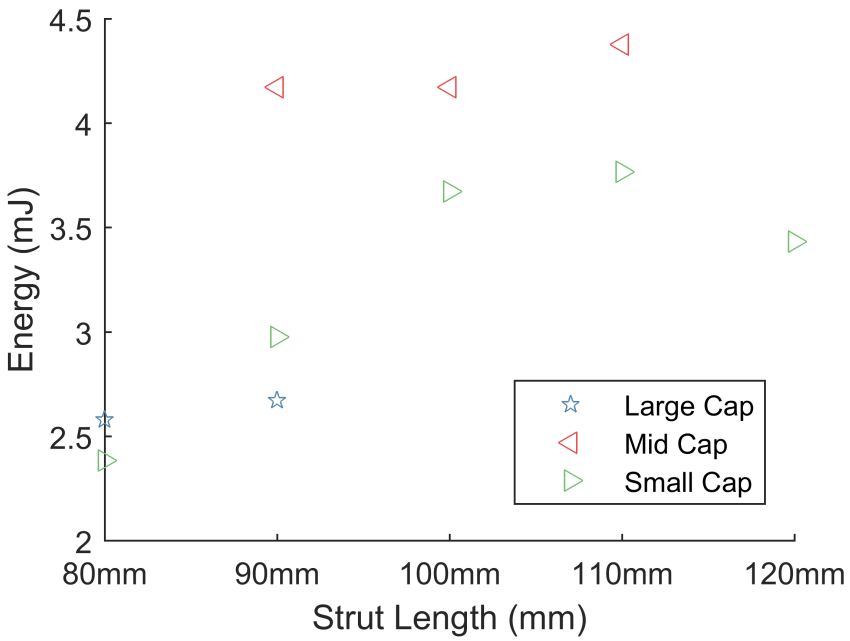

Figure 67: Plot of work output of single side actuation of antagonistic cone pair.

At an actuation voltage of 3.5kV each of the membrane work output was measured from the recorded free displacement and blocking force. The result aided selection of parameters to create a prototype. It can be seen that the maximum energy output was found in the mid-cap size cones (with the 110mm strut configuration providing the highest output). However, as the displacement of the actuator is of critical importance to maximising the utility of the device the relatively low displacement of this configuration was deemed inadequate (at 4.4mm). Thus, it was considered a lower energy output configuration with the highest displacement would be overall the best parameter set. Thus a configuration with a 100mm strut length and a small cap was chosen, which had only 15% reduction in energy output (of 3.75mJ) and approximately a 50% increase in displacement (to 6.4mm).

4.8 Lock Pin Functionality Test

The multi-state mechanism has been discussed in Section 4.5.3 (a 2D state transition diagram is shown in Figure 57). When this mechanism is used in a cylindrical form, it can be seen that a sequence of n-stable states can be created through the rotational movement of the wheel enabled through vertical travel produced by the translational actuator of the antagonistic dielectric cone.

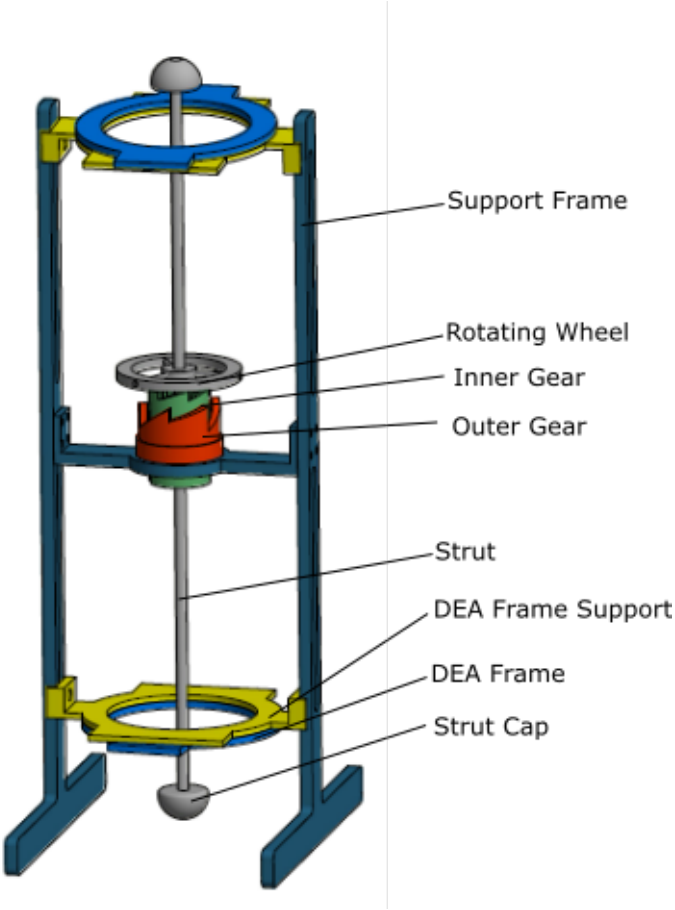

Figure 68: CAD desing of multi-state actuator prototype demonstration rig.

A design was created using Autodesk CAD, enabling the realisation of this circular instance of the bi-stable mechanism shown in Figure 68. In the figure, it can be seen

that the mechanism is between the antagonistic cones, which is to increase the potential for miniaturisation of the unit. The translation of the surface of the wheel provides the displacement for the pin forming a non-back-drivable multi-state end-effector. From the analysis of the cone characterisation energy plots (Figure 67) produced for the antagonistic cones, the highest work output actuator was selected and paired with the mechanism and tests under real conditions for the application.

An illustration of the degrees of freedom of the mechanism is shown in Figure 69:

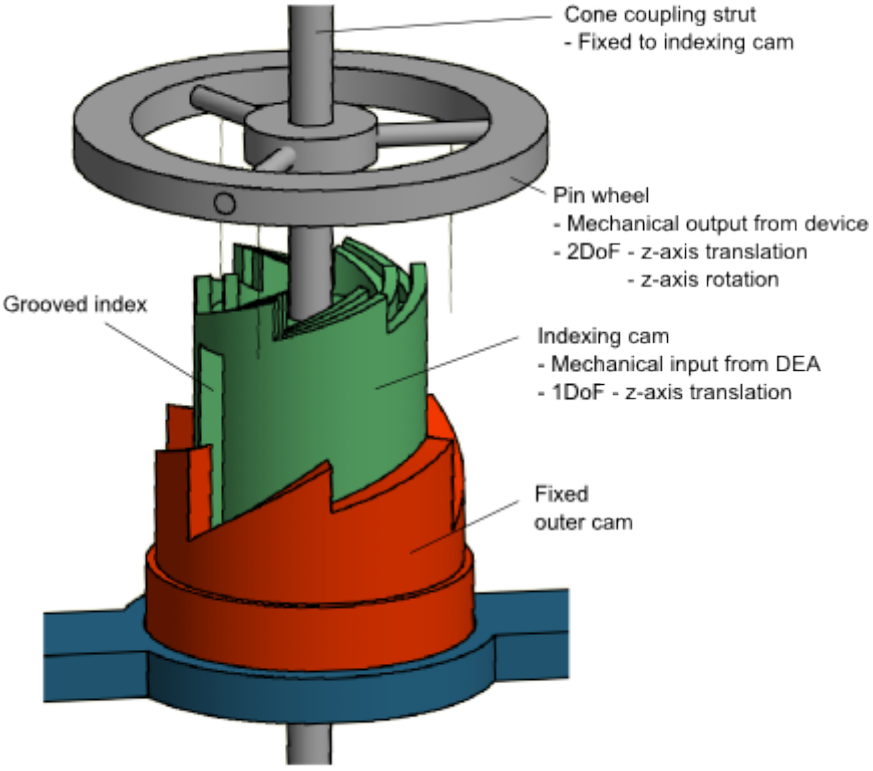

Figure 69: Illustration of defrees of freedom of multi-state mechanism design

The pin wheel is freely moving along the strut, but during an actuation cycle, the strut would move with the pin wheel. The pin wheel would encounter some frictional losses on rotation as it moved along the teeth of the cams and rotated around the strut.

It was considered that the weight of the pin wheel would overcome these losses. The indexing cam is attached to the strut and moves along an indexing groove keeping it from rotating.

4.9 Experimental Setup

As the confirmation of the concept would be made through the repeatable state transition of the multi-state device, the setup involved a freestanding actuation system as shown in the exploded view in Figure 68. The actual setup is shown in Figure 70.

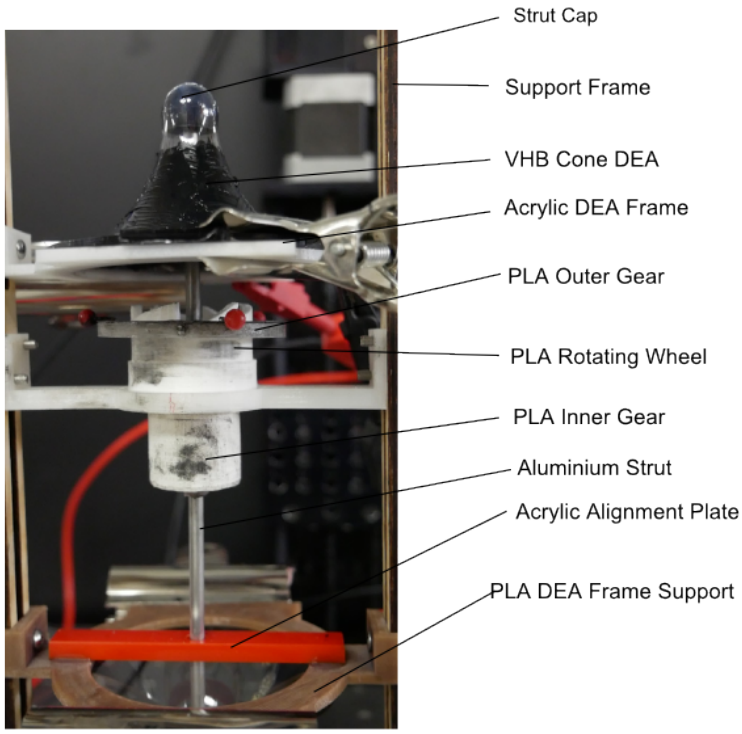

Figure 70: Photo of multi-state actuator with component descriptions.

In order to fabricate the device, the moving components need high accuracy and low weight. For the strut and indexing cam combination of aluminium rod and 3D printed PLA was used to meet these requirements. Hollow 3D printed parts allowed low weight and high accuracy, and the aluminium rod as smooth for low friction (and stiction), while

keep the weight low. The pin wheel was again constructed of aluminium rod and a PLA wheel for the same reasons. An acrylic plate was used to ensure accurate alignment of the strut in the mechanism, through laser cut holes which minimised additional frictional losses.

4.10 Concept Proof Results

Figure 71 shows the actuator displacement in active and passive states respectively As can be seen in the active state, there is significant wrinkling of the actuation membrane. This is due to equilibrium stress being reached in the circumferential plane of the cone. However, there is still tension in the radial direction. Although wrinkling tends to show the membrane is approaching limits of operation, the membranes performed reliably in repeatable actuation cycles at this voltage.

The images shown in Figure 71 show the state transitions as described in Section 4.5.3. The Figures 71(a-e) represent the states in Figure 57 (a-e) showing the pin wheel transitioning from high to low repeated twice. The actuator was able to achieve the required displacement using a 5kV actuation voltage. It is believed that the higher voltage was required to overcome stiction and to achieve the desired displacement to enable transition. Although the voltage was larger than expected the actuator was able to perform multiple cycles without failure.

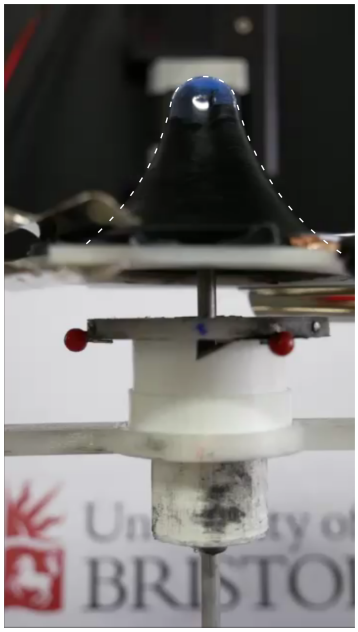

(a) State 1 - Initial State of device (HIGH state)

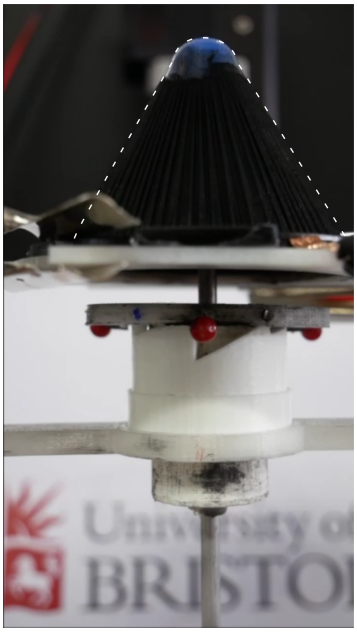

(b) State 2 - DEA Actuated (Vertical lift and rotation to inner teeth limit)

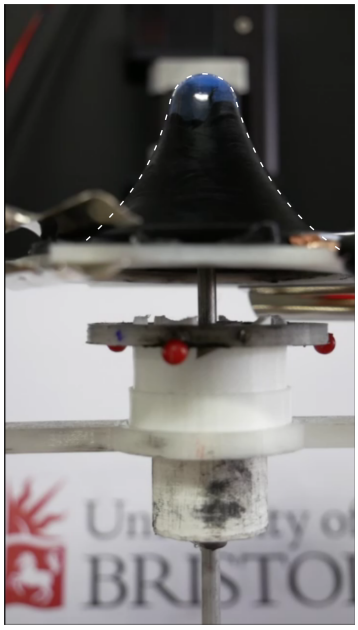

(c) State 3 - DEA Off - (Rotation to outer teeth limit to LOW state)

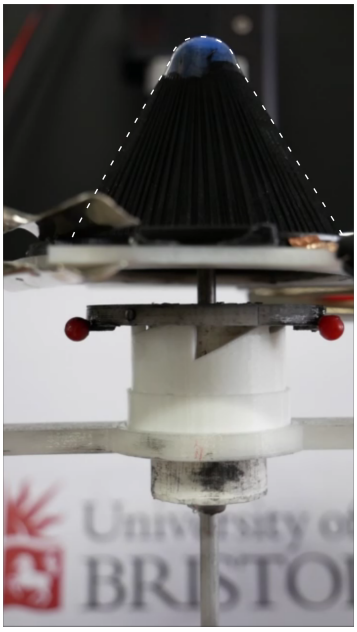

(d) State 4 - DEA Actuated (Vertical Lift and rotation to inner teeth limit)

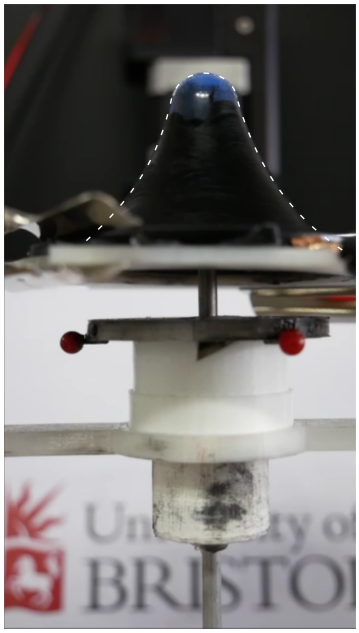

(e) State 5 - DEA Actuated (Rotation to outer teeth limit to HIGH state)

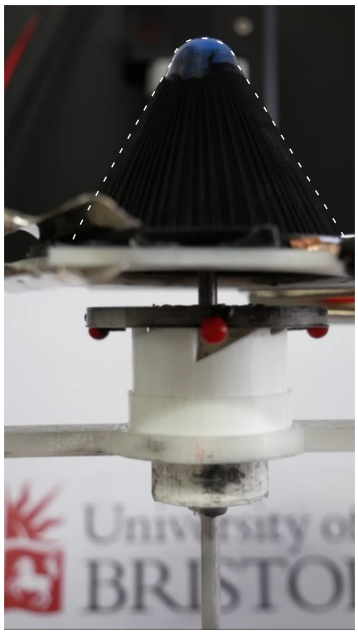

(f) State 6 - DEA Actuated (Rotation to inner teeth limit)

(g) State 7 - DEA Off - (Rotation to outer teeth limit to LOW state)

Figure 71: Series of figures showing state steps of actuation cycle of prototype unit.

For the experimental actuation of the device Figures 73 and 72 show the rotational angle displacement about the axis of the coupling strut of the actuator and translational displacement of the rigid end effector of the actuator along the axis of the strut during the DE actuation. This information was attained through calibrated tracking of the dots attached to the pin wheel.

Analysing Figure 72, the z-axis translation (along the axis of the strut) is plotted. The dashed line shows the ideal displacement of the pin wheel. It can be seen that there is some time displacement (particularly on the first application of voltage), where the wheel takes 0.2 seconds to rise to the required displacement for state transition of 5mm - this displacement is required for the wheel to pass over the teeth of the outer cam. There is some overshoot and undershoot of the position which was observed as the wheel 'bounced' at the maximum displacement. This bounce is mostly clearly observed by the high variation in displacement as the actuator transitioned from low to high state between 3.25 and 4.25 seconds.

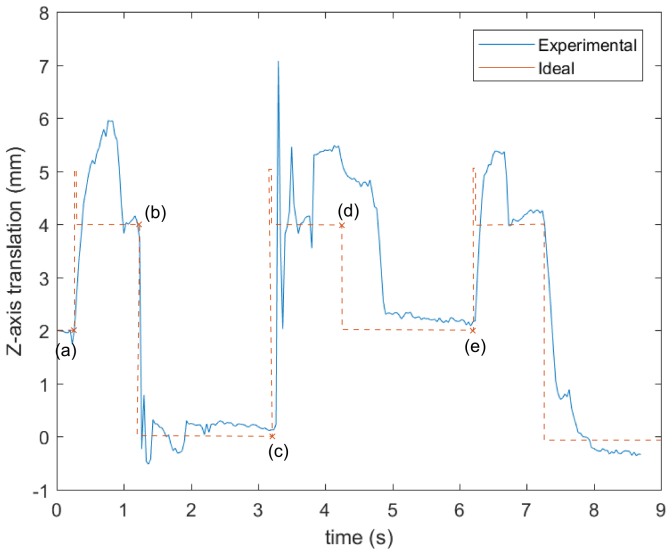

Figure 72: Plot of translational displacement of end effector along the axis of DEA actuation displacement. (Letters a-e mark states referred to in Figure 71).

Considering the plot in Figure 73, the dotted line shows the ideal transitional steps. The states from Figure 57 are labelled and depicted by crosses on this line. The blue solid line shows the retrieved data of the polar rotation in degrees from the test. When compared to the experimental data it can be seen that the ideal line significantly differs from the experimental results, however the wheel does rotate and transition between states. The differences are due to the delayed response in displacement of the actuator vertically, slowing the rotational displacement, which can be seen clearly at multiple steps (for example (a) to (b)). It was also noted that the wheel seemed to over-rotate (for example between (c) and (d)), however this may have been related to the 'bounce' observed between in the translation data in Figure 72. The wheel did under-rotate in the transition to low states (e.g. (b) to (c)), however it did travel far enough to allow the state change to occur, but not as accurately as expected.

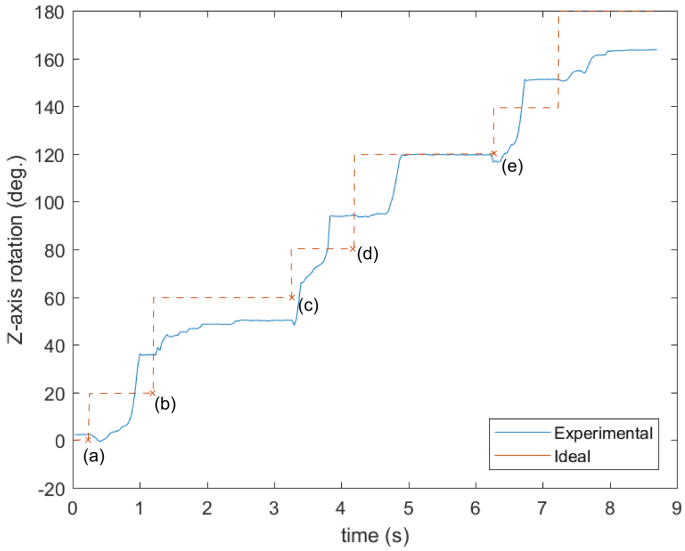

Figure 73: Plot of the rotational displacement of the end effector about the axis of DEA actuation displacement. (Letters a-e mark states referred to in Figure 71).

The bistable concept did deliver output transition between high and low states of a non-back-drivable rigid end effector through the application of translational actuation

from an antagonistic cone pair and whilst in the locked states required no energetic input. It can be seen that the actuator only uses energy when changing state, producing a very efficient device for numerous applications.

4.11 Summary

In this chapter, a system using DE actuator coupled to a non-back-drivable mechanism with a rigid end-effector has been presented. A review of soft robotic actuation technologies and the methods developed to couple soft actuators with rigid bodies was undertaken. The initial concept aimed at producing a device that combined soft actuators with a bistable mechanism aimed at zero-energy fixity. The review showed a lack of comparable device and as such this was a novel implementation of DEAs.

A review of coupled actuators led to the testing and characterisation of antagonistic cone actuators to provide the energetic source and rigid output of the actuator to the mechanism (through the coupling strut). The characterisation of the coupled DEA at a voltage of 3.5kV showed a maximum displacement of 6.4mm was attained with a small cap (15mm cap size) and 100mm strut, but the highest force generated by a medium cap (20mm cap size) with a 110mm strut, whilst producing a displacement of 4.4 mm. Additionally a cap of 20mm was found to generate larger energetic output over the range of strut lengths with an output of 4.4mJ. However, for the device actuation to be effectively utilised a high displacement was deemed advantageous and a 15% reduction in maximum force resulted in a ≈50% increase in displacement (of 2mm).

A mechanism concept was created, redesigning reference implementations [Sclater, 2011], to enable a bistable barrel cam to generate axial displacement of an end effector. Once formulated the design concept was expanded to include multiple multi-state output systems, which have potential for use in a host of applications. The mechanism is actuator type agnostic and hence could be powered by a range of conventional or non-conventional actuators. The use of a non-back-drivable mechanism separates actuation from external

loading, hence allows a stable state to be maintained with no power consumption.

For the subsequent proof of concept device, materials were chosen to minimise weight applied to the antagonistic cone pair using aluminium and low density 3d printed parts and using low friction parts (such as laser cut acrylic for alignment). The system was designed in a way that the soft actuator can be isolated from external forces, whilst providing rigid end effector output.

Due to scaling and complexity issues the scale of the device was much larger than the envisaged application, however the prototype showed the operation worked in practice. A characterised displacement of 6.4mm enabling a zero-energy fixity bi-stable displacement along the axis of the strut of 110mm to be achieved using a voltage of 5kV. The prototype also showed repeatable operability, and the use of a non-back-drivable mechanism separates actuation from external loading, hence allows a stable state to be maintained with no power consumption.

5 Development of an Actively Sensing Pneumostatic Probing Device

5.1 Introduction

This chapter will discuss the development of a novel sensing unit, which uses a combination of dielectric elastomer actuation in a pneumatically coupled arrangement, and a flexible membrane with surface protrusions paired with an optical sensor. The novel concepts used, and the innovations made to develop the active sensor will be discussed and an appraisal made of the sensing capability of a prototype unit for object shape detection.

The continued research and innovation in the field of sensory feedback devices is carried out to enable robots - and wider electro-mechanical systems - to more precisely understand the environment in which they operate and objects which they are tasked with manipulating. This in turn enables the development of better control of the robotic system and more precise fulfilment of functional requirements. The sense of touch is of particular interest; it facilitates exploration of the proximal environment to the robot and enhances understanding of the environment's mechanical properties. Paired with an actuation system (such as a robotic arm), the sense of touch allows the physical exploration of the environment.

Creating a robotic equivalent of nature's senses has been a long held ambition of roboticists. It is firstly a fully functional solution that we can characterise and model; it can be reverse engineered to produce a robotic equivalent, which we know can work effectively; finally nature's solutions lend themselves to a large spectrum of useful tasks we wish robots to perform, namely those already performed by humans for which our senses have evolved to complete effectively. Due to the level of complexity of humans' sensors, and the functional requirements of robots, humans are often used as inspiration from nature. For example, the finger has a dense somatosensory system providing the body with information to be evaluated, providing environmental feedback such as tem-

perature, touch, pressure, pain, and vibration [Van Putte et al., 2015, pp. 240 - 243]. As an example of its feedback and control potential, touch alone can be used as a means of navigation without visual information*.

Producing a tactile sensory skin (ignoring other sensory capabilities found in human's skin) is a complex task due to the multiple functional requirements of skin in the bodies interactions with the external environment. Consider, for example, in mimicking the finger, the ability to perform manipulation and grasping tasks must be maintained in a humanoid robot of human scale - the scale should be similar in order to perform the bulk of tasks robots are expected to carry out -, whilst providing highly parallelised sensory capability†.

Current state-of-art sensor implementation use technologies including (but not limited to) flexible capacitive, fluidic resistivity, piezoresistive, and optical sensors. These and a plethora of alternative sensors, while individually producing an analogue to a unique neuronal receptor found in nature, are hard to scale in number and density, in a way that can replicate or approach the tactile sense of human skin. When delving deeper into the formative sensors that enable the sense of touch, it can be considered to be generated by singular point sensors, the functionality of which, has been replicated using a variety of sensors. However, this is not sufficient to *feel* an objects features. Increased density of sensors used in implementations provide a better approximation of human tactile sensing, but are much more complex to implement due to connectivity, bulk (volume and weight), materials, sensor wiring and control integration.

It should be noted that although nature is a huge resource for inspiration, sensors do not have to replicate its complete feature set to provide useful function in the robotic paradigm, but it does form the basis of systems for targeted emulation, for use in many

*A knowledge of surrounding structures (an internal map) must be known to allow directed navigation - analogous to landmarks when using sight.

†When considering possible novel technologies, it should be noted that parallelised sensory capability is consider to act as an addition rather than replacement to current sensing technologies such as passive sensory end-effectors.

areas of the robotic field. This is not only due to the inspiration for unit function, but that the environment of intended operation - the structure and unstructured physical domains on earth - are well adapted to by nature.

Tactile sensing found in nature can be considered to be active-touch. Active-touch defines the act of touching, rather than passive contact, or being touched [Gibson, 1962]. It effectively allows a system to recover more information from a passive sensor's interaction [Visell et al., 2016]. For example, the BIOTACT EU project Whiskerbot was developed to explore the use of vibrissal mimetic active sensors as part of a system and in the design of a modular single sensors [Pearson et al., 2007]. Active-touch exploits the inferred dynamics of a physical interaction to further enhance the modelling required for a robotics system to meet functional requirements [Lepora and Ward-Cherrier, 2016]. Active-touch is a very dynamic and influential research topic at present due to the capability found in nature and the potential increase of sensing performance for robotics applications.

The combination of accurate sensing of a region - rather than point based - at a discrete time, and the actuation of the sensing surface, provides an extremely useful tool in developing active-touch sensors that could be attached to robotic systems for use in visually occluded and physically limited environments. This could be as part of a robotic armature or limb, an autonomous exploratory robot, or as a stand-alone self-active sensory device.

The aim of this chapter is to develop and active touch system, hence requiring:

1. Development of a sensory membrane providing high resolution feedback.
2. Create a coupled or direct actuation method to allow for active-touch or palpation of a surface.
3. Create a soft sensor that can provide dynamic sensing.
4. Ensure versatility of system through providing robust and scalable design.

Key performance criteria are:

- Develop a system that provides sensory palpation over an effective distance (relative to the size of the unit).
- Produce a highly parallelised sensing capability, able to deliver zonal sensing, whilst being lightweight.
- Ensure reliable and repeatable sensing.

In order to meet these criteria, this work will investigate existing technologies that provide elements of the function desired. The novel concepts mooted will be discussed and characterised in the aim of producing an active-touch unit.

5.2 Understanding Tactile Sensing and Nature's Design

Tactile sensing in robotics is crucial to providing feedback for position control or operation in complex dynamic unstructured environments. Considering this complex case, the information necessary to control and safely locomote a manoeuvrable robot requires considerable computation for path calculation and dynamic error-minimisation. To gain a more complete understanding of an environment, more sensors can be used. These sensors inform modelling of the surroundings by a robot, and allow movements to be made on that basis. The task of navigating an environment can be made easier by reducing effects of locomotion error, for example by having a lower centre of gravity so that the robot is more stable, utilising high precision components. However, an alternative approach could be to follow nature's design by using soft and temporarily deformable structures with flexible high density sensory interfaces. Perception of the environment in robotic systems is usually captured by cameras or distance sensors providing both far-field and near-field information, which is a common standardised approach. In more complex unstructured environments, robots interact with objects in their environment

- from uneven floors to obstructions, tactile sensing gives a proximal sensory feedback allowing a robot to probe and capture valuable information to enable it to negotiate the environment. Considering tactile sensing, more sensors allow a robot to gain a greater understanding of its proximal environment at a given time. Through this information the robot will be able to anticipate problems which other sensors (such as optical or more coarse tactile sensors) will not detect. This is something seen in nature across a broad range of species, locomotion methodologies and sensor availability.

5.2.1 Tactile Sensing

In somatosensory systems, the breadth of the information retrieved at any given instant is very significant in the computation of a reaction. Tactile sensing uses an array of sensors to give a system an understanding of its interaction with the surrounding environment. Sensing external forces at a single point on a body will give very little information about the force experienced by the whole body.

The disambiguation of touching and feeling must be clearly expressed to understand tactile sensing and how it can be engineered to provide useful feedback control to a system in robotics.

> **Touch** *(n) - the act or state of passively touching.* [Gibson, 1962]
>
> **Feel***(n) - [an act of touching something] to obtain the kind of stimulation which yields a perception of what is being touched.* [Gibson, 1962]

For example, a robot (or other actor) can touch an object and know where it touched it and describe the location in Cartesian space, and how much force acted in the act of touch, using a single point touch sensor; this can be defined as point sensing. This method provides enough feedback to allow a robot to perform grasping tasks, some proximity calculation and position error reduction (mainly used in industrial robotics). Point touch sensors can be used in increased numbers to provide a greater resolution

of touch. Further, an array of sensors can provide greater feedback information on a surface. This expands point sensing to zonal sensing, where a group of sensors can feedback on a local area, providing information on roughness, edges and sharpness.

When evaluating an external surface with sensors spread over a controlled limb, the material properties of the limb become a key factor in the limbs interactions with the surface. A rigid locally flat body surface will, through mechanical limitations, have limited contact with an irregular external surface. Consequently the sensory data retrieved of the external surface will be limited. Considering the sensing of a region (enabling feeling) of a surface, multiple sensing elements are required to be in contact with the unknown surface. Thus, compliance is essential in this endeavour to promote conforming of limb to surface and hence, its examination.

5.2.2 Nature's Design

As one of the main areas of physiological and psychological study for the advancement of understanding of touch, we (humans) are a key resource in the development of systems which emulate Natures tactile sensing. Empirical evidence shows that the sense of touch is invaluable in manipulation and control of objects using hands in humans [Gibson, 1962, Kikuuwe et al., 2004, Dahiya et al., 2010]. The somatosensory system found in humans has a broad range of environmental senses, which includes temperature, chemical, touch (both static and dynamic over a range of frequencies), and pain (detecting potentially damaging intrusions) [Van Putte et al., 2015, pp. 240 - 244]. The tactile sensing investigated here, is focused on increasing the complexity of touch sensors to improve environment interaction in robotics. Whilst this is a complex task, it still simplifies some significant sensory inputs used in the processing of interactions in nature. This focus is used to reduce system complexity to the minimum and limit hardware complexity requirements whilst still aiming to provide enhanced function.

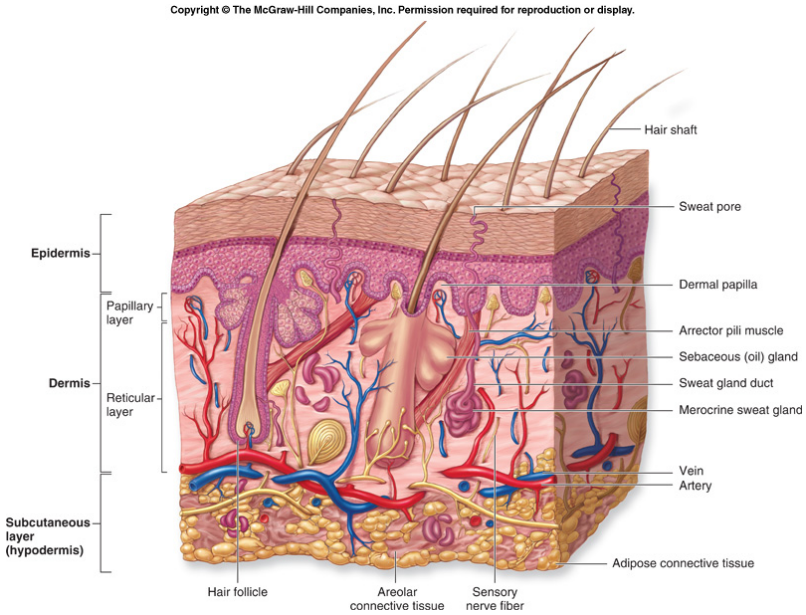

(a) Drawing of cross-sectional detail of skins features (reproduced from [Mescher, 2003]).

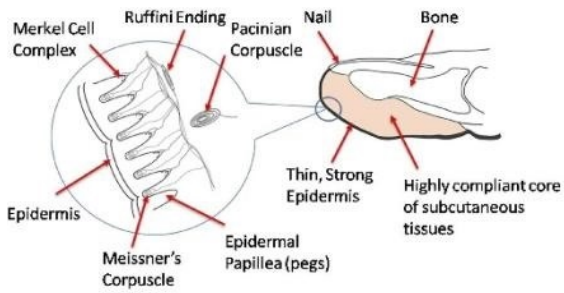

(b) An illustration of how the human finger is constructed with specific focus on haptic sensing (reproduced from [Chorley et al., 2010]).

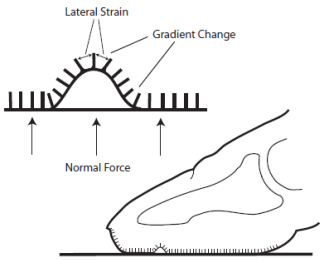

(c) Schematic of the resultant deformation of the human finger structure resultant from a normal force (reproduced from Chorley et al [Chorley et al., 2009]).

Figure 74: Images of human finger structure and illustration of the use of papillae in haptic sensory feedback.

In humans, the finger is one of the most densely packed sensory appendages. This specific sensory digit has developed through evolutionary pressure found in the command and manipulation of objects. The fine motor control in manipulation tasks performed by humans has been shown to be heavily influenced by the feedback from the dense array of mechanoreceptors in the fingers. The finger has numerous types of mechanoreceptor adding to the layers of sensing it is capable of. A cross-section is shown in Figure 74a.

The mechanoreceptors are used to evaluate the sensations of touch, which encompasses four types of skin receptor operating over stimuli of varying vibration ranges. The sensory information provided from these mechanoreceptors forms the feedback required for the human to actively interact with surfaces, detecting environment or object features and textures following the controlled trajectories navigated through the actuation of muscles in the body and digit [Berryman et al., 2006].

The mechanical structure of human digits (and many other sensory appendages in nature) are evolved to optimise utility. Figure 74b shows the ridged papillae structure which interact with the Meissners corpuscle to provide the touch sensitivity to external objects. In the case of the finger, the dermal layer and supporting sub-dermal tissues form a compliant, but resilient material, which envelops surfaces and provides feedback through encapsulated sensors forming an embodied sensor. The compliance helps the grip of an object, and the mechanoreceptors help with feature recognition [Feix et al., 2015, Monzée et al., 2003]. Individual sensors must be employed in large number to provide the sensing required to emulate human skins touch sensing capability. Considering the physical design, Figure 74c illustrates how an external object would interact with the skin, causing strain and compression, augmented by the papillae, to provide the broad range of touch sensitivity humans can analyse and use.

5.3 Touch Sensing Modes

Research groups and commercial enterprises have produced numerous touch sensing systems [Winstone et al., 2013, Rahbar et al., 2014, Bloor et al., 2006, Kawasaki et al., 2002, Valdivia Y Alvarado et al., 2012, Metta et al., 2008]. In its most basic point-sensing form, the sense of touch has been widely used in robotics - especially in industrial automation - by utilising highly accurate, but sparsely distributed sensors. These touch sensors can be used to provide a robot an affirmation of its location in a workspace using predetermined physically grounded points in a referenced Cartesian space. The sensors are also used to ensure factory output dimensions are within designed tolerances, for example. However, to sense more complex, temporally unique, actions in unmapped environs, a robot needs a more intricate sensing system. To meet its functional requirements a robot needs a sensory network providing regional tactile sensing over external surfaces that interact with the environment (i.e. it's skin). The system could provide accurate perception of external materials' properties whilst enabling a robot to control and manipulate external objects. To this end, to capture adequate information of its proximal environment, the tactile sensor may need to perceive shapes, grain, edges and other features of dynamic materials in an unspecified environment. Multiple features that have less than millimetre order dimensions are detected even at low normal forces in human fingertips [Berryman et al., 2006].

This level of functionality has yet to be satisfactorily achieved by robotic systems, where simple tasks, such as manipulation of an egg, or fruit picking currently use 'workaround' solutions, which avoid the sensing of the object and use materials that are soft and compliant to wrap or differential pressure to pick up target objects [Stoll,].

To try to implement a sensory array on the surface of an end effector capable of controlled manipulation - usually a digit or limb -, sensors able to evaluate normal and shear forces to a high accuracy must be densely pack and appropriately distributed over a useful surface area. The information must be processed and made available to the

control system for the calculation of actions in near real time so that robots can react in a similar time frame to natural mimetics; nature's response has been optimised by evolution to enable perception and reaction to facilitate survival.

5.3.1 Robotic Tactile Sensing Implementations

The sensors described in the Literature Review Section 2.11 have been used in a number of robotic system designs with specialised functional scope; some humanoid and others mimicking the advantages of other natural inspiration such as rodents. One of the main applications of tactile sensors is in the emulation of touch, focussing on the emulation of humanoid manipulation. This is essential in facilitating the replication and repeatability of skilled human physically demanding jobs. As such, this is an area of interest in a large proportion of the work; combining sensors into a workable system enabling feedback control to advance the capabilities of humanoid robots. The integration of multiple sensors into a robotic hand gives rise to complexity issues such as the number of connections, overall system bulk, and the trade off between localised and global processing.

The iCub fingertip is an implementation of capacitive sensing that is used in a distributed sensory system aiming to match the anatomy of the fingertip for use on a humanoid hand. A flexible PCB is used to arrange 12 rigid capacitive sensors around the finger, which is overlaid by a compliant foam silicone coating and a grounded encapsulating outer electrode. The fingertip is designed to emulate the resilience to manipulation control errors of human fingers, whilst providing broad area tactile feedback [Schmitz et al., 2010]. The capacitance is calculated locally to each fingertip and a global CAN - Controller Area Network - is used to feed the data back to a central control board. A relatively complex microcontroller capacitive measurement PCB is employed locally to the fingertip, but which requires only minimal spatial volume at the tip. The digits are linked together to form a full hand [Jamali et al., 2008].

The GIFU Hand III is designed as a robotics research platform providing humanoid

characteristics such as opposable thumb and sensory feedback. It features a high number of sensing points; 859 in total [Mouri et al., 2002], however few are presented on the fingertip as they are spread from fingertip to base of palm resulting in approximately 7 sensors per tip. The sensors are based on conductive ink separated by a thin film, which varies resistivity proportionally to pressure [Kawasaki et al., 2002].

The implementations described are examples of current state-of-art humanoid hands. The sensor density in both examples is relatively low, and hence could be considered as multiple single point sensors rather than a 'sensory skin' that provides zonal sensing. The lack of sensors effectively limits the extent of manipulation tasks due to the inability to track surface shape and contours.

5.4 TACtile sensor and artificial fingerTIP - TACTIP

The TACTIP sensor is part of a class of optical tactile sensory devices used to detect external force stimuli. It is designed to use optical input and a structured FOV - Field of View - emulating cutaneous components found in the human finger to provide high resolution tactile sensing of a region of interaction of the device with a surface [Chorley et al., 2009] shown in Figure 75. The tactile sensing it provides, achieves the goal of retrieval of highly accurate external surface details. Other devices based on similar optical technology have been presented [Yong, 2009, Ohka et al., 2006], however the research and optimisation of TACTIP have made it a class leading technology.

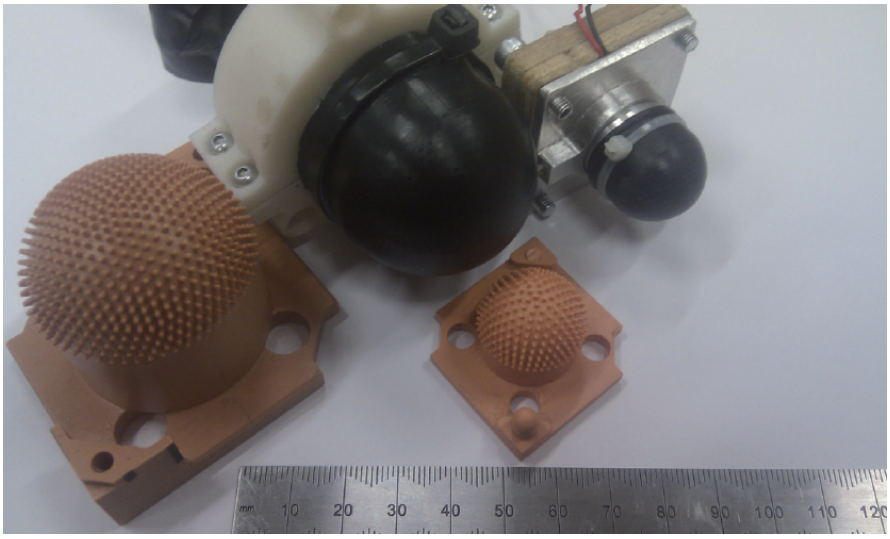

Figure 75: Photo of original TACTIP device and corresponding casting moulds (reproduced from [Chorley et al., 2009]).

The fingertip - the biological inspiration for this device - uses a number of uniquely specialised sensory nerve cells to discern any tactile stimulation. Of these sensors, Meissners corpuscles are located between dermal papillae in the papillary layer of the skin (Figure 74a). The spatial location and physical attributes of these sensors are hypothesised to detect the lateral strain developed orthogonally to the surface [Chorley et al., 2009].

When the TACTIP sensor comes into contact with an external surface, its compliant skin flexes following the undulations of the surface. This flex orientates the internal pins (or papillae) orthogonally to the gradient of the external surface. This gradient can be assumed to approximately match that of the contact surface. This is dependent on how closely the membrane can conform to the surface and the comparative difference between feature size and pin separation. The relative displacement of the papillae tips is recorded by the camera over a wide FOV and gives rise to its exceptional tactile sensing performance.

Human skin features inelastic but flexible outer layer and papillae, combined with the soft and deformable sub-dermal internal construct. This can be mimicked using

elastomeric compounds. Having replicated the structure of the skin, the retrieval of the parallelised touch sensory information is needed. In most cases this is a difficult task to solve due to problems of scaling, mechanical interference of sensory structure, and complexity of parallelism etc. However, the novel use of an optical sensor, is an essential part of the TACTIPs capability. It provides high resolution, high refresh rate capture of large image based datasets. Fabricating the device to emulate the finger's mechanical structure and using a translucent internal gel allows the internal optical sensor to accurately capture the papillae movement. The performance is further optimised by reducing interference from external ambient light, using infrared as the illumination medium for capturing the papillae tip locations. The tips are painted white to maximise reflection and contrast to the outer shell of the TACTIP (painted black). The camera is adjusted such that the focal depth matches the range over which the pin tips will move.

The TACTIP is a device with high density tactile sensing when compared to the current state-of-art alternatives described. Whilst very promising in sensing capability, the overall size of the standard TACTIP module is quite large (diameter of 50mm). However, it has been shown to be scalable to a size comparable to that of a human fingertip [Winstone et al., 2013], whilst maintaining effective zonal sensing.

The TACTIP approach to sensing a scene allows the capture of stimuli at many sensory points simultaneously with maximal sensory contact surface - the entirety of the contact surface of the tip is sensory as opposed to alternative implementations where areas are used for connections and circuitry. The operation over an hemispherical surface is innovative and effective for capturing point force and scene contact features using the papillae to mechanically amplify the forces.

5.5 Embodied Active Touch

Active perception is used in literature to describe the use of displacement to facilitate sensing of an environment [Gibson, 1962, Lepora, 2015]. This definition includes the use

of active sensors (such as electromagnetic or ultrasonic sensors), but also encompasses the controlled movement of a passive sensor to receive external stimulus. Relating active perception to the sensory paradigm of touch, which is manifested in mammals as the somatosensory system, the perception is narrowed to the physical inference of the environmental state (through sensory feedback) and known as active touch.

The differentiation of active touch (from passive touch) could seem a needless and dispensable clarification, especially when related to the field of robotics, where movement and controlled interactions are inherent. However, there is reason to separate the two; to allow there to be a distinction between which object is considered to be in control of movement relative to the sensor. A passive touch sensor can receive sensory stimulus from a dynamic environment without moving. Active sensing requires the sensor to be controlled in its interaction with the environment. An example cited is the focal adjustment of the eye [Bajcsy, 1988]. The eye and body is orientated to the region of interest, the lens is adjusted to bring a target object or zone into focus, the retina retrieves the targeted information.

we do not just see, we look - Ruzena Bajcsy [Bajcsy, 1988]

In the perception of physical contact characteristics, active touch describes the movement of a tactile sensor relative to a surface, to learn more about the surfaces form and composition using dynamic stimulus and feedback analysis. The embodiment of active touch can therefore be made through a variety of novel architectures using passive sensor technologies ranging from capacitive to optical, to receive information whilst manipulated. Active touch has been specifically developed on a number of platforms [Visell et al., 2016, Pearson et al., 2007, Lepora and Ward-Cherrier, 2016]. The use of other passive sensors will also be discussed as a means of providing a robot with active touch through the manipulation of its limbs. This distinction is made to discern systems that have been developed with active touch as a focus, and those developments that can

provide active touch as the passive touch component of an active system.

The sensory units described in this chapter thus far are passive. They cannot enable or control their interaction with their surrounding environment. Each sensor must rely on external manipulation. Some sensors are not designed to be used for active touch; *StretchSense*^{TM} has been developed and produced as a physiological aid or telemetric sensor rather than for their use in robotic systems [O'Brien et al., 2014]. When a passive tactile sensing unit is specifically designed for, and deliberately paired with, a robotic system, which enables a method of control through sensing dynamic interaction with an environment, that sensor has the characteristics of an embodied touch system; It is no longer passive in its interaction. The iCub robot is an example of a system with active touch. When attached to the end of a controllable end-effector the capacitive sensor array can be used to purposefully interact with its surroundings. Similarly this can be used to describe other humanoid sensing hands.

Although humanoid robots are a focus of a large proportion of research for sensory systems, other approaches have been investigated for their use in exploratory systems. Some approaches found in nature are highly tuned to visually occluded environments such as seals and rodents [Hanke et al., 2010]. These specialised methods are a useful inspiration for a novel approach to sensing.

Developed as part of the BIOTACT EU project, Whiskerbot is a robot which was designed to emulate the vibrissae of rodents [Pearson et al., 2007]. This system uses actuated whisker sensors to detect local stimuli including surface characteristic information from the dynamic interactions of the whisker on the near-field environment. This performs an exploratory function, but also protection (object avoidance) in visually impaired operation scenarios with dynamic environments. The system explored the use of modular active touch single point sensors in an array of 24 whiskers. The perturbation effects of external stimuli on the expected sensory feedback from a predetermined patterned oscillation of an array of whiskers is used to determine location, shape and

texture of external objects.

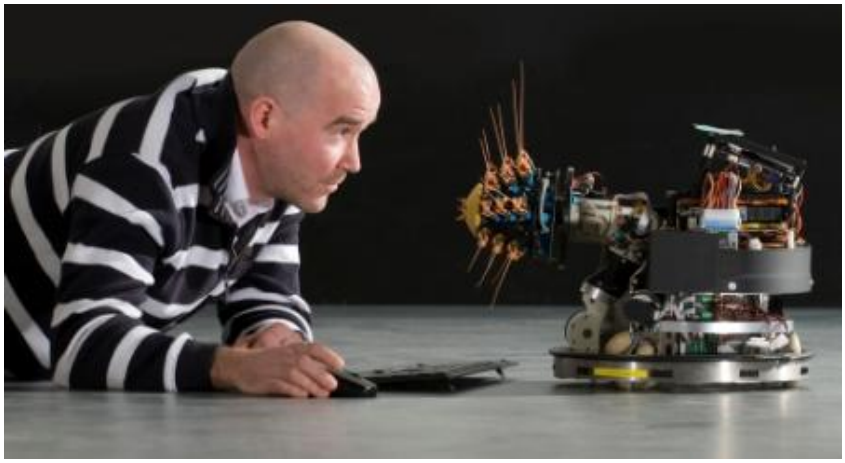

Figure 76: Photo of prototype Whiskerbot.

Pinnipeds (e.g. seals, sea lions) use their whiskers to track potential food via the vortices the prey produce as they move through the water [Hanke et al., 2010]. The mammals generate a whisking motion using their follicle sinus complex (FSC) [Valdivia Y Alvarado et al., 2012] to actuate the whisker. The whisker movement is then interpreted by mechanoreceptors in the follicle to understand the flow perturbations generated by prey.

The active touch implementations described are entire robotic systems, which are built from the ground up, with the robot as an essential part of the dynamic control of the passive sensor. Modularising an active touch unit allows the separation of active touch from the holistic system control of a robot. In situations of physical constraints and low visual stimulus - for example opaque fluid in a complex piping systems found in industrial complexes - the robot may not be able to provide consistent repeatable control over short distances due to the environmental constraints. An active module that has an optimised control could be invaluable in certain scenarios.

5.6 Pressurised Active-Touch Sensing Module

The TACTIP is a single variant of visual touch sensing technology. It is a passive sensor implementation, primarily designed for robustness and durability, and in recent developments has been explored for use applications in industrial conventional robotics as part of a robotic end effector sensing system [Lepora and Ward-Cherrier, 2016, Ward-Cherrier et al., 2016]. Although the unit can act as a sensor in a robotic implementation, it is inherently passive as a stand-alone unit. It is designed as a passive sensor, requiring the attachment of an external actuator - either from a controlled system or uncontrolled environmental stimulus - to the sensor in order for the sensory unit to move around and retrieve information actively. However, the TACTIP is not the only method of implementing the innovative optical sensing system. The essential elements of the TACTIP - sensory membrane with papillae and optical sensor - can be re-engineered into a module design as a novel self-contained active sensor. Considering it for use in lightweight soft robots, the original design is too heavy and rigid. In this work a set of novel developments have advanced the sensor for its use in soft robotics.

5.6.1 Pressurised Vessel Sensor

The TACTIP uses a spherical cap shape to provide a localised tactile sensor. The spherical cap can be replicated using pressurised air using the pressure difference from inside the capsule to the external environment to form an inflated skin. Using an airtight cylinder with a planar skin membrane, a hemispherical cap enables the creation of a spherical sensor. The pneumostatic vessel idea takes inspiration from nature in the form of similar vessels in mammals and invertebrates (e.g. earthworm, elephant trunk, octopus tentacle, and fish swim bladder). In these the hydrostatic body allows antagonistic coupling between muscles and sensory surfaces. In all mammals, muscular hydrostatic structures are used to perform manipulation and the outer skin provides sensory feedback

adding an extra layer of complexity (e.g. the tongue).

The envisioned pressurised vessel creates a comparable field-of-view (FOV) for the camera whilst allowing the removal of the transparent gel inside the membrane of TACTIP. Although the gel replicates the fatty tissue found in human fingers, it is not essential to the visual sensing of a surface, rather emulating the biological structure of the finger. Omission of the gel makes the sensor much lighter, but the pressurisation of the vessel maintains and enables enhancement of the essential functionality; the membrane is now free to stretch with pressure variation of the internal pneumo-static volume.

The development of a pneumatically supported thin sensor membrane creates a much less constrained skin. The membranes which form the pressurised spherical caps at the ends of the vessel can be tailored to provide specific mechanical characteristics; For the actuation membrane through the variation of dielectric material composition and the use of pre-strain, for the sensory membrane through material and papillae dimensions, density, zonal patterning, external surface texture etc. These characteristics enable the use of the conceived device to carry out specific tasks and in specific environments. Variation of the material properties not only aids in the shaping of the sensory surface, but through the DEA allows it to be dynamically extended, thus creating an implementation of active-touch. The pairing of an elastic membrane and a pneumatically pressurised vessel enables the modularisation of a dynamic sensor, which can be controlled by modulating the pressure inside the pneumatic vessel.

5.6.2 Sensory Skin Actuation

To modulate the pressure, a number of methods could be used:

- A compressor could be used, which would allow pressure control through electromechanical valves.
- An actuated syringe with external fixed volume could be used to modulate the

internal volume and hence pressure within the sensor module.

These possibilities require external components which add bulk and weight that essentially tie down the sensor to fixed location applications and remove its modular capabilities.

Considering less conventional actuation options, developments in soft materials have allowed thin membrane actuators to be provide a pressure differential to modulate pressurised vessels to form pumps [Lotz et al., 2009, Carpi et al., 2010b, Hines et al., 2016]. Exploring the development of a pressure difference, it can be seen that DEAs can be used as an integral pressure pump. Combining this novel actuation with the idea of a pressurised cylinder a module can be formed with a sensing membrane on one end, and the other end to be encapsulated using a DEA membrane. As such both membranes oppose each other when the module is pressurised through pneumostatic coupling. The pressure can be modulated by the application of voltage to the DEA membrane causing the skin membrane to dynamically stretch, and extend or retract as required. The DEA is lightweight, potentially proprioceptive, scalable and as a continuous surface, seals the pressure vessel. The sensory membrane could also be made active - functioning as a DEA - to increase the displacement of the membrane, as the materials used in its fabrication are capable of dielectric actuation. However, the antagonistic membrane is a preferable actuator for actively deflecting the membrane, as it separates the contact surface from the high voltage surfaces required to provide actuation.

5.7 ActivePneumostaticTIP Concept

The abstractions discussed in this chapter thus far are the formative innovations of an active-touch antagonistically coupled pneumostatic sensor, based on an optical tactile system. Named ActivePneumostaticTIP or APTIP - the combination of the pressurised DEA antagonistically paired with a pressurised sensory membrane to form an active device -, it is an implementation of the sensor as a proof of concept showing the func-

tionality of the actively sensing module and its potential uses. Figure 77 illustrates how the ActivePneumostaticTIP would operate.

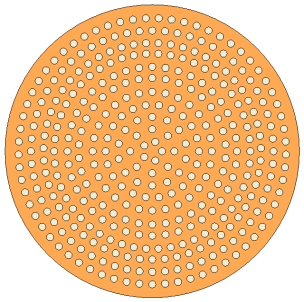

(a) Spread of Actuated Pins

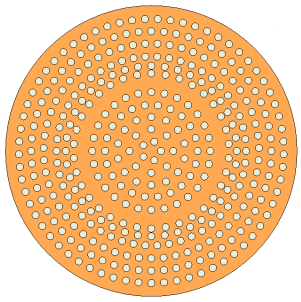

(b) Spread of Relaxed Pins

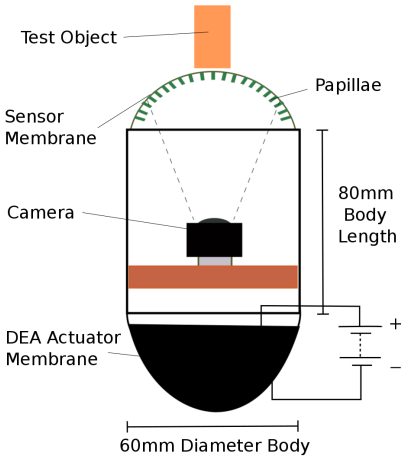

(c) Actuated DEA APTIP

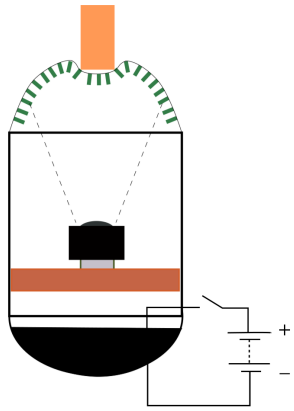

(d) Relaxed DEA APTIP

Figure 77: Diagrammatic representation of APTIP actuation and sensing of object.

As discussed the DEA would protract the sensory membrane allowing it to explore artefacts in its immediate surroundings. The concept of an ActivePneumostaticTIP physical device consists of four principal parts, the skin, optical sensor, pressurised vessel and actuator. The pneumostatic vessel uses an acrylic tube to form an inextensible cylindrical body as shown in Figure 78c & 78d. Each end has a soft membrane attached. The sensor membrane depicted in Figure 78c is comprised of a silicone skin, cast with papillae, and forms a passive membrane used with the camera sensor sealing one end of the vessel. Sealing the opposing end of the tube is a pre-strained DEA actuator. The

pressurisation of the vessel enables the coupling of the active and passive membranes through the pneumatic pressure in the vessel. The silicone skin is protracted through the contraction of the DEA actuator (through discharging the actuator). The silicone membrane is passive and is only moved through the coupling of the membranes on the ends of the pneumostatic vessel. The ActivePneumostaticTIP is designed so that it is inherently safe for human robot interaction (HRI) at the sensory end. The palpating surface is passive and the high voltage isolated inside the rear of the cylinder. In the event of a puncture or DEA breakdown, deflation of the pneumostat will occur, retracting the membrane from surface interaction.

The internal camera is used to track the individual papillae and map the surface of the membrane. Actuation of the coupled DEA enables the membrane to envelop and probe a surface. Figures 78c & 78d show the ActivePneumostaticTIP unit in actuated and relaxed states, the switching of which enables the probing of an object. The field-of-view (FOV) of the camera is shown in the diagrammatic representation and captures images of the domed silicone membrane shown in Figure 78a & 78b. If considered from the camera's perspective, the pin head density can be seen to increase around this specific test object, decrease at the object edge and stay approximately constant at the centre, for the APTIP states actuated (retracted) and relaxed (protracted) respectively. This is useful for detection purposes through the measurement of pin density.

The DEA actuator membrane and silicone skin form domed ends to the APTIP. With the pressurisation the membranes form a coupled pair. In order for the device to palpate a surface, the DEA actuator must be first in an actuated state (relaxing the DEA membrane) prior to the sensor approaching the surface; With the DEA in its actuated state the skin is retracted. The skin is then protracted by discharging the DEA actuator.

Development Note - The development of a soft sensor required the combining of two ideas using similar membrane based concepts. However, the function and materials of

these membranes were not comparable. The membranes are inflated, forming spherical caps as part of the pneumostatic design, which strains the membrane non-uniformly. The materials used in the design are different for each function (e.g. actuation, moulding to form sensory papillae) as it required specific design. This has meant that the pairing is complex and has material features such as pins, which make predictive analysis of the active or passive material very complex. For this reason the focus was on empirical analysis.

5.8 Materials and Methods

The proposed concept design shown in Figure 77 requires the integration of four major components:

- An air tight vessel
- Internally sealed and externally connected Camera
- Fabrication and attachment of a DEA
- Fabrication and attachment of a sensory membrane

The cylinder required an air tight seal to maintain the pneumatic pressure to couple the two antagonistic membranes of the DEA and the sensory membrane. Air was chosen as the medium for coupling the membranes, as this allowed the sensor to be lightweight and limited the need for further isolation of the camera module and high voltage membrane. Inside the vessel a camera would be mounted with a transmission line sealed through the vessel wall. Additionally an air inlet would be required. As such holes were drilled and sealed using epoxy resin once the cable was fitted. The vessel was made of two halves allowing the fabrication of the actuation and sensory membrane to be separable. The arrangement also allows for adjustment of the camera for optimisation

of FOV without adjusting the membranes. The diameter of the tube affects the design specification of the camera mount and the membranes.

Based on the limitations of the FOV and DEA sheet material dimensions, the APTIP module was constructed from a 2-part body made of acrylic tube of diameter 60mm, length 80mm and thickness 3mm. The sensory and DEA membranes were each attached to a body section. The two parts were joined with an airtight seal using duct tape. The module was inflated to a determined pressure and used in the experimental setup shown in Figure 81.

The camera module used a standard CMOS sensor on a board of 30mm x 30mm dimensions. The internal camera captured video at the maximum frame rate and resolution of the sensor (720x540 at 30fps - the frame rate varied with frame data size). This was the highest frame rate that could be attained from a commercially available video capture product in the price range to make a low cost proof of concept, which required heavy customisation to reduce weight and size. It was thought that the frame rate and resolution were sufficient for gathering of active-touch data. The camera included a manual focusing thread adjusted lens. A USB camera was mounted on a 3d printed cylindrical frame and inserted into the tube with the lens facing the sensing membrane.

The FOV of the camera was recorded using a simple measurement test whilst maintaining required focal length. A scale on a piece of paper was placed in front of the camera at a set distance. The focal distance was adjusted to match the distance from CMOS sensor to membrane, once inflated. The aim of the focusing was to allow the FOV to match the range of protraction of the sensory membrane. This could be further fine-tuned in the module experiments as required to optimise image clarity. From these tests the FOV was calculated as 45mm at a focal range of 40mm. This measurement was used to position the camera mount inside the vessel.

The APTIP uses a hemispherical sensory membrane which could be formed from a domed mould as used with TACTIP. This would use an optimised fabrication method,

however the diameter of the hemisphere would be dictated by the mould and hence influence the module size and limit variability for optimisation. Although this form could have been modified to counteract some of these constraints, however the membrane coupling - forming the basis of the active-touch functionality - would be compromised due to the form and lack of flexibility of the domed mould. The resulting form from an inflated flat membrane is comparable to that of a domed membrane. As a flat cast, the membrane specifications including thickness, size, pin spacing and length could be modified rapidly. Due to the number and influence of these factors a flat membrane design was chosen.

To create the flat sensory membrane, a material was required that could be easily moulded, would be light, compliant and elastic, whilst being resilient to some wear. A low shore hardness silicone was chosen, as it met these requirements owing to the variety of stiffness available, ease of use through prior experimentation - and as such, ease of use -, and the wealth of research in its use and fabrication methods in the soft robotic field. The material was also chosen due to its potential for DE actuation, if a two-sided module could be developed. Xiameter 3483 (Shore A -13) [Dow Corning, 2011] was the silicone chosen as it offered a good compromise between resilience, flexibility and elasticity [Dow Corning, 2018].

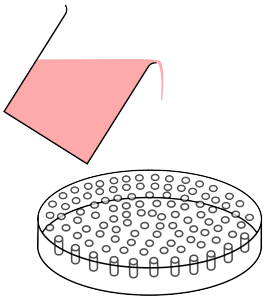

(a) Step 1: Pouring of degassed silicone in to acrylic mould.

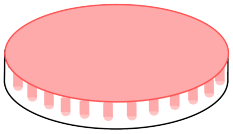

(b) Step 2: Allow silicone to cure.

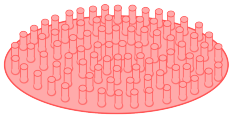

(c) Step 3: Demould and refine finish.

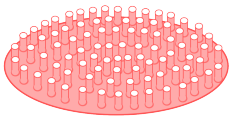

(d) Step 4: Paint tips of papillae.

Figure 78: Fabrication steps for production of silicone sensory membrane.

Figure 78 shows the steps used to create the silicone sensory membrane. A drop cast process was used to produce a thin layer with pins. An acrylic mould was laser cut with holes to create papillae and a small spacer below the mould was used to ensure the silicone flowed through and holes in the mould filled fully. A pin width of 0.75mm was chosen, trading flexibility for resolution, after some experimentation (examples are shown in Figure 79; the thinner the pin the more its tip would displace, while increasing diameter resulted in a stiffer pin, but also leading to a more inflexible membrane due to area of attachment of pin to membrane at the base Additionally practical limitations of available substrate material - the laser cut acrylic was available in millimeter increments. A pin length of 6mm generated a papillae head translation of +/- 3mm (assuming generated angle from axis orthogonal to surface of 30 degrees) to enable external object sensing

and tracking. This is shown in Figure 80. The membrane was made using Xiameter 3483 - with a Shore hardness of 13 -, which was deemed to have a balance of flexibility, strain, and robustness. The silicone was prepared using a vacuum to remove any air that could affect the quality of the membrane or pins - and hence affect the integrity of the pneumo-stat or the sensing capability of the device.

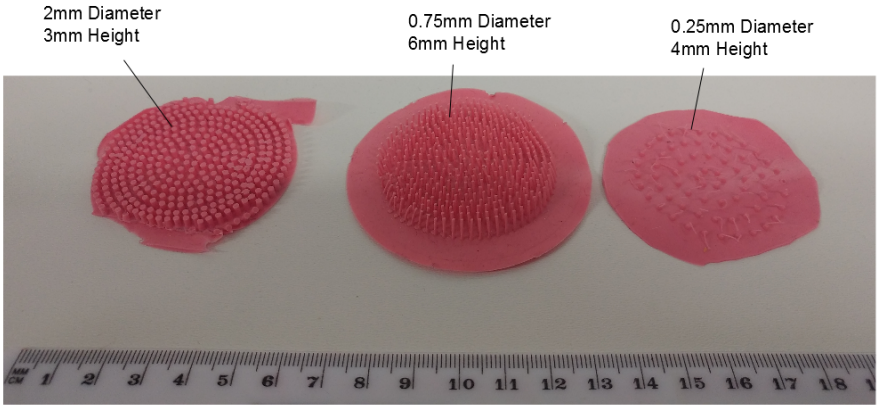

Figure 79: Photo of test pieces of sensory membrane.

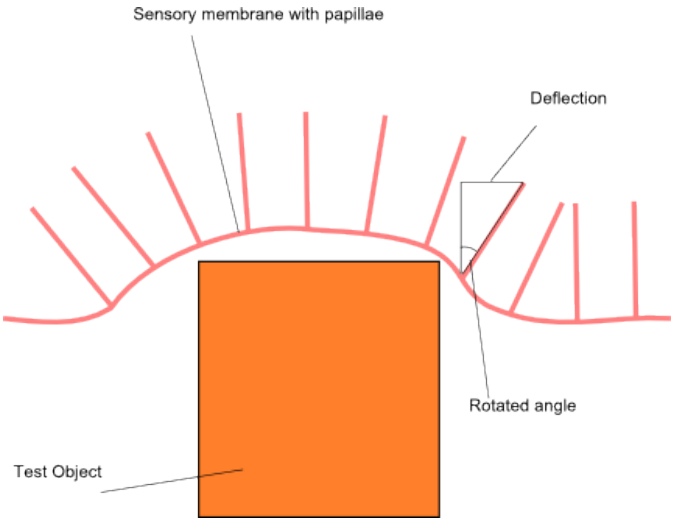

Figure 80: Illustration of deflection of papillae on sensory membrane resultant from contact with test object.

To control the thickness of the sensory membrane layer, laser cut acetate layers of

known thickness were used to precisely specify the membrane. For the specification of the pins, holes were laser cut into an acrylic sheet of precise size and length. Figure 78 shows an illustration of the finished membrane, where painted tip papillae are distributed over the soft inflatable membrane. The pin tips were painted to differentiate the tips from the background of the membrane, aiding in the calculation of pin displacement in image processing.

The DEA is designed to produce the force to protract the sensory membrane and allow it to interact with the environment. In its low energy state - with no voltage applied - the membrane is extended to a displacement established from the developed pressure in the pneumostatic vessel from the contained air. The application of a high voltage across the DEA membrane causes it to biaxially strain, and the dome it forms to expand and protract from the body of the vessel. This shifts the static volume in the vessel retracting the sensory membrane. In turn, when the DEA is grounded, the tactile sensor is protracted.

The DEA material chosen was VHB^{TM} 4905. This was selected due to its reliable and high volume fabrication by 3M^{TM}, enabling repeatable tests. Furthermore, previous research has characterised the optimal properties for maximising radial expansion of the membrane through the application of specified high voltage based on pre-strain. This known relationship allows repeatable, reliable tests to be performed, which can be replicated expediently in the event of failure.

To effectively couple the DEA to the sightly thicker and stiffer silicone sensory membrane, the VHB^{TM} acrylic membrane was biaxially pre-strained to 4.5 times its initial size. This enabled good volume matching at each end of the pneumostat over a range of volumetrically useful initial pressures. An initial pressure of ≈20mbar was chosen as this gave a good initial protracted displacement of the sensory membrane.

5.9 AP-TIP Characterisation

5.9.1 Experimental Setup

Using the methods described, an APTIP module was created and used to confirm and characterise the displacement of the active-touch sensory membrane, from its retracted position. An inflation pressure was applied to provide a predetermined steady state displacement of the active DEA membrane for optimisation of strain, and hence volumetric displacement. A laser was placed orthogonally aligned to the tip of the hemispherical pressurised membrane. The experimental layout is shown in Figure 81.

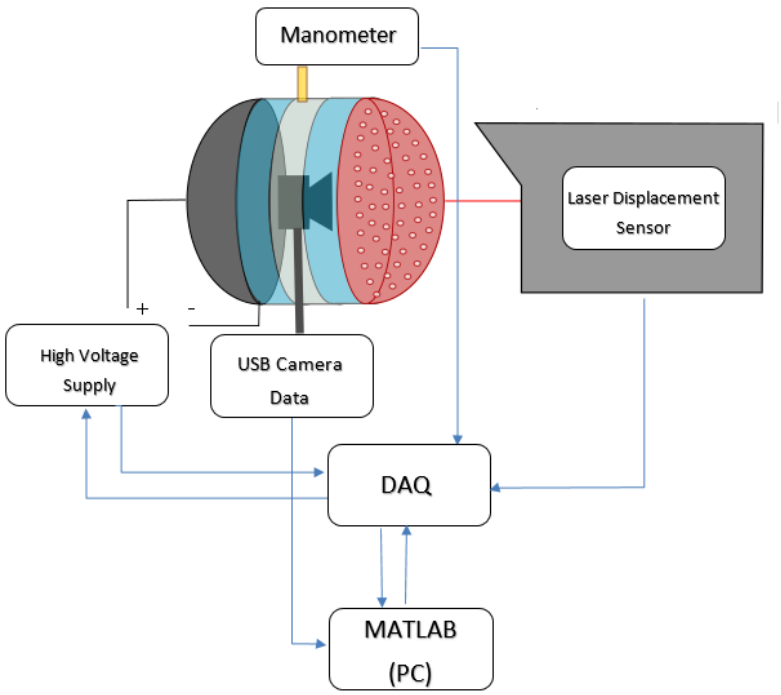

Figure 81: Schematic of characterisation rig setup for APTIP.

5.9.2 APTIP Static Tests

To maximise the displacement of the sensory membrane, and hence its active palpating capability, the module was tested over a range of input voltages in its pneumostatic con-

figuration at a fixed initial pressure. For each test, the voltage was held low for 2 seconds to retract the membrane, then held high for 2 seconds to allow for the displacement to stabilise and finally held low for two further seconds to allow the membranes to settle - allowing for any residual viscoelastic deformation. The pressure and displacement were recorded at each of the voltages tested, to provide some insight into the coupling of the membranes.

From the experimental setup, two sets of data were obtained - an orthogonally aligned external video capture of the APTIP and a set of synchronised pressure and laser displacement data measured with varying voltage. For the experiments the following equipment was used:

- DAQ - NI USB 8343
- Laser Unit - Keyence LK-GD500
- PC - computer running MATLAB software

Strict safety protocol was used in the experiments, using an insulated test space and isolated high voltage supply. The setup is further described in Appendix C.

Video Analysis

In the recordings captured of the individual tests, snapshots of maximum displacement show features of the actuator with successive application of increasing voltage, as shown in Figure 82. Figure 82a shows the membrane as an idealised hemispherical cap. Figure 82b shows the relaxation due to actuation, which extends the DEA along the longitudinal axis of the vessel, but also shows some expansion at the edges. In Figure 82c, the expansion seems to be predominately circumferential expansion as the membrane balloons outwards. Finally in Figure 82d the sideways expansion is even more noticeable, with some wrinkling clearly visible on the membrane surface.

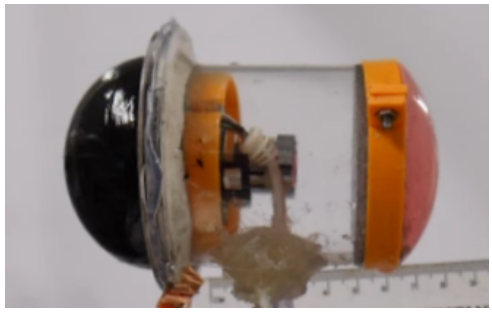

(a) Snapshot of passive state (0kV)

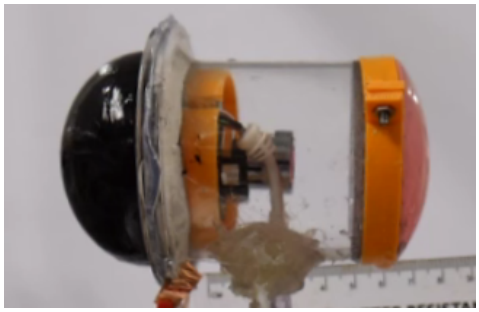

(b) Snapshot of active state (3kV)

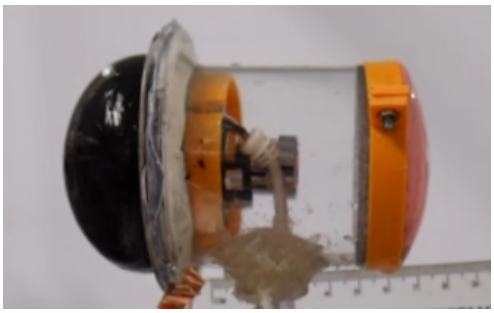

(c) Snapshot of active state (4kV)

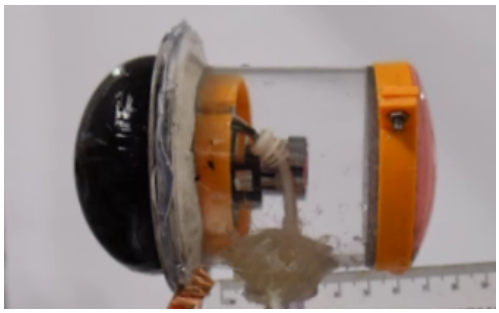

(d) Snapshot of active state (4.75kV)

Figure 82: Actuation of APTIP at varying voltages

Wrinkling

As mentioned, at higher applied voltages, wrinkling artefacts are clearly visible on the DEA membrane near the interface with the rigid vessel frame. Under the influence of uniform orthogonal stress a planar compliant membrane will strain uniformly biaxially.

When considering a spherical expansion with an inflating pressure, there is significant deviation from ideal biaxial strain. The conditions at the edge of the membrane are highly non-uniform, due to the boundary effects of the rigid acrylic frame to which the DEA membrane is attached and the elastic membrane itself. This adhesion restricts the strain circumferentially near the edge of the actuated section of the dielectric membrane. As the strain increases this effect becomes more pronounced. The deviation from biaxial strain is apparent through the wrinkling seen at the side of the membrane shown in Figure 83b, which, when compared to the unactuated form of the membrane shown in Figure 83a. Figure 83c shows how the wrinkling affects a large band at the outside of the

actuated surface. The effect is pronounced on an inflated membrane where the effective circumferential stress reduces to zero. This is possible where the inflation pressure reduces significantly or the strain is very high, which have both shown to be the case in these experiments.

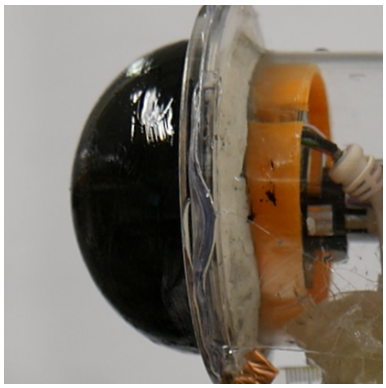

(a) Passive (unactuated) DEA membrane

(b) Actuated wrinkling DEA membrane

(c) Close-up image showing wrinkling details of DEA membrane

Figure 83: Photographic evidence of wrinkles on pneumostatic DEA when actuated with voltages approaching material breakdown.

Wrinkling was found to occur from 4kV. After wrinkling was present it was noted that the displacement began increasing again with higher actuation voltage before electric breakdown of the membrane occurs. Thus a safe optimum application voltage can be identified for the tests at 3.5kV.

Data Analysis

The synchronised pressure and pole height data is shown in Figure 84. The laser displacement data was converted to provide a precise pole height measurement of the sensory membrane. It can be seen that there is a close link between the pressure and pole height, both following the same curve. The relationship in region (i) follows typical DEA behaviour (as expected from a coupled diaphragm system, where the pole height has an inverse square relationship with voltage [Carpi et al., 2007]), with Figure 84 showing the pole height of the opposing sensory membrane (measured) falling with increased voltage. There are two significant non-linear features in the data. In region (ii), between 4.25kV and 5kV, the pole height increases by approximately 1.5mm or 20 percent of total pole height. It is hypothesised that the increase of pole height of the sensory membrane is due to droop described in the data in Figure 86. This droop may have caused the volume in the actuator spherical cap to drop and hence increase the pressure and inflate the sensory membrane. It may also be affected by the coupling of two different non-linear materials in an antagonistic configuration.

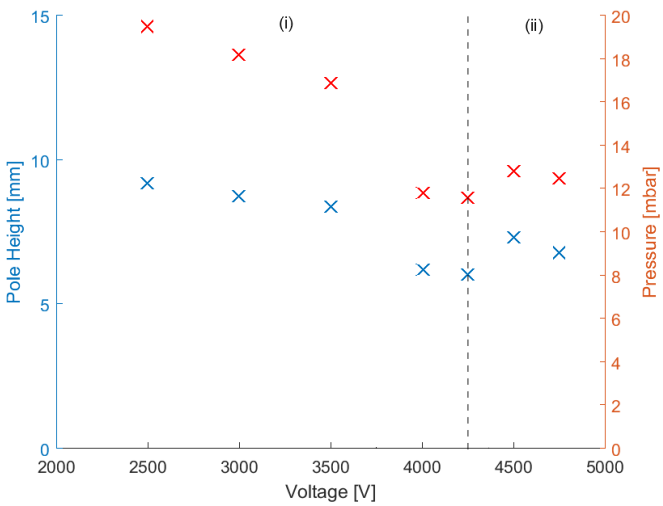

Figure 84: Plot of pole height and pressure against voltage for pneumostatic characterisation.

The shape of sensory skin affects the distribution of the papillae from which information is recovered. From Figure 85 the membrane can be approximated to ideal and thus the skins strain and the position of the pins can be calculated over the actuation cycle.

Assessing possible drivers for these effects, the video capture was found to provide some insights. Figure 82 shows the retraction displacement of the membrane at 0V (initial state), 3, 4, and 4.75kV. To investigate how the sensory membrane deflects with increasing voltage, Figure 85 shows the membrane outlines overlaid. The results show that the sensory membrane can be considered to be an approximately ideal spherical cap throughout its retraction and protraction cycle. The shape of sensory skin affects the distribution of the papillae from which information is recovered. As the membrane can be approximated to ideal, thus the skins strain and the position of the pins could be calculated over the actuation cycle, to model and negate any pin deviation effects.

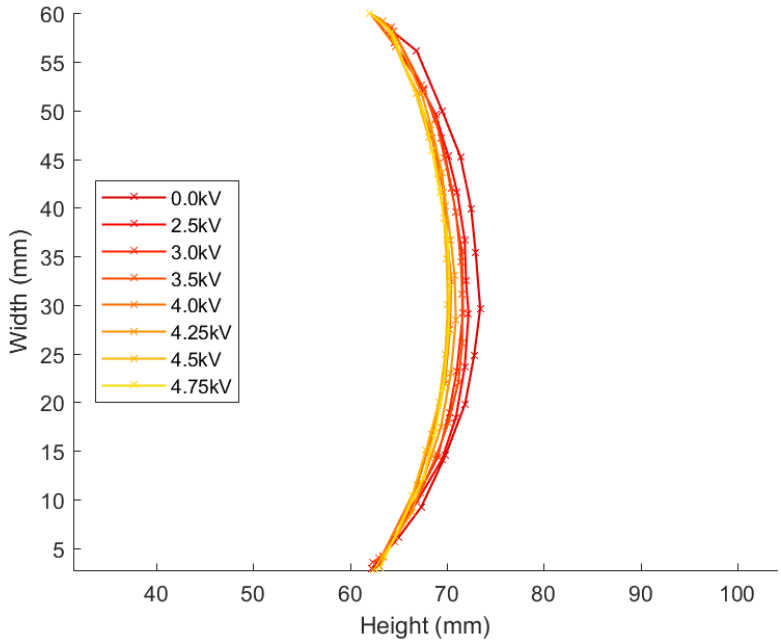

Figure 85: Plot of sensory membrane retraction on actuation recorded from video frames.

Due to equipment limitations of laser displacement sensors, the pole height of the active membrane was not precisely measured. The shape and characteristics can be investigated from the video. Initially in Figure 82a, the membrane can be seen to be of ideal shape, but under actuation at 4.75kV shown in Figure 82d, the expansion is non-ideal forming a squashed dome. Additionally wrinkling can be seen on the outer edge of the actuated membrane. Using the same evaluation method as previously, the membrane protraction can be overlaid to see how it varies with voltage shown in Figure 86. Although volumetrically initially larger, the pole height of the actuated membrane does not increase as much as expected. From this figure, it can be clearly seen that the ideal cap, expected to be formed by the active membrane, does not deform solely longitudinally, but laterally, forming a squashed dome. The membrane is also seen to droop slightly, which is assumed to be due to the influence of gravity.

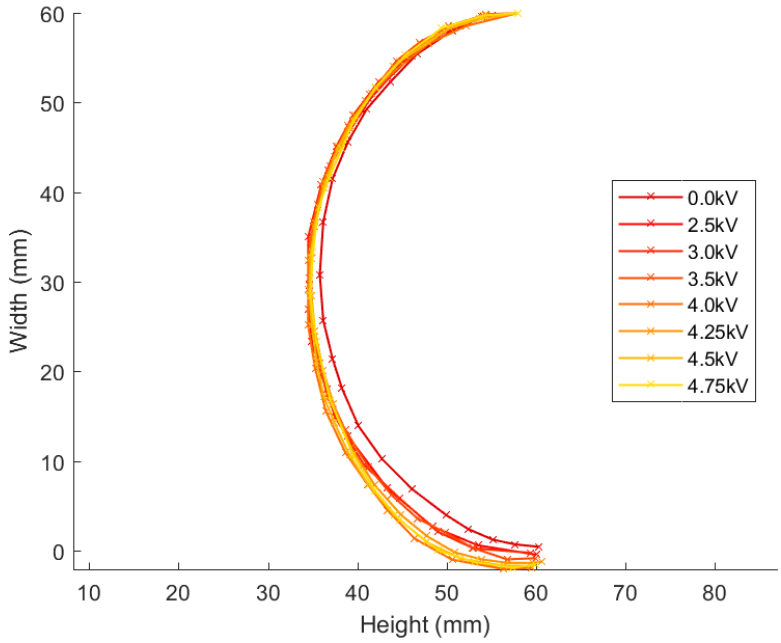

Figure 86: Plot of actuator membrane expansion on actuation recorded from video frames.

The droop of the membrane is caused by the weight of the membrane (and carbon grease electrodes) distorting. The pressure drop associated with the relaxation of the membrane reduces the pressurisation of the membrane as it extends, which led to the slight asymmetry. The droop was calculated as having a maximum of 4mm over a 60mm membrane. The asymmetry of the spherical caused by the gravitational droop will affect the volumetric displacement and hence the maximum retraction of the sensory membrane. Although the experimental vessel orientation could have been altered and the tests re-run, the gravitational effect would have still been present. If held vertically the gravitational effect of the heavier sensory membrane would have limited the displacement.

The antagonistic coupling between the opposing membranes underpins the active-touch capability of the sensing module. Considering the air inside the cylinder as an ideal gas at the operational pressures <20mbar, the expected pressure-volume relationship can be simply described using Boyles law - assuming temperature is constant -, and it can be assumed that any effects of compressibility of the gas are negligible enough to be ignored.

$$p1.V1 = p2.V2 \tag{15}$$

The illustration in Figure 87 shows the antagonistic arrangement and the volume shift. The volumetric sections of the APTIP have been separated and labelled such that:

$$p1.(V_{A1} + V_{B1} + V_{C1}) = p2 * (V_{A2} + V_{B2} + V_{C2}) \tag{16}$$

The internal initial volume can be predicted from the shape of the membranes in the non-actuated state where both membranes are approximately ideal. However, as discussed, at high actuation voltages required for optimal sensory skin displacement, the DEA does not form an ideal hemisphere, thereby limiting measurement of the internal

volume [Fleisher, 2002].

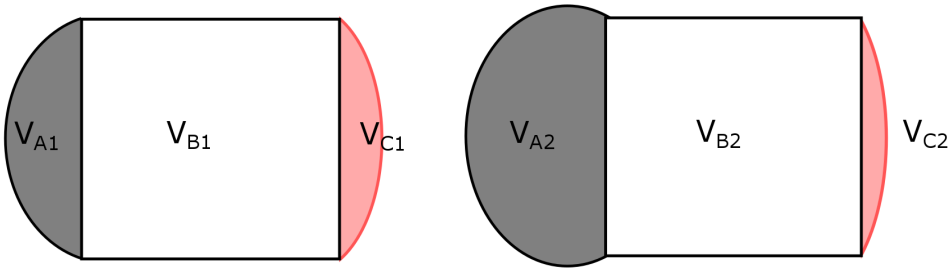

(a) APTIP with sensory membrane in protracted state.

(b) APTIP with sensory membrane in retracted state.

Figure 87: Illustration of APTIP volumetric changes between states.

Any air volume in the tubing to the manometer can be considered negligible.

DEA Membrane Breakdown

The tests of the APTIP module were concluded with the electrical breakdown failure of the DEA membrane. This was recorded and an anomalous displacement reading found. On further inspection it was found that immediately following breakdown the membrane was protracted momentarily by 2.3mm. This unexpected displacement was found to be due to the near instantaneous retraction of the DEA membrane. In its actuated inflated state, the membrane is at a maximal (given a specific voltage) energy state. When the dielectric membrane breaks down, this causes two effects. Firstly the short-circuit of the electrically charged plates (carbon grease); Secondly the resultant spark causes (in most cases) an air outlet from the pneumostat. Due to the size of the hole the first effect is dominant. It is hypothesised the discharge releases the elastic energy stored in the membrane producing a pressure wave inside the vessel, which protracts the membrane. The pressure then equalises between the internal and external surfaces of the pneumostat, causing both sensory and actuating membranes to retract.

Although not applicable to this work this momentary pressure variation causing some protraction may be of use in some developments. However, the eventuality of a

breakdown or failure of the membranes are shown to cause the retraction and inherently safe failure of the high voltage actuator.

5.9.3 APTIP Dynamic Tests

Figure 88 was created to generically describe the relationship between pole height, vessel pressure, and voltage input for the vessel. It can be seen that the pressure is inversely proportional to the applied voltage. At Figure 88 sector (i) the conductive plates of the DEA are grounded; there is no voltage applied across the actuator membrane, and the sensor membrane is protracted. As the voltage across the DE membrane is increase, it relaxes, expanding and reducing the pressure inside the vessel in sector (ii). In sector (iii) the sensory membrane is fully retracted (minimum pole height), the vessel pressure stabilises at a new level, as the voltage across the DEA is at its maximum.

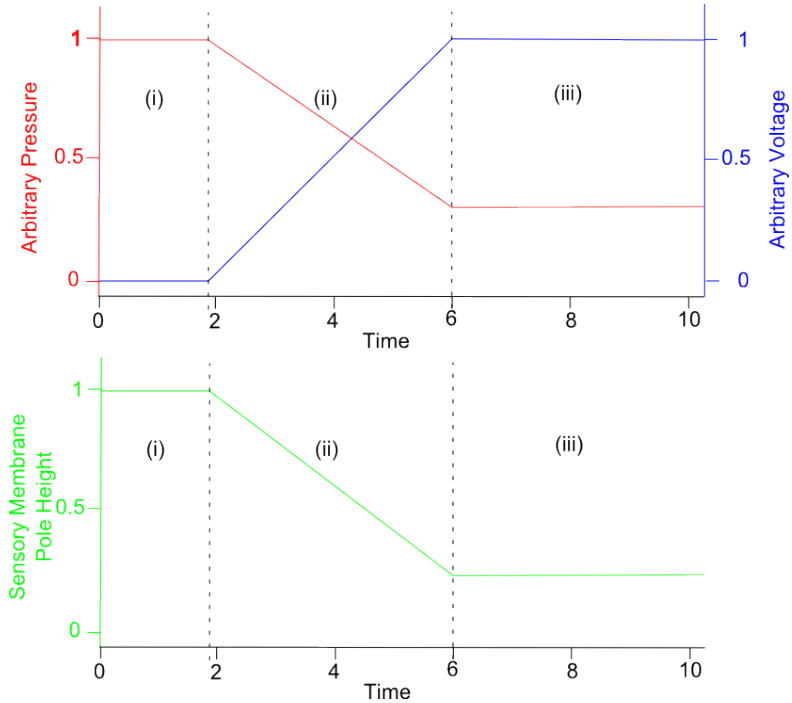

Figure 88: Illustrative plot of dynamic variation of parameters with actuation of DEA pneumostat.

To evaluate the dynamic functionality (protraction and retraction of the sensory membrane) of the active-touch, a test object was placed within range of the sensor and a test actuation cycle performed. The voltage, DEA membrane displacement, and internal pressure of the vessel were recorded, with the internal video captured by the camera. A square wave input voltage was applied to the DEA.

Figures 89 show the particle image velocimetry (PIV) of internal frames displaying the FOV of the camera. The frames sequence show the protraction distancing the pins from the camera (Figure 89b), their dynamics splaying (Figure 89c) as they conform to the object, and final resting protracted state (Figure 89d).

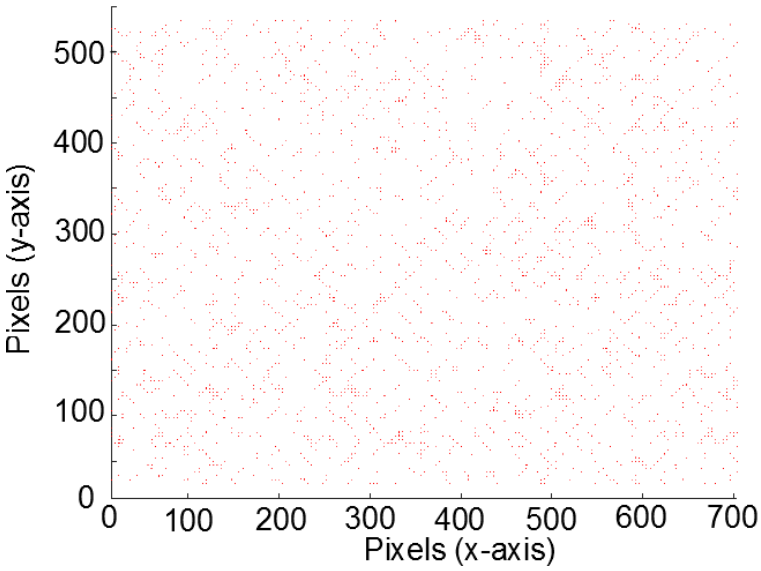

(a) Protraction Frame 2

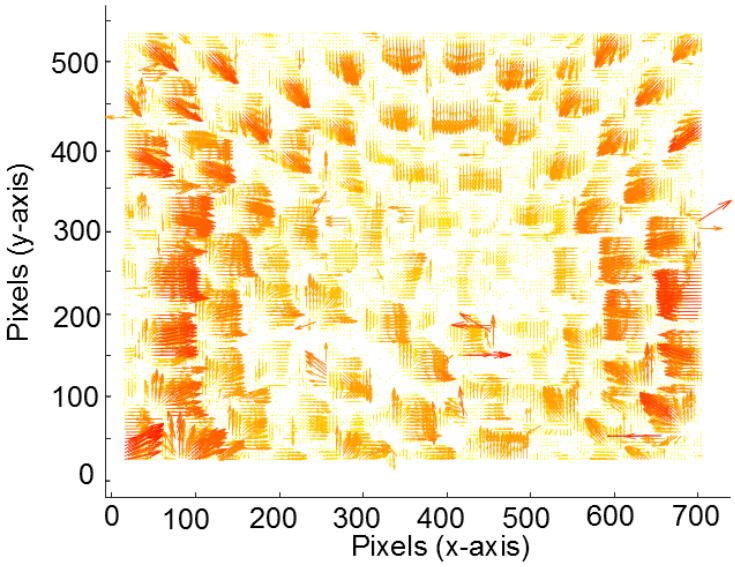

(b) Protraction Frame 4

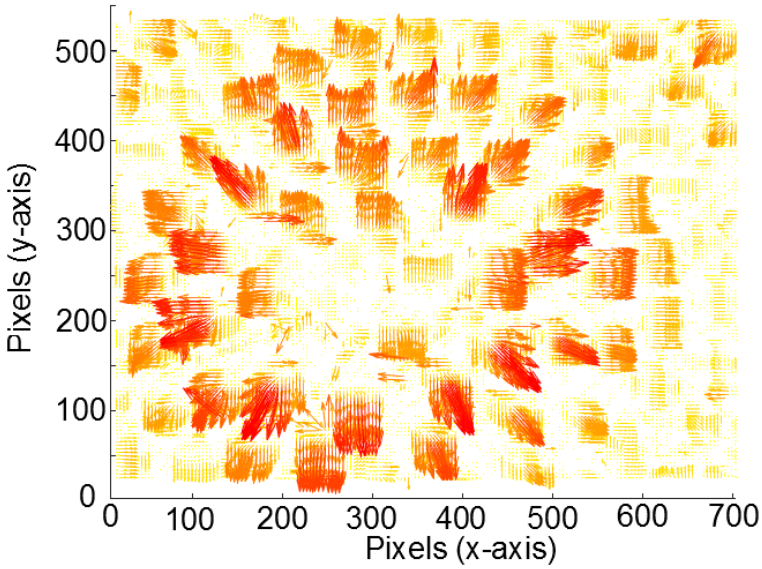

(c) Protraction Frame 8

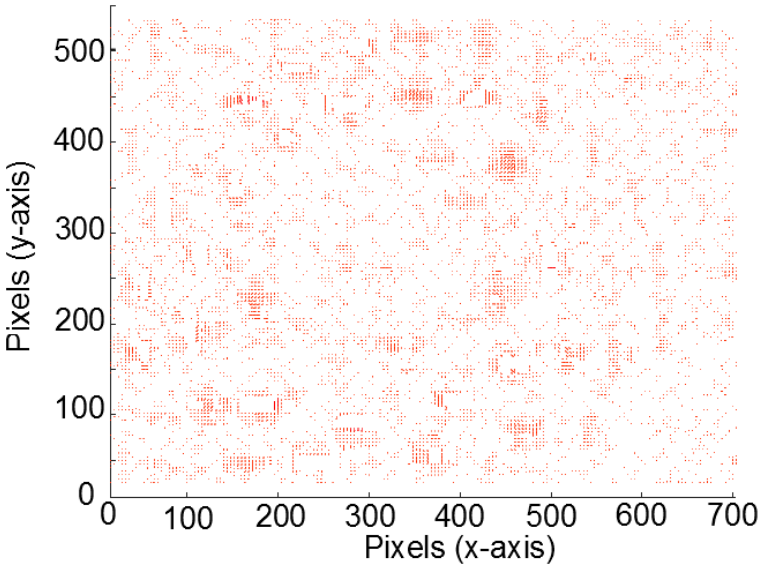

(d) Protraction Frame 12

Figure 89: Processed data of internal camera video frames of sensory membrane protraction.

5.10 APTIP Module Object Palpation

Having confirmed the parameterisation of the APTIP through characterisation, and optimisation of the pairing of active and sensory membranes to maximise protraction, the module was tested with the aim of retrieving scene-wide features in an environment. For these tests a series of test objects were identified and fabricated. A range of objects with multiple features, some with sharp angles, were constructed - a prism, cylinder, cuboid. The 2D shape of the end face was of particular interest. Additionally, the interaction of the tactile sensor with a featureless planar surface was also used, to capture the effect of the pins on membrane conformance to a flat obstruction or wall. The test objects were aligned end face towards the membrane to maximise the feature impression and measured 10mm across. This was chosen to allow the membrane enough 'free' contact surface to conform to the edges of the object. The experimental set up is shown in Figure 81 , with the addition of the test object (shown in Figure 92). The pneumo-stat and external object are in fixed relative positions with a spacing of 5mm. The external object was placed within range of the active sensor, and with its end face in the same plane as the end of the APTIP body.

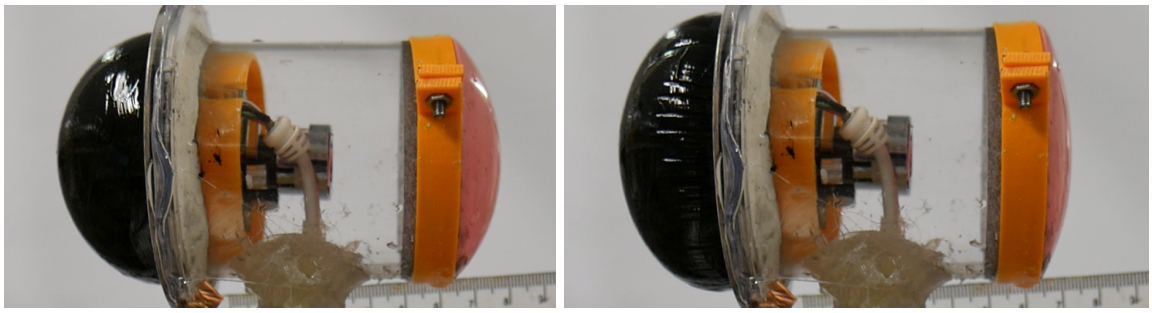

(a) Photo of APTIP with sensory membrane in protracted state.

(b) Photo of APTIP with sensory membrane in retracted state.

Figure 90: External Photos of ActivePneumostaticTIP

The camera recorded the papillae movement during this time and a single actuation cycle was used to analyse the sensory feedback for each of four test objects (cylindrical

block, cuboid block, and triangular prism block) shown in Figure 91.

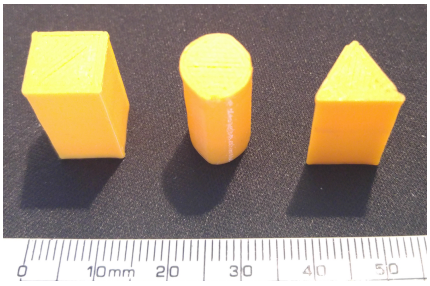

Figure 91: Photo of test blocks used in sensory membrane object detection tests

5.11 Experimental Setup

A similar setup was used for the experimental test interactions of the APTIP with test objects, however the displacement was not recorded due the the orthogonal alignment of the test object to the hemispherical sensory membrane. The image below illustrates the changes made to the set up in Figure 81 - replacing the laser displacement sensor with test objects.

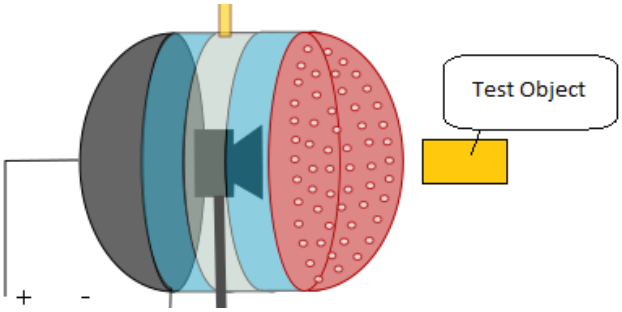

Figure 92: Schematic of APTIP set up for object detection tests

5.12 Image Processing of Camera Video

As discussed in Section 5.8 and Section 5.2.2, the pins remain orthogonal to the membrane as an object is touched. The membrane conforms to the object and at edges or

angled surfaces, this causes the pins tips to translate in the 2D plane of the field of view of the camera. The raw image data of the initial and final resting conditions of the pins during a protraction cycle are shown in Figure 93. In each case, it can be clearly seen that a discernable shift in pins is visible in the FoV of the camera, however it is not immediately obvious in which direction each pin has shifted.

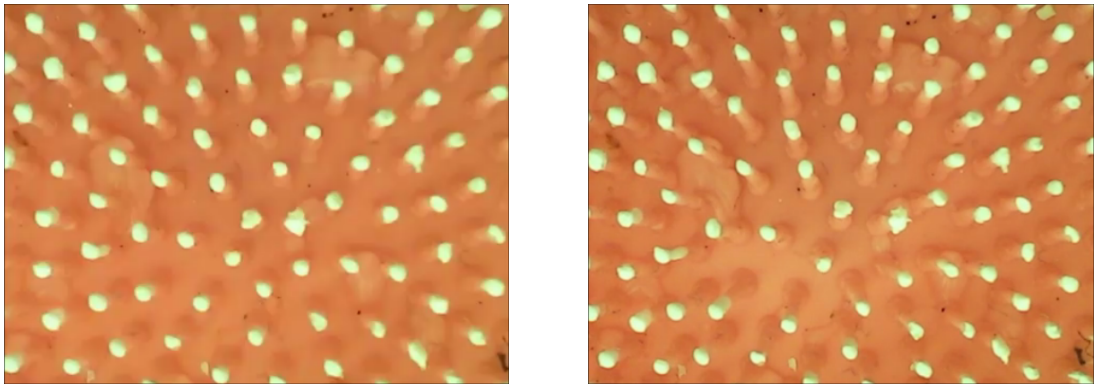

(a) Internal image of sensory membrane pins with membrane retracted

(b) Internal image of sensory membrane pins with membrane protracted on circular object

Figure 93: Unprocessed frames from camera of circular object test

5.12.1 Image Processing Methods

To analyse the movements of the pins in more detail to capture the resultant sensing from the protraction of the membrane onto the test objects, a number of image processing methods were considered:

Particle Image Velocimetry (PIV)

PIV is a processing technique which analyses the velocity of particles over a planar (2D field) to create a velocity field. Comparison of pixel blocks of an image provide a velocity vector; repeating this process over the whole image gives a velocity vector field. A matlab tool called OpenPIV was used to process the images [Taylor et al., 2010].

Pseudocode Algorithm:

1. Divide video into a set of frames.
2. Use interrogation windows to identify speckling.
3. For all interrogation windows across consecutive frames:
   (a) Locate speckles, and calculate velocity and size.
   (b) Calculate velocity for each window.
4. Plot velocity vector field.

For each of the test case objects, PIV - particle image velocimetry - was used to confirm whether objects could be identified. In each case the PIV images the travel of the pins is represented by a heatmap of vector arrows showing the amount of pin movement during the object palpation. Multiple sample rates were tested to try to maximise the object recognition. When a global optimum PIV parameters were found, the parameters were fixed for PIV analysis across all tests objects. An interrogation window of 64x64 pixels was used with a 8 pixel window spacing for the PIV. Using the PIV across the full set of frames from the video of the membrane protraction, the computed vector field was found to have low amplitude for many frames (Appendix D). It can be seen in Figure 94 that as the voltage drops across the actuated membrane, the sensory membrane and associated pins protract, resulting in the inward pin movement in the FOV as the distance between camera and pins increases, shown in Figure 94 a. Once the membrane contacts the test object the pins then splay around the edges of the object causing an outward movement of the pin tips shown in Figure 94 b.

A simplified version of PIV was considered, due to the limitations of the frame rate on attaining useful data from the PIV. As the captured active-touch was found to be limited to approximately two frames (dependent on frame to voltage application timing), binary digital image correlation would enable the analysis of the data of the

touch captured to be processed. This uses a pair of images and considers the velocity of particles in the same way as PIV. Using this method both the initial protraction of the sensory membrane and the contact with the test object can be captured. The examples in Figure 94 show the results for a circular test object:

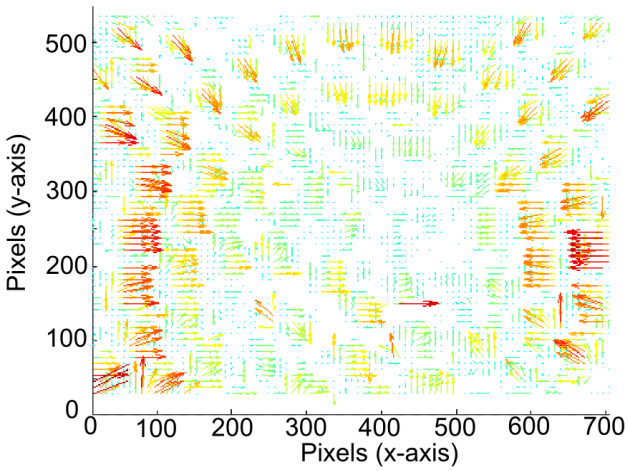

(a) PIV between frames 4 and 5 on DEA relaxation

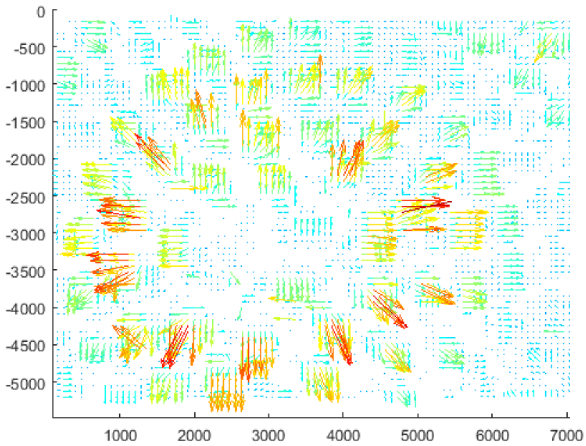

(b) PIV between frames 8 and 9 on sensory membrane contact with test object.

Figure 94: PIV of succcessive frames at key state changes.

Using a binary PIV of sequential frame pin positions resulted in a clear, interpretable

vector field showing the movement and the shape made on protraction of the membrane and contact with the object. The output shows the movement of the pin tips and tracks their displacement.

Pin Centroid Tracking

Instead of considering velocity vector field, which assumes that elements of an image could be moving in all of the field, a second algorithm was considered using centroid tracking. To do this the image was scanned for pins by looking for concentrations of high luminance in a grayscale thresholded image of the FoV of the camera. The centroids were then located in subsequent images and then correlated to the centroids of the previous image. This was repeated over the complete set of images from the protraction of the membrane onto a test object.

Pseudocode Algorithm:

1. Divide video into a set of frames.
2. Grayscale frames.
3. For all frames:
   (a) Locate centroids of high luminance pixel clusters of threshold size.
   (b) Find closest centroid in previous frame.
4. Plot paths of pins.

The path of individual pin tracking is shown in Figure 95:

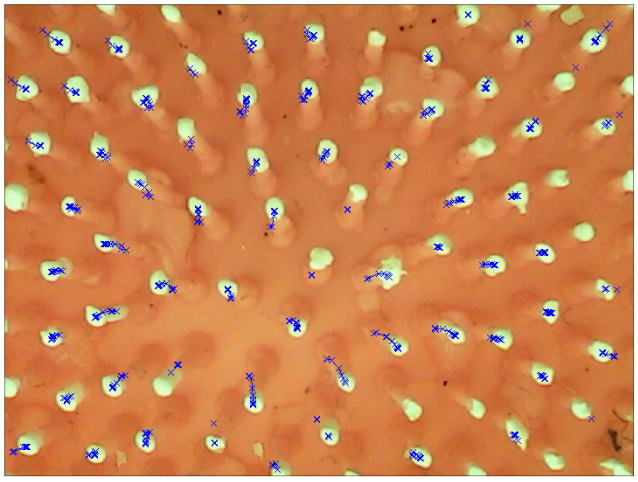

(a) Vector tracking of individual pins for circular object detection test.

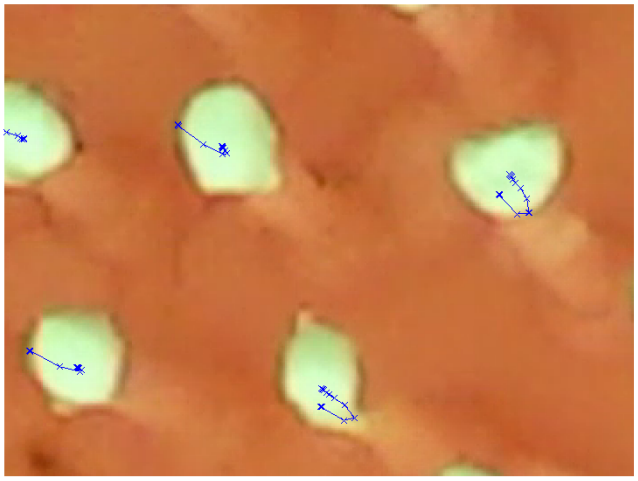

(b) Vector tracking close up of small group of pins for circular object detection test.

Figure 95: Circle object test individual pin vector tracking.

The centroid tracking shows the full path of the pin through protraction and conforming to the test object. In Figure 95a the tracking shows 'U-turn' trajectories of the pins, where the path vectors are shown overlaid on the final resting state of the membrane. The U-turns are shown in a magnified section of the image in Figure 95b. As the

membrane protacts, it moves away from the camera, and as such the FoV covers more of the membrane and the pins appear closer together. This has caused the displacement of the pin towards the centre of some of the pins. The membrane then contacts the surface of the test object causing the pins to incline and displace relatively on the edges of the object as the pins moved orthogonally to the membrane as it enveloped the object.

Pin Centroid Correlation

In a similar method to two frame PIV, the pin tracking algorithm can be simplified to process the frames only involved in the contact with the test object. The distance travelled was use to create a velocity vector for each of the pins.

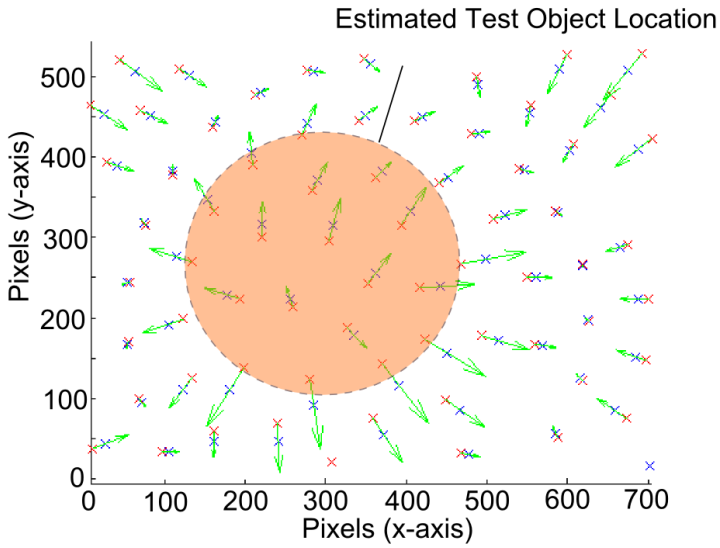

(a) Image of test object pin vectors (green) from consecutive video frames (marked red and blue respectively).

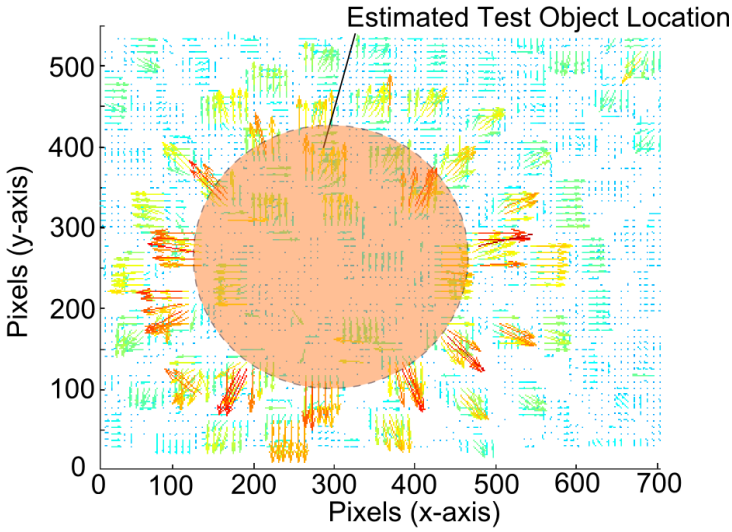

(b) Two frame PIV vectors from consecutive video frames using image processing tool.

Figure 96: Output of image processed frames from circular object detection test

The pin overlay figures for each test case show the retracted (red pins) and protracted (blue pins) states of the membrane with arrows depicting the cumulative movement vector.

5.12.2 Summary of Image Processing Development

PIV processing has shown that a higher frame rate camera may allow more complex analysis of the palpation of a test object. The current proof of concept is only able to provide two frame PIV output for the palpation as the whole pin deflection occurs within the window between two frames. Further analysis with a high speed camera (externally) may enable the specification and selection of a camera for this module for future tests. However, the resultant algorithm producing a single vector field resulting from the membrane contacting the test object does enable quicker processing and output of useful information on the local deflection of windows scanned on the membrane.

Pin tracking was also affected by the frame rate, but did confirm (as found in PIV analysis) that two stages of protraction and encapsulation of the object can be identified. The algorithm developed was able to identify pins and return its inter-frame displacement. This produced exact tracking information rather than a velocity vector field.

Following the analysis of methods of image processing and considering the nature of the data retrieved during the test (specifically the frame rate limitations which affected the number of frames over which the touch affected the pin positioning), two-frame PIV and pin centroid correlation were investigated further with multiple test objects focussing on the encapsulation frames of the videos recorded from the camera:

5.13 Analysis of Test Objects Contact

Through the analysis of the pin displacement when contacting multiple objects, it was hypothesised that key elements of the movement could be identified. With the frame rate limiting the data retrieved, the investigation focused on whether the test object could be identified and how the pins moved on contact with the test object.

Figure 97a shows the relative pin positions (blue - retracted, red - protracted). the arrow vectors show the direction of travel of the pins. It can be seen there is a square block with approximately 30° rotation shown, where pins have only minimal movement in the central region of the image (depicted by short blue arrows). Surrounding pins can be seen to spread and conform to the sides of the object.

Figure 97b shows the PIV analysis of the initial and final sample images. As with the pin movement vectors a discernable object is recognisable with minimal movement in the centre and larger movements to the sides of the square palpated object. The corners of the square cause a rounding of the pin spread, increasing displacement, as the membrane conforms to the sharp intersection (red arrows). It can be seen that at the corners of the external test object, the pins splay in the direction the corner is pointing (on the middle left hand side of Figure 97b. A higher number of pins could decrease the rounding effect this demonstrated in the test module. The pin density and length will have to be optimised to improve the sensor accuracy.

In this test there is negligible lateral movement reflected in the very low vector magnitude inside the central region shown in Figure 97b.

5.13.1 Square Object Test

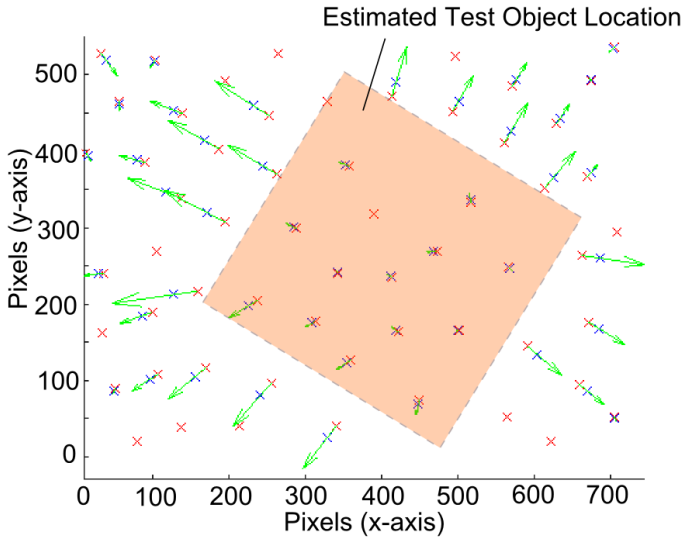

(a) Image of test object pin vectors (green) from consecutive video frames (marked red and blue respectively).

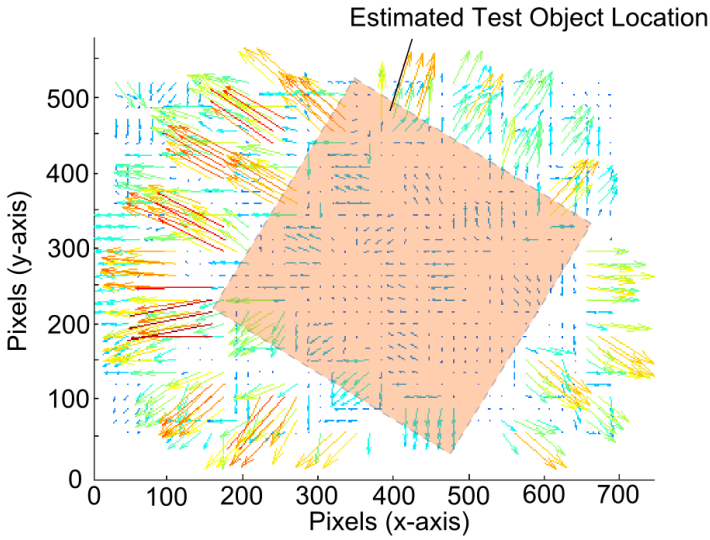

(b) Two frame PIV vectors from consecutive video frames using image processing tool.

Figure 97: Output of image processed frames from square object detection test

5.13.2 Triangular Object Test

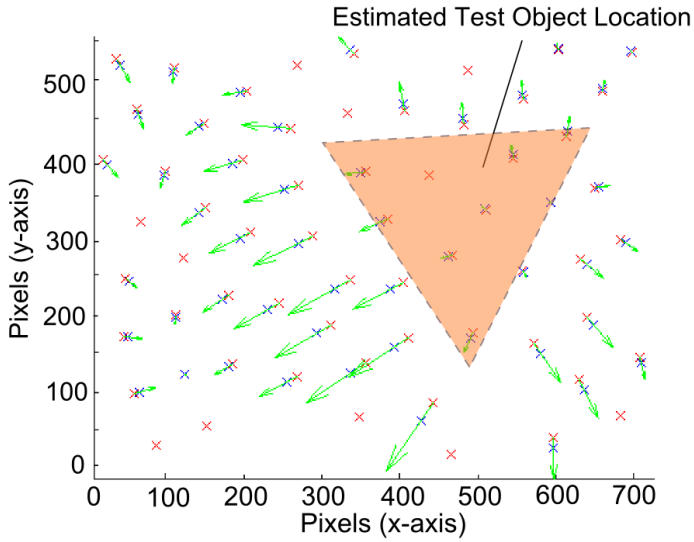

(a) Image of test object pin vectors (green) from consecutive video frames (marked red and blue respectively).

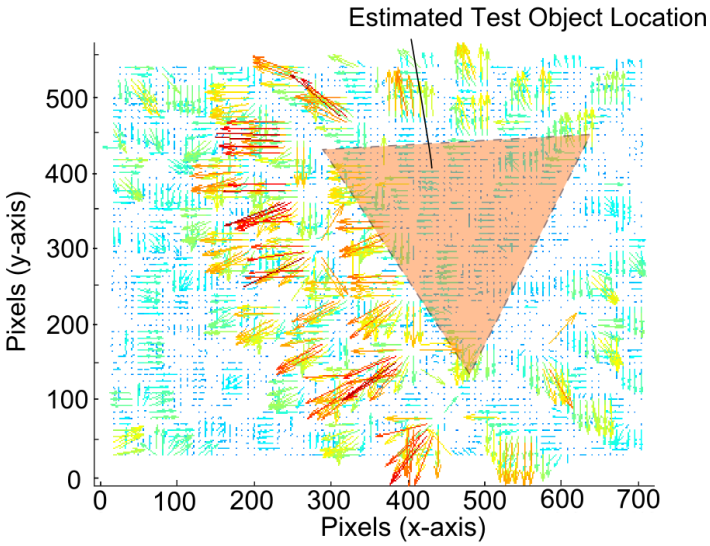

(b) Two frame PIV vectors from consecutive video frames using image processing tool

Figure 98: Output of image processed frames from triangular object detection test

Figure 98a shows the pin vectors over the period of protraction. The left hand side of the image shows a clear edge detection with pins splaying out on the edge and pins on the extreme of the FOV moving inwards as predicted. Although the triangle is not central

to the palpation, edges are still discernable on the right hand side.

In Figure 98b PIV vectors correspond to the triangular shape, with the left hand side edge of the triangle detected strongly. The membrane is conforming to the surface and, at the edges of the applied shape, showing a large change in density. The object is slightly misaligned in its mount leading to only a partial shape detection with both methods. The PIV also shows that the tip moulds around the most central edge, deforming the membrane along the side of the block, leading to a higher concentration of particle vectors and an increased pin density.

5.13.3 Circular Object Test

Figures 96a & 96b show post-processed data highlighting the differences in the protracted and retracted states. Figure 96a shows the circular spreading of the pins in the protracted state (blue pins) in the left of the image around a central pin. There seems to be only a very limited movement at the centre.

As discussed in Section 5.9.3, the internal image data shows a circular contraction of the pins on the edge of the image as the membrane moves away from the camera (Figure 94 a). The central spread occurs momentarily later in the protraction (Figure 94 b), which is due to the domed membrane flattening as it conforms to the shape, whilst around the edge of the cylinder, the direction of movement is highest, where the membrane envelops the object. At the furthest limits of the FOV corners, it can be seen that the pins are still moving inwards, where the membrane is not in contact with the object and the membrane returns to its domed shape.

It should also be noted there may be some lateral shift in the membrane to the right of the image. Without perfect alignment of the sensor and the object this will always occur, and shows the type of mechanical shift that will have to be accounted for in future work. The analysis of the pin overlay is backed up by the PIV tracking of the pins (Figure 96b) . The vectors show a circular expansion around a central point region.

The pin tracking analysis shown in Figure 96a) depicts a pin spread at the centre, and increased density of pins in the 2D image just beyond the circumference of the cylinder where pins move outwards and pins on the extremities of the FOV move inwards. This is replicating the expected response as shown in Figure 74c.

During the test, it was observed that the membrane did seem to rise in the centre of the circular object. As a result the membrane flexibility may need to be further optimised to fully conform to object details. The experiment shows that there is an inherent lower limit of object size, from which shape information can be retrieved for a given papillae density. The membrane will however, still detect the object, but not all of its detail.

5.14 Summary

In this chapter, the harnessing of DEAs and soft materials for an innovative zonal sensing technology has been presented. This has culminated in the development of a novel type of active-touch sensor, combining soft actuation technology and soft sensors in a pneumostatic modular frame. This innovation has been demonstrated through a proof-of-concept, developed to characterise the actuation and optimise the performance of active membrane palpation, thus providing an effective and dynamic sensor.

The coupling of the membranes at the pressures required was found to be more complex than originally anticipated, but the parameters could be tuned to produce a displacement in the order of 5mm. When considering that it is possible to reduce the cylindrical module length to near zero, this actuation can be significant and useful for a range of applications. It can be concluded that the module can be optimised to provide a useful millimetre range deflection active-touch sensor for feature detection.

The experiments have also shown that the implementation of an optical sensor in a lightweight module, with a soft actuator can still perform reliable shape detection whilst

adding the extra capability of active palpation of near-field environment features. The current pneumatic solution has not been tested with object manipulation and the thin membranes and low pressure will not be optimal for most tasks. But, with the increase in sensory membrane thickness and a stack DEA actuator, combined with an increased pressure, the benefits of the proof-of-concept module should be maintained whilst enabling direct interaction and manipulation of heavier dynamic external structures.

As discussed in section 5.7, the APTIP is a self-sensing active module, which can be applied to a number of tasks. It can be used as a statically located sensor, externally locomoted sensor, conventional robotic attachment, or as part of an self-locomoting soft robot. It's capability for sensing dynamic or static environments expands the range of applications. The modular design can, not only be used independently of external actuation, but can be attached to conventional and non-conventional robotic systems to enhance, for example, sensing in visually occluded environments, where delicate and dynamic sensing may be required. For these applications further characterisation of the vessel with different membrane thicknesses and pressures would allow optimisation to environmental conditions. Additionally, the effects of using different actuator materials would enable the benefits of high frequency palpation to be explored.

6 Conclusions and Further Work

6.1 Introduction

The integration of DEAs in coupled systems is still an area of intense research focus. These actuators have been shown to be efficient and can be tailored to a range of tasks, as well as having useful features such as proprioception. However, the route to creating high performance actuators through a repeatable automated fabrication using soft materials remains elusive. Additionally, the soft nature of the materials used makes integration into or with conventional actuation frameworks difficult. There is potential for reliability issues and exposure to high voltage if these problems are not resolved.

In this thesis, a number of research avenues have been explored to expand the capability and integration of DEAs:

The first aim was to explore multi-layer actuators and see how the current state-of-art could be improved, where significant limitations in extracting the performance found in single layer actuators meant limited progress has been made. The investigation showed that optimisation of individual layers and the mitigation of impacts of stacking (such as passive margin size) were the main issues experienced, although additional issues seemed under-explored such as laminate tensile strength. A number of optimising parameters have been characterised and combined in the formation of a novel multi-layer stack actuator. An optimal conductive layer was fabricated with a carbon black weight of 5%, and formed into a multi-layer actuator with captured pre-strained. These steps have aimed to remove some of the key barriers to developing an optimised stack actuator with performance characteristics comparable to mammalian muscle.

Secondly, integration of DEAs with rigid components is difficult due to the soft nature of the actuator materials and the potential for mechanical breakdown due excessive stress concentrations leading to membrane rupture. Hence, the separation of non-linear actuation dynamics from work output is extremely beneficial. The work has included

the design of a novel arrangement to separate the output from the soft actuator and produce an output that with multiple stable states allowing it to be used for a host of applications.

Lastly, the ability to sense in DEAs has been shown to be useful, however up-scaling its capacitive sensing leads to huge complexity for zonal sensors and would reduce performance if used for both actuation and sensing. Alternative sensing methods are available. This work has investigated and analysed how zonal sensing can be achieved in a soft body and has led to the production and characterisation of a novel soft active-touch sensor.

6.2 Conclusions

This thesis is split into three parts, which cover the individual topics of *integration and coupling of DEAs* investigated. The following conclusions were drawn from the work:

1. Developed Multiple Advances in Stacked Multi-layer Actuators.

- *Conductive silicone composite layers of thickness 100 microns can be produced with a carbon black loading of 5% by weight.*
- *A multi-layer DEA can be created using bonded layers to enhance passive mechanical strength, whilst maintaining a completely soft body.* A review of existing stacking methods has shown that bonded electrode and dielectric layers have not been utilised. Literature shows the use of adherence and encapsulation; methods which have been shown in tensile strain tests in this thesis to provide a far weaker mechanical strength under tension than bonded layers or mammalian muscle. This is an insight that led to the use of bonding to produce a layered actuator with bio-mimetic properties.
- *Pre-strain can be captured in an inherently soft bonded actuator.* The concept of

using all-silicone interpenetrating networks (S-IPN), which have been previously produced [Brochu et al., 2013], has been reconfigured to using the silicone conductive compound to enable the capture of pre-strain in dielectric layers. A new method for capturing pre-strain was developed to create a two layer dielectric actuator using a cured conductive compound to bond the pre-strained layers. This pre-straining enhances the performance of the actuator whilst providing the extra benefit of compression of the conductive layer improving range of operational strain*. To demonstrate the pre-straining method on an increased scale, an actuator with multiple dielectric layers was created using a manual stacking method; Conductive layers with a thickness of 65 microns and a carbon black weight of 5% was used to bond together three pre-strained laminated dielectric layers of 100 microns (initial thickness). When cured together they formed an actuator with dielectric retained pre-strain of 29%. The actuator produced a thickness mode contraction of 16%; an output which is comparable to mammalian muscle.

- *DEA stacks can be produced with 100's of layers using the advances described (pre-strain and conductive layer bonding.* A demonstrator stack actuator sample was produced with 16 pre-strained dielectric layers (each with an initial 100micron thickness) on a device capable of stacking >100 layers, to show that a method of stacking that could be up-scaled had been produced. Large multi-layer DEA stacks can be fabricated but the process is complex and intricate, especially with the introduction of performance enhancements such as capturing of pre-stretch. DEA stacks are still confined to academic research due to fabrication and operational limitations as the actuator technology is too immature.

2. Integration of Soft DEAs into Rigid Actuation Systems.

- *The use of flexible actuators to drive rigid end-effector displacement is currently*

*operational strain would be limited by the strain of the conductive silicone composite, where strain would temporarily break chains of connection and cease conductivity

under explored in the field of soft robotics. The field of soft robotics covers a broad array of technologies. Some of these technologies mimic biology using soft bodies and soft actuators to perform complex tasks that are difficult for conventional rigid robots to complete (such as gripping and squeezing through gaps [Bogue, 2012]). Mammals (among a broad set of other examples in nature) use soft muscle with rigid skeletons to enable forceful interaction with their surroundings. The review of literature found this is under-explored, which can in part be explained by the lack of high-power actuators of the scale and power density to mimic biological muscle effectively. However, this work aimed to use a combination of soft muscle and rigid links. The separation of actuator and output in soft actuator technologies enables a wide breadth of unitised actuation systems based on soft actuator technologies.

- *Characterisation of an antagonistic cone pair has shown that the force-displacement relationship is linear.*, which has since been confirmed independently by other works [Cao and Conn, 2017]. The characterisation of multiple cap and rod combinations led to the identification of the highest energy output pairing of 4.4mJ, with a mid-range size cap (20mm) and mid size strut (110mm). This was found to be different to the arrangement with maximum displacement of 6.4mm - with the combination of small cap (15mm) and strut length 100mm.

- *A novel mechanism has been conceived and an accompanying design space to produce a number of modes of operation of zero-energy fixity multi-stable devices.* The development of a non-back-drivable mechanism for a bi-stable concept was expanded to include a possible range of mechanisms which could use the energetic output of the antagonistic cone pairs linear displacement to produce:

  - Lock pin
  - N-State Translational Output
  - Stepper motor

  - Linear Screw drive
  - Other mechanisms are also possible

- *A non-back-drivable bistable actuator prototype with rigid output has been developed and has proved the concept can operate effectively.* The device was tested to provide bistable rigid output from a soft actuator.

- *Coupling arrangements can be developed for the coupling of soft DE actuators with rigid external forces using an approach which disconnects the actuator from the end-effector through mechanical coupling.* This idea could be used to bring soft actuation into use for applications traditionally reserved for solely rigid mechanical systems.

3. Develop a novel method of sensing using soft active touch.

- *A novel concept has been developed for a soft active-touch sensor.* Pairing of soft membranes in form prototype active pneumostatic vessel to provide zonal sensory feedback is an innovative idea, which may have a range of possible applications, which are further evaluated in Section 6.3.

- *A sensory membrane with papillae can be fabricated, and biased out-of-plane through pressurisation into a spherical cap and paired with a camera to produce a zonal sensor with an FOV of 45mm.* A pneumatic optically based sensor has been developed generating a comparable function to TACTIP [Chorley et al., 2009], whilst decreasing weight and widening the application space through the inclusion of modular active sensing.

- *An active-touch pneumostatic module (APTIP) can actively protract a sensory membrane 5mm using a DEA in an antagonistic pneumostatic configuration, and conform to the surface of an object and retrieve information of its shape.* DEA

actuators can be used in conjunction with the developed pneumatic sensor to produce an active touch coupled unit facilitating dynamic sensing of environments.

- *Multiple algorithm implementations can be used to tracking pins.* Both PIV and pin centroid tracking were able to detect pin deflection. Further investigation would be required to consider the trade off with data retrieve and speed of calculation for evaluation of real-time processing.

6.3 Discussion of Applications of Developed Technologies

The following section considers the application of the developed technologies to real-world applications.

6.3.1 Multi-Layer Actuator Optimisation and Fabrication

The focus of the study on multi-layer actuators has been on creating higher power soft actuators. Additionally the aim has been to create a contractile actuator with similar properties to mammalian muscles. The reason for this is to enable the creation of high efficiency artificial muscles that can deliver the tensional forces in passive and active loading to emulate biological muscles, or more specifically human muscles. This work was aimed at steps to making this a reality. The resultant actuator could be used in a plethora of systems and as such its applications span robotic technologies, medical prosthetics and beyond (from biomimicry to pumps and valves). The advantageous feature of proprioception could be used in addition to provide position feedback.

Biomimetic Muscle

The contractile actuation resulting from the stack actuator configuration could be used in a prosthesis to replace a missing limb. The efficient and silent actuation would enable long lasting and inconspicuous devices to be developed. The scale of these devices

could be limbs, but could also could replace small extremities such as fingers:

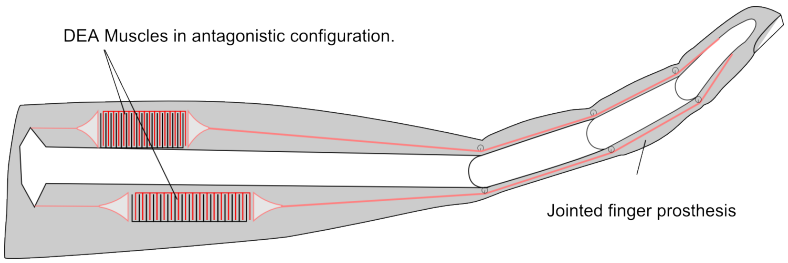

Figure 99: Concept of an antagonistic finger prosthesis

6.3.2 Multi-state Device Future Development

The design tested for a binary multi-stable mechanism was fabricated to produce a proof of concept device using a particular form of the broad range of modes of operation the device can be used to develop. The electro-mechanical structure and possible arrangements that could be used for many applications.

Valves

There exists a group of actuation systems used as control actuator forming a critical component of high-power systems e.g. pneumatic actuation valve in a system such as a McKibben muscle [Shadow Hand,]. This is essential in the control of the system, just as a transistor will control current flow in an equivalent electrical actuation system. However, due to the physical medium used in pneumatics, for example, a mechanical flow control is required.

For systems involving high-power pneumatics or hydraulics, there is a requirement to distribute pressurised fluids from vessel to actuator where flow is controlled by an actuated disc (or other method/configuration) [FISHER, 2005]. The valve is an enabling actuator, producing a low-power switching function to a high-power system. The precise control and variability of such a device is essential in the optimisation and control of the high-power actuator. Using conventional technologies, a popular example would be

a rotary motor actuating a disc butterfly valve. These can be bulky and can require constant current consumption in holding a desired position. Given these characteristics, the multi-state device described may be able to compete with conventional technologies used for this purpose.

Tactile Display

The suggestion of using DEAs for a Braille reader has been the subject of research since it was first discussed [Runyan and Blazie, 2010]. This is a significant target within from the group of novel actuators to develop e-Braille.

Braille displays are made up of dots. These dots are either created or adjusted to a predetermined height from the ground surface of the display. The difference in height is used by the reader to feel the symbol denoted in a Braille cell. The Braille cell is a collection of (most commonly) eight dots arranged as two columns of four rows. The dots in the cell are spatially arranged based on a defined standard. The requirements set out for Braille devices are not clearly defined, but are characterised in a review paper [Runyan and Blazie, 2010]. Currently Braille readers consist of a single row of up to 40 cells using linear actuators to power the pins. This technology leads to higher power consumption and bulk [Runyan and Blazie, 2010] leading to heat dissipation issues. An example is shown in Figure 100:

Figure 100: Photo of common braille display device (reproduced from [Runyan and Blazie, 2010])

The multi-state actuators use as an electronic Braille reader as part of the accessible technologies available to the blind or visually paired was chosen. In this application the device is shown in one of it's most rudimentary designs. The use for e-Braille is also useful for comparison with other DEA arrangements. This is because the use of DEAs as a solution to enable the production of a Braille reading tablet has been previously postulated. As a result examples exist of DEAs in alternative configurations in designs for this application. There are some problems that may arise from creating a miniaturisable mechanism that meets the needs of the Braille standard and this would need to be explored.

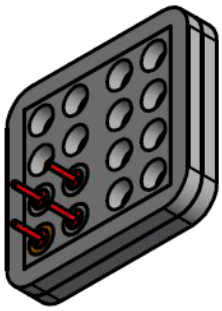

Figure 101: Illustration of conceptual DEA braille display device.

The operational characteristics of a tactile display are not tied to that of a Braille reader, hence some devices have been created which extend or alter the mode of stimulation for the communication of information to the sensory reader. This could be further explored with the multi-state actuator design, and a conceptual illustration is shown in Figure 101.

6.3.3 Soft Active-Touch Sensor

The formulated design of the ActivePneumostaticTIP is a complete encapsulated self-active sensing module. It can be applied to a range of tasks:

1. - As an attachment to a robot arm the self-active sensor can be used in areas of physically constrained workspace. In such situations actuation of the whole robot arm may damage, interfere with the environment being sensed, or more importantly the actuation may not be smooth or repeatable over small displacements required in some potential applications. The nature of the materials used allow for this sensing to be performed at a high frequency of protraction. For detection of the dynamic response from changeable localised characteristics of a surface, the ActivePneumostaticTIP could be employed providing controlled minimal actuation.

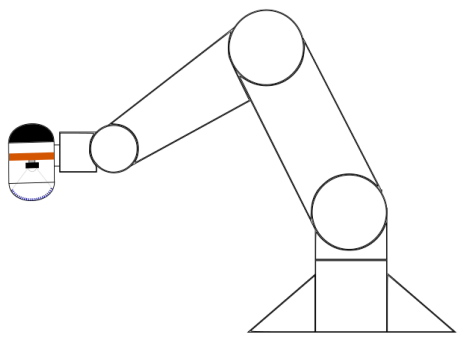

Figure 102: Illustration of APTIP as a robotic arm attachment

2. - The module could be used with a biomimetic novel exploratory robot probe. In the field of soft robotics wheeled transit is primarily replaced by biologically inspired locomotion such as snakes or simple legged robots [Plante and Dubowsky, 2007, Nguyen et al., 2014]. As such, a sensory end-effector enhancing or providing primary exploring capabilities of a self-propelled autonomous robot, in an environment with no external visual acuity (i.e. operating in soft material such as earth, or opaque liquids). The active touch could double as embodied touch with particular advantages for operation in potentially damaging physical objects.

Figure 103: Ilustration of active pneumostatic device as worm end effector

3. - Furthermore, the module could be used as an externally locomoted stand-alone self-active sensor. For example, it could be used for the observation of dynamic response of surfaces within the GI tract or vascular system or intra-body cavity. Gently probing of the normally inaccessible body surfaces can be used to find visually occluded objects of interest. Its soft body and compliant form can be used where rigid bodies are highly likely to damage delicate structures.

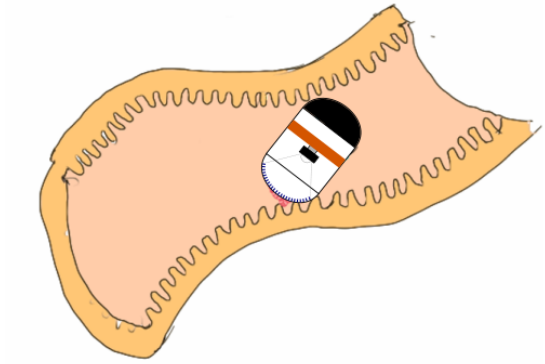

Figure 104: Concept of APTIP as standalone senory device

6.4 Further Work

Each of the parts of the thesis have created novel development to the field of soft actuators and have opened up opportunities for further research:

6.4.1 Multi-Layer Actuator Optimisation and Fabrication

The multi-layer actuator implementation has shown it is possible to optimise and imbue a layered actuator with characteristics currently only found in single films and additional properties such as mechanical strength. However, even with the processes described in this thesis, further work is required in:

- Scaling up the presented fabrication method to produce a reliable high layer number stack actuator (100-1000 layers) .
- Testing of stack actuators for ultimate tensile strength and force-displacement characteristics.
- Analysis of the practical efficiency and mechanical strength achievable with these multi-layer actuators using the novel design approaches presented.

6.4.2 Multi-state Device Future Development

The multi-state actuator concept opens up a variety of possibilities for further work including development of mechanisms based on the concept presented, but additionally it exposes a new area of research of encapsulation (using soft or rigid materials) in soft robotics and their potential for use to protect the core components in more dangerous* environments. For example lightweight low-power valves could be created using this concept. The precise control and variability provided by the implementation of the concept as a valve would enable suitable control of flow.

6.4.3 Soft Active-Touch Sensor

Particularly, when considering the APTIP in a soft robot, it could be added as a sensory attachment to an inch worm pneumostatic robot [Conn et al., 2014b]. The additional capability this provides to the robot for search and rescue, industrial, and exploratory applications would expand the possible uses and environments the robot could be used in. Although created for the experimental tests described, the module was also created to be as lightweight as possible with the intention of pairing it with an existing inch-worm locomoting robot enabling sensing.

Another method to expand upon the palpative displacement of the APTIP is to consider utilising inherent non-linear instabilities that can be developed using particular material and fluid parameters (particularly pressure). This can lead to the use of pneumatically controlled snap-through of the DEA membrane creating increased volume shifts and hence sensor displacement.

*Dangerous in this context is referring to environments which could damage unprotected DEAs

References

[ABB, 2018] (2018). Articulated Robots. https://new.abb.com/products/robotics/industrial-robots Date Accessed: 01-06-2018.

[Fes, 2018] (2018). Bionic Learning Network. www.festo.com/group/en/cms/10156.htm Date Accessed: 12-04-2018.

[Albert, 2016] Albert, K. C. P. (2016). Ant-roach www.pneubotics.com/history/.

[Alsteens, 2005] Alsteens, B. (2005). *Mathematical modelling and simulation of dispersive mixing.* PhD thesis, UCL.

[Altalhi et al., 2017] Altalhi, T., Khanam, N., Feng, P., Rahaman, M., Bhandari, S., Aldalbahi, A., and Govindasami, P. (2017). A New Insight in Determining the Percolation Threshold of Electrical Conductivity for Extrinsically Conducting Polymer Composites through Different Sigmoidal Models. *Polymers*, 9(12):527.

[Anderson et al., 2011] Anderson, I. a., Tse, T. C. H., Inamura, T., O'Brien, B., McKay, T., and Gisby, T. (2011). Flexidrive: a soft artificial muscle motor. 7976.

[Araromi et al., 2011] Araromi, O. A., Conn, A. T., Ling, C. S., Rossiter, J. M., Vaidyanathan, R., and Burgess, S. C. (2011). Spray deposited multilayered dielectric elastomer actuators. *Sensors and Actuators, A: Physical*, 167(2):459–467.

[Araromi et al., 2015a] Araromi, O. A., Gavrilovich, I., Shintake, J., Rosset, S., Richard, M., Gass, V., and Shea, H. R. (2015a). Rollable multisegment dielectric elastomer minimum energy structures for a deployable microsatellite gripper. *IEEE/ASME Transactions on Mechatronics*, 20(1):438–446.

[Araromi et al., 2015b] Araromi, O. A., Rosset, S., and Shea, H. R. (2015b). Versatile fabrication of PDMS-carbon electrodes for silicone dielectric elastomer transducers.

2015 Transducers - 2015 18th International Conference on Solid-State Sensors, Actuators and Microsystems (TRANSDUCERS), pages 1905–1908.

[Araromi et al., 2014] Araromi, S., Gavrilovich, I., Shintake, J., Rosset, S., and Shea, H. (2014). Towards a deployable satellite gripper based on multisegment dielectric elastomer minimum energy structures. *Proceedings of SPIE*, 9056.

[Ata et al., 2012] Ata, S., Kobashi, K., Yumura, M., and Hata, K. (2012). Mechanically durable and highly conductive elastomeric composites from long single-walled carbon nanotubes mimicking the chain structure of polymers. *Nano Letters*, 12(6):2710–2716.

[Bajcsy, 1988] Bajcsy, R. (1988). Active perception. *Proceedings of the IEEE*, 76(8):966–1005.

[Bar-Cohen, 2004] Bar-Cohen, Y. (2004). *Electroactive Polymer (EAP) Actuators as Artificial Muscles*. SPIE Press, second edi edition.

[Bergström and Boyce, 1998] Bergström, J. and Boyce, M. (1998). Constitutive modeling of the large strain time-dependent behavior of elastomers. *Journal of the Mechanics and Physics of Solids*, 46(5):931–954.

[Berryman et al., 2006] Berryman, L. J., Yau, J. M., and Hsiao, S. S. (2006). Representation of object size in the somatosensory system. *Journal of neurophysiology*, 96(1):27–39.

[Bloor et al., 2005] Bloor, D., Donnelly, K., Hands, P. J., Laughlin, P., and Lussey, D. (2005). A metal-polymer composite with unusual properties. *Journal of Physics D: Applied Physics*, 38(16):2851–2860.

[Bloor et al., 2006] Bloor, D., Graham, a., Williams, E. J., Laughlin, P. J., and Lussey, D. (2006). Metal-polymer composite with nanostructured filler particles and amplified physical properties. *Applied Physics Letters*, 88(10):10–13.

[Bogue, 2012] Bogue, R. (2012). Artificial muscles and soft gripping: a review of technologies and applications. *Industrial Robot: An International Journal*, 39(6):535–540.

[Boonstra, 1979] Boonstra, B. (1979). Role of particulate fillers in elastomer reinforcement: a review. *Polymer*, 20(6):691–704.

[Breazeal and Bar-Cohen, 2003] Breazeal, C. and Bar-Cohen, Y. (2003). Biologically Inspired Intelligent Robots. *SPIE - Conference on Smart Strutures and Materials 2003: EAPAD*, 5051.

[Brochu and Pei, 2010] Brochu, P. and Pei, Q. (2010). Advances in dielectric elastomers for actuators and artificial muscles. *Macromolecular Rapid Communications*, 31(1):10–36.

[Brochu et al., 2013] Brochu, P., Stoyanov, H., Niu, X., and Pei, Q. (2013). All-silicone prestrain-locked interpenetrating polymer network elastomers: free-standing silicone artificial muscles with improved performance and robustness. *Smart Materials and Structures*, 22(5).

[Cao and Conn, 2017] Cao, C. and Conn, A. (2017). Elastic actuation for legged locomotion. *Electroactive Polymer Actuators and Devices (EAPAD) 2017*.

[Carpi et al., 2015] Carpi, F., Anderson, I., Bauer, S., Frediani, G., Gallone, G., Gei, M., Graaf, C., Jean-Mistral, C., Kaal, W., Kofod, G., Kollosche, M., Kornbluh, R., Lassen, B., Matysek, M., Michel, S., Nowak, S., O'Brien, B., Pei, Q., Pelrine, R., Rechenbach, B., Rosset, S., and Shea, H. (2015). Standards for dielectric elastomer transducers. *Smart Materials and Structures*, 24(10).

[Carpi et al., 2010a] Carpi, F., Frediani, G., and De Rossi, D. (2010a). Hydrostatically coupled dielectric elastomer actuators. *IEEE/ASME Transactions on Mechatronics*, 15(2):308–315.

[Carpi et al., 2011] Carpi, F., Frediani, G., Turco, S., and De, R. D. (2011). Bioinspired tunable lens with muscle-like electroactive elastomers. *Advanced Functional Materials*, 21(21):4152–4158.

[Carpi et al., 2008] Carpi, F., Gallone, G., Galantini, F., and De Rossi, D. (2008). Enhancement of the electromechanical transduction properties of a silicone elastomer by blending with a conjugated polymer. *Proceedings of SPIE*, 6927.

[Carpi et al., 2010b] Carpi, F., Menon, C., and De Rossi, D. (2010b). Electroactive elastomeric actuator for all-polymer linear peristaltic pumps. *IEEE/ASME Transactions on Mechatronics*, 15(3):460–470.

[Carpi et al., 2005] Carpi, F., Migliore, A., Serra, G., and Rossi, D. D. (2005). Helical dielectric elastomer actuators. *Smart Materials and Structures*, 14(6):1210–1216.

[Carpi and Rossi, 2007] Carpi, F. and Rossi, D. D. (2007). Contractile folded dielectric elastomer actuators. *Smart Materials and Structures*, 6524:1–13.

[Carpi et al., 2007] Carpi, F., Rossi, D. D., Kornbluh, R., Pelrine, R., and Sommer-Larsen, P. (2007). Dielectric Elastomers as Electromechanical Transducers.

[Chang et al., 2017] Chang, M., Wang, Z., and Liang, W. (2017). A visco-hyperelastic model characterizing the electromechanical behavior of nonhomogeneous soft material. *AIP Advances*, 7(9):1–8.

[Chang et al., 2013] Chang, W. L., Šabanović, S., and Huber, L. (2013). Use of seal-like robot PARO in sensory group therapy for older adults with dementia. In *ACM/IEEE International Conference on Human-Robot Interaction*, pages 101–102.

[Chiba et al., 2008] Chiba, S., Waki, M., Kornbluh, R., and Pelrine, R. (2008). Innovative Power Generators for Energy Harvesting Using Electroactive Polymer Artificial Muscles. *Electroactive Polymer Actuators and Devices*, 6927.

[Chirikjian, 1994] Chirikjian, G. (1994). A binary paradigm for robotic manipulators.

[Chorley et al., 2009] Chorley, C., Melhuish, C., Pipe, T., and Rossiter, J. (2009). Development of a tactile sensor based on biologically inspired edge encoding. *2009 International Conference on Advanced Robotics*.

[Chorley et al., 2010] Chorley, C., Melhuish, C., Pipe, T., and Rossiter, J. (2010). Tactile edge detection. *Proceedings of IEEE Sensors*, pages 2593–2598.

[Cianchetti et al., 2014] Cianchetti, M., Ranzani, T., Gerboni, G., Nanayakkara, T., Althoefer, K., Dasgupta, P., and Menciassi, A. (2014). Soft Robotics Technologies to Address Shortcomings in Today's Minimally Invasive Surgery: The STIFF-FLOP Approach. *Soft Robotics*, 1(2):122–131.

[Conn and Rossiter, 2011] Conn, A. and Rossiter, J. (2011). Antagonistic dielectric elastomer actuator for biologically-inspired robotics. *Proceeding of SPIE*, 7976.

[Conn, 2008] Conn, A. T. (2008). *Development of Novel Flapping Mechanism Technologies for Insect-Inspired Micro Air Vehicles*. PhD thesis.

[Conn et al., 2007] Conn, A. T., Burgess, S. C., and Ling, C. S. (2007). Design of a parallel crank-rocker flapping mechanism for insect-inspired micro air vehicles. *Proceedings of the Institution of Mechanical Engineers, Part C: Journal of Mechanical Engineering Science*, 221(10):1211–1222.

[Conn et al., 2014a] Conn, A. T., Hinitt, A. D., and Wang, P. (2014a). Soft segmented inchworm robot with dielectric elastomer muscles. *Proc. SPIE*, 9056(2):90562L.

[Conn et al., 2014b] Conn, A. T., Hinitt, A. D., and Wang, P. (2014b). Soft segmented inchworm robot with dielectric elastomer muscles. *Proc. SPIE*, 9056.

[Conn and Rossiter, 2012a] Conn, A. T. and Rossiter, J. (2012a). Harnessing electromechanical membrane wrinkling for actuation. *Applied Physics Letters*, 101(17):1–5.

[Conn and Rossiter, 2012b] Conn, A. T. and Rossiter, J. (2012b). Towards holonomic electro-elastomer actuators with six degrees of freedom. *Smart Materials and Structures*, 21(3).

[Conn and Rossiter, 2010] Conn, A. T. and Rossiter, J. M. (2010). Radially expanding mechanism for dielectric elastomers. *Proceedings of SPIE*, 7642:76420P.

[Cox, 2012] Cox, D. (2012). Development of a deposition system for patterned compliant electrodes. Technical report, University of Bristol.

[da Silva et al.,] da Silva, L. F. M., Öchsner, A., and Adams, R. D. *Handbook of Adhesion Technology.*

[Dahiya et al., 2010] Dahiya, R. S., Metta, G., Valle, M., and Sandini, G. (2010). Tactile sensing-from humans to humanoids. *IEEE Transactions on Robotics*, 26(1):1–20.

[Dow Corning, 2011] Dow Corning (2011). *Material Safety Data Sheet: XIAMETER® RTV-3483 Base and XIAMETER® RTV- 3083 Curing Agent-In.* Dow Corning.

[Dow Corning, 2018] Dow Corning (2018). Product Information SILASTIC ® 3483 Base and SILASTIC ® 83 Curing Agent - Date Accessed 01/05/2018. Technical report.

[El-Kady et al., 2012] El-Kady, M. F., Strong, V., Dubin, S., and Kaner, R. B. (2012). Laser scribing of high-performance and flexible graphene-based electrochemical capacitors. *Science*, 335(6074):1326–1330.

[Feix et al., 2015] Feix, T., Romero, J., Schmiedmayer, H.-b. B., Dollar, A. M., and Kragic, D. (2015). The GRASP Taxonomy of Human Grasp Types. *IEEE Transactions on Human-Machine Systems.*

[Festo, 2018] Festo (2018). BionicCobot. www.festo.com/group/en/cms/12746.htm Date Accessed: 28-05-2018.

[FISHER, 2005] FISHER (2005). Control Valve Handbook. *EMERSON Process Management*.

[Fleisher, 2002] Fleisher, P. (2002). *Liquids and Gasess: Principles of Fluid Mechanics*. Lerner Publications.

[Follador et al., 2014] Follador, M., Conn, A. T., Mazzolai, B., and Rossiter, J. (2014). Active-elastic bistable minimum energy structures. *Applied Physics Letters*, 105(14).

[Follador et al., 2015] Follador, M., Conn, A. T., and Rossiter, J. (2015). Bistable minimum energy structures (BiMES) for binary robotics. *Smart Materials and Structures*, 24(6).

[Foulger, 1999] Foulger, S. H. (1999). Electrical properties of composites in the vicinity of the percolation threshold. *Journal of Applied Polymer Science*, 72(12):1573–1582.

[Gent, 1996] Gent, A. N. (1996). A New Constitutive Relation for Rubber. *Rubber Chemistry and Technology*, 69(1):59–61.

[Gibson, 1962] Gibson, J. (1962). Observations on active touch. *Psychological review*, 69(6):477–491.

[Gisby et al., 2013] Gisby, T. A., Brien, B. M. O., and Anderson, I. A. (2013). Self sensing feedback for dielectric elastomer actuators. 193703(2013):10–14.

[Gisby et al., 2011] Gisby, T. a., O'Brien, B. M., Xie, S. Q., Calius, E. P., and Anderson, I. a. (2011). Closed loop control of dielectric elastomer actuators. *Polymer*, 7976.

[Gu et al., 2017a] Gu, G. Y., Zhu, J., Zhu, L. M., and Zhu, X. (2017a). A survey on dielectric elastomer actuators for soft robots. *Bioinspiration and Biomimetics*, 12(1).

[Gu et al., 2017b] Gu, G. Y., Zhu, J., Zhu, L. M., and Zhu, X. (2017b). A survey on dielectric elastomer actuators for soft robots. *Bioinspiration and Biomimetics*, 12(1).

[Guo et al., 2015] Guo, J., Xiao, R., Park, H. S., and Nguyen, T. D. (2015). The Temperature-Dependent Viscoelastic Behavior of Dielectric Elastomers. *Journal of Applied Mechanics*, 82(9).

[Haines et al., 2014] Haines, C. S., Lima, M. D., Li, N., Spinks, G. M., Foroughi, J., Madden, J. D. W., Kim, S. H., Fang, S., Jung de Andrade, M., Goktepe, F., Goktepe, O., Mirvakili, S. M., Naficy, S., Lepro, X., Oh, J., Kozlov, M. E., Kim, S. J., Xu, X., Swedlove, B. J., Wallace, G. G., and Baughman, R. H. (2014). Artificial Muscles from Fishing Line and Sewing Thread. *Science*, 343(6173):868–872.

[Hanke et al., 2010] Hanke, W., Witte, M., Miersch, L., Brede, M., Oeffner, J., Michael, M., Hanke, F., Leder, A., and Dehnhardt, G. (2010). Harbor seal vibrissa morphology suppresses vortex-induced vibrations. *The Journal of experimental biology*, 213(Pt 15):2665–2672.

[Haruna et al., 2007] Haruna, M., Kubo, K., Fukusumi, K., and Tamida, T. (2007). Development of soft actuator: mechanism with vibration element using dielectric elastomer to generate large displacement. *Proceedings of SPIE*, 6524.

[Hines et al., 2016] Hines, L., Petersen, K., and Sitti, M. (2016). Inflated Soft Actuators with Reversible Stable Deformations. *Advanced Materials*.

[Hong, 2011] Hong, W. (2011). Modeling viscoelastic dielectrics. *Journal of the Mechanics and Physics of Solids*, 59(3):637–650.

[Horowitz and Hill,] Horowitz, P. and Hill, W. The Art of Electronics.

[Huang et al., 2012] Huang, J., Li, T., Chiang Foo, C., Zhu, J., Clarke, D. R., and Suo, Z. (2012). Giant, voltage-actuated deformation of a dielectric elastomer under dead load. *Applied Physics Letters*, 100(4).

[Huu Chuc et al., 2008] Huu Chuc, N. H., Thuy, D. V., Park, J., Kim, D., Koo, J., Lee, Y., Nam, J.-D., and Choi, H. R. (2008). A dielectric elastomer actuator with self–sensing capability. *Electroactive Polymer Actuators and Devices (EAPAD)*, 6927.

[IARC, 2010] IARC (2010). IARC monographs on the evaluation of carcinogenic risks to humans. *IARC Monographs on the Evaluation of Carcinogenic Risks to Humans*, 93.

[Jamali et al., 2015] Jamali, N., Maggiali, M., Giovannini, F., Metta, G., and Natale, L. (2015). A new design of a fingertip for the iCub hand. *IEEE International Conference on Intelligent Robots and Systems.*

[Jamali et al., 2008] Jamali, N., Metta, G., and Natale, L. (2008). iCub Tactile Sensing System : Current State and Future Directions. Technical report.

[Jha, 2008] Jha, V. (2008). Carbon Black Filler Reinforcement of Elastomers.

[Jung et al., 2008] Jung, K., Kim, K. J., and Choi, H. R. (2008). Self-Sensing of Dielectric Elastomer Actuator. 6927.

[Kalpakjian S., 2000] Kalpakjian S. (2000). Manufacturing Engineering and Technology.

[Kawasaki et al., 2002] Kawasaki, H., Komatsu, T., and Uchiyama, K. (2002). Dexterous Mnthropomorphic Robot Hand With Distributed Tactile Sensor: Gifu Hand II. *IEEE/ASME Transactions on Mechatronics*, 7(3):296–303.

[Keplinger et al., 2012] Keplinger, C., Li, T., Baumgartner, R., Suo, Z., and Bauer, S. (2012). Harnessing snap-through instability in soft dielectrics to achieve giant voltage-triggered deformation. *Soft Matter*, 8(2):285–288.

[Kiil and Benslimane, 2009] Kiil, H.-E. and Benslimane, M. (2009). Scalable industrial manufacturing of DEAP. *Proc. of SPIE*, 7287.

[Kikuuwe et al., 2004] Kikuuwe, R., Sano, A., Mochiyama, H., Takesue, N., Tsunekawa, K., Suzuki, S., and Fujimoto, H. (2004). The tactile contact lens. *Sensors, 2004. Proceedings of IEEE*, pages 535–538.

[Kornbluh et al., 1991] Kornbluh, R., Eckerle, J., and Andeen, G. (1991). Artificial muscle: the next generation of robotic actuators. In *4th World Conference of Robotics Research*, Pittsburgh.

[Kornbluh et al., 1998] Kornbluh, R., Pelrine, R., Eckerle, J., and Joseph, J. (1998). Electrostrictive polymer artificial muscle actuators. *Proceedings. 1998 IEEE International Conference on Robotics and Automation*, 3:2147–2154.

[Kovacs, 2006] Kovacs, G. (2006). Arm wrestling robot driven by dielectric elastomer actuators. *Proceedings of the First IEEE/RAS-EMBS International Conference on Biomedical Robotics and Biomechatronics, 2006*, pages 260–265.

[Kovacs and Düring, 2009] Kovacs, G. and Düring, L. (2009). Contractive tension force stack actuator based on soft dielectric EAP. *Proc. SPIE*, 7287.

[Lepora, 2015] Lepora, N. F. (2015). Biomimetic Active Perception with Tactile Fingertips and Whiskers. 9:1–12.

[Lepora and Ward-Cherrier, 2016] Lepora, N. F. and Ward-Cherrier, B. (2016). Tactile Quality Control With Biomimetic Active Touch. *IEEE Robotics and Automation Letters*, 1(2):646–652.

[Lichter et al., 2001] Lichter, M. D., Sujan, V. a., and Dubowsky, S. (2001). Experimental Demonstrations of a New Design Paradigm in Space Robotics. pages 219–228.

[Lotz et al., 2008] Lotz, P., Matysek, M., Lechner, P., Hamann, M., and Schlaak, H. F. (2008). Dielectric elastomer actuators using improved thin film processing and nanosized particles. *Polymer*, 7976.

[Lotz et al., 2009] Lotz, P., Matysek, M., and Schlaak, H. F. (2009). Peristaltic Pump made of Dielectric Elastomer Actuators. 7287.

[Lotz et al., 2011] Lotz, P., Matysek, M., and Schlaak, H. F. (2011). Fabrication and application of miniaturized dielectric elastomer stack actuators. *IEEE/ASME Transactions on Mechatronics*, 16(1):58–66.

[Low and Lau, 2014] Low, S.-h. and Lau, G.-k. (2014). Bi-axially crumpled silver thin-film electrodes for dielectric elastomer actuators. *Smart Materials and Structures*, 23(12).

[Low et al., 2012] Low, S. H., Tan, A. W. Y., Shiau, L. L., and Lau, G. K. (2012). Actuated strains in excess of 100% in dielectric elastomer actuators using silver film electrodes. 8340.

[Lu and Kim, 2014] Lu, N. and Kim, D.-H. (2014). Flexible and Stretchable Electronics Paving the Way for Soft Robotics. *Soft Robotics*, 1(1):53–62.

[Maas et al., 2015] Maas, J., Tepel, D., and Hoffstadt, T. (2015). Actuator design and automated manufacturing process for DEAP-based multilayer stack-actuators. *Meccanica*, 50(11):2839–2854.

[Marchese et al., 2014] Marchese, A. D., Onal, C. D., and Rus, D. (2014). Autonomous Soft Robotic Fish Capable of Escape Maneuvers Using Fluidic Elastomer Actuators. *Soft Robotics*, 1(1):75–87.

[Matysek et al., 2010] Matysek, M., Lotz, P., Flittner, K., and Schlaak, H. F. (2010). Vibrotactile display for mobile applications based on dielectric elastomer stack actuators. *Proceeding of SPIE*, 7642.

[Matysek et al., 2009] Matysek, M., Lotz, P., and Schlaak, H. F. (2009). Tactile display with dielectric multilayer elastomer actuators. *SPIE Smart Structures and Materials + Nondestructive Evaluation and Health Monitoring*, 7287.

[McKay et al., 2009] McKay, T. G., Calius, E., and Anderson, I. a. (2009). The Dielectric Constant of 3M VHB: a Parameter in Dispute. *Proc. of SPIE*, 7287.

[Medalia and Heckman, 1969] Medalia, A. and Heckman, F. (1969). Morphology of aggregates. *Journal of Colloid and Interface Science*, 36(2):173–190.

[Mescher, 2003] Mescher, A. L. (2003). *Junqueira ' s Basic Histology Text & Atlas*. Number November 2015.

[Metta et al., 2008] Metta, G., Sandini, G., Vernon, D., Natale, L., and Nori, F. (2008). The iCub humanoid robot: an open platform for research in embodied cognition. *Proceedings of the 8th Workshop on Performance Metrics for Intelligent Systems*, pages 50–56.

[MG Chemicals, 2012] MG Chemicals (2012). Carbon Conductive Grease 846 Technical Data Sheet. pages 1–4.

[Mirvakili et al., 2014] Mirvakili, S. M., Rafie Ravandi, A., Hunter, I. W., Haines, C. S., Li, N., Foroughi, J., Naficy, S., Spinks, G. M., Baughman, R. H., and Madden, J. D. W. (2014). Simple and strong: twisted silver painted nylon artificial muscle actuated by Joule heating.

[Monzée et al., 2003] Monzée, J., Lamarre, Y., and Smith, A. M. (2003). The effects of digital anesthesia on force control using a precision grip. *Journal of neurophysiology*, 89(2):672–683.

[Mouri et al., 2002] Mouri, T., Kawasaki, H., Yoshikawa, K., Takai, J., and Ito, S. (2002). Anthropomorphic Robot Hand : Gifu Hand III. *Iccas2002*, pages 1288–1293.

[Nenno and Wetzel, 2014] Nenno, P. T. and Wetzel, E. D. (2014). Rate-dependent extensional "dynamic ligaments" using shear thickening fluids. *Spie*, 9057.

[Nguyen et al., 2017] Nguyen, C. T., Phung, H., Hoang, P. T., Nguyen, T. D., and Jung, H. (2017). A novel bioinspired hexapod robot developed by soft dielectric elastomer actuators. pages 6233–6238.

[Nguyen et al., 2014] Nguyen, C. T., Phung, H., Nguyen, T. D., Lee, C., Kim, U., Lee, D., Moon, H., Koo, J., Nam, J.-d., and Choi, H. R. (2014). A small biomimetic quadruped robot driven by multistacked dielectric elastomer actuators. *Smart Materials and Structures*, 23(6).

[O'Brien et al., 2014] O'Brien, B., Gisby, T., and Anderson, I. A. (2014). Stretch sensors for human body motion. *Proceedings of SPIE - The International Society for Optical Engineering*, 9056.

[Ogden, 1972] Ogden, R. W. (1972). Large Deformation Isotropic Elasticity: On the Correlation of Theory and Experiment for Compressible Rubberlike Solids. *Proceedings of the Royal Society A: Mathematical, Physical and Engineering Sciences*, 328(1575):567–583.

[O'Halloran et al., 2008] O'Halloran, A., O'Malley, F., and McHugh, P. (2008). A review on dielectric elastomer actuators, technology, applications, and challenges. *Journal of Applied Physics*, 104(7).

[Ohka et al., 2006] Ohka, M., Kobayashi, H., Takata, J., and Mitsuya, Y. (2006). Sensing precision of an optical three-axis tactile sensor for a robotic finger. *Proceedings - IEEE International Workshop on Robot and Human Interactive Communication*, pages 214–219.

[OtherLab,] OtherLab. Robots Made from Interesting Materials. Technical report.

[Pang et al., 2016] Pang, Y., Tian, H., Tao, L., Li, Y., Wang, X., Deng, N., Yang, Y., and Ren, T. L. (2016). Flexible, Highly Sensitive, and Wearable Pressure and Strain Sensors with Graphene Porous Network Structure. *ACS Applied Materials and Interfaces*, 8(40):26458-26462.

[Parker,] Parker. Films - promo.parker.com/promotionsite/eap/us/en/the-technology.

[Pearson et al., 2007] Pearson, M. J., Pipe, a. G., Melhuish, C., Mitchinson, B., and Prescott, T. J. (2007). Whiskerbot: A robotic active touch system modeled on the rat whisker sensory system. *Adaptive Behavior*, 15(3):223–240.

[Pede et al., 1998] Pede, D., Serra, G., and De Rossi, D. (1998). Microfabrication of conducting polymer devices by ink-jet stereolithography. *Materials Science and Engineering: C*, 5(3-4):289–291.

[Plante and Dubowsky, 2006] Plante, J.-S. and Dubowsky, S. (2006). Large-scale failure modes of dielectric elastomer actuators. *International Journal of Solids and Structures*, 43(25-26):7727–7751.

[Plante and Dubowsky, 2007] Plante, J. S. and Dubowsky, S. (2007). On the performance mechanisms of Dielectric Elastomer Actuators. *Sensors and Actuators, A: Physical*, 137(1):96–109.

[Poole and Booker, 2008] Poole, A. and Booker, J. D. (2008). Classification and selection of actuator technologies with consideration of stimuli generation. *Proceedings of SPIE*, 6927.

[Pourazadi et al., 2017] Pourazadi, S., Shagerdmootaab, A., Chan, H., Moallem, M., and C, M. (2017). On the Electrical Safety of Dielectric Elastomer Actuators in Proximity to the Human Body.

[Rahbar et al., 2014] Rahbar, a., Rahbar, M., and Gray, B. L. (2014). Flexible touchpads based on inductive sensors using embedded conductive composite polymer. *Nanosensors, Biosensors, and info-tech Sensors and Systems*, 9060.

[Randazzo et al., 2008] Randazzo, M., Buzio, R., Metta, G., Sandini, G., and Valbusa, U. (2008). Architecture for the semi-automatic fabrication and assembly of thin-film based dielectric elastomer actuators. *Proc. of SPIE*, 6927.

[Romasanta et al., 2011] Romasanta, L. J., Hernández, M., López-Manchado, M. a., and Verdejo, R. (2011). Functionalised graphene sheets as effective high dielectric constant fillers. *Nanoscale Research Letters*, 6(1):508.

[Rosset et al., 2016] Rosset, S., Araromi, O. A., Schlatter, S., and Shea, H. R. (2016). Fabrication Process of Silicone-based Dielectric Elastomer Actuators. *Journal of Visualized Experiments*, (108):1–13.

[Rosset et al., 2007] Rosset, S., Niklaus, M., Dubois, P., Dadras, M., and Shea, H. R. (2007). Mechanical properties of electroactive polymer microactuators with ion-implanted electrodes. 6524.

[Rosset and Shea, 2015] Rosset, S. and Shea, H. R. (2015). Towards fast, reliable, and manufacturable DEAs: miniaturized motor and Rupert the rolling robot. 9430.

[Rossiter et al., 2010] Rossiter, J., Takashima, K., and Mukai, T. (2010). Dielectric elastomer actuators with zero-energy fixity. *Electroactive Polymer Actuators and Devices*, 7642.

[Runyan and Blazie, 2010] Runyan, N. and Blazie, D. (2010). EAP actuators aid the quest for the "Holy Braille" of tactile displays. *Spie*, 7642.

[Schmitz et al., 2010] Schmitz, A., Maggiali, M., Natale, L., Bonino, B., and Metta, G. (2010). A tactile sensor for the fingertips of the humanoid robot iCub. *IEEE/RSJ 2010*

International Conference on Intelligent Robots and Systems, IROS 2010 - Conference Proceedings, pages 2212–2217.

[Sclater, 2011] Sclater, N. (2011). *Mechanisms and Mechanical Devices Sourcebook, 5th Edition.*

[Shadow Hand,] Shadow Hand. Shadow Robot - www.shadowrobot.com/products/.

[Shahinpoor and Thompson, 1995] Shahinpoor, M. and Thompson, M. S. (1995). The Venus Flytrap as a model for a biomimetic material with built-in sensors and actuators. *Materials Science and Engineering C*, 2(4):229–233.

[Smith and Cheeseman, 1986] Smith, R. C. and Cheeseman, P. (1986). On the Representation and Estimation of Spatial Uncertainty. *The International Journal of Robotics Research*, 5(4):56–68.

[SRI, 2010] SRI (2010). SRI EPAM. https://www.sri.com/engage/products-solutions/epam Date Accessed: 01-06-2018.

[Stauffer and Bunde, 2008] Stauffer, D. and Bunde, A. (2008). Introduction to Percolation Theory . *Physics Today*, 40(10):122–123.

[Stoll,] Stoll, W. FlexShapeGripper Gripping modelled on a chameleon's tongue.

[Sugino et al., 2012] Sugino, T., Shibata, Y., Kiyohara, K., and Asaka, K. (2012). CNT/conductive polymer composites for low-voltage driven EAP actuators. *Proc. SPIE Electroactive Polymer Actuators and Devices (EAPAD) 2012*, 8340.

[Suo, 2010] Suo, Z. (2010). Theory of dielectric elastomers. *Acta Mechanica Solida Sinica*, 23(6):549–578.

[Taylor et al., 2010] Taylor, Z. J., Gurka, R., Kopp, G. A., and Liberzon, A. (2010). Long-duration time-resolved PIV to study unsteady aerodynamics. *IEEE Transactions on Instrumentation and Measurement*, 59(12):3262–3269.

[Tepel et al., 2014] Tepel, D., Hoffstadt, T., and Maas, J. (2014). Automated manufacturing process for DEAP stack-actuators. 9056.

[Tiwana et al., 2012] Tiwana, M. I., Redmond, S. J., and Lovell, N. H. (2012). A review of tactile sensing technologies with applications in biomedical engineering. *Sensors and Actuators, A: Physical*, 179:17–31.

[Tolley et al., 2014] Tolley, M. T., Shepherd, R. F., Mosadegh, B., Galloway, K. C., Wehner, M., Karpelson, M., Wood, R. J., and Whitesides, G. M. (2014). A Resilient, Untethered Soft Robot. 1(3):213–223.

[Tse et al., 2011] Tse, T. C. H., O'Brien, B., McKay, T., and Anderson, I. a. (2011). A validated finite element model of a soft artificial muscle motor. *Polymer*, 7976.

[Valdivia Y Alvarado et al., 2012] Valdivia Y Alvarado, P., Subramaniam, V., and Triantafyllou, M. (2012). Design of a bio-inspired whisker sensor for underwater applications. *Proceedings of IEEE Sensors*, pages 1–4.

[Van Putte et al., 2015] Van Putte, C., Regan, J., and Russo, A. (2015). *Seeley's Essentials of Anatomy & Physiology*. McGraw-Hill Eductaion, 9th edition.

[Viry et al., 2014] Viry, L., Levi, A., Totaro, M., Mondini, A., Mattoli, V., Mazzolai, B., and Beccai, L. (2014). Flexible three-axial force sensor for soft and highly sensitive artificial touch. *Advanced Materials*, 26(17):2659–2664.

[Visell et al., 2016] Visell, Y., Lepora, N., Hartmann, M. J. Z., and Hayward, V. (2016). Biology to Technology in Active Touch Sensing - Introduction to the Special Section. *IEEE Transactions on Haptics*, 9(2):155–157.

[WackerChemie, 2014] WackerChemie (2014). New Horizons through innovative applications with Elastosil film.

[Wanhao, 2016] Wanhao (2016). Wanhao Duplicator 4S. Technical report.

[Ward-Cherrier et al., 2016] Ward-Cherrier, B., Cramphorn, L., and Lepora, N. F. (2016). Tactile Manipulation With a TacThumb Integrated on the Open-Hand M2 Gripper. *IEEE Robotics and Automation Letters*, 1(1):169–175.

[Winstone et al., 2013] Winstone, B., Griffiths, G., Pipe, T., Melhuish, C., and Rossiter, J. (2013). TACTIP - Tactile fingertip device, texture analysis through optical tracking of skin features. 8064 LNAI:323–334.

[Wolff and Wang, 1993] Wolff, S. and Wang, M.-J. (1993). Carbon Black Filler Reinforcement of Elastomers. *Carbon Black: Science and Technology*, (October):460.

[Xiao et al., 2014] Xiao, H., Jiang, J., Li, H., and Wang, G. (2014). Design of strain sensors based on the resistivity-percolation curves and piezoresistivity curves of different conductive composites. 9061.

[Yao et al., 2005] Yao, G., Ren, W., Akhras, G., Yang, G., Mukherjee, B. K., and Szabo, J. P. (2005). The strain response of silicone dielectric elastomer actuators. *Smart Structures and Materials 2005: Electroactive Polymer Actuators and Devices (EAPAD)*, 5759:134.

[Yong, 2009] Yong, C. P. (2009). Dynamic sensing in mimicking cutaneous mechanoreceptors - 3d sensor applying reception by vision. *2009 IEEE International Workshop on Imaging Systems and Techniques, IST 2009 - Proceedings*, pages 17–21.

[York et al., 2010] York, A., Dunn, J., and Seelecke, S. (2010). Experimental characterization of the hysteretic and rate-dependent electromechanical behavior of dielectric electro-active polymer actuators. *Smart Materials and Structures*, 19(9).

[Yuan et al., 2008] Yuan, W., Hu, L., Ha, S., Lam, T., Grüner, G., and Pei, Q. (2008). Self-Clearable Carbon Nanotube Electrodes for Improved Performance of Dielectric Elastomer Actuators. *Electroactive Polymer Actuators and Devices*, 6927.

[Yuan et al., 2007] Yuan, W., Lam, T., Biggs, J., Hu, L., Yu, Z., Ha, S., Xi, D., Senesky, M. K., Grüner, G., and Pei, Q. (2007). New electrode materials for dielectric elastomer actuators. *Proceeding of SPIE*, 6524(2007).

[Zhang et al., 2006] Zhang, R., Lochmatter, P., Kunz, A., and Kovacs, G. (2006). Spring Roll Dielectric Elastomer Actuators for a Portable Force Feedback Glove. *Smart Structures and Materials 2006: Electroactive Polymer Actuators and Devices (EAPAD)*, 6168(0).

Appendices

A Equilibrium Mechanics of L-IPNs

We will now consider the effects of the lamination on the structure of the material. The elastomeric films in stages of the lamination process are represented in Figure 105. A layer of elastomeric material can be produced such that it can be considered isotropic and approximately incompressible. Biaxial pre-strain causes a uniform strain in the $\boldsymbol{x}$-$\boldsymbol{y}$ plane, and reduction in the thickness plane (comparing Figure 105a and Figure 105b). Due to the use of biaxial plane any measurement in $\boldsymbol{x}$ and $\boldsymbol{y}$ can be considered equal to planar length $\boldsymbol{p}$ of an element.

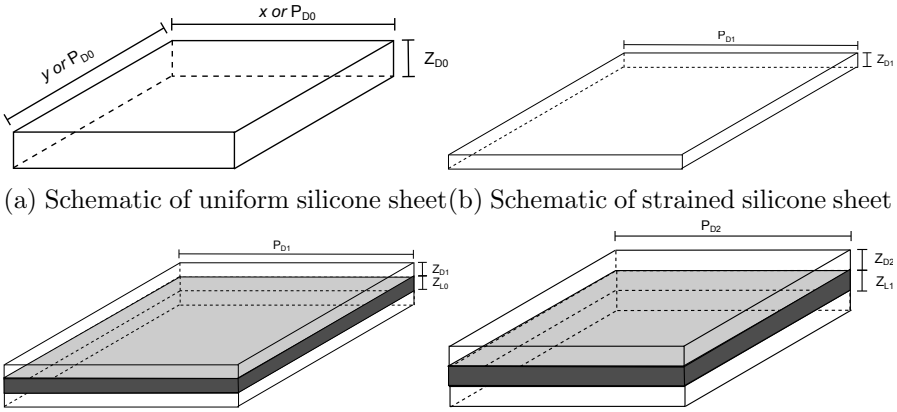

(a) Schematic of uniform silicone sheet

(b) Schematic of strained silicone sheet

(c) Representation of pre-strained laminated 3-layer silicone sheet.

(d) Image of resultant L-IPN from released pre-strained laminate.

Figure 105: Set of schematics illustration the strain mechanics in producing a layered actuator with captured pre-strain.

When the pre-strained laminate is released from its supporting structure, the ratio of conductive composite to dielectric remains constant as shown in Equation 17. From Equation 8 & 9, and applying this to the element lengths described in Figure 105, it can be seen that the dielectric to electrode thickness ratios in Figures 105c & 105d are the

same.

$$\frac{z_{D2}}{z_{L1}} = \frac{z_{D1}.\lambda_{z_{D1,2}}}{z_{L0}.\lambda_{z_{L0,1}}} = \frac{z_{D1}.p_{D2}}{z_{L0}.p_{D1}} = \frac{z_{D1}}{z_{L0}}\,, \tag{17}$$

where z_L, p_L are thickness and planar lengths respectively, and λ_p, λ_l are the respective stretches.

If an adhesive element is applied between two pre-strained elastomeric layers, and is assumed to form a uniform bond with each, the adhesive undergoes a compression when relaxed. In equilibrium, the compressive stress on the adhesive will equal the retained pre-strain stress of the elastomeric layer in the thickness plane. Due to the repeatability of the structure, this result can be extended to a stack. Due to the symmetry of the lamination in the envisaged stack, there will be no out-of-plane moment, given that the forces in repeated layers can be assumed to be equal.

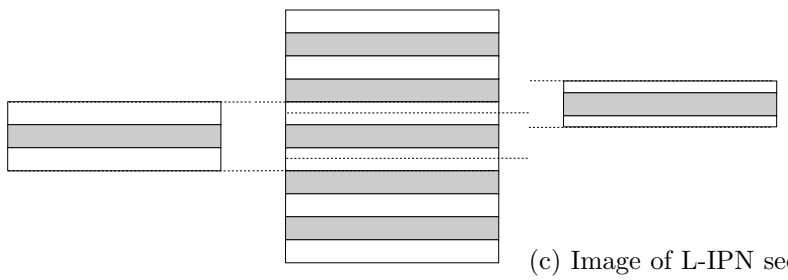

(a) Image of single L-IPN (b) Image of laminated multi-layer stack (c) Image of L-IPN section in planar equilibrium.

Figure 106: Laminations In an Envisaged Stack

B DE Membrane Fabrication For Multilayer Actuators

DEA actuator fabrication requires the formation of a high purity (i.e. no particulates) uniform dielectric membrane. This enables the maximisation of the electric field of a membrane of a given thickness.

B.1 Spin Coating

Spin coating has been discussed in the literature as one method of producing thin film actuators out of silicone material. It benefits from the following attributes:

- Consistent uniform layers
- Relatively large sheets
- Can be batch produced for consistency
- The material thickness can be customised
- The material stiffness can be customised through type of silicone and addition of silicone oil.

To characterise the sheets of material, an elastomer used in previous works was used and the thickness compared across a range of spin speeds [Lotz et al., 2011].

B.2 Spin Coating Sample Analysis

For a number of rotational speeds (as per Lotz et al [Lotz et al., 2011]), a layer of spun Dow Corning 3483 silicone was cured and the variation of thickness of a centre-line cross-section was measured. The results confirmed layers were of a similar composition to initial findings [Lotz et al., 2008] showing uniformity across the entire cross-section with a slight thickness increase at the centre and edge of the film disc. Figure 107a shows the cross-section along which the thickness was measured. The thickness was affected by the mix batch of silicone, but was found to be consistent within the batch. A spinning program was created to produce films of approximated 100μm thickness. Figure 107b shows an example of the uniformity of the sample.

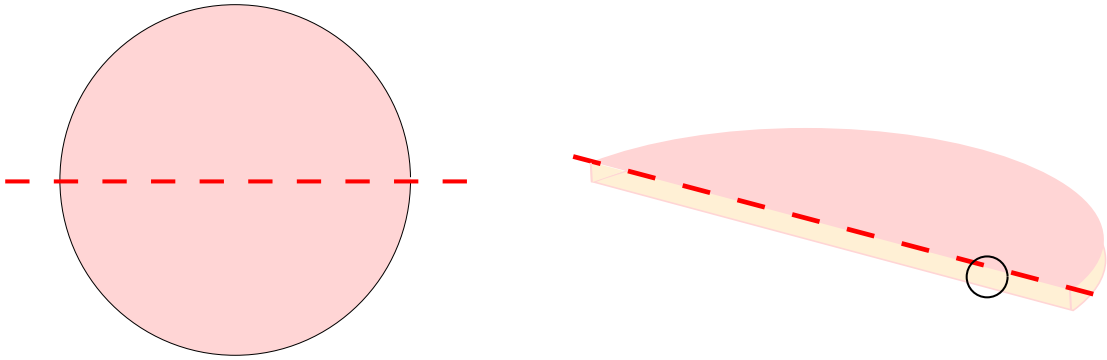

(a) Illustration of silicone cross-sectional slice used for microscopy image.

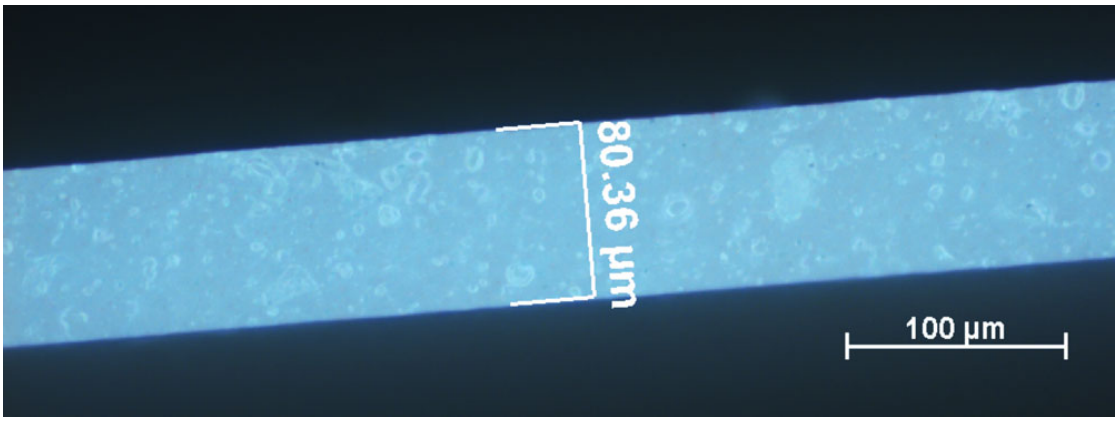

(b) Silicone sheet cross-sectional microscopy image

Figure 107: Illustration of measurements of spun silicone sheet

C High Voltage Test Rig

In order to test the DEAs, a test rig was required that provided a safe experimental area. A bespoke electrically insulated rig has been created by the group for DEA testing. It consists of a perspex box with a magnetic interlock to ensure high voltage grounding if the door is open. The high voltage boxes are controlled by a remote low voltage control box, which is also sealed. The high voltage boxes are separated from the main test area by an electrically insulated floor panel of Perspex. All recording equipment is electrically insulated from possible high voltage sources. The outputs of the devices

are then connected to a PC for control of experiments and data recording. The setup is shown in Figure 108 and a photo is shown in Figure 109.

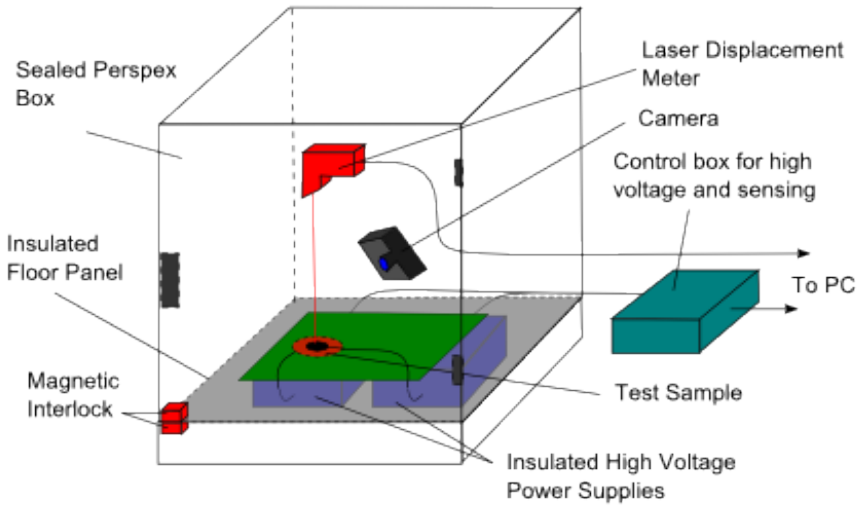

Figure 108: Depiction of high voltage experimental rig.

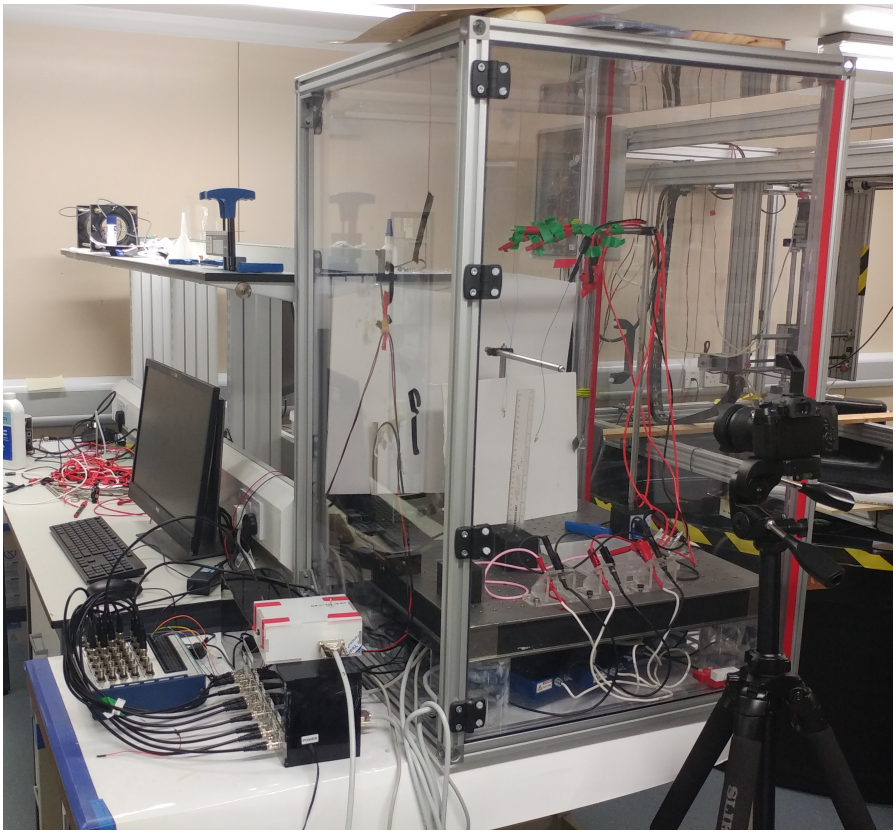

Figure 109: Photo of high voltage experimental rig.

D PIV Frames of Palpation of Circular Object

The PIV tool (OpenPIV) produced a series of between frame PIV vector frames shown below from which a selection have been used in describing the dynamic process of palpation onto an object.

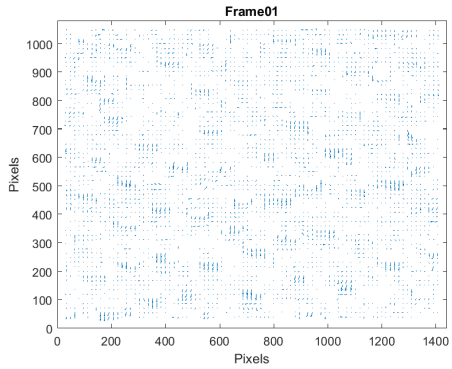

(a) Internal video of circle object test palpation; Frame 01

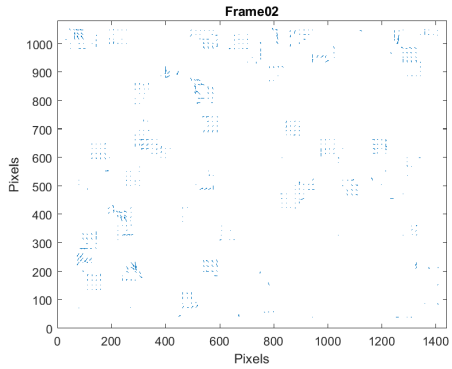

(b) Internal video of circle object test palpation; Frame 02

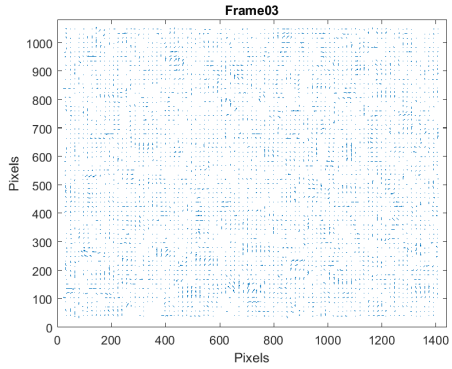

(c) Internal video of circle object test palpation; Frame 03

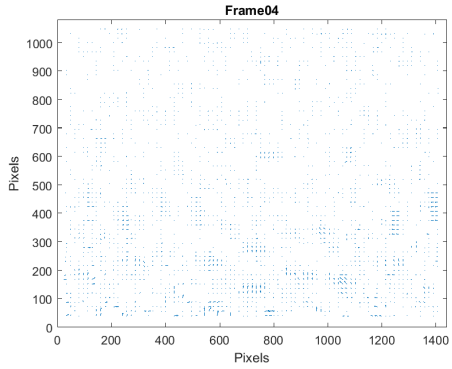

(d) Internal video of circle object test palpation; Frame 04

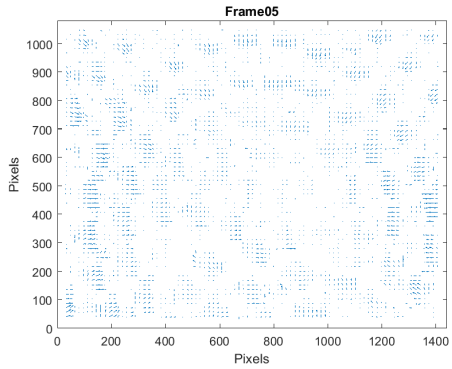

(e) Internal video of circle object test palpation; Frame 05

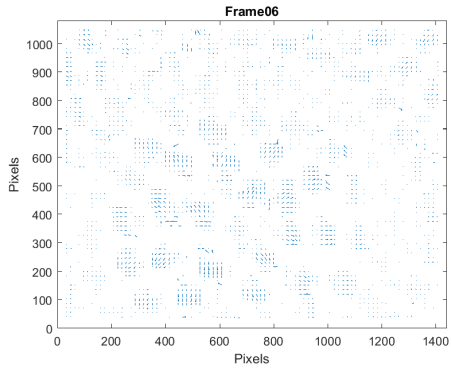

(f) Internal video of circle object test palpation; Frame 06

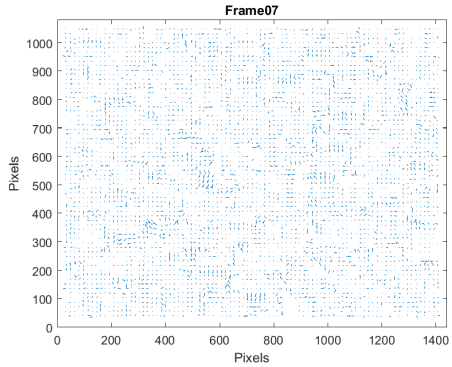

(g) Internal video of circle object test palpation; Frame 07

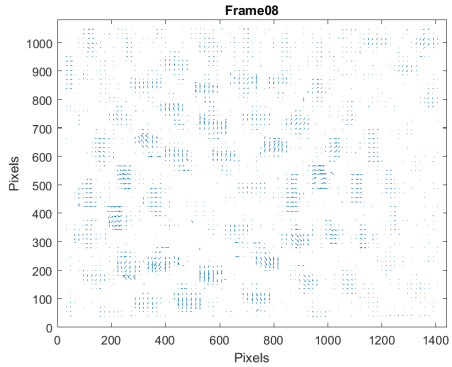

(h) Internal video of circle object test palpation; Frame 08

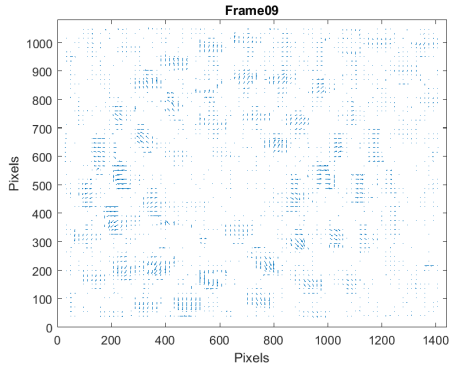

(i) Internal video of circle object test palpation; Frame 09

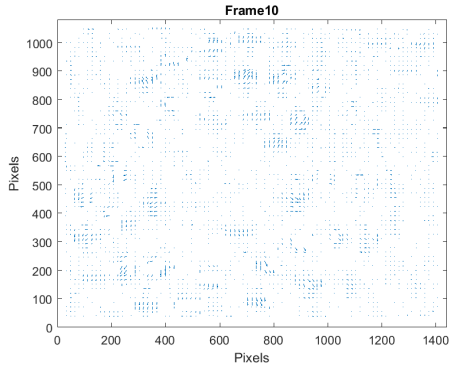

(j) Internal video of circle object test palpation; Frame 10

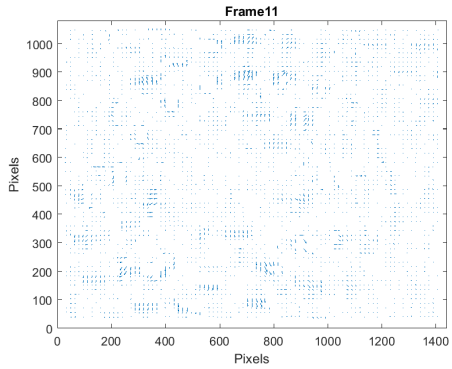

(k) Internal video of circle object test palpation; Frame 11

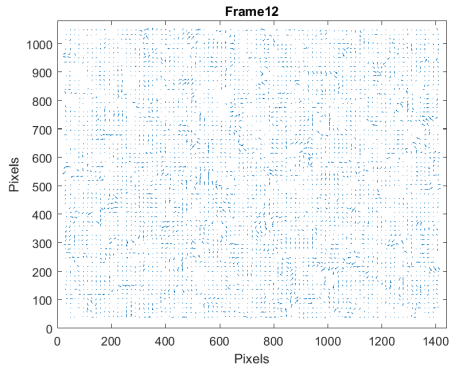

(l) Internal video of circle object test palpation; Frame 12

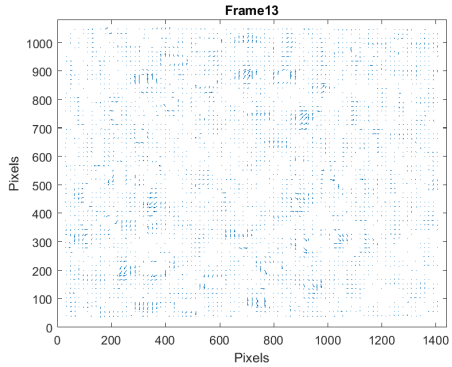

(m) Internal video of circle object test palpation; Frame 13

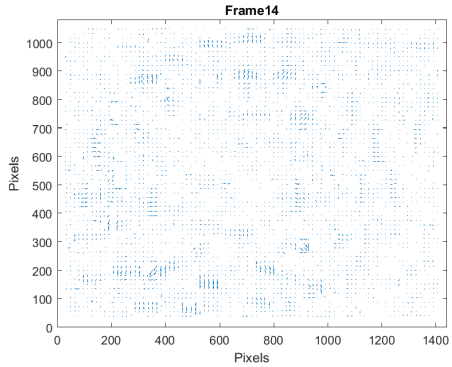

(n) Internal video of circle object test palpation; Frame 14

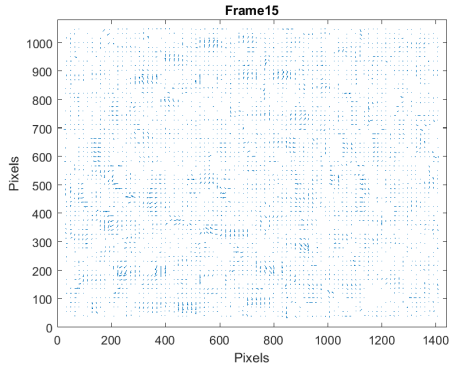

(o) Internal video of circle object test palpation; Frame 15

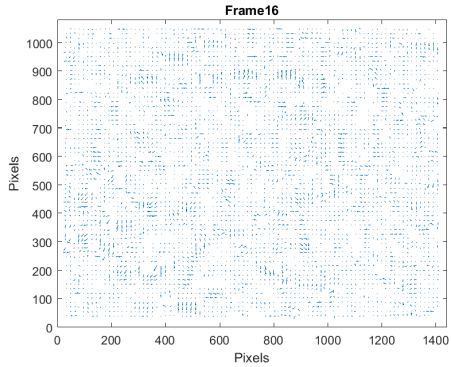

(p) Internal video of circle object test palpation; Frame 16

Figure 110: Complete set of frames of video of circular object test palpation.